



The
University
Of
Sheffield.

A Study on the Numerical Characterisation of Short Fibre Reinforced Composites

by

Ioannis Ioannou

A Thesis submitted for the degree of

Doctor of Philosophy

In the

Composite System Innovation Centre

Department of Mechanical Engineering

September 2014

Abstract

This thesis aims to investigate the macroscopic influence of micromechanical parameters in short fibre thermoplastic reinforced composites (SFTRC). A numerical simulation using the finite element method has been carried out under the concept of Representative Volume Element (RVE). For the short fibre composite material under investigation, all the properties were studied on the linear elastic response.

The microstructure was created by implementing an algorithm to solve the packing problem and create periodic microstructures. Various microstructures were developed in order to study the influence of the dominant parameters. The developed algorithm is able to create microstructures which can be separated into two main categories. The first one regards microstructures consisting of uniform fibre length while the second one regards microstructures made of non-uniform fibre length. The uniform length developed microstructures were studied with respect to the following parameters: Fibre Orientation Distribution (FOD), three cases of orientation were considered: Aligned, misaligned and random orientation, three cases of fibre Aspect Ratio (AR): AR=1, AR=5, AR=10, and three cases of UC size. The non-uniform length microstructures were studied with respect to: Fibre Orientation Distribution (FOD), three cases of orientation were considered: Aligned, misaligned and random orientation, and two cases of UC size.

The developed algorithm was programmed in order to create periodic microstructures considering a number of parameters introduced by the user. The role of the algorithm was focused on creating elliptical shapes and assigned them with various constant and random parameters. Ellipses were representing short fibres placed in a stochastic manner in space (random coordinates) for the cases of randomly oriented fibres, mis-oriented fibres and aligned fibres and for three cases of aspect ratio: AR=1, AR=5, AR=10. The cases of random orientation and length distribution were seeded from a pseudo-random number generator by following a uniform distribution. The case of misaligned fibres was achieved by seeding fibre's orientation with the same pseudo-random generator but restricting the maximum achievable fibre angle to achieve a negative exponential distribution.

A statistical test was implemented in order to quantify the influence of the stochastic parameters in the macroscopic response and derive the representative results which must be independent from any stochastic parameter. A Chi-square test was used for 97% accuracy and for two degrees of freedom. The test was applied on the results (for all the properties under investigation) of the five realisations and it consisted of a comparison between the observed value, defined through the analysis, and the expected value defined as the average quantity of the observed values.

The developed models were subjected to three kinds of periodic boundary conditions; kinematic boundary conditions for the effective transverse and longitudinal stiffness and shear stiffness (E_1, E_2, G), thermal boundary conditions for deriving the effective thermal conductivity (K_1, K_2) and thermo-mechanical boundary conditions for the case of Coefficient of Thermal Expansion (CTE) (α_1, α_2). In the investigation of the thermal and thermo-mechanical properties, results were obtained for the steady state case.

A study on the effect of RVE size was carried out, and in the case of uniform fibre length results show that representativeness of the size is a parameter strongly dependant on the combination of AR and FOD. Chi-square results show a small dependency between the macroscopic response and the size with regard to the uniform fibre length. In the case of fibre length distribution, chi-square results show a very strong dependency of the effective properties with the developed realisations. Conclusions about the representative size can be made once parameters as FOD, FLD, AR and C_{Inh} are considered. Once results from representative sizes of UCs were obtained a further comparison of all the properties (mechanical, thermal and thermo-mechanical) with analytical predictions took place.

Acknowledgments

First of all I would like express my sincere gratitude to my supervisors Professor Alma Hodzic and Dr. Inna Gitman for their excellent supervision, without which this work would have been impossible. In particular, I would like to thank Professor Alma Hodzic for her patience, her encouragement and for guiding me and advising me accordingly during these years, for which I am deeply grateful. Secondly I would like to thank Dr. Inna Gitman for her support and her assistance and also for providing the necessary conditions that made the completion of this work possible. I am also grateful to Professor Costas Soutis who co-supervised my early PhD years. His contribution was critical for setting a strong basis for the continuation of my PhD. I would like to express my gratitude to Dr Sofia Pavlopoulou for all her valuable advice. Throughout these years I had the opportunity to collaborate with a number of people who critically contributed to this work. All my colleagues have provided the best possible working environment. Special thanks go to Alon, Steve, Khaled, Pete, Muliady, Diyar, Tedy and Dr. Tim Swait for all of their help and companionship. My family and my friends have played a key role all these years with their encouragement and understanding. Sincere thanks go to my parents Chrysostomos and Maria, my brother Angelos and my sister Eirini and to Charis, for being there for me all these years, for sharing my joyful moments and for keeping me going when things went wrong. Also special thanks to Markos Andronikou and Panayiotis Apostolelis. In conclusion I would like to acknowledge the financial contribution of the Qatar Science and Technology Park.

Contents

1	Introduction	15
1.1	General aspects.....	17
1.1.1	Manufacturing processes.....	18
1.2	Analytical-Theoretical approach	24
1.3	Numerical-computational approach.....	26
1.3.1	Thermal and thermo-mechanical properties.....	31
1.4	Experimental approach.....	35
1.5	Homogenisation.....	40
1.6	Conclusions	41
1.7	Aim and scope of this study.....	42
1.8	Outline.....	44
2	Mechanical and thermal properties – characterisation of a SFRT composite.....	46
2.1	Material homogeneity	46
2.1.1	Inclusion – inhomogeneity.....	46
2.2	Material symmetry.....	47
2.3	Dominant parameters affecting the macro-mechanical behaviour of SFRC	53
2.3.1	Physical and mechanical properties of fibres and matrix.....	54
2.3.2	Characteristics of fibres and matrix interface.....	63
2.3.3	Fibre length distribution or aspect ratio distribution.	64
2.3.4	Fibre orientation distribution	67
2.3.5	Volume fraction	72
2.4	Modelling strategies	73
2.4.1	Mean field approach.....	73
2.4.2	Periodic micro-field approach.....	75
2.5	Micromechanical models.....	76
2.5.1	Strain and stress concentration tensors	78
2.5.2	Voigt approximation	80
2.5.3	Reuss approximation	81
2.5.4	Shear lag model.....	82
2.5.5	Eshelby inclusion approximation	86
2.5.6	Eshelby’s approach on inhomogeneity.....	91

2.5.7	Self-consistent scheme	93
2.5.8	Mori Tanaka scheme	94
2.5.9	Halpin-Tsai model	95
2.5.10	Analytical models comparison-Elastic properties	97
2.6	Thermal Conductivity	98
2.6.1	Halpin's Model	98
2.6.2	Choy's model	99
2.6.3	Nielsen's model	100
2.7	Linear Coefficient of Thermal Expansion	101
2.7.1	Schapery's model	101
1.1.1.	Shear Lag model	102
2.7.2	Halpin and Pagano's model	102
2.8	Conclusions	103
3	Numerical modelling	105
3.1	Packing problem	105
3.2	Representative Volume Element (RVE)	108
3.2.1	Definition	109
3.2.2	Length scales	109
3.2.3	On the existence of RVE	110
3.3	Modelling SFRC	111
3.3.1	Implemented Algorithm	112
3.3.2	Inclusion's shape	117
3.3.3	In plane orientation distribution	118
3.3.4	Fibre's length distribution	119
3.3.5	Algorithm time response	120
3.4	Numerical models formation	122
3.4.1	Boundary conditions	124
3.5	Conclusions	128
4	Homogenisation approach	129
4.1	Computational homogenisation	130
4.1.1	Asymptotic homogenisation approach	132
4.1.2	Volume average method	135
4.1.3	Reaction force homogenisation approach	137
4.2	Macro-homogeneity condition	137

4.3	Effective properties under investigation	138
4.3.1	Elastic properties.....	139
4.3.2	Thermal properties	141
4.3.3	Thermo-mechanical properties	142
4.4	RVE approach.....	144
4.4.1	Chi-square test.....	144
4.4.2	Chi-square test and inclusion's orientation	145
4.4.3	Chi square and aspect ratio	147
4.4.4	Chi square and effective properties.....	149
4.5	Conclusions	150
5	Results and discussion	152
5.1	Mono-dispersed fibre's length.....	152
5.1.1	Chi-square results	152
5.1.2	Effective properties results	173
5.2	Non mono-dispersed fibre's length	184
5.2.1	Chi-square results	184
5.2.2	Effective mechanical properties	193
5.2.3	Effective thermal conductivity	197
5.3	Comparison with analytical models.....	201
5.4	Conclusions	205
6	Summary and conclusions	209
7	Bibliography	214

Table of figures

Figure 1.1 Stiffness of various material with respect to their density. Indication of specific stiffness	16
Figure 1.2 Extrusion compounding process.....	18
Figure 1.3 The number average of fibre length with respect to flight number towards the screw for glass SPS with weight fraction of 40%. Ramani et al. (1995).....	19
Figure 1.4 Maximum fibre volume fraction as a function of average fibre aspect ratio. Adapted from Milewski.....	19
Figure 2.1 A bounded inclusion and inhomogeneity.....	47
Figure 2.2 Displacement vector define between ϕ and φ	48
Figure 2.3 structure and material coordinate systems.....	51
Figure 2.4 Specific stiffness and specific strength for various engineering materials.....	55
Figure 2.5 Schematic representation of manufacturing process of carbon fibres.....	56
Figure 2.6 The repeating unit of Aramid fibres.....	57
Figure 2.7 A typical example of a tetrahedral bond of silica with oxygen.....	58
Figure 2.8 Glass fibres manufacturing process.....	60
Figure 2.9 A configuration of polypropylene structure.....	61
Figure 2.10 A conformation of polyethylene structure.....	61
Figure 2.11 degradation of fibre length as a function of flight number for three different screw designs.....	Error! Bookmark not defined.
Figure 2.12 Reduction of average fibre length as fibre's content increase.....	64
Figure 2.13 Slice of specimen along Z axis. Fibres are projected as ellipses.....	68
Figure 2.14 Fibre orientation distribution function for various cases of shape functions.....	69
Figure 2.15 Distribution of fibre orientation coefficient for various combinations of shape functions.....	70
Figure 2.16 Orientation distribution for various values of λ	71
Figure 2.17 Schematic representation of the Voigt and Reuss models.....	82
Figure 2.18 Schematic representation of the Shear-Lag model.....	82
Figure 2.19 A single elliptical inclusion embedded in a matrix domain.....	86
Figure 2.20 The first step involves the removal of the inclusion from the surrounding domain.....	87
Figure 2.21 The second step involves the application of a surface traction on the boundaries of the inclusion.....	87
Figure 2.22 The third step of the virtual experiment regards the return of the inclusion into its original position within the matrix.....	87
Figure 2.23 The final step of the process involves the removal of the applied traction and the application of an opposite and equivalent force acting on the surface of the inclusion.....	88
Figure 2.24 A schematic representation of the EIM.....	92
Figure 2.25 Schematic representation of the SCS.....	93
Figure 2.26 Flow chart of the SCS solver.....	94
Figure 2.27 A comparison of predictions of longitudinal and transverse stiffness for aligned fibres orientation.....	97
Figure 2.28 Prediction of effective stiffness in the case of randomly oriented fibres.....	97
Figure 2.29 Comparison of analytical models predictions for Thermal conductivity.....	101
Figure 2.30 Comparison of analytical predictions for the Coefficient of Thermal Expansion.....	103
Figure 3.1 Three dimensional ellipses and two dimensional elliptical shape representing fibres.....	106

Figure 3.2 A very basic structure of a packing algorithm.....	107
Figure 3.3 SEM picture of short fibre composite	107
Figure 3.4 Three different lengths involved in a multi-scale approach.	110
Figure 3.5 Unit cell structures of randomly distributed circular inclusions. Left unit cell has a defined wall effect while the unit cell on the right contains more flexible boundaries.	112
Figure 3.6 Simple structure of a packing algorithm.....	113
Figure 3.7 Calculation of distance between inclusions was based on centre to centre distance calculation.....	113
Figure 3.8 Flow chart of the initial algorithm able to produce a microstructure that consists of circular inclusions.....	114
Figure 3.9 Flow chart of the algorithm used to develop various cases of SFRC microstructure.	115
Figure 3.10 Implementation of geometrical periodicity.....	116
Figure 3.11 Aspect Ratio is defined as the ratio between length of a fibre over the diameter.	117
Figure 3.12 Orientation distribution for in-plane randomly oriented fibres.	118
Figure 3.13 Distribution of fibres orientation for misaligned fibres.	119
Figure 3.14 Distribution of fibre length-AR.....	120
Figure 3.15 Time response of the developed algorithm for various values of AR and orientation...	121
Figure 3.16 Plane stress element CPS3.....	123
Figure 3.17 Typical mesh sample of randomly oriented UC.	123
Figure 3.18 Dirichlet boundary conditions.....	124
Figure 3.19 Neumann boundary conditions.	125
Figure 3.20 Periodic boundary conditions.	125
Figure 3.21 Boundary conditions for calculating longitudinal thermal conductivity.....	126
Figure 3.22 Boundary conditions for calculating Coefficient of Thermal Expansion.	126
Figure 3.23 Loading conditions for effective longitudinal, transverse stiffness and effective shear stiffness.....	127
Figure 3.24 Symbolic representation of the developed stress field for longitudinal stiffness on the left and transverse stiffness on the right.	127
Figure 3.25 Figure 3.26 Symbolic representation of the developed stress field for longitudinal thermal conductivity on the left and transverse thermal conductivity on the right.	127
Figure 4.1 An illustration o the concept of homogenisation and length scales.	130
Figure 4.2 Schematic representation of the multi-scale approach.....	131
Figure 4.3 Asymptotic Homogenisation approach	132
Figure 4.4 Plane stress triangular element with a single integration point.....	136
Figure 4.5 Applied boundary conditions for calculation of the CTE	143
Figure 4.6 Five realisations of a UC consisting of the same V_f the same AR the same orientation distribution and the same UC size.	146
Figure 4.7 Chi-square values for longitudinal stiffness for realisations with AR=10 and three cases of orientations.....	146
Figure 4.8 Chi-square values for transverse stiffness for realisations with AR=10 and three cases of orientations.....	147
Figure 4.9 Chi-square value for longitudinal effective stiffness of aligned fibres as a function of AR.	148
Figure 4.10 Chi-square value for transverse effective stiffness of aligned fibres as a function of AR.	149

Figure 4.11 Chi square values for different mechanical properties for aligned fibres with AR=10....	150
Figure 5.1 From every case of parameter combination, five realisations were developed in order to study statistically the results.....	153
Figure 5.2 Chi-square results for uniform length aligned fibres.....	156
Figure 5.3 Chi-square results for uniform length misaligned fibres.	159
Figure 5.4 Chi-square results for uniform length randomly oriented fibres.	161
Figure 5.5 Chi-square results regarding the thermal conductivity for aligned uniform length fibres.	164
Figure 5.6 Chi-square results regarding the thermal conductivity for misaligned uniform length fibres.	165
Figure 5.7 Chi-square results regarding the thermal conductivity for randomly oriented, uniform length fibres.	166
Figure 5.8 Chi-square results regarding the coefficient of thermal expansion for uniformly oriented-aligned fibres.....	169
Figure 5.9 Chi-square results regarding the coefficient of thermal expansion for misaligned fibres.	170
Figure 5.10 Chi-square results regarding the coefficient of thermal expansion for randomly oriented fibres.	171
Figure 5.11 Effective mechanical properties results for uniform length fibres. Results are presented with respect to AR for all the cases of orientation under investigation.	174
Figure 5.12 Effective shear properties results for uniform length fibres. Results are presented with respect to AR for all the cases of orientation under investigation.	176
Figure 5.13 Effective thermal conductivity results for uniform length fibres. Results are presented with respect to AR for all the cases of orientation under investigation.	179
Figure 5.14 Effective CTE results for uniform length fibres. Results are presented with respect to AR for all the cases of orientation under investigation.....	182
Figure 5.15 Chi-square results regarding the mechanical properties for non mono-disperse fibre length distribution, for three cases of orientation.	185
Figure 5.16 Chi-square results regarding the thermal conductivity for non mono-disperse fibre length distribution, for three cases of orientation.	189
Figure 5.17 Chi-square results regarding the coefficient of thermal expansion for non mono-disperse fibre length distribution, for three cases of orientation.....	191
Figure 5.18 Mechanical effective properties for non mono-disperse fibre length for the three cases of orientation.	194
Figure 5.19 Thermal conductivity effective properties for non mono-disperse fibre length for the three cases of orientation.....	197
Figure 5.20 Coefficient of thermal expansion for non mono-disperse fibre length for the three cases of orientation.	199
Figure 5.21 Comparison of FEA results with various analytical models for longitudinal transverse and shear stiffness	201
Figure 5.22 Comparison of FEA results with various analytical models for the case of randomly oriented and misaligned fibres	202
Figure 5.23 Comparison of FEA results with various analytical models for thermal conductivity for aligned and misaligned fibres.	203
Figure 5.24 Comparison between FEA results and analytical models for coefficient of thermal expansion for aligned misaligned and randomly oriented fibres.	204

List of tables

Table 2-1 Common fibre's material and their filament size.	55
Table 2-2 Main commodity thermoplastics for structural applications	61
Table 2-3 Main thermoset resins used for composite structures.....	63
Table 2-4. Stress, strain and displacement field for the inclusion and the matrix according to Eshelby's approach.	88
Table 2-5. Parameters of the Halpin-Tsai model.	96
Table 3-1. Elastic and thermal properties of glass fibres and polypropylene.....	122
Table 4-1 Properties under investigation	138
Table 5-1 Chi-square results for mechanical properties.....	162
Table 5-2 Chi-square results for thermal properties.	167
Table 5-3 Chi-square results for thermos-mechanical properties.....	172
Table 5-4 Results for mechanical effective properties.	177
Table 5-5 Results for effective thermal properties.....	180
Table 5-6 Results for thermos-mechanical effective properties.	183
Table 5-7 Chi-square results for mechanical properties of RLD.	187
Table 5-8 Chi-square results for thermal properties of RLD.	190
Table 5-9 Chi-square results for thermos-mechanical properties of RLD.	192
Table 5-10 Results of effective mechanical properties of RLD.	195
Table 5-11 Results of effective thermal properties of FLD.	198
Table 5-12 Results of the effective thermos-mechanical properties of FLD.	200

Nomenclature

Acronyms

SFRC	Short Fibre Reinforced Composite
AR	Aspect Ratio
FO	Fibres Orientation
SFRTC	Short Fibre Reinforced Thermoplastic
IM	Injection Moulding
RSA	Random Sequential Absorption
LRS	Laminate Random Strand
DoF	Degrees of Freedom
ITZ	Interfacial Transition Zone
RDSF	Randomly Distributed Short Fibres
TRDSF	Transversely Random Distributed Short Fibres
SFRP	Short Fibre Reinforced Polymer
EIM	Equivalent Inclusion Method
MFI	Melt Flow Index
HDT	Heat Deflection Temperature
TMA	Thermo-Mechanical Analysis
CTE	Coefficient of Thermal Expansion
LCTE	Linear Coefficient of Thermal Expansion
IFSS	Inter-facial Shear Stress
ESCS	Effective Self Consistent Scheme
IDD	Interaction Direct Derivative
SCS	Self-Consistent Scheme
MCM	Monte Carlo Method
EIAS	Equivalent Inclusion Average Stress
CLT	Composite Laminate Theory
LRSM	Laminate Random Strand Method
UC	Unit Cell
RVE	Representative Volume Element
GETVRM	Abaqus subroutine
USDFLD	Abaqus subroutine
C_{Inh}	Degree of Inhomogeneity
T_g	Glass transition temperature
LF	Long Fibre
SF	Short Fibre
FOD	Fibre Orientation Distribution
FLD	Fibre Length Distribution
RoM	Rule of Mixtures
IRoM	Inverse Rule o Mixtures
LAA	Laminate Analogy Approach
FEM	Finite Element Method
DMA	Dynamic Mechanical Analysis
CVD	Chemical Vapour Deposition
LCP	Liquid Crystal Polymer
V_f	Fibres Volume Fraction
V_m	Matrix Volume Fraction
M_n	Molecular Weight

W_f	Weight fraction
f_L	Fibre Length
m	Orientation-Length Distribution Shape Parameters
n	Orientation-Length Distribution Shape Parameters
a	Orientation-Length Distribution Shape Parameters
b	Orientation-Length Distribution Shape Parameters
ρ_f	Fibre's Density
ρ_m	Matrix Density
r	Fibres Diameter
R	Fibre to Fibre centre distance
C^P	Polarisation Tensor
C^{Ref}	Reference Homogeneous Media Tensor
ε_{ij}^*	Eshelby's eigen-strain
ε_{ij}^e	Elastic strain-(equivalent to eigen-strain)
ε_{ij}^c	Constrained field strain
σ_{ij}^c	Constrained field stress
G_{ij}	Green's function
n_k	Unit vector
S_{ijkl}	Eshelby's tensor
δ_{ij}	Delta of Kronecker
A_{ijkl}	Strain concentration tensor
B_{ijkl}	Stress concentration tensor
t_i	Surface traction
σ_{ij}	Normal stress
τ_{ij}	Shear stress
ε_{ij}	Normal strain
γ_{ij}	Shear strain
E	Young's modulus
G	Shear modulus
ν	Poisson ratio
λ	Kacir's model shape parameter, Cox 's model parameter, characteristic length of structure scale.
μ	Chin's model parameter
s	Chin's model parameter
θ	In plane orientation angle
P, q	Shape parameters for fibre orientation distribution model
f_θ	Fibre orientation coefficient factor
θ_{mean}	Mean fibre orientation angle
θ_{mod}	Most probable fibre's angle
$\rho(\theta)$	Fibre orientation distribution
$g(\theta)$	Orientation cumulative distribution function
c	Orientation-Length Distribution Shape Parameters

1 Introduction

Composite materials are known as new generation, lightweight and very strong-stiff materials, yet this kind of material has existed in nature for thousands of years now. Materials like wood, bamboo, bones amongst many others are a few examples of composite materials existing long before the modern engineering community thought of developing the first composite material. The beginning of composite materials starts in the third decade of the 20th century; however composite structures can be found as far back in time as 1500 BC when ancient Egyptians and Mesopotamians mixed mud and straw in order to create a strong and durable structural material for buildings. Later on, around 1200 AD the Mongolian army of Genghis Khan used a bow made out of composite material consisting of wood, bone and animal glue, all of which were wrapped together with birch bark. These signs indicate that humans understood the advantages of a composite system of materials, in structures, centuries ago. Nowadays with the existing manufacturing technologies and the significant improvements in theoretical knowledge, composite materials are the sharp edge of materials technology.

In general a composite material is a material made from two or more distinct materials with significantly different physical or chemical properties, which produce a material with properties different from the individual components. The second phase of composite material is called “matrix” and its main purpose is to keep the reinforcing agent together and also to transfer the load to the reinforcing agent. The main matrix materials are polymers, metals and ceramics. Polymeric materials are the result of the polymerisation process of monomers and they exist in two types, natural polymers and synthetic polymers. Natural polymers exist in nature in the form of natural silk or natural wool or proteins. The second type of polymeric structures is the synthetic polymers. Examples of synthetic polymeric structures, amongst others, include nylon, polyethylene, polyester, and epoxy. Scientists developed the first synthetic polymers at the beginning of the 20th century. Plastics like vinyl, phenolic, polyester and polystyrene were developed in the early 1900s and were the first synthetic polymers. In the case of synthetic polymers two big categories can be found - thermoplastic and thermoset polymers. The primary physical difference is that thermoplastics can be re-melted back into a liquid form, whereas thermoset plastics will always remain in a permanent solid state. However in order to create a strong-stiff material, further that a polymeric matrix, reinforcement is needed. Historically the first fibre reinforcement appears in 1935 from Owens Corning by introducing the first glass fibre. Since then a period of developing composite materials began and extreme growth occurred during World War II. By 1970 the sector of composite materials was well established, new types of resins with better properties were developed and new types of fibre reinforcement like carbon and aramid were introduced into the market. Reinforcing agents can be fibres (continuous, long or short), particles, nanotubes or nanoparticles. A relation between mass and Young’s modulus for various reinforcing materials can be seen in Figure 1.1.

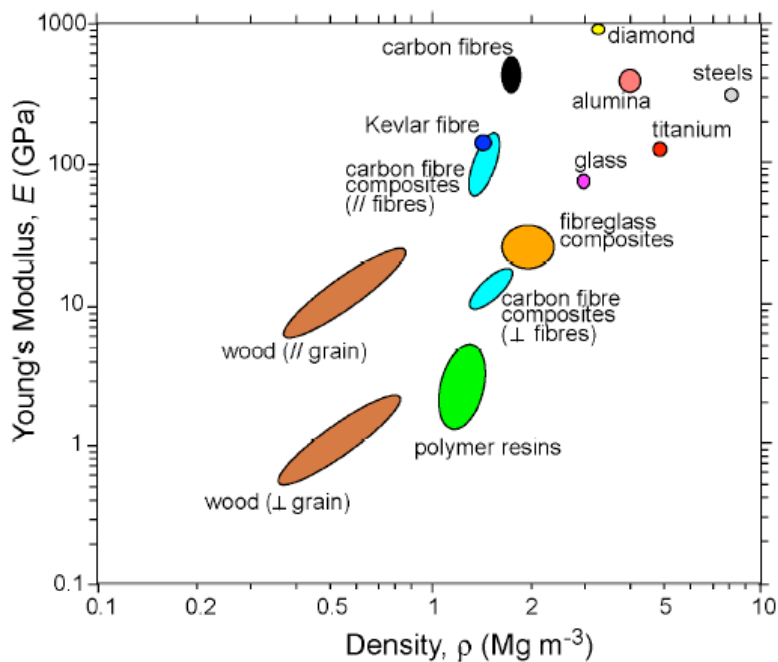


Figure 1.1 Stiffness of various materials with respect to their density. Adapted by D. Hull

The composite material to be further discussed will be polymeric thermoplastic matrix reinforced with short glass fibre composite. Short fibre reinforced composites (SFRC) are materials with many advantages. Amongst others, SFRC are not expensive composite materials, they have a relatively low cost and easy process of manufacturing and they exhibit superior mechanical properties over the parent polymers. These are the main reasons for the extent of development and usage of SFRC. Large scale production of SFRC is possible by using extrusion compounding and injection moulding processes. These conventional fabrication techniques are the main reason for making the manufacture of SFRC efficient and inexpensive in comparison with the manufacture of continuous fibre composite.

The following chapter provides a background for the mechanical, thermal and thermo-mechanical characterisation of short fibre composite materials. Prediction of effective mechanical, thermal and thermo-mechanical properties of short fibre reinforced composites (SFRC) has been a field of study for various researchers and it consists the main influence for the following chapters. Through this chapter different approaches that have been developed by numerous researchers through the years will be presented. The chapter begins by discussing the main aspects of the manufacturing process of short fibre composite, which is a process which introduces major factors affecting the behaviour of the material, and continues by addressing the major fundamental theoretical approaches on micromechanical analytical modelling.

The chapter is separated in three main sections. During the first section a review of various analytical approaches on the field will be presented, followed by numerical approach and

experimental work. Finally the chapter concludes with a review of the homogenisation approach. All of the sections presented in this chapter are of important interest for material characterisation.

1.1 General aspects

Short fibre composite materials have been attractive to the industry since their invention. SFRC received much attention as a material due to its mechanical and physical properties, with those properties being strongly influenced by the morphology and the type of the reinforcement, as well as by the bonding efficiency between the fibres and the matrix. Various manufacturing processes have been developed throughout the years. Mainly SFRC manufactured using the injection moulding process exhibit properties that strongly depend on the aspect ratio (AR), fibre's orientation (FO), fibre's content, fibre's length and the interfacial strength. Considering its superior mechanical properties in combination with the low manufacturing cost, it makes it easier to understand why this family of materials were used and studied so widely. In any case of different combinations of matrix and reinforcement materials, or in any case of different AR or FO, the macroscopic behaviour of the composite material will be different. For this purpose a wide range of investigations have been done in order to clarify the limitation and the potential of such materials in any loading or environmental conditions.

Earlier theoretical micromechanical models were able to predict the macroscopic effective properties of SFRC by using the micromechanical parameters of the material. Simple and relatively complex theoretical models have been developed in order to satisfy this purpose. Analytical models are based on the accurate mathematical modelling of the physical phenomenon-mechanism that takes place on a system of materials as a composite material. Through the revolutionary development of computational power and the improvement of numerical methods, a more comprehensive computational approach was made possible and a new era of computational mechanics began. There are five main factors dominating the physical and mechanical behaviour of SFRC:

- Properties of the individual constituents
- Fibre volume fraction
- Fibre orientation distribution (FOD)
- Fibre length distribution (FLD)
- Fibre-matrix interface strength.

1.1.1 Manufacturing processes

Theoretical models predicting stiffness, strength and fracture among other properties strongly depend on the aforementioned five factors-parameters. FOD and FLD in particular, are properties strongly dependant on the manufacturing process. As mentioned in the introduction, manufacturing processes such as extrusion compounding and injection moulding are most often used to manufacture short fibre reinforced thermoplastic composite (SFRTC) . The process of extrusion compounding shown in Figure 1.2 involves a screw (single or double) as a transport media due to its ability to perform all the necessary steps of the process: feeding, pumping, melting and mixing. Its advantage to include a relatively large quantity of compound material, including screw technology for the extrusion compounding offers a good homogeneity of the melt and an accurate temperature control. A good degree of homogeneity is always an aim for short fibre manufacturing processes. As reported by many authors, screw technology for extrusion compounding SFRTC products leads to a dramatic reduction of the fibre length distribution.

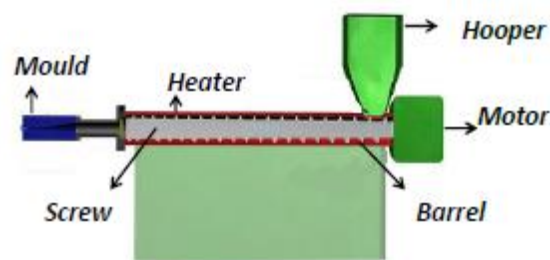


Figure 1.2 Extrusion compounding process.
Adapted by B.T. Astrom

As it has been reported by (Ramani, 1995) there is an effect on the final fibre length with the geometry of the screw. Figure 1.3 demonstrates that the average fibre length is dramatically reduced in relation to the actual geometric design of the screw and the numbers of flights. During the process of compressing and mixing the polymer with the short fibres and especially during the process of melting, extremely high shear stresses take place in the melted material.

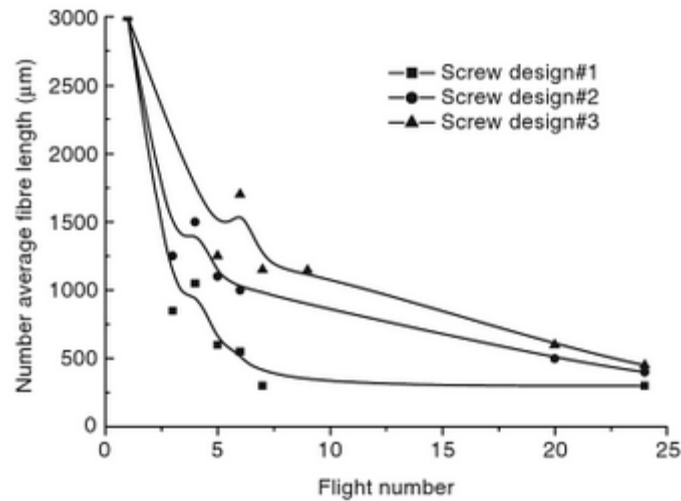


Figure 1.3 The number average of fibre length in respect with flight number towards the screw for glass SPS with weight fraction of 40%. (Ramani, 1995)

As a result, the fibres which appear between the screw and the walls of the extruder break due to the high shear stresses. Also, as reported by (Fu, et al., 2009) the major causes of fibre damage can be:

- Fibres interacting with a fibre-stress concentration due to abrasion of fibres surface,
- Fibres overlapping can cause high bending stresses, which will result in fibre breakage, and
- High viscous forces introduced into the system by the matrix melt may cause fibre fracture.

For high Volume Fraction (V_f), or densely populated flow of fibres there is a high possibility of fibre to fibre interaction. As a result, (Milewski, 1974) presented a relation between fibre aspect ratio and the maximum achievable volume fraction, shown in Figure 1.4, showing that high volume fraction for randomly oriented SFRC is only possible for low aspect ratio. In other words, the higher the aspect ratio, the lower the maximum achievable volume fraction.

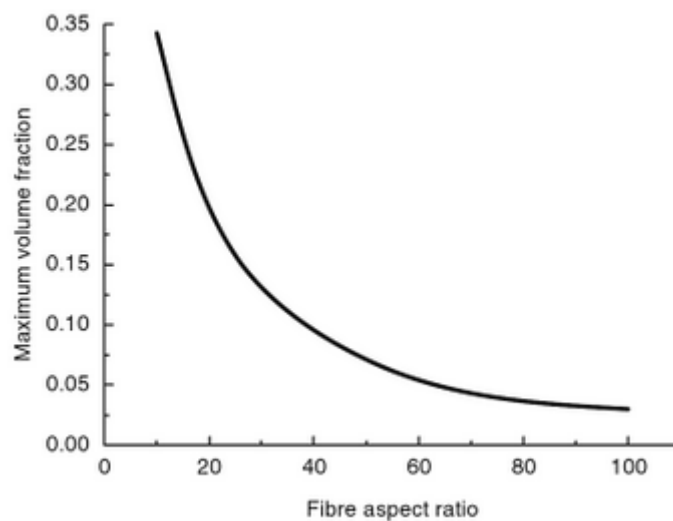


Figure 1.4 Maximum fibre volume fraction as a function of average fibre aspect ratio. Adapted from (Milewski, 1974).

It has also been reported by (Fu, et al., 2009) that the process of extrusion compounding for fibre filled polymer manufacturing has a practical processing limit on the maximum fibre content of 40-45% weight fraction.

As reported by (Rosato, 2000), injection moulding (IM) is principally a mass production method and has the advantage of cost-effective economy, vast quantity and no post-moulding operations, and that is predominantly why IM is used to produce at least 50% (by weight) of SFRC. The IM process involves three basic mechanical units:

- Melting and injection unit,
- Mould, and
- Clamping cylinder.

First, the composite compound is introduced into a heater chamber and then the injection process follows under pressure into a mould cavity. After that the part solidifies. The final step involves the ejection of the product from the mould. In terms of fibre orientation for the IM manufacturing process, the high speed flow of the melt helps to achieve a higher degree of alignment. A combination of high speed flow with a narrow gate or a thin and confined wall helps fibres to be oriented towards the flow direction. This phenomenon occurs mainly due to the most probable interaction of fibres with the walls of a narrow passage. This interaction lead to high shear stresses which results in a higher degree of alignment for the fibres. The best known model to describe this situation is called the “skin-core-skin” model, in which two skin layers surround the core layer. Due to the interaction of the melt with the mould surface, fibres are prone to a higher degree of alignment in contrast with the core layer, located in the middle of the mould (without any contact with the cold mould surface) and the fibres tend to be more randomly oriented.

This case of orientation causes the material to display a more anisotropic behaviour. In terms of the aspect ratio, as in the case of the extrusion compound, there is a significant reduction of the fibre length during the process of IM. As reported by (Kamal, 1986), a significant reduction of fibre length was observed from 0.71mm to 0.27mm. According to (Vu-Khanh, 1991), the IM manufacturing process can be controlled by six variables:

- peak cavity pressure,
- holding pressure,
- back pressure,
- screw speed,
- melt temperature and
- barrel temperature profile.

Generally, fibre attrition is strongly influenced by these variables.

As reported by (Thomason, 1996) during the last decades the rapid increase in the use of structural composites led to the need to develop high performance SFRC. High performance of SFRC can be

achieved if the composite contains fibres with high AR, high volume fraction and aligned orientation; all of the aforementioned properties are strongly dependant on the manufacturing process of SFRC. On the other hand, the market demand for mass production of SFRC is in contrast with the quality of the manufacturing processes needed to achieve high AR and aligned FO. This led to the development of manufacturing techniques able to satisfy the needs of the market. Despite parameters like fibre content being relatively easy to control, other parameters such as AR and FO are still not easily controllable.

Regarding the manufacturing methods of short fibre composite with thermoset resins a wide range of methods are currently used in industry. The following paragraphs aim to describe the main manufacturing methods as:

- Hot press moulding
- Cold press moulding
- Hand lay-up
- Spray lay-up

During the hot press moulding, a matched metal tool is placed between the platens of a hydraulic press and heated to between 130°C and 170°C. The prepreg or reinforcement material is placed in the tool, which has a cavity in the shape of the component required. The tool is rapidly closed and the cure is completed within 2-3 minutes. The tool is opened and the component removed. In order to aid removal of the component from the tool, release agents are either incorporated into the resin mix or applied to the surface of the tool.

This method uses various compounds including SMC (Sheet Moulding Compound), DMC (Dough Moulding Compound) and BMC (Bulk Moulding Compound). The compounds use polyester resin, filler, catalyst, pigment and other additives. The fibre preforms are typically a sprayed chopped fibre and binder or thermally deformed Chopped strand mat containing a thermoplastic binder. This method does allow for a high production rate and is preferred by the automotive industry.

Some of the characteristics of the method are:

Table 1-1 Characteristics of hot press mould method.

key points		
Resin		Polyester, Epoxy
Fibre Type		Chopped strand mat
Cost	Press	30K-350K
	Tool	3K-70K
Application		Car body panel

In the case of cold press moulding, fibres in the form of mats are placed on the mould and overlap at the pinch-off area of the mould. The resin used consists of two batches mixed together, one batch contains the catalyst and the other contains the accelerator. The resin is poured into the mould, the press is lowered and the mould closed. The resin is forced to the edges of the mould but cannot escape due to the overlap of fibre at the pinch-off area. Over this area the fibre is compressed more

than over the rest of the mould. The effect is that the resin is contained in the mould but air can escape, hence creating a back pressure that ensures the resin flows into all parts of the mould. A cold cure process is used (although some increase in temperature is common) with an accelerator in place to achieve cure within a reasonable timescale (approximately 15 minutes). The curing process is exothermic so that care must be taken not to degrade either the mould or the product.

As the manufacturing pressures and temperatures are low, the tooling is relatively light duty and hence low cost. This method also allows for moderate production rates and can be considered for high volume production.

Some of the characteristics of the method are:

Table 1-2 Characteristics of the cold press method.

key points		
Resin		Polyester, Epoxy, Phenolic
Fibre Type		Glass or carbon filament mat, woven, roving and multi-axial reinforcement
Cost	Press	5K-30K
Application		High volume productions

For hand wet lay-up method, the fibre is positioned in or on the mould by hand. If the mould is a complex shape, small pieces of mat are cut to fit and then more layers are applied to achieve the required thickness. The liquid resin is poured over the fibre and rolled to ensure complete wetting of the fibre and removal of air bubbles. In general the resin cures at room temperature with the use of an accelerator and a catalyst. If a hot cure is used then there is no need to use an accelerator. Post curing of cold cured laminates is recommended.

Prior to application of the fibre and resin, the mould is prepared with either polyvinyl alcohol or non-silicon wax to aid release of the component. Release of the component is achieved by either tapping wedges between the mould and the component, or by the use of compressed air to gently force the pieces apart.

Chopped strand mat is the most commonly used fibre although woven roving is used when a stronger and stiffer laminate is required. A gel coat is applied to the mould surface to produce a resin rich smooth surface for appearance and protection purposes. For improved surface finish and corrosion resistance a surface veil is used which is applied with an embedded fabric for reinforcement or mixed with resin for smooth surface.

The advantage of this method is that it is simple and hence is widely used. There is low cost of capital equipment and no requirement for highly skilled labour. It is also possible to achieve relatively high fibre contents in the laminate. The disadvantages are that it is not suited for strength or weight critical primary structure as the fibre orientation and local resin content cannot be well controlled. The nature of the wet lay-up also has health and safety issues because low molecular weight resins can be harmful. The fumes from the curing process, especially with polyester resin, require appropriate extraction systems, especially to comply with emission levels for styrene.

Some of the characteristics of the method are:

Table 1-3 Characteristics of the hand wet lay-up method.

key points	
Resin	Polyester, Vinyl ester, Phenolic
Fibre Type	Chopped strand mat, Woven roving
Cost	<500
Application	Boats, Ducts, Wind turbine blades, Chemical tanks

The method of spray lay-up implies that glass fibre (Roving) is fed into a chopper on the spray gun and the resulting strands are blown into a stream of liquid resin. The spray is directed at a mould and the resulting composite has a random array of glass fibres. The resin must be liquid at room temperature to achieve adequate handling, wet out and fibre impregnation. In addition to this the gel time of the resin must be sufficient to allow complete lay-up of the part before solidification occurs. The laminate is rolled to conform the laminate to the mould surface and remove any air bubbles. There are two cure systems used, twin-pot and catalyst injection. Both systems begin the reaction process at the gun, which means fast curing resin systems may be used.

Prior to application of the fibre and resin, the mould is prepared with either polyvinyl alcohol or non-silicon wax to aid the release of the component. Release of the component is achieved by either tapping wedges between the mould and the component or by the use of compressed air to gently force the pieces apart.

Glass fibre is particularly suitable for this method as it is easily chopped into strands, has low static and fast wet through. Resins such as vinyl ester or polyester are commonly used owing to their high reactivity.

The spray method has the advantage on being a fast application method. It achieves better wetting of the fibre with fewer voids than with hand lay-up. This results in parts having better physical properties. However, it produces parts that are less uniform, particularly in thickness than hand lay-up. The laminates tend to be resin rich and hence heavier. This method requires a low molecular weight resin and the styrene emissions can be high, requiring tight health and safety controls.

Some of the characteristics of the method are:

Table 1-4 Characteristics of the spray lay-up method.

key points		
Resin	Polyester, Vinyl ester, Phenolic, Epoxy	
Fibre Type	Glass	
Cost	Machine	5K-10K
	Mould	150-15K
Application	Caravan bodies, Bathtubs, Shower trays	

1.2 Analytical-Theoretical approach

The mechanical characterisation of a short fibre composite was first approached analytically by the implementation of micromechanical models. An innovative work was released in 1889 by Voigt and in 1929 by Reuss. Both Voigt and Reuss models were reference models since the earlier developed models were mainly based on the Voigt model, known later as the Rule of Mixtures (RoM) while Reuss model became known as the Inverse Rule of Mixtures (IRoM).

A pioneering work was released in 1952 by (Cox, 1952) on stress distribution along the fibre, using the shear lag model. Prediction of the effective elastic modulus was enabled by calculating the fibre length factor and adding a modifying factor to the rule of mixtures (RoM). The shear lag model uses microstructural parameters such as fibre length and fibre to fibre distance in order to calculate macroscopic effective properties. A major contribution of the shear lag model is that by using few necessary assumptions it can accurately predict the normal and shear stresses distribution on the fibre and also can predict the saturation effect of fibre length.

(Hill, 1963) presented a general theoretical approach on the problem of two isotropic phases for any concentration by implementing the concept of the phase concentration tensor of stress and strain. Hill also mentions that the calculation of macroscopic elastic properties involves calculating the dependency of the macroscopic moduli on the relative concentrations, on the inclusion geometry, inclusion arrangement, inclusion distribution etc. A self-consistent method was introduced by (Hill, 1965) as a method that takes account of the inhomogeneity of stress and strain in a similar way to the crystalline aggregates theory. The model is able to predict the effective stiffness of a two phase composite material. Inclusions are assumed to be aligned ellipses and to have the same elastic properties as that of short fibres. The method is based on the solution of the auxiliary elastic problem involving a uniformly loaded infinite mass containing an ellipsoidal inhomogeneity.

In 1957, a revolutionary work was presented in the proceedings of the royal society by a British engineer named Sir Douglas Eshelby (Eshelby, 1957,). The method was promising solution of the stress and strain field in a composite by analysing an ellipsoidal inclusion embedded in an infinite matrix. Eshelby used the superposition method of linear elasticity, and by assuming four steps of a virtual experiment, he proved that the stress and strain field inside the inclusion are uniform, for an ellipsoidal inclusion in a homogeneous infinite matrix. Sir Douglas Eshelby's work consist a head cornerstone on the field of micromechanics.

Another work on the prediction of short fibre composite came from Halpin and Kardos (Halpin, 1976,) once they released a paper on the review of the Halpin Tsai equations. It should be mentioned that Halpin and Tsai established more useful expressions of Hill's self-consistent method, with approximations to make the model compatible for short fibre composites. As it will be discussed later, the limitation of the Halpin-Tsai model, for a very stiff or very complained material, led to variations of the RoM. The Halpin and Tsai model has been widely considered to be a reliable model, relatively easy to use, with closed analytical solutions. The model uses the degree of inhomogeneity and the geometry parameters of a short aligned fibre to predict its macroscopic behaviour.

A more complicated scheme was presented by (Mori, 1973) which aimed to discuss a new method of calculating the average internal stresses of a matrix in a material containing inclusions with transformation strain. The original work of Mori and Tanaka does not refer to composite materials, but to the plastic deformation that occurs in a material with transformation strain. In the paper the concept of average stress throughout the matrix is discussed, and also an expression of the average elastic energy by considering the effect of interaction between the inclusion and the free boundary. Benveniste's work in 1987, (Benveniste, 1987) suggested a new approach on the Mori Tanaka scheme for calculating the effective properties of composite materials. A direct approach on the applications of the theory is presented in the paper, through a method named EIAS (Equivalent Inclusion Average Stress). The method combines the concept of the equivalent inclusion method (EIM), introduced by (Eshelby, 1957), and the concept of average stress and strain, introduced by (Mori, 1973), considering the interaction between the inclusions. A detailed discussion of the aforementioned models, regarding the concept of average stresses, eigen-strain or the equivalent inclusion concept, can be found in the book of (Mura, 1987). Sufficient definitions of inclusions, inhomogeneities and the inhomogeneous inclusions are given based on the concept of eigen-strain.

All the previews of the aforementioned models are micromechanical models. They may have different approaches but all of them consider information derived from the microstructure of the material in order to calculate macroscopic effective or apparent properties. A different analytical approach came mainly from the work of (Halpin, 1976,) and co-workers, which is derived from a micromechanical (self-consistent) model, but this is more a semi-empirical approach.

The Laminate Analogy Approach (LAA) has been used by various researchers as a model able to estimate the effective mechanical properties of SFRC. The model uses a macroscopic approach on a composite material using the Classical Laminate Theory (CLT) and simulates the short fibre material as a stacking sequence of differently oriented laminates. The model indirectly uses results from the shear lag model, the Voigt model and the Halpin Tsai model in order to calculate micromechanical properties. Under this consideration information of the microstructure of the material are introduced into the model and treated with a macroscopic approach through CLT. Fibre orientation and fibre length are involved within the model in the same manner as in CLT.

The effect of fibre length and fibre orientation was deeply discussed by (Fu, 2000). In an analytical manner they presented a model of calculating the probability density distribution for the fibre length and fibre orientation. They proposed a fibre efficiency factor, which is a product of the fibre length efficiency factor and the fibre orientation efficiency factor. The article concludes with a tensile strength model which considers the main micromechanical parameters affecting the composite.

A more recent work from (Jules, 2004) presents a hybrid way of calculating effective properties. In this article a software is developed and presented, which calculates the effective properties using the Mori Tanaka scheme, by implementing numerical methods in order to assign random values in micromechanical parameters. The developed software has the ability to consider fibre orientation in three dimensional space and fibre length.

The preview paragraphs refers to analytical models, a theoretical approach based on the mathematical modelling of the mechanism that takes place in a two phase composite material behaviour on a micro scale. The fact that recently published works are still contributing to the field of analytical modelling is an indication that a more simple and holistic approach is possible. The

common base of the presented theoretical work in micromechanical aspects of SFC is the idealisation of the material's morphology. Assumptions like the equal distances between fibres, or the uniform length and orientation, the assumption of a single inclusion embedded in an infinite matrix, are ideal situations of the stochastic morphology of a short fibre composite. A closer examination of the material's morphology can be achieved by implementing a computational approach, a topic which will be discussed in the next paragraphs.

1.3 Numerical-computational approach

Since 1970, there has been a race to develop numerical methods that will be able to solve differential linear or non-linear equations, which describe the behaviour of materials under various loading conditions. The Finite Element Method is a well-established method and is one among others methods (Boundary Element Method, Finite Volume Method) used for computational structural analysis. Therefore, a more realistic approach on the microstructure of the composite is enabled and various geometric parameters can be evaluated through a computational approach. Through literature, one is able to find numerous papers which discuss computational mechanics for traditional engineering materials, as well as for more advanced materials such as composite materials. The following paragraphs will focus on scientific work dealing only with numerical models for short fibre composites and more specifically the literature considering microstructures or micromechanical properties of a short fibre composite material.

A relatively recent paper was released by (Hine, 2002) for the prediction of elastic and thermo-elastic properties of the aligned short fibre composites. Throughout the paper, a numerical approach is presented based on the Finite Element Method (FEM) and the thermo-elastic properties of the model are calculated using an iterative method, by minimising the strain energy using a conjugate gradient approach. Through the developed three dimensional model of the aligned short fibre composite, the author investigates the replacement of the length distribution in the morphology of the composite with a mono-disperse (uniform) fibre length which will show the same longitudinal modulus. The distribution of longitudinal and transverse Young modulus, as well as the shear modulus Poisson ratio and the coefficient of thermal expansion are presented as functions of volume fraction. Volume fraction was increased until 30%. For the case of $V_f = 15\%$ results for longitudinal Young modulus and CTE are presented as a function of AR. The work concludes that a replacement of the fibre length distribution can be done with the number average length of the fibres in a composite material. Predictions of the developed numerical model are compared with theoretical predictions of the Halpin-Tsai model and (Tandon, 1984) model.

In a later work, the author (Lusti, 2002) focuses on the second important microstructure variable, the fibre orientation. Elastic and thermo-elastic properties of three dimensional misaligned structures were calculated numerically and compared with experimental and analytical results. The stochastic parameter of orientation was seeded by sampling the measured distribution using the Monte Carlo method (MCM). In both papers the author uses three dimensional representations of the microstructure of a short fibre composite, experiencing geometric periodicity.

(Pan, 2008) also studied the effect of random fibre orientation on the macroscopic effective stiffness properties of a randomly oriented fibrous composite. Through the paper, the author underlines the difficulty of creating models that represent the geometry at micro-level for high volume fraction. A method of generating three dimensional, random fibrous realisations is presented which is based on the Random Sequential Absorption (RSA) algorithm. A modified RSA was used in order to overcome the “jamming problem”. The jamming problem can be described as the difference between the analytical predictions on V_f and the achievable V_f from the developed algorithm. Analytical predictions on the maximum achievable V_f were proposed by (Evans, 1986,) by implementing a linear function of AR. A modified version of RSA algorithms was used in order to overcome the jamming limit. The modification regards the ability of the algorithm to count for fibre kinks or fibre local bending. By implementing this technique (Pan, 2008) were able to achieve V_f up to 35.1% using inclusions with AR=20. Fibres were simulated as sphere-cylinders, which are cylinders with a hemisphere attached to both ends. By using this shape, stress singularities in the model were minimized. The developed RVE consisted of two kinds of sub-layers, the fibre reach sub-layer and the matrix reach sub-layer. Both layers are repeated six times and seven times respectively through thickness in order to build the RVE. The developed microstructure can be approached as macroscopically transversely isotropic behaviour due to the in-plane random orientation. Fibre length was assumed constant and fibre cross section or bundle cross section was approached as a dodecagonal shape. The size of the RVE was chosen based on a literature approach of scales as $L/l = 2$, where L represents the length of the RVE and l represents the length of the fibres. Effective stiffness properties were calculated using a homogenisation procedure based on six independent loading conditions. Results from the developed numerical model were compared with analytical approximations from the Halpin-Tsai equation.

In a subsequent paper the author (Pan, 2008) investigates the effect of interaction between fibres by considering two cases of models consisting of overcrossing fibres. The first model contains two overcrossing fibres or a single interaction pair and the second model contains twelve fibres or twenty interaction points. The interaction was measured in terms of stress concentration and the stress concentration was defined as the ratio of local stress over the average stress. The phenomenon of fibre overcrossing was studied as a function of two variables. The first was the distance between the fibres, and the second was orientation between them by changing the in-plane and out of plane angle. The effect of those two variables and the general effect of crossover fibres in the stiffness of the composite are evaluated for the through thickness direction C_{33} . The study concludes that the stress concentration factor for the case of a single interaction pair increases with decreasing the distance between the fibres, and also C_{33} slightly increases by decreasing the fibre’s distance. In the case of twenty interaction pairs, stress concentration was generally higher compared with the single interaction pair and shows the same dependency with fibre distance, C_{33} also increased while the distance was decreasing.

A similar approach was performed by (Iorga, 2008). An RSA-based periodic microstructure was analysed through FEA. Results for effective stiffness were compared with a windowing approach method named Laminar Random Strand method (LRSM) and analytical predictions of the Halpin-Tsai model. Two random angles (in plane Θ and out of plane Φ) and a random point in space were seeded to the RSA in order to produce a non-overlapping periodic microstructure of random short fibre composite. Two different cases of the same material were studied. A random fibre composite

with $V_f = 15.13\%$, $AR=10$ and Φ restricted in the range of $\pm 10^\circ$. The second case was the same material but now $V_f = 20\%$, $AR=20$ and Φ restricted in the range of $\pm 5^\circ$. For both cases the in-plane angle has no restrictions, so it was free to vary in the interval $[0^\circ - 360^\circ]$. The effective stiffness tensor was calculated based on a volume average scheme, of stresses and strains field as a result of the loading conditions. Numerical models were subjected to uniform kinematic boundary conditions for six static problems which corresponded to the six independent loading cases. Results from the random microstructure were compared with orientation averaged results, from aligned fibres and a relative error between the two different methods was calculated.

LRS is a method proposed by (Ionita, 2006) and is a windowing approach able to rapidly evaluate a large number of fibre arrangements for in-plane orientation. Calculations of effective properties are based on the classical laminate theory. The method is able to consider the effect of fibre kinks but not any out of plane orientation of the fibres. The method has the ability to measure the statistical inhomogeneity in the material by information derived from local region. A comparison between the LRS method and the direct finite element approach was performed and also results for the statistical homogeneity are presented as a function of the window size.

(Berger, 2007) investigate the elastic constants of short fibre composite materials using a three dimensional RVE. Fibres were simulated as cylinders for the case of random orientation and aligned fibres. The periodic microstructure was created using the RSA method with some modifications in order to avoid local areas with low quality mesh or element shape. These constraints lead to higher quality mesh, less distorted elements, and as a consequence more accurate results. The author discusses the limitation of V_f by using the RSA method for fibres with constant length ($V_f = 25\%$) and fibres with different lengths. Results are presented as a function of V_f from 10% up to 40% with a step of 10%. For every case of V_f five different samples of RVE were generated and the average mean of the effective property was calculated. By applying six particular loading cases, the nine material constants $[E_{11}, E_{22}, E_{33}, G_{12}, G_{13}, G_{23}, \nu_{12}, \nu_{13}, \nu_{23}]$ were calculated. In the case of random orientation, the material is assumed to be statistically isotropic and the mean value for E, G and ν was calculated. Results from the numerical models were compared with various micromechanical schemes. The macroscopic isotropic behaviour of the randomly oriented composite is evaluated by a direct comparison of the Young modulus in every main direction as a function of V_f . The effect of fibre orientation is also investigated by comparing the Young modulus in the three main directions for aligned and randomly oriented fibres.

(Gitman, 2007) studied the existence and the size effect of RVE for a three phase composite material. The composite under investigation consists of circular inclusions with random diameter (between 2.5mm - 5.0mm). The third phase is an Inter-phasiaal Transition Zone (ITZ) which surrounds the circular inclusion and is attached to the matrix. The developed RVEs experienced no wall-effect and geometric periodicity. The term wall-effect is understood as the ability of the inclusions to penetrate through the borders of the RVE. Four different RVE sizes were considered in order to study the size effect. For all the cases three different V_f were developed, $V_f = [30\%, 45\%, 60\%]$ and for the combination of different size and different V_f , five different realisations were generated. Realisations refer to different samples which consist of the same V_f and RVE size but different stochastic parameters - like the inclusion's position and size. The purpose of developing five realisations is to evaluate the influence of stochastic parameters at the macroscopic response.

A gradient damage model was used to describe the damage initiation in the material and elastic properties degradation during the test. The crack initiation occurs in the inter-phasic zone, because ITZ has the lowest crack initiation strain compared with matrix and inclusions. Periodic boundary conditions were implemented by using a penalty method for the uniaxial tension test. Results of the material behaviour are presented in the form of stress-strain curve for the elastic, the hardening and the softening region of the material. The elastic region is understood as the linear part of the stress-strain curve. The hardening region is the non-linear region before the peak of the curve and the softening region is the region after the peak, across which the material exhibits a softening behaviour. The existence of RVE is discussed through two different perspectives: the statistical and the deterministic approach. According to the statistical approach, an RVE exists if the mathematical expectation and the standard deviation of an up-scale property (such as stiffness) must converge to a specific value while RVE size is increasing. The deterministic approach involves the value of dissipated energy plotted for increasing values of RVE size. Dissipated energy is measured as the area under the stress-strain curve. Regarding the existence of RVE in the three different regions the author underlines the lack of RVE existence on the softening region. The author investigates the deviation of a single tested sample from the mean of its class of realisations, by implementing a chi-square test-criterion. The criterion calculates the effect of deviation for accuracy of 95% with two Degrees of Freedom (DoF). It was reported that for the hardening region a larger size of RVE was required when compared with the linear elastic region of the stress-strain curve where smaller size of RVE can be used.

As it was explained by (Kari, 2007) the main advantage of analysing SFRC using numerical models is the ability of computational models to approach, to a satisfactory degree, the real micro-structure of the material. The author suggests a method of overcoming the jamming problem and evaluates the effective mechanical properties of a Randomly Distributed Short Fibre Composite (RDSFC), for relatively high V_f . Two different types of composite were created in respect of the orientation: Randomly Distributed Short Fibres (RDSF) and Transversely Random Distributed Fibres (TRDF). TRDF models consist of aligned fibres - all the fibres are oriented towards one direction. Both micro-structures were created using a modified RSA algorithm. Modification regards the distance between the cylinders and the distance between the surface of the cylinder and the surface of the RVE. The second modification protects the model from errors introduced through bad mesh quality. A final modification is the deposit of fibres in a descend manner in order to achieve higher V_f .

The author points out the limitation of the developed algorithm to reach higher V_f with . identical size of inclusions. The suggested solution comes through a modification of the RSA algorithm, in order to deposit first high AR fibres, and once it reaches the jamming limit, to reduce the AR and to continue with the process. By using this technique the algorithm was able to generate 3D RVE with a V_f of 40%. For the two different types of composite, various models were created in order to evaluate the influence of V_f .

The influence of the RVE size on the macroscopic response of the Young modulus is presented for all major directions, with the relative error measured as the standard deviation. Results for E_1, E_2, E_3, G, ν regarding the RDSF composite are presented for various V_f from 10%-40% and are compared with predictions from analytical micromechanical models. A comparison between E_1, E_2, E_3 is used as a measure of the isotropic behaviour of the RDSF composite, with variations less than 1.5%. Finally, a comparison between the RDSF and TRDSF is performed, indicating the

influence of fibre orientation. The author concludes that for RDSF there is no significant influence by the AR, in contrast with the TRDSF material in which effective properties improved considerably with respect to AR increase. This is also reported for the randomly distributed case, V_f . Orientation appears to be a more dominant parameter when compared with AR.

(Wang, 2011) studied mechanical properties and developed a damage model for random composite materials. Mechanical properties and fracture properties were studied by performing computational experiments under the concept of RVE. For that purpose a 2D RVE was developed.

The packing problem of randomly distributed inclusions was solved by developing an algorithm able to approach the solution in two distinct steps. Through the first step named “criss-crossing”, the algorithm begins by placing circular inclusions in a periodic manner with constant distance between them in both X and Y coordinates. While the algorithm is still working on the first step, inclusions that belong to every even row or every odd column experience a move on X and Y axes respectively. During the second step, a zoom in approach is performed. The algorithm considers the neighbourhood of fibres close to each other. A concentric circle is then calculated for every fibre in the neighbourhood. The points where the concentric circle of an inclusion meets the concentric circle of another inclusion in the neighbourhood define the space where the inclusion can randomly move or rotate. The second step in the algorithm is essential in order to obtain randomly distributed inclusions.

That both materials matrix and inclusions are linear, transversely isotropic and perfect bonding was assumed between matrix and inclusions. Damage initiation and propagation was studied based on the maximum principal stress theory. Stresses were measured in every integration point and compared with a stress value calculated by the maximum principal stress theory. If the measured value exceeds the specific maximum principal stress, material stiffness is reduced locally in order to simulate damage initiation. Once the damage is detected, the elastic modulus is degraded by a factor of 10^{-5} in order to simulate the reduction of stiffness due to crack existence. Measurements of stress on the integration points took place by implementing a user-subroutine GETVRM and the damage criterion was implemented through the USDFLD subroutine. Results indicate a linear relation of load in respect to displacement. Agreement between computational predictions and experimental data of ultimate load was observed.

1.3.1 Thermal and thermo-mechanical properties

Apart from the mechanical properties of a composite material, of which a proper calculation is necessary for a complete engineering design, thermal and thermo-mechanical properties are equally very crucial parameters once an engineer designs a new material or extends the usage of an existing material. Especially in the case of polymeric composite materials, special care is needed once the polymer is thermoplastic, with mechanical properties strongly depending on the current temperature situation and also on the previews of thermal load.

An extensive article written by (Schapery, 1968) in 1968 studied different approximations of analytically calculating the coefficient of thermal expansion for a composite material in various cases. A further discussion on the manner of answering the volumetric and the linear coefficient of thermal expansion problem is presented. Through the paper, a new method for calculating upper and lower bounds on thermal expansion coefficients of isotropic and anisotropic composites can be found. The developed method is a combination of the complimentary and potential energy principles, with a procedure of minimizing the difference between upper and lower bounds. The author approaches solutions analytically, between the upper and lower bounds for the CTE, based on the expression of Gibb's free energy, implementing the elastic constants of the constituents of the composite, such as bulk modulus, compliance tensor and stiffness tensor. Through the study, the author discriminates a few cases in which a more exact approach, instead of upper and lower bound, is possible. For those cases the bounds coincide or are very close to each other.

In the case of a composite material in which the bulk modulus is equal to the lower bound, it represents a case of uniform stress distribution, in which an exact solution is possible through the "Rule of Mixture" (RoM). In the case in which strain in the composite is practically uniform, so the bulk modulus is close with the upper bound, the Turner prediction can be used to derive an exact solution. The case of a composite material consisting of different phases with the same Poisson ratio is another one case in which exact solution can be found.

(Hatta, 1985) published an article presenting a new analytical approach to study the problem of thermal conductivity for SFRP, for steady state heat conduction problems. The roots of the proposed approach are derived from the Equivalent Inclusion Method which is an analogous approach to the Eshelby EIM for the elasticity frame. Through the proposed method, a closed form solution can be achieved, with the formulation being based on a simple algebraic operation. By considering two types of fibre orientation distributions (uniform distribution and cosine type distribution), the author compares results of effective thermal conductivity using different analytical models as a function of AR, V_f and orientation angle. Results show that thermal conductivity increases in relation to V_f and decreases in relation to the orientation angle. Results of thermal conductivity as a function of AR show that there is a significant dependency between conductivity and AR for $AR \leq 50$.

(Chen, 1996) published an article in which they studied the thermal conductivity of a composite material consisting of mis-oriented short fibres of carbon or glass, dispersed in a poly-(pheylene sulfide) matrix. They made use of Kacir's single parameter exponential function in order to characterize the orientation distribution function of mis-oriented fibres.

Authors investigate in an analytical manner the thermal conductivity response of the composite material for the steady state condition. The analytical formulation is based on the mean field approach of Mori and Tanaka in conjunction with Eshelby's Equivalent Inclusion method. They studied thermal conductivity as a function of AR, V_f and fibre orientation. Throughout the analytical calculations, the interaction of fibres is considered by implementing the mean stress concept of Mori and Tanaka. The authors based their calculations on Taya and Mura's work by making use of the analogous thermal micro-parameters as those used by Eshelby's equivalent inclusion method. Terms like perturbed heat flux are introduced into the calculation to represent the analogous perturbed strain for the mechanical loading problem. In addition, the concept of inhomogeneities, the equivalent transformation temperature and the perturbed temperature gradient, with which they connect the Eshelby tensor were used.

By implementing a spherical coordinate system, the authors were able to create second order transformation tensors in order to consider fibres mis-orientation. The nature of the orientation distribution in the composite is mainly a result of the material forming, but also of the mould cavity, the melt behaviour of the polymer with the fibres or the geometry of the fibres. The orientation density function, for the fibre's orientation, is an exponential expression proposed by Kacir et al using a single parameter which takes values depending on the degree of fibre orientation.

The conductivity of the material is strongly dependant on the degree of inhomogeneity between fibres and matrix, on the conductivity of the constituents, on the AR, the V_f , and on the degree of orientation. Results from the analytical model are compared with experiments from a former publication of the author and results are found to have an acceptable agreement with less than 20% deviation. The author considers the skin core effect, in which during the process of forming the composite, all the fibres that are close to the mould walls experience a shear stress which forces them to have a higher degree of orientation when compared with the fibres in the middle of the composite, which do not experience the shear stress of the mould's wall and as a result end up with very low degree of orientation.

Results show an enhancement of the conductivity of the polymeric matrix, especially in the case of carbon fibres. Longitudinal thermal conductivity seems to have a strong dependency on AR, (AR<40), in contrast with the transverse thermal conductivity, which seems to be unaffected in respect of AR. The same behaviour was observed in the skin and in the core of the material. For short carbon fibre reinforced composites, the range of AR=15-20 shows a significant increase for the longitudinal conductivity. For both longitudinal and transverse directions of thermal conductivity, the dependency of the property with AR becomes saturated for AR=50.

Dependency of thermal conductivity with V_f was also studied for the range of $V_f = 0.1, 0.2, 0.3, 0.4$ as a function of the orientation parameter λ . Longitudinal conductivity increases with the increase of V_f and also increases for $\lambda \leq 10$. The opposite behaviour was observed for the transverse conductivity in respect of the orientation parameter λ . As long as λ increased, transverse conductivity also decreased. The effect became saturated above $\lambda = 10$. Considering that the author emphasized the importance of choosing the most appropriate process technique. The article concludes by underlining the strong enhancement on thermal conductivity caused by the two manufacturing dependant parameters such as AR and fibre orientation.

(Hua, 2013) study the thermo-mechanical behaviour of a metal matrix composite. Specifically, they investigate properties such as effective stiffness, the Poisson ratio and the Coefficient of Thermal Expansion for aluminium 2080 reinforced with SiC particles. The thermo-mechanical properties were investigated as a function of the constituent's stiffness, volume fraction, aspect ratio and orientation.

Analysis of the material and results were obtained by the Mori-Tanaka model and FE simulations. Both cases were compared with experimental results. The FE model was built under the concept of a representative volume element, by using an RSA to solve the packing problem and randomly disperse thirty inclusions of a sphero-cylinder shape in a square, without any intersection, and by sharing the same probability of orientation angle. The stress and strain field was obtained by applying periodic boundary conditions, through a uniform strain distribution of 2%. For the calculation of CTE, a temperature rise of 100 °C is implied. Results show a very good agreement between the MT model predictions and FE calculations, but both deviate from experimental results. This may be a result of the numerical simplification as the constant aspect ratio, the idealized orientation, or the perfect interface between fibre and matrix.

Based on the very good agreement between results from MT and FE, the authors compare the computational time needed for both cases and emphasise that the MT scheme is, without a comparison, a much faster method. In order to investigate the influence of particle stiffness, the author compares the effective properties with respect to volume fraction, for the stiffness of various particles. Results show that there is higher sensitivity for $V_f > 10\%$ with the maximum increase on growth rate existing at $V_f = 30\%$ and being equal to 36.8%.

The coefficient of thermal expansion and the Poisson ratio decrease with respect to the volume fraction and particle stiffness. The influence of AR was also investigated from AR=5-20 with a step of 5. Results show saturation on the AR dependency for $AR > 10$. The effect is known as the "classical shear lag" behaviour which describes the load transfer efficiency between phases as a function of the degree of inhomogeneity. The effect of particles orientation was studied through the Mori-Tanaka scheme. Results show that the effective modulus in the longitudinal direction was strongly dependent on the particle orientation, in contrast with the weak dependency of the transverse direction and particle orientation. Effective Poisson ratio and CTE decrease with respect to V_f .

(Annapragada, 2007) study the thermo-mechanical properties of an energetic composite material consisting of particles with various diameters. The author investigates the elastic properties of the energetic material using the FE method and the thermal properties using the finite volume method (FVM) under the concept of RVE. Effective properties such as the Young modulus heat conductivity and specific heat were examined for 2D RVE and 3D RVE. The author underlines the computational cost of a 3D simulation in comparison with the 2D.

For the 2D simulations, two different methods were used. The first method implies the analysis of a 2D RVE with a constant V_f . The second method uses slides of a 3D structure, along a different cross section. Effective properties are obtained by arithmetic averaging over results for all the sliced 2D RVEs. Effective mechanical properties, Young modulus and Poisson ratio were obtained by applying kinematic uniform boundary conditions, in a way that boundary nodes displacement paralleled to the boundary faces where couple and kinematic degrees of freedom were restricted.

A homogenization process of calculating the average stress and strain leads to the calculation of the effective Young modulus. Thermal conductivity was calculated by imposing a temperature difference on the boundaries of RVE and by measuring the total heat flux of the material. The constitutive equation of a steady state thermal conductivity was used in order to calculate the thermal conductivity. Effective specific heat was obtained through a two-step procedure. First, a heat flux is applied on the left side of RVE for a specific time Δt while the remaining sides are insulated. During the second step, adiabatic boundary conditions are applied to all walls and the system is allowed to reach an equilibrium temperature and the specific heat is calculated.

The composite material consists of estane matrix and glass particles in a weight fraction of 21% and 59%. The matrix was modelled as an isotropic material with temperature and strain rate dependant properties. Glass particles were also isotropic without any dependency on temperature or strain rate. The author also studied the effect of RVE's size. Five different RVE sizes were developed and convergence was obtained if a requirement of deviation was satisfied. Results show that thermal conductivity converges faster in comparison with specific heat, or in other words, specific heat shows higher dependency on the size of RVE when compared with thermal conductivity. A comparison between 2D and 3D models shows that results follow the same trend without significant deviation; however, the computational cost for 3D simulation is much higher.

(Berger, 2007) investigate the thermo-mechanical properties of unidirectional fibrous composite material and consider the existence of an interphase between matrix and fibres. A periodic unit cell of a three phase composite was developed with cylindrical fibres in a square packing array and coated with an interphase material. The bonding on the interphase between fibre and matrix was assumed to be perfect and all the constituents behaved isotropic and linear elastic.

Results are obtained by applying periodic boundary conditions on the surface of the unit cell and by coupling the kinematic degrees of freedom for all the nodal pairs opposite each other. For each virtual experiment, boundary conditions were imposed in such a way that only one macroscopic strain was not equal to zero each time, and as a result, the corresponding coefficients of effective stiffness were calculated. Volume average stresses and strains were calculated using a summation for the local values of stress, strain and volume.

By obtaining the coefficients of effective stiffness, a calculation of the coefficient of thermal expansion is possible. In order to calculate CTE the boundary conditions imply a kinematic restriction on the boundaries of the unit cell and a temperature difference between the two sides. Due to the temperature differences and the kinematic restriction on the boundary on the unit cell, a stress field will be induced into the system. With average stress, elastic stiffness and temperature difference known, the calculation of CTE can be performed. Results show that CTE decrease linearly with respect to V_f , and that the FEM has a perfect agreement with the asymptotic homogenisation method.

(Annapragada, 2006) study the effective thermal conductivity of particulate composite through numerical experiments. For the specific study, the material used for inclusions has higher thermal conductivity, and is used in order to improve the thermal conductivity of the composite material. Calculations of the effective thermal conductivity are based on the concept of RVE.

A random packing algorithm was developed for 2D and 3D simulations. The algorithm was able to ensure geometric periodicity and a random distribution of non-intersected circular or spherical inclusions. A temperature difference between two opposite faces while the rest of the faces of the RVE are insulated. The method of finite volume was used and the total heat flux was calculated. Results for the effective thermal conductivity were obtained through a method able to capture the effect of particle concentration, the degree of inhomogeneity and the particle population in the RVE.

Results for the 2D case are presented for low V_f and the effective thermal conductivity of the particulate composite. A linear relation with V_f and a relatively good agreement with the predictions of the Maxwell model were observed. For higher $V_f \leq 50\%$ results show a larger deviation from the predictions of the Maxwell model and are closer to the harmonic mean calculation. The same linear relation between effective thermal conductivity and V_f was detected. As reported in the paper, the distribution of effective thermal conductivity for values of $V_f = 0 - 40\%$ over the degree of inhomogeneity shows a saturation on the contribution of inclusions for values $K_{inh} \geq 20$. In contrast, by increasing the volume fraction of the composite, effective thermal conductivity always increases, with the major variation occurring between $V_f = 20 - 40\%$.

1.4 Experimental approach

Apart from the analytical and numerical approach on the characterization of a composite material, the most reliable way to obtain data most of the time is an experiment. Even if the cost of performing a virtual and a real experiment is not comparable, the need for experimental results is more than obvious, at least during the initial stage of numerical model development.

An extended study on mechanical and thermal properties of short fibre composite materials has been completed by (Thomason, 1996). In the first publication of this series, the author investigates the influence of fibre length and volume fraction of a composite consisting of short glass fibres embedded in a polypropylene matrix. Results are presented for the cases of different melt-flow index, molecular weight of the matrix and fibre-sizing.

Tensile properties were determined using an Instron 1195 according to ISO/R527-1996(E) and according to ISO/178-1975(E) for the flexural modulus. Experiments for tensile and flexural modulus were executed for a range of fibre lengths, sized fibres and a matrix with two different MFI and M_n . Results show that stiffness increases almost linearly with respect to fibre concentration $W_f \leq 60\%$. A similar dependency between fibre length and stiffness was observed, with the exception of very fine inclusions. Samples with a concentration of 60% also show a lower stiffness than the general trend. This may occur due to fibre packing considerations, and relatively long fibres, due to the high concentration, tend to orient out of plane. It was also observed that samples containing sized-fibres show no significant improvement in stiffness. However, the effect of sizing was clearly observed for the ultimate properties.

The molecular weight and MFI of polypropylene were also examined. Results show no sensitivity of stiffness on molecular weight and MFI changes for the specific laminates. The shear lag model developed by Cox is used for theoretical comparison. A good agreement between theoretical and

experimental results was observed, for fibre length $f_l \geq 0.5\text{mm}$ and $W_f = 40\%$. The author reports that deviation from the theoretical predictions may occur due to several factors affecting the behaviour of the material such as: the out of plane orientation, an increase in cross-over points between fibres, and also an increase of void content. All the aforementioned factors are related to the problem of packing a high volume fraction of inclusions with a high aspect ratio.

Experimental measurements of the void content show a significant increase for high fibre content $W_f = 60\%$. A recalculation of stiffness using the RoM, including the appropriate correction on the volume fraction, due to void content, for high volume fraction samples, shows a good agreement with experimental results. The author concludes by underling the linear increase of stiffness as a function of weight fraction for $W_f \leq 40\%$. Above that value, various mechanisms caused by the packing arrangement are activated, and the increase of stiffness is less. It was also observed that there is an independency of stiffness with fibre length for $f_l > 0.5\text{mm}$, however it must be emphasised that fibre length is directly related with the packing problem.

In a subsequent work (Thomason, 1996) investigate the thermal properties of short fibre glass polypropylene composite. A heat deflection temperature test and DMA test were performed in order to obtain the storage and loss modulus and also the heat deflection temperature. Results for HDT are plotted as a function of fibre content for $W_f \leq 40\%$ for various fibre lengths. According to the results, if a composite contains high levels of fibres with high AR, a plateau level of HDT close to the melting point of the matrix is possible, even for low fibre content. The author underlines this as evidence of improvement on the creep resistance due to long fibres or high AR.

The DMA test was also performed in order to study the ability of a material to retain stiffness at an elevated temperature, specifically for high value of HDT. Flexural storage modulus was obtained through the DMA test and is presented as a function of temperature for various fibre concentrations for a fixed fibre length. Reduction of stiffness is clear and can be separated in two steps: reduction at the glass transition temperature and further reduction at the melting temperature of polypropylene. Results also claimed that for high temperature, elevated stiffness can be obtained with high fibre content.

A comparison of DMA results with flexural test show a deviation of stiffness for temperatures of 23°C and 100°C and an agreement with results obtained from DMA at 23°C. Results of the flexural storage modulus as a function of temperature for various fibres' length show a significant increase of the modulus with respect to fibre's length and indicate the important role of long fibres on applications which involve elevated ambient temperature. Fibre's length was examined in the interval of 0.09-12mm.

The glass transition temperature T_g increases with respect to the fibre length and a comparison of experimental data with theoretical predictions of the Cox model shows good agreement. It was also observed during the DMA tests that samples experience the so-called lofting phenomenon for temperature above the polypropylene melting temperature. The phenomenon occurs because during the manufacturing process, the out of plain fibres are compressed and held together by the polymer. Once the temperature is close to the melting temperature, fibres may straighten out and they may return to their original thickness. The phenomenon was studied in more detail and the TMA test shows a steep increase in thickness once the temperature is close or above the

polypropylene melting temperature. The dependency of loft with weight fraction and fibre length was also examined. Results indicate that the phenomenon is more obvious for weight fraction slightly above 20%. Below that value, loft seems to be independent of fibre length, for values $f_L = 3 - 12\text{mm}$. However, for higher fibre content, the phenomenon is dominant and shows a strong dependency on fibre length.

Through the TMA test, the in-plane and out-of-plane linear coefficient of thermal expansion were calculated. Results show that both LCTE were relatively insensitive with respect to fibre length, but in contrast, a strong dependency was observed in respect to fibre concentration. The test was performed for temperatures between -20°C to 100°C . For the whole range of temperatures, in-plane LCTE decrease in relation to the fibre concentration. A closer look at the experimental data shows that LCTE can be approached as a constant for fibre content between 10%-40%. Fibre contents below or above this interval exhibit a strong dependency on temperature. Out-of-plane LCTE exhibits a complex behaviour with a peak between fibre content of 20%-30%.

A comparison of experimental data with theoretical predictions shows an excellent match for the in-plane LCTE. Out of plane LCTE was compared with the Schapery model and with an improved model proposed by the author. Results show a deviation from Schapery's model and a good agreement with the proposed model. Concluding, the author underlines the effect of void content on the deviation of theoretical models and emphasises that good correlation of experimental data and theoretical predictions occurs only when the effect of void is considered in the calculations.

In the third part of the studies, regarding the influence of fibre length and concentration on properties of glass fibre and polypropylene composite, (Thomason, 1996) investigate the strength and strain at failure of short fibre composites. Two series of samples were prepared with variation on fibre content, fibre length, MFI and molecular weight. Tensile and flexural strain at failure were examined in respect to fibre content for fibre length values between 0.1-12mm.

It is clear from the experimental data that increasing the fibre content results in lowering strain at failure. This behaviour may result from the increase of local stress concentration points at the boundaries of a fibre. High stresses at the end of a fibre may lead to the matrix cracking if the surrounding material cannot support the load. By increasing fibre content, the number of concentration points increase and the material fails within lower strains. A contribution to this phenomenon is due to the fact that longer fibres have the ability to transfer-bear higher stresses. In that case, stress concentration will be higher and failure may occur within a lower strain rate. Evidence of a dependency between fibre length and failure strain was not clear.

According to the flexural test, results seem to converge for high fibre length, to a specific value of failure strain, almost for every fibre's content. Ultimate strength for the tensile and flexural tests was plotted as a function of fibre concentration and fibre length. Results for tensile strength with respect to fibre content exhibit a linear behaviour. Tensile strength increases linearly with respect to fibre concentration for $W_f \leq 60\%$. It was also observed that sized fibres show a higher level of tensile strength. A similar trend was observed for the flexural test. A linear increase of flexural strength was observed for fibre content up to 30%. For higher values of fibre content, flexural strength exhibits a plateau. When tensile and flexural strength is plotted over fibre length, it can be observed that for very short fibres, the strength of the composite tends towards the matrix strength. As fibre length increase, strength increases, and they experience saturation for lengths above 3mm.

Samples with higher molecular weight matrix were tested and compared with the previous experiments. The comparison shows that there is no sensitivity of the tensile strength to matrix molecular weight. It was also observed that for tensile strength, increasing the fibre content for small fibre length leads to a lower tensile strength. A comparison of tensile strength with theoretical predictions of the Kelly-Tyson model indicated a deviation on the predictions of elastic critical fibre length. According to the theoretical predictions, a much greater value of critical length is needed in order to obtain 90% of the maximum attainable strength. A comparison of tensile strength predictions of the Kelly-Tyson model with experimental results shows a large scatter. This deviation may be a result of the simplifications of the theoretical model, such as: fibre orientation, voids and distribution of fibre length. The author introduces a correction factor in the equation to consider the orientation effect and a modification of the ineffective fibre length. After the introduction of the correction factor, results from the modified Kelly-Tyson model show an excellent agreement with experimental data. Concluding, the author emphasises that the tensile strength of short fibre composites is mainly dominated by the fibres with the same orientation as the loading direction. A failure of those fibres will lead to material failure.

With their subsequent work, (Thomason, 2002) studied the influence of fibre length and concentration for injection moulded long and short glass fibres embedded in a polypropylene matrix. The author aims to explain the structure-processing performance relationship of various forms of glass fibre polypropylene composites. Long discontinuous fibre composites are regularly manufactured through the pultrusion process using continuous glass fibres. On the other hand, short glass fibre composites are mainly produced through the extrusion compounding of chopped glass fibres. For the specific experiments, the diameters of long and short fibres didn't vary. Long fibres were between $16 - 20\mu\text{m}$ and short fibres between $14 - 17\mu\text{m}$.

Two other variables of the manufacturing process of the two materials involved in this study were viscosity and temperature. Long fibres polypropylene composites require low viscosity resin, achieved by high MFI and elevated processing temperatures. Short fibre polypropylene was manufactured with lower MFI and lower processing temperatures. A coupling agent was added in the composite in order to improve the adhesive conditions between fibres and matrix.

Experiments were performed in ambient temperature of 23°C with 50% relative humidity, and for three different parameters combined: LF19, SF19 and SF14 which stand for long fibres with a diameter of $19\mu\text{m}$ and short fibres with a diameter of 19 and $14\mu\text{m}$. Results were obtained for flexural tests, the Izod and modified Charpy impact test, and also the multi-axial impact test. Fibre length distribution and fibre diameter were measured by an image process analysis and optical microscopy. The dependency of fibre length reduction with respect to the manufacturing process and the initial fibre length was studied.

Results of fibre length are presented with respect to fibre content. Results show a general reduction of the fibre length in respect to weight fraction. It was also observed that long fibre composite seems to be less sensitive to the fibre's length reduction, in comparison with short fibre composite. This may be due to the different compound processes of the long fibres and short fibres. Results from the tensile test indicate a linear relation between Young's modulus and weight fraction. Results show no significant improvement for long fibres and no important changes for smaller diameter of fibres (increasing the aspect ratio). Again, it has been clear that Young's modulus is firstly affected by

the elastic properties of the constituents and then by the orientation properties of fibres, and that it is less sensitive to fibre length. A reason that the effect of fibre length does not contribute to the increase of Young's modulus may be that it is directly related to the orientation of fibres. Longer fibers give slightly lower orientation and the effects cancel each other out.

A similar trend was observed for flexural modulus. Results for tensile strength also show an increase with fibre content. Long fibre composite has the higher tensile strength. It can be expressed as a linear function of weight fraction with a threshold between 40-50%. Regarding short fibre samples, SF14 with a smaller diameter shows higher tensile strength. Results for flexural strength show higher absolute values when compared with tensile strength, but generally the same behaviour was observed. Tensile elongation decreases with respect to the fibre content, indicating a more brittle response in higher weight fractions. A steep drop was observed with the addition of fibres and then a linear decrease of up to 50% weight fraction. Long fibres show a higher tensile performance in general, however regarding short fibres, samples with smaller diameter, show higher tensile performance.

Notched Izod and notched Charpy impact test were performed. Results are plotted over fibre content and have a similar trend for both tests. The comparison between long and short fibres indicates higher performance by long fibres. Results for short fibres portray that fibres with higher AR perform better. An impact test for lower temperature was performed and compared with impact test results at an ambient temperature. Results show a very brittle behaviour at -40°C for short fibre samples, indicating less energy absorption capabilities when compared with the ambient temperature.

Long fibre samples seem to be unaffected by the temperature. Stress levels of the three materials were compared for strain values of 1% and 2%. Results indicate that there is an increasing difference in relative modulus as the applied strain increases. In general, long fibre composites and higher aspect ratio samples show higher stress levels. A comparison with previous experimental work by Thomason and Vluc is presented for various properties as a function of fibre length. Tensile modulus, tensile strength and impact normalized properties are compared for fibres with lengths up to 100mm. Results show that the effect of saturation exists for different fibre lengths in each property. A direct comparison of fibre length, needed to reach 90% of its property performance, shows that for tensile modulus it is 1mm, for tensile strength it is 7mm and for the impact test it is 16mm.

In a later work (Thomason, 2002) study micromechanical parameters from macro-mechanical measurements on glass fibre reinforced polypropylene. A series of E-Glass specimens with $W_f = 0, 10, 20, 30, 40\%$ were prepared and exposed to tensile and flexural load. Data for fibre length and fibre orientation were extracted by applying a high temperature ashing procedure on the specimens and a direct measurement of the fibre length. Orientation distribution was obtained by taking systematically optical micrographs across the thickness. The elliptical profile of a fibre on a cross section can provide useful information for the fibre's orientation. An average value of orientation was approximated, and based on that approximation, an orientation factor was calculated.

Two different composites are compared with and without a coupling agent. Results for tensile modulus show a linear dependency with fibre content. Increasing the volume fraction leads to a

linear increase of tensile stiffness. Results for tensile strength also indicate an increase with respect to volume fraction, but in this case the relation is not linear. It is also very clear from the plot that the coupling agent is a major contributor to the increase of tensile strength.

A similar trend was observed for the flexural strength test in which a non-linear dependency of volume fraction with flexural strength was detected and a clear enhancement effect for the specimens with a coupling agent in comparison with the specimens without a coupling agent. Tensile elongation at failure was also calculated. Results show high sensitivity for the initial addition of fibres. For values $V_f \geq 10\%$, a linear decrease with respect to volume fraction was observed. Samples containing the coupling agent exhibit higher elongation at break.

Fibre length after the injection moulding process was also examined through a range of volume fraction. Results show that fibre length decreases linearly with respect to fibre content. It must be noted that an increase in melt viscosity leads to higher bending forces on fibres during compounding or moulding. This decrease in fibre length with respect to volume fraction may be a reason for the strength properties reduction, showed with respect to volume fraction. The author also proposes a macro approach for determining the micromechanical parameters and dominating short fibre composite strength. It is clear through the process of calculating micromechanical parameters that the method is simple, inexpensive and also appears as an ideal tool for industrial product developers. By using this macro-approach and by deriving relations from a stress-strain curve of the material, values for the interphase shear strength can be obtained for the two types of composite.

Results indicate the improvement of the material's IFSS with the addition of the coupling agent, and also a degradation on IFSS with respect to fibre content. The improved stress transfer from matrix to the fibre as a result of the coupling agent has been reported by many authors. Finally, a comparison between experimental results and predictions of the macro-approach indicate a very good agreement and a serious reduction of tensile elongation in respect of the fibre content. The author concludes by underlining the significant effect of residual interfacial radial compressive stresses on the interface shear strength.

1.5 Homogenisation

An investigation of various homogenization models and of multi-phase elastic composites was carried out by (Klusemann, 2010). Six homogenization models were compared regarding the degree of inhomogeneity as a function of volume fraction. The authors introduce two new approaches, the Effective self consistent scheme (ESCS) approach and the interaction direct derivative (IDD) approach.

The authors summarize the common process of homogenization methods in two steps. Firstly, a local problem of a single inclusion has to be solved in order to obtain the local response and secondly a process of averaging the local behaviour to obtain the global response takes place. Predictions of the homogenisation approaches of Voigt, Reuss, the self-consistent scheme, the Mori Tanaka method, the Hashin and Shtrikman bounds and the Lielens method were calculated for $V_f = 0 - 1$ and for the degree of inhomogeneity $C_{inh} = 0 - 20$.

Results show that there is a bigger deviation between the predictions of various homogenization methods, as long as C_{inh} is increasing. More specifically, the author underlines the disadvantage of the MT scheme to predict accurate results for $V_f > 50\%$. This is caused by the fact that the MT method treats the matrix material as the one to have the higher concentration in the composite. For relatively small V_f , predictions for the MT scheme, the self-consistent method and the Lielens scheme coincide with each other. Results show a strong dependency between predictions of various homogenization schemes with the degree of inhomogeneity, especially for high V_f .

Results from the aforementioned homogenization schemes were compared with results from FEM simulations. FEM simulations were developed for a cubic 3D micro-structure consisting of spherical inclusions. Linear kinematic boundary conditions were applied and the effective Young modulus was calculated. A comparison with the homogenization schemes for $C_{inh} = 10$ and $V_f = 0 - 0.35$ shows an increase of the effective Young's modulus with respect to V_f and an agreement with SCS, the Lielens model and lower H-S bound. For constant $V_f = 0.3$ and $C_{inh} = 1 - 20$, the effective Young's modulus experiences a linear increase with respect to the degree of inhomogeneity, but a saturated behaviour can be observed for $C_{inh} \geq 10$.

Porosity of the same material was also calculated for $V_f = 0 - 1$, the homogenization schemes, and $V_f = 0 - 0.35$ for the numerical approach. Results show a significant reduction of the effective Young's modulus with respect to voids content. Predictions of the homogenization schemes show higher deviation for higher V_f . Concluding, the author emphasizes that the homogenization method should be checked for its behaviour in the case of a high degree of inhomogeneity.

1.6 Conclusions

Through the aforementioned presented work on the field of characterising the effective properties of short fibre reinforced composite materials, the section of dominant manufacturing parameters which affect the response of short fibre composite was initially covered. The main theoretical models developed through the years followed, and computational research on composite material characterisation was then reviewed. Finally the literature review concludes with a review of the experimental research and some homogenisation aspects.

Even if the field is well covered from all the reported aspects, lots of effort needs to be made in order to be fully and optimally covered. Regarding the manufacturing processes, a lot of optimisation need to take place in order to constrain all the dominant parameters of the manufacturing process because, as it was presented, those parameters exert a high level of influence on the macroscopic response of the material.

Analytical and semi-analytical models developed through the years provide a useful tool for material characterisation. It is a cost ineffective process which can lead to very useful conclusions about the material behaviour. The main drawback regarding implementation of analytical models for material characterisation is that simple to use models may include assumptions that deviate from the real nature of material but play a crucial role in materials behaviour. On the other hand, very complicated models may overcome this barrier of assumptions but they require the implementation of high level mathematical calculations. In any case, a good analytical model must be characterised

by its ability to predict the macroscopic behaviour of a material in a broad range of parameters, to have a clear physical meaning (including all the physical mechanisms that take place during the material's reaction), and to be as simple as possible to use.

The field of numerical-computational simulations was the last one developed when compared with the analytical modelling and the experimental characterisation of materials. This is mainly due to the delay in developing and optimising numerical methods in relation to software, and also the development and optimisation of high performance computers in order to accurately simulate materials or structures behaviour. The main barrier to numerical simulations is the computational cost needed for an appropriate numerical model and also the accurate development of the microstructure in order to capture all the phenomenon happening at a lower scale.

Experimentation is a necessary process in order to obtain the real reaction of the material without considering assumptions of the analytical models or errors and uncertainties introduced by a numerical simulation. The main drawback of experiments is the fact that some parameters cannot be fully controlled during the manufacturing processes and cannot be accurately measured during the experiment.

1.7 Aim and scope of this study

Taking all the aforementioned into consideration the objective of this thesis is to offer a new approach to the numerical modelling and characterisation of short fibre composite. The following work is based on computational modelling of short fibre composite through a Representative Volume Element for a variety of parameters that play an important role in the mechanical, thermal and thermo-mechanical effective properties of SFRC.

Of particular interest for this study is the commercially attractive composite consisting of thermoplastic polymer and chopped glass fibres. In order to approach the problem of material characterisation, an in depth knowledge of composite material micro-structure and composite material responses is needed. Considering a computational approach for material characterisation, the finite element method was used in order to derive the response of the material for various loading cases.

The direct aim of the project is to:

- Create representative microstructures of SFRC consisting of 30% fibres by volume. The developed microstructures will be used as a tool to study the macro-mechanical, thermal and thermo-mechanical effective properties.
- Fully characterise the SFRC regarding thermal mechanical and thermo-mechanical properties

- Study the influence of
 - FOD
 - FLD
 - AR
 on the effective properties.
- Study the representative size of SFRC micro-structures with high degree of inhomogeneity $C_{inh} = 60$.
- Study the influence of FOD, FLD and AR on the size of RVE.

By meeting the previous targets it will be able to create mapping between the effective properties and the optimum micromechanical parameters. This map will be a tool for designing with SFRC which will consider changes in FOD, FLD and AR in order to approach an optimum combination for the designer. It will be also possible to create a parameters/properties-size mapping regarding the influence of the aforementioned parameters (FOD, FLD, AR) and properties under study ($C_{11}, C_{22}, C_{66}, K_{11}, K_{22}, \alpha_{11}, \alpha_{22}$) with the representative size.

In order to fulfil these objectives the following actions are considered:

- Understanding the limitation and disadvantages of short fibre composite on the manufacturing process.
- Understanding how the dominant micromechanical parameters influence the performance of the material and also ways to implement those parameters into the numerical model.
- Development of microstructure able to mimic the actual packing behaviour of fibrous composite materials. The development of microstructure for numerical models plays the same role as the manufacturing process for the experimental approach. Development of the microstructure includes all the parameters under investigation.
- Creation of an algorithm able to reproduce random micro-structures, and able to consider FOD and FLD.
- In line with the previous action for uniform fibre length a study on the influence of aspect ratio on the effective properties needs to take place.
- Expose the RVE to various loading conditions. Through the following chapters mechanical, thermal and thermo-mechanical effective properties will be analysed theoretically and numerically.
- In order to consider a statistical study on the results of every UC, a set of realisations need to be created for each combination of parameters and each loading case.
- Finally a comparison of numerical results with well-developed theoretical models is used as an evaluation of the accuracy of the models.

The generic question of the study is the ability of the short fibre thermoplastic material to fulfil several structural or semi-structural applications. The individual questions of the study can be summarised as:

- What are the effective
 - Mechanical properties (C_{11}, C_{22}, C_{66})
 - Thermal properties ($K_{11}, K_{22},$)
 - Thermo-mechanical properties ($\alpha_{11}, \alpha_{22},$)

of the developed material?
- What is the representative size of SFRC microstructures?
- How do the microstructure parameters influence the representative size of the RVE, regarding:
 - Fibre orientation distribution
 - Fibre aspect ratio
 - Fibre length distribution
- How the aforementioned parameters influence the effective properties?

1.8 Outline

Chapter 1 provides a background for the mechanical, thermal and thermo-mechanical characterisation of short fibre composite materials. The prediction of effective mechanical, thermal and thermo-mechanical properties of short fibre reinforced composites (SFRC) has been a field of study for various researchers and consists the main influence for the following chapters. Throughout this chapter different approaches that have been developed by numerous researchers through the years will be presented. The chapter begins by discussing the main aspects of the manufacturing processes of short fibre composite, which is a process introduce major factors effective the behaviour of the material. The chapter continues by addressing the major fundamental theoretical approaches on micromechanical analytical modelling. The chapter is separated into three main sections. During the first section a review of various analytical approaches in the field was presented followed by a numerical approach and experimental work. Finally, the chapter concludes with a review of the homogenisation approach.

Throughout chapter 2, various aspects of mechanical and thermal characterization of materials are discussed. The concept of eigen-strains is presented and very basic definitions of homogeneous and inhomogeneous media are given. The micromechanical definitions of inclusion and inhomogeneity are presented, as well as the assumption that follows each degree of homogeneity. The general formulation of Hooke's law is further discussed and the influence of the material's symmetry on the material's stiffness tensor is presented. An additional analysis of the parameter's influence on the macroscopic behaviour of short fibre composite follows. The following section presents analyses of various modelling strategies. The advantages and disadvantages of various computational micromechanical approaches are discussed in a subsequent section. The chapter concludes with an analysis and discussion about various micromechanical analytical models. The main assumptions of micromechanical models are presented and compared. In addition, a discussion of the micromechanical parameters that each model considers was performed and the influence of those

parameters are further discussed. A comparison between the analytical micromechanical predictions as a function of AR takes place for all the properties under investigation.

Throughout chapter 3 the development of the numerical models is presented. Firstly the development of a packing algorithm is discussed. The main challenges of packing algorithm development are presented while at the same time solutions to overcome those problems are suggested. The main thinking behind the algorithm structure is explained, while the limitations, the advantages and the modifications of the algorithm in order to cover various cases of FO and AR follow. The main assumptions of the developed models are given, with a discussion on the potential inaccuracy these will cause. A detailed discussion of the concept of RVE takes place with various definitions and a report on the length scale assumptions and on the existence of RVE. The chapter offers a detailed description of the geometric periodicity of the UC and the inclusion's shape on a two dimensional space. The topics of fibre orientation distribution and fibre length distribution are also discussed, while the time efficiency of the packing algorithm is presented as a function of fibre orientation and fibre aspect ratio. Finally, the chapter concludes with a report on the mechanical, thermal and thermo-mechanical applied boundary conditions.

Chapter 4 consists of a report on computational homogenisation processes. Throughout the chapter a definition of homogenisation approaches is given while the main homogenisation methods are presented. An extended discussion on the formulation and on the main assumptions of each homogenisation method took place. Advantages and limitations of each method are also discussed. The requirements of using a homogenisation method are presented, while various schematic representations of the method are given. A report on the macro-homogeneity condition is given while the properties under investigation are further discussed. For all the presented homogenisation approaches the one which will be used is further explained by addressing in detail the formulation of the method in each step. Finally, the chapter concludes with a report on the representative element approach and on the implementation of the chi-square test.

Throughout chapter 5 results from the developed numerical models are presented. The chapter is separated into two sections, which refer to uniform fibre length and fibre length distribution. For both sections results are presented as a function of the parameters under investigation. Results from the chi-square test are presented first in order to clarify the representative sizes, and as a consequence, the valid results. The fifth chapter concludes with a direct comparison of the representative results with various theoretical models as a function of the aspect ratio.

Chapter 6 includes all the conclusion remarks. This chapter discusses all the results of chapter five in a qualitative and quantitative manner. Useful conclusions can be made regarding the representative size of such a material and how it is influenced by different parameters. Also the combinations of parameters that influence the representativeness of the material are under investigation. The quality of the effective property values is discussed and the importance of combining the information included in the results with the information included in the chi-square test was addressed. Finally, the chapter concludes with a discussion of the comparison of numerical results and theoretical predictions and the main reasons for any deviations.

2 Mechanical and thermal properties – characterisation of a SFRT composite

Throughout the following chapter, various aspects of mechanical and thermal characterization of materials are discussed. The concept of eigen-strains is presented and very basic definitions of homogeneous and inhomogeneous media are given. The micromechanical definitions of inclusion and inhomogeneity are presented, as well as the assumption that follows each degree of homogeneity. The general formulation of Hooke's law is further discussed and the influence of the material's symmetry on the material's stiffness tensor is presented. A further analysis of the parameters' influence on the macroscopic behaviour of short fibre composite follows. The following section presents analyses of various modelling strategies, and the advantages and disadvantages of various computational micromechanical approaches are discussed. The chapter concludes with an analysis and discussion about various micromechanical analytical models. The main assumptions of micromechanical models are presented and compared. In addition, a discussion on the micromechanical parameters that each model considers was performed and the influence of those parameters is further discussed.

2.1 Material homogeneity

Throughout the introduction and the literature review, at various instances, the reinforcing agent was referred to as inclusions. The term inclusion has a specific meaning once the scale of observation or the description of the mechanism is with respect to the micro scale. In order to accurately distinguish the differences of an inclusion with an inhomogeneity, it is crucial first to present definitions of eigen-strain and homogeneous, inhomogeneous material.

A homogenous material is anything made of matter that is uniform in composition. More specifically, a material is said to be homogeneous if the material's elastic properties are the same at all points of the body. An inhomogeneous material is any material which has elastic properties which are not the same for every point in the material.

2.1.1 Inclusion – inhomogeneity

The term eigen-strain is relatively new and is a generic name first reported in the literature by a German engineer, H. Reissner, in 1931 in a study regarding residual stresses. The concept of using the eigen-strains method for further micromechanical analyses has become more popular since 1957, when Sir Douglas Eshelby presented his work referring to an analytical solution of the stress and strain field for an ellipsoidal domain.

This work inspired a great number of scientists to apply a different approach to developing micromechanical models for material characterisation. Throughout his original work, Eshelby referred to eigen-strains as stress free transformation strains. This definition is a result of a process within the material, observed to have stress-free transformation strains. Such a process may be a phase transformation on austenitic alloy, which will lead to a strain field. However, those strains do not result through a stress field applied on the material, but are a result of phase transformation.

In a slightly different context, however with the same basic idea, Kroner introduces the term of “elastic polarisation” in order to refer to eigen-strains of a non-homogeneous poly-crystal deformation. A similar term for the use of residual stresses was 2.8 from engineers in order to describe the self-equilibrated internal stresses when they remain in materials after the manufacturing process.

In general, eigen-strain is a name for non-elastic strains which may exist due to misfit strains, initial strains, phase transformation, plastic strain or thermal expansion. The self-equilibrated internal stresses, caused by the aforementioned eigen-strains, on a body free from external force or surface constrains, are called eigenstresses. The incompatibility of eigen-strains is the reason behind the existence of eigenstresses. Generally, any type of strain which exists in a material in the absence of an applied stress field can be treated as eigen-strain. An inclusion is defined as a sub-domain where non-vanishing eigen-strains dominate, while in the rest of the domain eigen-strains are zero. The surrounding domain is called matrix. It must be emphasised that the inclusion is defined only when the elastic moduli of the subdomain/inclusion are the same with the surrounding domain/matrix. Figure 2.1 shows a bounded sub-region K of a homogeneous region L.

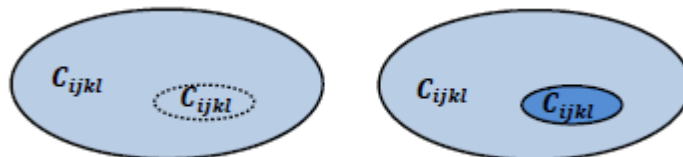


Figure 2.1 A bounded inclusion and an inhomogeneity

The subdomain is called inhomogeneity when its elastic moduli differ from the elastic moduli of the surrounding domain. As reported by (Mura, 1987), for an inhomogeneous sub-domain a uniform applied stress at infinity is not uniform at the neighbourhood of the subdomain. However, this stress disturbance due to the inhomogeneous sub-domain can be approached by an eigen-stress field caused by an inclusion, with the proper selection of eigen-strain. Further discussion takes place in the following paragraphs.

2.2 Material symmetry

For designing purposes, or during the manufacturing process, composite materials are keen to exhibit an anisotropic behaviour. It then becomes crucial to discuss the general expression of Hooke’s law. According to the structure of the material under investigation, the degree of anisotropy of the material changes and that has a reflection on Hooke’s equation. According to the theory of

elasticity, the constitutive equation relating stress and strain, under the condition of infinitesimal small strain, is stated by Hooke's law. Equation 2.1 expresses Hooke's law in a tensor form. Hooke's law is a linear equation which relates stresses to strains by a constant tensor.

$$\sigma_{ij} = C_{ijkl}\varepsilon_{kl} \quad \text{Equation 2.1}$$

For the above equation, stress and strain are second order symmetric tensors. Strain tensor is defined through differentiation of the displacement field, while the displacement field can be seen in Figure 2.2 and expressed through Equation 2.2.

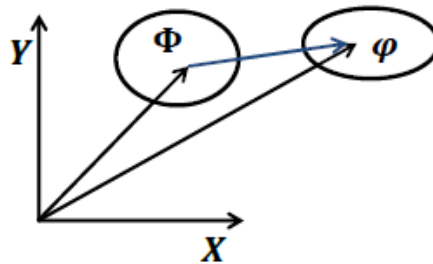


Figure 2.2 Displacement vector define between Φ and φ

$$u(x) = \varphi - \Phi \quad \text{Equation 2.2}$$

$$\varepsilon_{ij} = \frac{1}{2}(u_{i,j} + u_{j,i}) \quad \text{Equation 2.3}$$

$$\begin{bmatrix} \varepsilon_{xx} & 2\varepsilon_{xy} & 2\varepsilon_{xz} \\ 2\varepsilon_{xy} & \varepsilon_{yy} & 2\varepsilon_{yz} \\ 2\varepsilon_{xz} & 2\varepsilon_{yz} & \varepsilon_{zz} \end{bmatrix} = \begin{bmatrix} \frac{\partial u_1}{\partial x_1} & \left(\frac{\partial u_1}{\partial x_2} + \frac{\partial u_2}{\partial x_1}\right) & \left(\frac{\partial u_1}{\partial x_3} + \frac{\partial u_3}{\partial x_1}\right) \\ \left(\frac{\partial u_1}{\partial x_2} + \frac{\partial u_2}{\partial x_1}\right) & \frac{\partial u_2}{\partial x_2} & \left(\frac{\partial u_2}{\partial x_3} + \frac{\partial u_3}{\partial x_2}\right) \\ \left(\frac{\partial u_1}{\partial x_3} + \frac{\partial u_3}{\partial x_1}\right) & \left(\frac{\partial u_2}{\partial x_3} + \frac{\partial u_3}{\partial x_2}\right) & \frac{\partial u_3}{\partial x_3} \end{bmatrix} = \begin{bmatrix} \varepsilon_1 & \gamma_6 & \gamma_5 \\ \gamma_6 & \varepsilon_2 & \gamma_4 \\ \gamma_5 & \gamma_4 & \varepsilon_3 \end{bmatrix} \quad \text{Equation 2.4}$$

Under the concept of continuum mechanics, stresses can be expressed as the internal forces reacting for an infinitesimal volume of the material, when it is subjected to an external force. Stress has a physical meaning of force over the cross section area and is fully defined by a second order symmetric tensor as proposed by Cauchy as expressed in Equation 2.5.

$$\sigma_{ij} = \begin{bmatrix} \sigma_{xx} & \sigma_{xy} & \sigma_{xz} \\ \sigma_{xy} & \sigma_{yy} & \sigma_{yz} \\ \sigma_{xz} & \sigma_{yz} & \sigma_{zz} \end{bmatrix} = \begin{bmatrix} \sigma_{xx} & \tau_{xy} & \tau_{xz} \\ \tau_{xy} & \sigma_{yy} & \tau_{yz} \\ \tau_{xz} & \tau_{yz} & \sigma_{zz} \end{bmatrix} \quad \text{Equation 2.5}$$

The tensor relating linear elastic strain with stresses is known as the elastic stiffness tensor and since stress and strain are symmetric second order tensors, by definition the fourth order stiffness tensor experiences minor symmetry, Equation 2.6.

$$C_{ijkl} = C_{jikl} = C_{ijlk} = C_{jilk} \quad \text{Equation 2.6}$$

For the elastic medium under discussion, a potential function is assumed which satisfied Equation 2.7. Combining Equation 2.1 and Equation 2.7, the fourth order elastic stiffness tensor can be expressed as shown in Equation 2.8.

$$\sigma_{ij} = \frac{\partial W}{\partial \varepsilon_{ij}} \quad \text{Equation 2.7}$$

$$C_{ijkl} = \frac{\partial^2 W}{\partial \varepsilon_{ij} \partial \varepsilon_{kl}} \quad \text{Equation 2.8}$$

Since the order of differentiation is irrelevant, the existence of Equation 2.9 can be proven. What Equation 2.9 stated is called major symmetry on the elastic stiffness tensor. Due to that property of the potential function, it can be shown that the fourth order elastic tensor has a major symmetry and that the inverse tensor exists and is also symmetric.

$$C_{ijkl} = C_{jkli} = C_{klij} = C_{lijk} \quad \text{Equation 2.9}$$

The inverse tensor is known as the compliance tensor, Equation 2.10.

$$S_{ijkl} = C_{ijkl}^{-1} \quad \text{Equation 2.10}$$

In general, a fourth order tensor consists of 81 constants, however, for a fully anisotropic material, only 21 out of the 81 are independent. The remaining 60 components of an anisotropic stiffness tensor can be expressed as a function of the 21 independent constants. Due to the major symmetry of the elastic stiffness tensor, as expressed in Equation 2.9, the total number of elastic constants is reduced to 36. A fully populated elastic stiffness tensor is shown in expression 2.11 while 2.12 defines the same equation in a contracted notation form.

$$\begin{bmatrix} C_{1111} & C_{1122} & C_{1133} & C_{1112} & C_{1123} & C_{1131} & C_{1121} & C_{1132} & C_{1131} \\ C_{2211} & C_{2222} & C_{2233} & C_{2212} & C_{2223} & C_{2231} & C_{2221} & C_{2232} & C_{2231} \\ C_{3311} & C_{3322} & C_{3333} & C_{3312} & C_{3323} & C_{3331} & C_{3321} & C_{3332} & C_{3331} \\ C_{1211} & C_{1222} & C_{1233} & C_{1212} & C_{1223} & C_{1231} & C_{1221} & C_{1232} & C_{1231} \\ C_{2311} & C_{2322} & C_{2333} & C_{2312} & C_{2332} & C_{2331} & C_{2321} & C_{2332} & C_{2331} \\ C_{3111} & C_{3122} & C_{3133} & C_{3112} & C_{3132} & C_{3131} & C_{3121} & C_{3132} & C_{3131} \\ C_{2111} & C_{2122} & C_{2133} & C_{2112} & C_{2132} & C_{2131} & C_{2121} & C_{2132} & C_{2131} \\ C_{3211} & C_{3222} & C_{3233} & C_{3212} & C_{3232} & C_{3231} & C_{3221} & C_{3232} & C_{3231} \\ C_{3111} & C_{3122} & C_{3133} & C_{3112} & C_{3132} & C_{3131} & C_{3121} & C_{3132} & C_{3131} \end{bmatrix} \quad 2.11$$

Contracted notation is also known as Voigt notation and it is a way of representing a symmetric tensor by reducing its order. There are a few variants on the process of contracting indices, coming from different researchers, however the approach differs only on the certain weights attached to the selected element of the tensor.

$$\begin{bmatrix} C_{11} & C_{12} & C_{13} & C_{14} & C_{15} & C_{16} \\ C_{21} & C_{22} & C_{23} & C_{24} & C_{25} & C_{26} \\ C_{31} & C_{32} & C_{33} & C_{34} & C_{35} & C_{36} \\ C_{41} & C_{42} & C_{43} & C_{44} & C_{45} & C_{46} \\ C_{51} & C_{52} & C_{53} & C_{54} & C_{55} & C_{56} \\ C_{61} & C_{62} & C_{63} & C_{64} & C_{65} & C_{66} \end{bmatrix} \quad 2.12$$

During the following paragraph, an explanation of material symmetry will take place with a further report on the reflection of material symmetry on the elastic stiffness tensor. We assume that an elastic medium is reported with respect to two coordinate systems (x_1, x_2, x_3) and a second coordinate system (x'_1, x'_2, x'_3) , Figure 2.3. Symmetry of the two coordinate systems must be reflected on the symmetry of the material structure. Directions towards the principal axes of the two coordinate systems must have the same elastic properties; as a result, Hooke's law will be the same for the two coordinate systems.

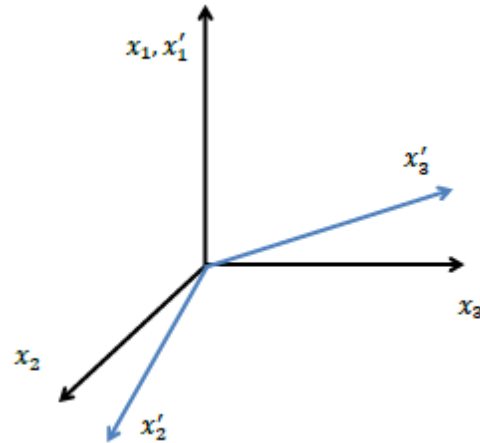


Figure 2.3 structure and material coordinate systems.

Anisotropic elastic materials exhibit a degree of symmetry within their structure, which is reflected on the symmetry of elastic properties. Due to that symmetry, many of the elements of elastic stiffness vanish or are simply related to others. Beginning with the higher degree of anisotropy, a triclinic material, as shown in Equation 2.13, has a fully populated elastic stiffness tensor with 36 constants of which 21 are independent. A solution to such a problem is not trivial and is needed for mono-crystal triclinic systems. Such a material has properties that change drastically with the orientation.

$$\begin{bmatrix} C_{11} & C_{12} & C_{13} & C_{14} & C_{15} & C_{16} \\ C_{21} & C_{22} & C_{23} & C_{24} & C_{25} & C_{26} \\ C_{31} & C_{32} & C_{33} & C_{34} & C_{35} & C_{36} \\ C_{41} & C_{42} & C_{43} & C_{44} & C_{45} & C_{46} \\ C_{51} & C_{52} & C_{53} & C_{54} & C_{55} & C_{56} \\ C_{61} & C_{62} & C_{63} & C_{64} & C_{65} & C_{66} \end{bmatrix}$$

Equation 2.13

A step higher in elastic symmetry is the monoclinic material. A monoclinic material has a plane of symmetry, and every direction in the media which is symmetric with respect to the symmetry plane, has the same properties. For a monoclinic material the elastic stiffness tensor is partially populated with 20 constants from of which 13 are independent Equation 2.14.

$$\begin{bmatrix} C_{11} & C_{12} & C_{13} & 0 & 0 & C_{16} \\ C_{21} & C_{22} & C_{23} & 0 & 0 & C_{26} \\ C_{13} & C_{23} & C_{33} & 0 & 0 & C_{36} \\ 0 & 0 & 0 & C_{44} & C_{45} & 0 \\ 0 & 0 & 0 & C_{54} & C_{55} & 0 \\ C_{16} & C_{26} & C_{36} & 0 & 0 & C_{66} \end{bmatrix}$$

Equation 2.14

A material which has two vertical planes of symmetry which impose the existence of a third vertical plane is called orthotropic. It can be shown that if two orthogonal planes of symmetry exist, there is always a third orthogonal plane of symmetry. Single ply composite materials show an orthotropic behaviour. The elastic constants of the stiffness tensor are reduced to 12, of which 9 are independent, Equation 2.15.

$$\begin{bmatrix} C_{11} & C_{12} & C_{13} & & & \\ C_{12} & C_{22} & C_{23} & & & \\ C_{13} & C_{23} & C_{33} & & & \\ & & & C_{44} & 0 & 0 \\ & & & 0 & C_{55} & 0 \\ & & & 0 & 0 & C_{66} \end{bmatrix}$$

Equation 2.15

An elastic media with an axis of elastic symmetry is called transversely isotropic material, Equation 2.16. An axis of elastic symmetry is the one with the entire vertical direction, elastic equal and every vertical on the elastic axis plane has isotropic properties. It is obvious that the transversely isotropic material experiences a higher degree of symmetry and that is reflected in the elastic stiffness tensor as 12 constants with 5 of them independent.

$$\begin{bmatrix} C_{11} & C_{12} & C_{12} & & & \\ C_{12} & C_{22} & C_{23} & & & \\ C_{12} & C_{23} & C_{22} & & & \\ & & & \frac{(C_{22} - C_{23})}{2} & & \\ & & & & C_{66} & \\ & & & & & C_{66} \end{bmatrix}$$

Equation 2.16

The highest degree of symmetry exists in isotropic materials. Elastic media in which all the directions are elastically equal is called isotropic, Equation 2.17. Isotropic material has an infinite number of

planes of symmetry, meaning that the properties are independent of the orientation. For an isotropic material the elastic stiffness tensor has 12 elements with 2 independent constants.

$$\begin{bmatrix} C_{11} & C_{12} & C_{12} & & & \\ C_{12} & C_{11} & C_{12} & & & \\ C_{12} & C_{12} & C_{11} & & & \\ & & & \frac{(C_{11} - C_{12})}{2} & & \\ & & & & \frac{(C_{11} - C_{12})}{2} & \\ & & & & & \frac{(C_{11} - C_{12})}{2} \end{bmatrix} \quad \text{Equation 2.17}$$

Throughout the previous subsection, the concept of material symmetry was discussed. The reflection of material symmetry on the elastic stiffness tensor was presented for the cases of triclinic, monoclinic, orthotropic, transversely isotropic and isotropic materials.

As reported by (Nye, 1949), this symmetry can be summarised as: for a material element and for its physical properties, every material symmetry transformation of the material element is a physical symmetry transformation of the physical property. Also, the definition of inclusion and inhomogeneity was given as defined in micromechanics. The definition of inclusions and inhomogeneity was defined through the concept of eigen-strain and eigenstresses. Clarification of the aforementioned definitions and concepts was found necessary due to the following analysis of micromechanical models and due to the assumptions on material symmetry for the numerical models.

2.3 Dominant parameters affecting the macro-mechanical behaviour of SFRC

The mechanical and thermal performance of a short fibre composite is strongly influenced by various parameters mainly originating from the properties of the constituents and the manufacturing processes. Throughout the following sub-chapter those major factors are described and analysed. Also, what influences those factors is discussed and useful conclusions about high performance of SFRC are presented. A general discussion and details on the physical and mechanical properties which are influenced by these major factors will take place during the following chapter.

A strong disadvantage of pure polymer structures is their low strength and stiffness in comparison with traditional engineering materials. On the other hand, pure polymeric structures have numerous advantages that render their implementation in structure applications necessary. In order to

overcome this difficulty and make use of the strong advantages of polymeric structures, the introduction of reinforcing inclusions is needed.

The rapid engagement of reinforcing inclusions in the polymeric structures is a result of the manufacturing process. Without huge difficulties, injection moulding methods and extrusion compounding methods were able to manufacture reinforced polymeric structures, and also the manufacturing time is much shorter compared with manufacturing continuous composite materials. High performance short fibre composite materials can be obtained if the major factors affecting their performance are satisfied. The major factors that play a critical role in determining high performance short fibre composite materials are:

- Physical and mechanical properties of fibres and matrix.
- Characteristics of fibres and matrix interface.
- Fibre length distribution or aspect ratio.
- Fibre orientation distribution and
- Volume fraction.

It is then crucial for any micromechanical analytical model to include information about those factors. However, not all the parameters have the same influence for every property under investigation. It is important then to clarify the influence of every factor for the properties under investigation.

2.3.1 **Physical and mechanical properties of fibres and matrix**

Throughout the following paragraphs some of the main properties of fibres and matrix materials will be analysed. Physical properties as dimensions of a filament or a tow are presented among with mechanical or elastic properties of fibres and matrices. The sub-chapter is divided into two sections. The first section refers to properties of fibres and the second refers to the properties of matrix materials.

2.3.1.1 *Fibres*

Fibres comprise the main reinforcing agent for advanced composite materials. Production of fibres for commercial purposes started in 1931 with glass fibres, but the advanced fibres for structural applications were developed in the late 1950s for boron fibres and the 1960s for carbon fibres. Advanced fibres have the characteristic of high specific mechanical properties. The term specific mechanical property refers to the ratio between the property (Young's modulus, Shear modulus, strength etc.) over density. Some of the most common fibre materials and their filament size can be seen in Table 2-1.

Table 2-1 Common fibre material and their filament size.

Fibre type	Filament size (μm)	Filament per tow
Glass fibre S-2	6-14	2000
Kevlar	12	1000
Carbon AS4	8	12000
Carbon IM8	5	12000
Ceramic Nicalon (SiC)	15	500
SCS-6 (SiC)	20	1

As can be seen in Table 2-1 fibres exist in tows comprised of filaments which vary in diameter. The micro size of filaments and the population of them in a tow result in a very flexible fibre. The main type of fibres will be presented with emphasis on glass fibres as the material under consideration. Figure 2.4 shows a map of materials placed in a position indicating their specific stiffness and specific strength. Materials placed in the lower left corner are characterised by low specific stiffness and strength. On the contrary materials placed towards the top right corner are characterised by high specific properties.

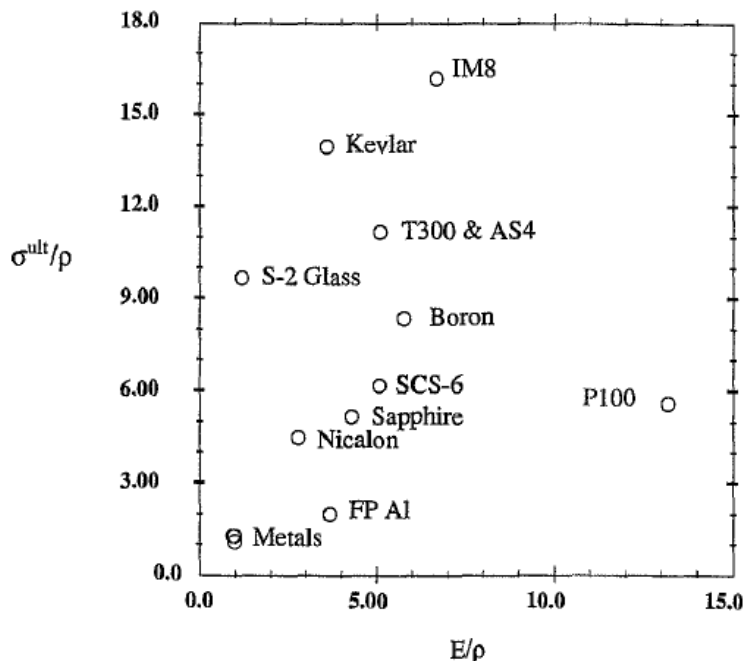


Figure 2.4 Specific stiffness and specific strength for various engineering materials. Adapted by D. Hull

2.3.1.1.1 Carbon fibres

Carbon fibres are widely used in advanced lightweight structures. These are mainly produced by a chemical decomposition, heat –controlled pyrolysis of a precursor material. The precursor material can be Polyacrylonitrile, rayon or petroleum pitch. The manufacturing process involves heat treatment of the precursor material to a temperature range between 1000 *and* 3000 °C. For the first two cases of precursor material the start point of the manufacturing process is textile fibres. A schematic representation of manufacturing carbon fibres can be seen in Figure 2.5. Filaments of carbon have a diameter that ranges from 4 – 10 μ m and tows consist of between 3000 *and* 300000 filaments. A tow is what is known as a carbon fibre. Carbon fibres are flexible with elevated stiffness and strength properties.

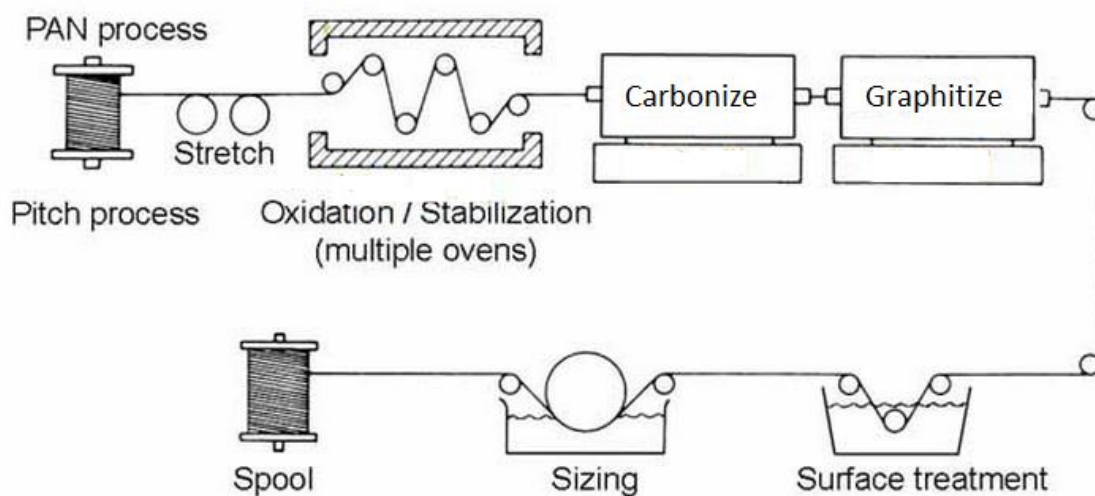


Figure 2.5 Schematic representation of manufacturing process of carbon fibres. Adapted by B.T. Astrom.

2.3.1.1.1.1 Manufacturing carbon fibres

The process of manufacturing carbon fibres starts from drawing and oxidizing the fibres at a temperature below 400°C. The purpose of that step is to ensure that the material will not melt in the subsequent steps of the process. During the first step drawing and oxidizing may occur consequently. Fibres then undergo heat treatment at temperatures above 800°C in the absence of oxygen (a process known as pyrolysis) in order to remove non-carbon elements. Generally common carbon fibres consist of 80 – 95% of carbon while graphite fibres, which are also carbon fibres, consist of 99% carbon. The following steps involve carbonization and graphitization of fibres at temperatures above 1000°C. During the process of carbonization and graphitization further drawing may occur in order to reach a higher degree of orientation for the fibres. The last steps involve surface treatment and sizing of the fibres. The properties of fibres mainly depend on the carbon-carbon bonds between the graphene layers and the orientation of these layers.

2.3.1.1.2 Boron fibres

Boron fibres are produced by chemical vapour deposition (CVD) of boron on a tungsten core. The diameter of boron fibres ranges between $33 - 400\mu\text{m}$ with an average diameter of $140\mu\text{m}$. Boron fibres are characterised by a brittle behaviour with low flexibility. Boron fibres consist of two different materials and can be seen as a composite system. As a result of the two materials existence during the fabrication cool-down process, residual stresses raise due to the mismatch of coefficient of thermal expansion. Boron fibres are characterised by elevated strength and stiffness properties. Usually they are not used in combination with polymer matrices but they are usually combined with metal matrices.

2.3.1.1.3 Aramid fibres

Kevlar-Aramid fibres are organics fibres produced by melt-spun of a liquid polymer solution. Kevlar fibres are available in four grades. Kevlar 29, which is a special type of Kevlar exhibiting high toughness properties, Kevlar 49 and Kevlar 149 which are Kevlar fibres with high and ultra-high modulus. Kevlar fibres were first introduced in the early 1970s as a reinforcement in automobile tyres. Aramid filaments have relatively low diameter ($d \approx 12\mu\text{m}$) due to which they have a very flexible behaviour. They consist of radially arranged crystalline sheets and as a consequence they behave highly anisotropically. Aramid fibres have high strength properties on tension but low performance on compressive strength and Young's modulus. It is a well-known material for its ballistic properties - the ability to absorb energy.

2.3.1.1.3.1 Manufacturing of aramid fibres

The raw material for producing aramid fibres is polyamide which is a liquid crystal polymer (LCP). The solution spinning process for producing aramid fibres starts by dissolving polymer powder in sulphuric acid and extruding the product through small holes at 80°C at a speed rate of $0.1 - 6\text{ m/s}$. Fibres then pass through a water bath of 1°C in order to solidify. Most of the time aramid fibres do not need any surface treatment due to their ductile behaviour. Figure 2.6 shows the repeating unit of a Kevlar material.

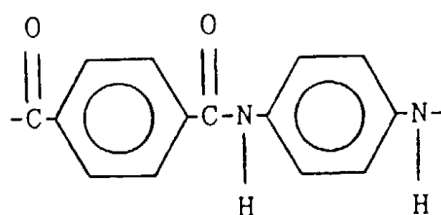


Figure 2.6 The repeating unit of Aramid fibres. Adapted from H.H. Yang

The advantages of Kevlar fibres are their improved toughness properties and damage tolerance, very good mechanical properties and relatively high temperature tolerance, good corrosion resistance and good electrical properties. Major disadvantages of aramid fibres are that it is an expensive material, relatively sensitive to moisture and also due to its extensive toughness properties it is very difficult to do any machining process with it.

2.3.1.1.4 Glass fibres

Glass fibres have the highest percentage of use for discontinuous fibre composite materials. Due to their inexpensive process of production, the good physical and mechanical properties they exhibit—such as high strength, high stiffness, low specific weight, good chemical resistance and good insulation properties—glass fibres comprise over 90% of the fibres used in short fibre composite polymers. They were first commercially released in 1931 from a company in Illinois but the first glass fibre was produced back in 1893.

Nowadays different types of glass fibres exist in the market for use for different purposes. Despite that the majority of glass fibres are silica based structures (SiO_2), which exists as a polymer, with additives such as oxides of boron, sodium, calcium, aluminium and iron. Glass generally exists in an amorphous structure or with a small degree of crystallinity after a post-manufacturing process. The atomic structure of glass is what defines the elastic properties and strength of the material. Figure 2.7 shows a typical example of a tetrahedral bond of silica with oxygen at the corners.

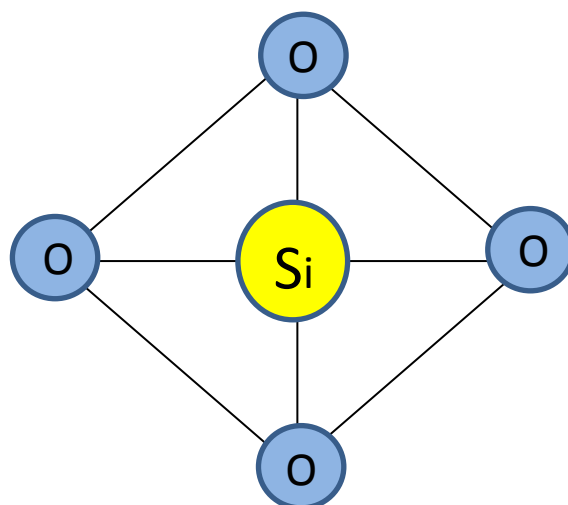


Figure 2.7 A typical example of a tetrahedral bond of silica with oxygen

Tetrahedral structures are connected together by sharing the oxygen at the corners. In such a way a 3D network structure is developed. The existence of elements like *Ca* or *Na* on the corners of the tetrahedral structure tends to improve the formability of glass but they have a negative contribution on the stiffness and strength of the material because they tend to break up the network by forming ionic bonds with oxygen atoms.

The main types of glass fibres are:

- E-glass: This is the most common type of glass. “E” stands for “Electrical” since this type of material has elevated electrical and weathering properties. It also exhibits good strength and stiffness. It consists of alumino-borosilicate glass with less than 1% (Weight fraction) of alkali oxide.
- C-glass: This is the type of glass used when demanding corrosion properties are needed. “C” stands for corrosion and compared with E-glass it has better corrosion resistance but lower strength. It consists of alkali-lime glass with a high boron-oxide content.
- S-glass: This is the most expensive type of glass. “S” stands for strength since S-glass fibres have higher strength, temperature resistance and Young’s modulus when compared with E-glass and S-glass fibres. It consists of alumina silicate glass with a high *MgO* content.

2.3.1.1.4.1 *Manufacture of glass fibres*

Glass fibres are produced by extruding a melt of silica mixed with other oxides, through holes in a platinum-alloy plate. Holes have a diameter between 0.8 – 3.2 *mm* and are usually extruded in the thousands. Fibres are drawn at a linear velocity of 60 *m/s* and the final diameter of the fibres depends on the size of the hole, the viscosity and temperature of the melt, the cooling rate and the drawing velocity. Figure 2.8 shows the basic concept of the glass fibre manufacturing process.

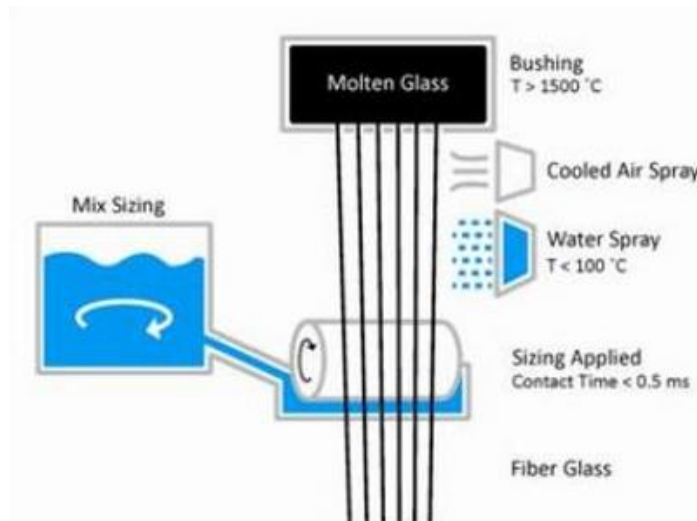


Figure 2.8 Glass fibres manufacturing process. Adapted from Michelman

2.3.1.2 Matrix materials

Matrix is the constituent used in composite materials which manages to hold the reinforcing agents (fibres) together and also transfers the load through shear stresses on the interface to fibres, and last but not least, it protects the reinforcing agents from adverse environmental effects. More than that matrix is the constituent of a composite which is responsible for preventing any buckling of fibres in compression and also for transferring the load to surrounding fibres in the case of individual fibre fracture. The dominant materials used as matrices are:

- Polymers
- Metals
- Ceramics

Throughout the following sub-section the three main types of matrix materials will be presented with emphasis on the polymer matrices.

2.3.1.2.1 Polymers

For composite materials, the matrix is usually a polymer, however, different materials are used depending on the application. The term polymer comes from the Greek language and means “many-building blocks”, and refers to the repeating units-monomers of a macromolecule or a long chain. A polymer is the result of a process called polymerisation. Polymerisation is a process whereby monomer molecules react together in a chemical reaction to form a long chain of a network molecule. Polymers are highly molecular weight compounds consisting mainly of carbon and hydrogen atoms connected together by primarily or covalent bonds. Figure 2.9 shows a configuration of polypropylene while Figure 2.10 shows a conformation of polyethylene.

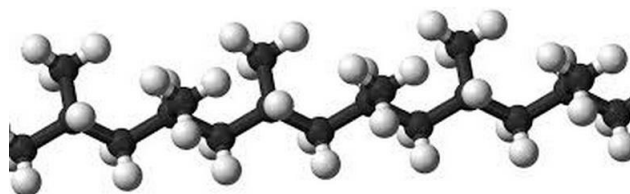


Figure 2.9 A configuration of polypropylene structure.

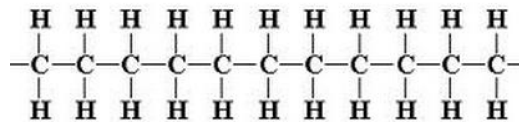


Figure 2.10 A conformation of polyethylene structure.

Polymers macroscopic behaviour is strongly influenced by the configuration and conformation of the molecular structure. This dependency can be ascribed to the relative mobility of molecules which can be on the intramer structure, on the intramolecular structure or on the intermolecular structure of the chain. In the first case the polymer's properties are strongly influenced by the type of elements presented and the kind of bond between them. In the second case macroscopic properties are influenced by the location of the functional groups in the polymer chain.

Most polymers have an amorphous structure but sometimes a degree of crystallinity may occur with an amorphous phase. In the case of gradual heating the amorphous phase of the polymer will always melt before the crystalline region. This happens mainly because crystal structures consume more energy in order to dislodge the molecules. This process is endothermic. The ability to change phases from solid to liquid and back to solid happens because mainly only secondary bonds (van der Waals bonds) act between the molecules. A polymer exhibiting such behaviour is called thermoplastic.

In general there are two main families of polymer- thermoplastic and thermosets. Thermoplastics are polymers consisting of long molecular chains held together by secondary bonds, which is the reason that they can melt and solidify theoretically infinite times. Thermoplastic polymers usually have an amorphous structure, especially in the case of irregular and stiff molecules structure. On the contrary, in the case of regular and flexible molecular structures, thermoplastic polymers tend to be partially crystalline. The degree of crystallinity can be controlled through the cooling rate during the manufacturing process. Table 2-2 shows some of the main thermoplastics used in structural or semi-structural applications.

Table 2-2 Main commodity thermoplastics for structural applications

Material	Density (Mg/m^3)	Young's Modulus

		(GPa)
Nylon 6.6	1.1-1.4	1.4-2.8
Polypropylene	0.9	1.0-1.4
PEEK	1.26-1.32	3.6

Behaviour of thermoplastics with respect to the temperature depends on the degree of crystallinity and the molecular weight of the polymer. Amorphous thermoplastics tend to experience the glass transition at lower temperatures when compared with semi-crystalline thermoplastics, since crystallinity works as a barrier to the polymer melting. In the same way thermoplastics with high molecular weight tend to need higher temperatures in order to lose their secondary bonds.

Glass transition temperature is defined as the temperature at which a region of rapid loosening of the secondary bonds take place and relatively large segments of the molecules gain extra kinematic degrees of freedom. Between the glass transition temperature and melt temperature amorphous thermoplastics seems to experience what is known as rubber plateau. Rubber plateau is a behaviour of amorphous thermoplastics in which the material does not experience any stiffness degradation but deformation occurs as a result of molecules sliding past one another.

As a generic note it must be emphasised that amorphous thermoplastics tend to shrink much less than semi-crystalline thermoplastics. This happens mainly because there is no crystallisation during the solidification stage and so molecules do not change their structure dramatically. In the case of amorphous thermoplastics, molecules keep a random position. This has as a result a very good surface finish for thermoplastic structures. On the other hand, the existence of crystallinity in a polymer improves the resistance to solvents, mainly because regions with crystalline structures prevent dissolution. Also, crystallinity improves creep resistance and stiffness, whilst at the same time reducing properties such as toughness and ductility. As reported by (Astrom, 1997) an optimum percentage of crystallinity in thermoplastics is about 20 – 35%.

In the case of thermosets polymers, initially they consist of long molecules connected only with secondary bonds, although the presence of carbon-carbon double covalent bond results in solidification of the polymer resin. As long as these intermolecular bonds cannot be broken without breaking the intramolecular covalent bond, thermoset polymers cannot melt. In general thermosets polymers consist of amorphous structures.

Initially thermoset resins are in a liquid form. By initiating a chemical reaction crosslink bonds are created between neighbouring molecules. At the end of this process an enormous three dimensional network is created between cross-linked molecules. The process of crosslinking neighbouring molecules is an exothermic process, mainly because it leads to lower energy state into the system comparing with the random structure of molecules in the initial liquid form. On the contrary with thermoplastics, thermosets exhibit a different behaviour with respect to temperature. Due to their amorphous structure thermosets have an extended rubber plateau and never melt once covalent

bonds hold the three dimensional chain together. Further application of heat on a thermoset will lead to a charred carbon structure. The main thermoset resins used for composite structures can be seen in Table 2-3.

Table 2-3 Main thermoset resins used for composite structures

Material	Density (Mg/m^3)	Young's Modulus (GPa)
Epoxy Resins	1.1-1.4	3-6
Polyesters	1.2-1.5	2.0-4.5

2.3.2 Characteristics of fibres and matrix interface

As reported while analysing the contribution of fibres in the previous sub-chapter, fibres are also a source of crystallization for the matrix. The region defined between the fibre and matrix is called the interface. The general definition of an interface, as reported by (Fu, et al., 2009), is a boundary demarcating distinct phases such as fibre and matrix.

An interphase may be a diffusion zone, a chemical reaction zone, or the bounds between two polymers in a polymer blend. The role of the interface or interphase is very crucial for properties such as strength or toughness. It does not affect properties such as the elastic modulus because the modulus is calculated under the assumption of infinitesimal strains, resulting in a perfect interfacial bonding which can be assumed without losing any accuracy in the calculations. In contrast, once the material is loaded over the elastic region, elevated stresses in the matrix must transfer to the fibres, otherwise the composite will fail from high stresses in the matrix. If the interface is not strong enough to transfer stresses to the fibre, the composite will show lower strength and probably a matrix failure, or a de-bonding mode of failure.

Interface can be improved by adding any coupling agent in the composite. This will positively affect the interfacial shear stress and will result in a higher stress transfer degree. The interfacial shear strength, and as a consequence, interfacial bonding, are directly related to what is known as critical fibre length through the shear lag model. Definitions and further details about critical length will be given in the next paragraph.

2.3.3 Fibre length distribution or aspect ratio distribution.

Through the following chapter two very important micromechanical parameters for short fibre composites will be analysed. The influence of fibre length and fibre orientation on the macroscopic elastic behaviour of discontinuous fibre composites will be examined. The length of a short fibre composite is a result of the manufacturing method. During the two main methods of manufacturing short fibre composite, Injection moulding and extrusion compounding, certain length degradation on fibre takes place due to the elevated temperature and the high shear stresses developed through the melting and compounding process. Figure 1.3 shows the degradation of fibre length as a function of flight number for three different screw designs.

Another reason for fibre breakage during manufacturing is the high viscous resins. When a high viscous polymer is injected with fibres into a mould, there is a high possibility that fibres will break due to the high shear stresses developed from the viscous polymer. As observed from Figure 1.3 at the end of this manufacturing process, fibre length undergoes a serious degradation. The final length distribution of a short fibre composite is a parameter dependant on various manufacturing factors.

As reported by Fu et al. and by Thomason et al. these factors mainly include the fibre content, the processing condition, matrix viscosity characteristics and the nature of fibres. During the manufacturing process the most common reasons for a fibre breakage are fibre-fibre interaction, fibre-matrix interaction and fibre in contact with the surface of the manufacturing equipment. It was observed by Fu et al. that with the increase of fibre content, fibre-fibre interaction increases and causes more damage to the fibre and leads to lower mean fibre length. Mean fibre length is inversely proportional to the fibre content. Reduction of fibre length with fibre content can be seen in Figure 2.11 as it was reported by (Thomason, 2002).

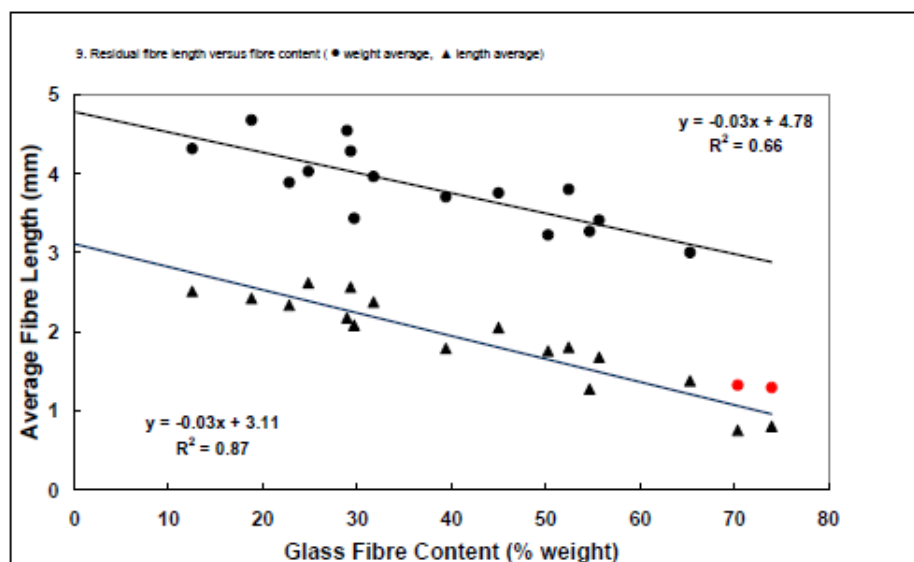


Figure 2.11 Reduction of average fibre length as fibre's content increase.
Adapted from Thomason et al.

The literature reports that a direct relation between fibre length and mechanical-physical properties exists. In order to accurately study the influence of fibre length in the elastic properties, the strength and the fracture toughness of a short fibre composite- an accurate measurement of the fibre length need to take place. The most common experimental way of fibre length measurement is direct measurement through resin burnout. Fibres are collected after burning the resin and dispersed in a solution whereby a direct measurement can take place, usually through an image analysis method. It is crucial to use the appropriate tools in order to define a probability density function which describes the length distribution of short fibres.

Various characteristics of the fibre length distribution can be defined for a probability density function $f(l)$, between fibre length l and dl and a cumulative distribution function $F(l)$ for the probability that the fibre length is equal or less than a specific length l . (Fu, 1996) propose a relationship between probability density function and cumulative distribution function as shown in Equation 2.18 and Equation 2.19.

$$F(l) = \int_0^l f(x)dx \quad \text{Equation 2.18}$$

$$\int_{l_{min}}^{l_{max}} f(x)dx = 1 \quad \text{Equation 2.19}$$

Short fibre length distribution can be described by a two parameter Weibull distribution function, as shown in Equation 2.20. In Equation 2.20 m and n are shape parameters and L is the fibre length. It was reported within the literature that the distribution describes accurately the experimental observations of glass-polypropylene short fibre composites.

$$f(L) = (m/n)(L/n)^{m-1}e^{-(L/n)^m}, \text{ for } L > 0 \quad \text{Equation 2.20}$$

A different form of Weibull distribution is Tung distribution, Equation 2.21. For the above equation a and b are scale and shape parameters respectively. The two equations are related through the shape parameters.

$$f(L) = abL^{b-1}e^{-aL^b}, \text{ for } L > 0 \quad \text{Equation 2.21}$$

The cumulative distribution function can be expressed in terms of a and b as shown Equation 2.22. The mean fibre length and the most probable length (mode length) are shown in Equation 2.23 and

Equation 2.24. The most probable length can be obtained by differentiating the probability density distribution and allowing the resultant equation to equal zero. The solution of l in that case will indicate the peak on the probability density distribution plot.

$$F(L) = 1 - e^{-aL^b}, \text{ for } L > 0 \quad \text{Equation 2.22}$$

$$L_{mean} = \int_0^{\infty} Lf(L)dL = a^{-1/b} \Gamma\left(\frac{1}{b} + 1\right) \quad \text{Equation 2.23}$$

$$L_{mod} = \left[\frac{1}{a} - 1/(ab)\right]^{1/b} \quad \text{Equation 2.24}$$

For a specific length l_1 and l_2 the cumulative fibre length distribution is known by Equation 2.22. Then, a solution for the shape parameters is possible. Equation 2.25 and Equation 2.26 show the solution of a and b shape parameters.

$$b = \frac{\ln\{\ln[1 - F(l_1)]/\ln[1 - F(l_2)]\}}{\ln(l_1/l_2)} \quad \text{Equation 2.25}$$

$$a = \frac{\ln[1 - F(l_1)]}{l_1^b} \quad \text{Equation 2.26}$$

Two different approaches for the probability distribution function were proposed by (Chin, 1988). The probability density distribution and the mean length are presented in Equation 2.27 and Equation 2.28. For the density function b and c represent shape parameters and for the mean length, Γ is the gamma function.

$$f(l) = \frac{c}{b} \left(\frac{l}{b}\right)^{c-1} e^{-(l/b)^c} \quad \text{Equation 2.27}$$

$$L_{mean} = b\Gamma\left(\frac{1}{c} + 1\right) \quad \text{Equation 2.28}$$

The second approach by (Chin, 1988) is a logarithmic-normal distribution expressed in Equation 2.29, where s and μ are model parameters and l is the fibre length.

$$f(l) = \frac{1}{\sqrt{2\pi sl}} e^{[-(\ln l - \mu)^2 / 2s]} \quad \text{Equation 2.29}$$

Mean fibre length and the most probable length are presented in Equation 2.30 and Equation 2.31, where an expression of the model parameters as a function of mean and most probable length, is shown in Equation 2.32 and Equation 2.33.

$$l_{mean} = e^{\left[\mu + \frac{s^2}{2}\right]} \quad \text{Equation 2.30}$$

$$l_{mod} = e^{\left[\mu - s^2\right]} \quad \text{Equation 2.31}$$

$$s = \sqrt{\frac{2}{3}(\ln l_{mean} - \ln l_{mod})} \quad \text{Equation 2.32}$$

$$\mu = \frac{2\ln l_{mean} + \ln l_{mod}}{3} \quad \text{Equation 2.33}$$

As reported by various authors, (Cox, 1952), (Thomason, 2002), effective properties of a short fibre composite are strongly influenced by fibre length distribution, up to a certain fibre length or AR. It has been shown analytically and experimentally that there is saturation on the reinforcing phenomenon for fibre length, and the threshold is defined by the critical fibre length. A unique answer for the critical fibre length cannot be given because as it was shown experimentally by (Thomason, 1996), the critical length varies depending on the property under investigation. Properties such as strength or impact resistance show a more sensitive response to fibre length and larger fibres are needed to reach the critical threshold.

2.3.4 Fibre orientation distribution

The second parameter with a strong influence on the mechanical and thermal properties of short fibre composite is fibre orientation. As with the previous parameter, fibre orientation is strongly influenced by the manufacturing process.

It is reported by (Thomason, 1996) that parameters of fibre length and fibre orientation are costly effective for the manufacturing process but they also strongly influence the mechanical and physical

properties of a short fibre composite. For a short fibre composite, orientation will always have a random nature. Even with a manufacturing process aimed at orienting fibres towards the flow direction, fibres will never be fully aligned, nonetheless a certain degree of alignment can be achieved.

The symmetry of the material, as reported in the previous sub-chapter, is strongly influenced by the fibre orientation. The higher degree of symmetry for short fibre composite is transversely isotropic, and it can be achieved with random in plane orientation. A short fibre composite, with a degree of orientation, tends to have an orthotropic behaviour. It has been reported in literature that injection moulded samples exhibit a skin-core-skin behaviour with respect to the fibre orientation. The skin-core-skin structure is a result of the manufacturing process, as a consequence of which fibres at the boundaries of the specimen become more aligned towards the flow direction, in comparison with the fibres in the middle of the specimen, which were found to have a more random distribution.

Fibre orientation can be measured through image process analysis. Image analysis requires that slices of the specimen are taken transversely to the Z axis and to undergo a polish process. Images of the slices are then taken. Fibres are projected as ellipses, as shown in Figure 2.12, for any possible orientation and as circles for all the fully aligned fibres. The orientation of each fibre can be characterised in 3D space by two Euler angles (θ and ϕ). The in plane angle θ can be defined as in Equation 2.34.



Figure 2.12 Slice of specimen along Z axis. Fibres are projected as ellipses.

$$\theta = \cos^{-1}(b/a)$$

Equation 2.34

Where a and b represent the major and the minor semi-axis of the elliptical cross-sections respectively. It has been reported by (Fu, et al., 2009) that for composites with a high degree of alignment, calculation of circular projections can introduce an error of 8% for angle. This uncertainty can be minimized to 0.5% if the cross-section is taken at an angle with respect to the Z axis. As in the case of fibre length, fibre orientation distribution can be defined as shown in Equation 2.35, in which θ is the in plane orientation.

$$g(\theta) = \frac{\sin \theta^{2p-1} \cos \theta^{2q-1}}{\int_{\theta_{min}}^{\theta_{max}} \sin \theta^{2p-1} \cos \theta^{2q-1} d\theta} \quad \text{for } 0 \leq \theta_{min} \leq \theta \leq \theta_{max} \leq \pi/2 \quad \text{Equation 2.35}$$

p and q are shape parameters, which are used to determine the shape of the distribution. The combination of p and q can indicate high alignment to any direction or a random orientation as can be seen in Figure 2.13. The plot indicates that the combination of p and q parameters determines the degree of fibre alignment in the composite.

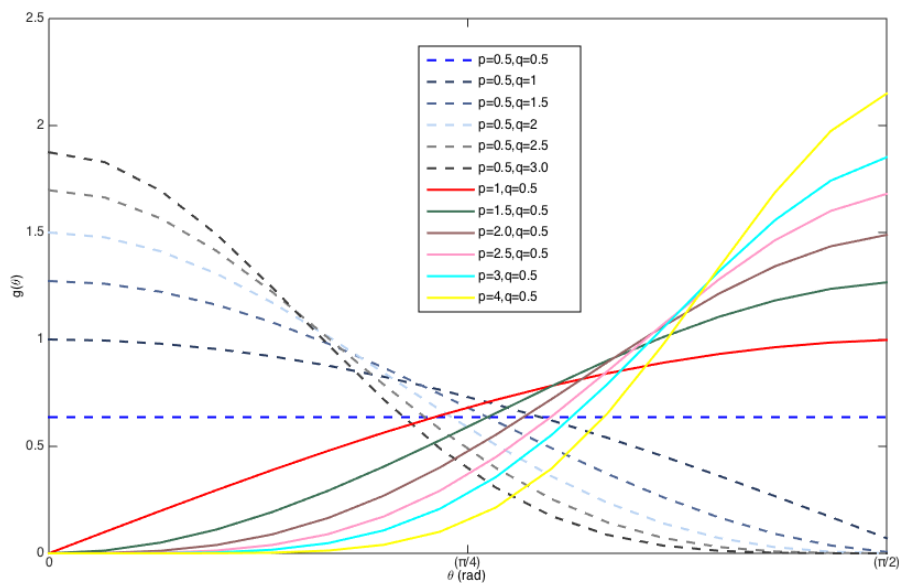


Figure 2.13 Fibre orientation distribution function for various cases of shape functions.

The fibre orientation coefficient factor can be defined according to (Fu, 1996) through an integration of Equation 2.35 which leads to Equation 2.36. A schematic representation of the equation can be seen in Figure 2.14 where value of $f_{\theta} = 1$ denotes a perfect alignment of fibres towards the first-principal direction, while $f_{\theta} = 0$ defines the 2D random orientation distribution.

$$f_{\theta} = 2 \int_{\theta_{min}}^{\theta_{max}} g(\theta) \cos^2 \theta d\theta - 1$$

Equation 2.36

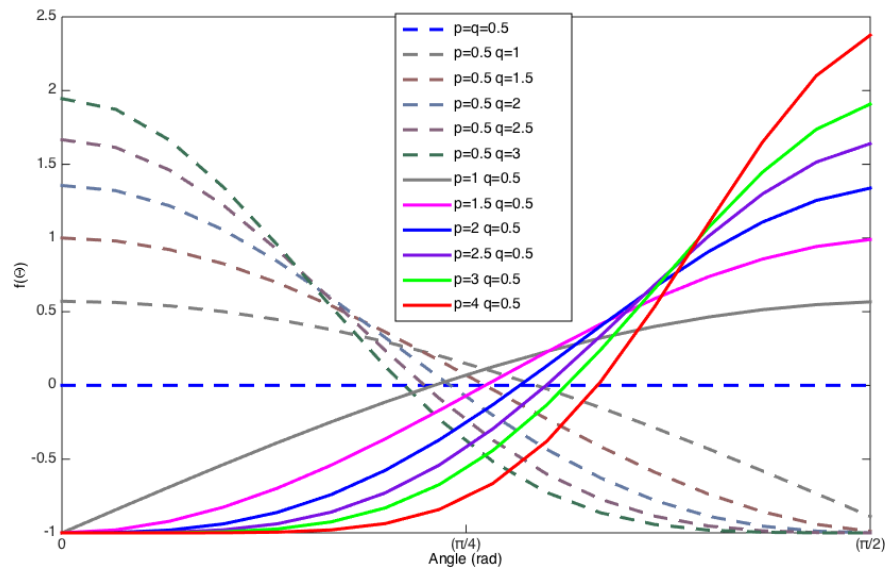


Figure 2.14 Distribution of fibre orientation coefficient for various combinations of shape functions.

The mean fibre orientation angle can be calculated as shown in Equation 2.37. The most probable angle as defined in Equation 2.38 is the result of differentiating $g(\theta)$ and allowing it to equal to zero.

$$\theta_{mean} = \int_{\theta_{min}}^{\theta_{max}} \theta g(\theta) d\theta$$

Equation 2.37

$$\theta_{mod} = \arctan\{[(2p - 1)/(2g - 1)]^{1/2}\}$$

Equation 2.38

(Chin, 1988) presented a modified (Kacir, 1975) single parameter exponential function to describe fibre orientation distribution. According to (Kacir, 1975) probability density function is given as in Equation 2.39.

$$\rho(\theta) = \lambda e^{-\lambda\theta} \quad \text{Equation 2.39}$$

where λ is a shape parameter, which has a low value for random orientations and a large value for a major preferential alignment. It has been reported in literature that the distribution function is suitable for large values of λ . The density distribution function for various values of λ is given in Figure 2.15.

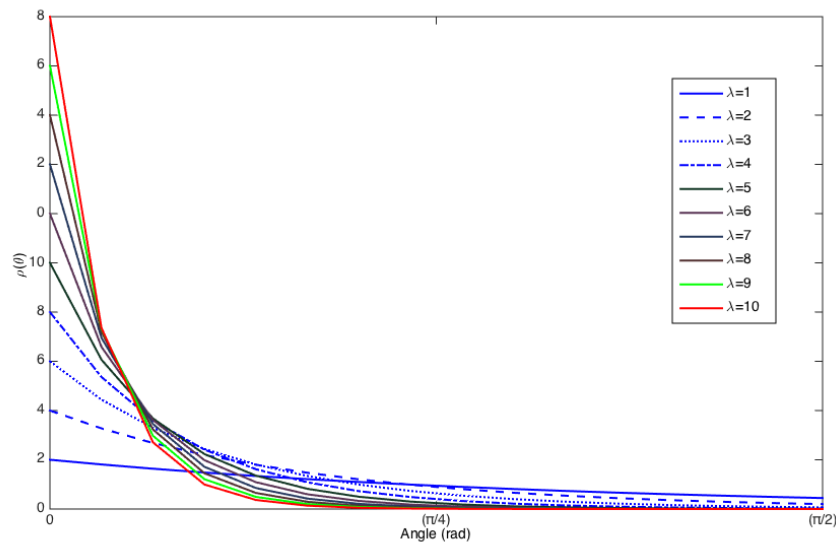


Figure 2.15 Orientation distribution for various values of λ .

A normalised version of Kacir's model has been proposed by (Chin, 1988). As shown in Equation 2.40, Kacir's model has been normalised with $\left(1 - \lambda e^{-\frac{\pi}{2}\lambda}\right)$. It can be observed from the cumulative distribution function, Equation 2.40, that for values of $\theta = \pi/2$, $F(\theta) = 1$ which indicates that the possibility of an angle being between $(0 - \pi/2)$ is 100%.

$$g(\theta) = \frac{\lambda e^{-\lambda\theta}}{1 - \lambda e^{-\frac{\pi}{2}\lambda}} \quad \text{Equation 2.40}$$

2.3.5 Volume fraction

The last parameter under discussion for short fibre composites is the volume fraction. Volume fraction is defined as the volume of fibres over the total volume of the composite, Equation 2.41.

$$V_f = \frac{V_{fibres}}{V_{composite}} \quad \text{Equation 2.41}$$

The volume fraction of a matrix can be defined in the same way as fibre volume fraction, Equation 2.42 or it can be expressed as a function of fibre volume fraction. Industrial applications of short fibre composites usually require a volume fraction of up to 35%.

$$V_m = \frac{V_{matrix}}{V_{composite}} = 1 - V_f \quad \text{Equation 2.42}$$

Usually, during the preparation of short fibre composites, weight fraction is measured. Equation 2.43 expresses the density of the composite as a function of the density and weight of the constituents. Subscript f indicates fibres while subscript m indicates matrix. W_f and ρ_m indicate the fibres' weight fraction and matrix density respectively.

$$\rho_c = \frac{W_f \rho_f \rho_m}{W_f \rho_m + W_m \rho_f} \quad \text{Equation 2.43}$$

By employing the same approach, the density of the composite can be calculated using Equation 2.43. This theoretical calculation of density deviates from experimental measurements for various reasons. A dominant parameter affecting this deviation is the porosity of the material or the void content. Furthermore, during the curing of the composite material, fibres act as a source of crystallisation for the matrix, and as a result, the density of the matrix changes.

The maximum achievable volume fraction is strongly dependant on the packing arrangement. Regular packing arrangements as square or hexagonal can be expressed by Equation 2.44 and

Equation 2.45. For those arrangements, volume fraction is a function of fibre ratios r and fibre to fibre distance R .

$$V_f^{Sqr} = \frac{\pi}{2\sqrt{3}} \left(\frac{r}{R}\right)^2 \approx 0.785 \quad \text{Equation 2.44}$$

$$V_f^{Hex} = \frac{\pi}{4} \left(\frac{r}{R}\right)^2 \approx 0.907 \quad \text{Equation 2.45}$$

A random packing arrangement can be approached by Equation 2.46 which is a modified version of the Evans and Gibson model. Maximum achievable volume fraction is a function of fibre diameter and fibre length.

$$V_{f,max} = \frac{4d}{l} \left(\frac{1}{1 + d/l}\right) \quad \text{Equation 2.46}$$

For the short fibre composite manufacturing process, volume fraction is also a limitation. It has been reported that it has a negative contribution on the final fibre length and on the void content. The effect of volume fraction on the effective elastic properties will be further analysed through analytical models.

2.4 Modelling strategies

Throughout the following subchapter, various micromechanical modelling approaches will be presented. The following modelling methods are used for material properties characterization through simple uniaxial loading conditions. Micromechanical constitutive equations have a strong advantage when compared with semi-empirical models due to their ability to implement information from a local phase and also to have a clear physical basis. Localization can be defined as the estimation of the local response, for any phase or constituent, as well as for a known far field applied load. The modelling approaches throughout the following chapter can be divided into two groups. The first group regards methods which consider interactions between distinct reinforcements or different phases, while the second group considers approximations which aim to thoroughly reflect interactions between micro-geometries.

2.4.1 Mean field approach

Mean field methods use the phase-average in order to calculate the microfield response. The phase average field is expressed in terms of uniform stresses and strains. Information of the microstructure's geometry is introduced into the calculations in terms of volume fraction, aspect ratio or phase topology. Representative models for the mean field approach are the Mori-Tanaka type models, although almost all mean field descriptions in continuous micromechanics are based on the results of Eshelby. Eshelby offers a theory considering a description of the microfield, by relating stress free strains to far field applied strains with what is known as Eshelby's tensor. A modified version of the theory, known as the equivalent inclusion method, makes it compatible for calculating stress and strain field inside an inhomogeneity. Eshelby's model will be further analysed in the next chapter. Considering Eshelby's model assumption, mean field approaches were originally compatible only for a dilute matrix inclusion composite. By the term 'dilute', a composite that satisfied Equation 2.47 is described.

$$V_f \ll 10\%$$

Equation 2.47

The case of dilute concentrations has the same unique characteristics that do not affect the analysis or the results. Any expression of the concentration tensor becomes independent of volume fraction. Distances between inhomogeneity are considered to be relatively far, due to the dilute concentration, and as a consequence there is no interaction between them.

The assumption of non-interaction between inhomogeneities is considered to be correct with respect to the fibre concentration. However, for short fibre composites, usually their industrial application demands higher volume fraction. As reported in the literature, fluctuations of the stress and strain field due to interaction between inhomogeneities are not calculated by mean field approaches, which can be referred to as the "non-interactive" method. However, the mean field approach can be modified in order to be able to count for fibres' interaction. Image stresses, background stresses or perturbed stresses, are defined as the stresses acting on the inhomogeneity due to the interaction with neighbouring inhomogeneity. Introduction of those stresses in the main calculation enables the model to count for that interaction. Perturbed stresses can be superimposed on the far field stresses through a proper modification of the average matrix stress.

Mean field theories can be implemented successfully for material characterization. They can be solved by computer programs using explicit algorithms of linear algebra, once expressions of Eshelby's tensor exist. Despite all the aforementioned limitations and disadvantages of the approach, mean field schemes are a very useful tool for material characterization of aligned inhomogeneous composite.

A different mean field approach for estimating the effective thermo-mechanical properties of a composite material rests on the effective medium theories. According to the effective medium theory, the inhomogeneity is embedded in an infinite medium which has unknown mechanical properties. The system can provide a solution for the effective medium using an iterative scheme approach.

There are two effective medium approaches which are used often, the classical self-consistent method and the generalised self-consistent method. Predictions using the classical self-consistent scheme show good agreement with lower Hashin-Shtrikman bound for low volume fraction, and for a higher volume fraction results tend to agree with the upper bound of Hashin-Shtrikman. Even if it is not considered to be the best choice of modelling for composite materials, CSCS offers acceptable results and very accurate predictions for functionally graded materials. From a computational point of view, CSCS is by definition an implicit problem and the computational time and power needed for a solution are higher when compared with the Mori-Tanaka scheme.

Another mean field approach is the differential scheme. The differential scheme can be described as a procedure for adding an infinitesimal concentration of inhomogeneity by repeated circles, and for every circle to apply a homogenization process. Solutions for thermo-elastic properties from differential schemes can be obtained through numerical integration executed by standard numerical algorithms. Due to their mathematical complexity, differential schemes experience a non-broad use in the field of composite material characterization.

The Hashin-Shtrikman approach is based on a comparison between the inhomogeneous and a reference homogeneous material. Using the polarization tensor as defined in Equation 2.48, various forms of concentration tensors can be defined. Where C^P corresponds to the polarization tensor, C^{ref} is the elastic properties of the reference homogeneous media and C represents the elastic properties of the inhomogeneous material. As reported in literature, Equation 2.48 'is a starting point for deriving mean field concentration tensors.' Calculation of thermo-mechanical properties according to the Hashin-Shtrikman approach involve the use of Eshelby's tensor and Hill's influence tensor.

$$C^P(x) = (C(x) - C^{ref})\varepsilon(x) \quad \text{Equation 2.48}$$

In contrast with mean field methods, bounding methods do not have the ability of zooming in the material and offer a local description. Bounding methods are restricted to homogenization procedures. Classical bounds methods involve expressions of the minimum potential energy. Some of the representative models of this approach are: Hill bounds which consist of the Voigt and Reuss bounds, and the Hashin-Shtrikman bounds. Both models will be further analysed in the following chapter. The aforementioned modelling approaches belong to the mean field approach. The Mori-Tanaka-type estimations, the classical self-consistent method, the differential scheme method and the Hashin-Shtrikman estimations have been presented, while the basic bounding methods of Hill and Hashin-Shtrikman were discussed. Generally, mean field approaches are usually expressed as phase concentration tensors which can be calculated with a relatively low computational cost and have been reported to successfully describe the thermo-mechanical behaviour of composite materials.

2.4.2 Periodic micro-field approach

A different approach from the mean field, which aims to fully describe the interaction between phases, is the periodic micro-field approach, or unit cell method. A material with periodic geometry and with the ability for infinite extension is implemented by the method in order to approximate the micro field of an inhomogeneous material. A material with periodic geometry is understood as a material with a repeated microstructure throughout the whole volume. Results can be obtained through numerical analysis. The periodic micro field approaches are considered to be accurate methods of material characterization for a linear thermo-elastic response, but they are also used for the non-linear range. A strong advantage of the method is that it can describe highly complex phase arrangements and also offers a high resolution of the micro field. Due to the high resolution and the detailed information of the local field, periodic micro field approaches tend to be computationally demanding.

The embedding approach is a different configuration in which an effective medium surrounds a composite material consisting of discrete phases. Properties of the surrounding material are not known in advance and are calculated through an interactive scheme such as the self-consistent approach. Far field loads are applied in the surrounding region. Embedded cell approaches are widely used for material characterization but much like the previous methods, they are computationally very expensive.

The last approach from the second group is the windowing approach. According to this method, randomly chosen squares are selected from a given phase arrangement and subjected to specific boundary conditions. It has been reported that through the method, the apparent macroscopic properties are defined instead of effective properties. Approaches such as the aforementioned are appropriate methods for material characterization which are also able to count for the interaction effect. With the exception of the windowing approach, the previous two approaches offer useful information on the microstructure. Those methods are generally characterized by a high computational demand.

2.5 Micromechanical models

The micromechanics of materials are considered to be the analysis of heterogeneous materials on the level of the individual constituents. Composite materials exhibit an inherent inhomogeneous nature. A closer inspection of any kind of material will indicate that a degree of heterogeneity exists. The deviation from the homogeneous state exists due to various reasons such as particles, cracks, voids, regions of different phase or grain boundaries. Within the literature, they are referred to as defects in a generalized sense.

One of the main aims of micromechanics is to evaluate the contribution of those defects to the macroscopic behaviour of the material and to link mechanical relations on different length scales. As a consequence of that inhomogeneous nature, on the present of a far field load on the boundaries of the composite material, non-uniform distribution of stresses developed throughout the composite media. Evaluation of this distribution, for the aim of material characterization, has always been a challenge for engineers.

The microstructure of a short fibre composite material is mainly created during the manufacturing process. Engineers have a limited ability to control the formation of the microstructure during the manufacturing process, mainly because this geometrical arrangement on the second phase material is a consequence of a complex interacting micromechanical process which takes place during the manufacture of the material. The nature and geometrical properties of the microstructure strongly influence the macroscopic properties of short fibre composites. This fact results in some deviation from the ideal microstructure considered for numerical or analytical models.

By considering a fine length scale, on the micro level, defects on the microstructure can be related to a material point on the macro level. In such a way micromechanical problems can be approached under the framework of continuum mechanics. Micromechanical problems of defect can be separated in two different approaches regarding the point of interest. The problem can be formulated in order to approach the behaviour of the defect and characterization of the properties on that scale, micro-scale, or the problem can be formulated in order to describe the influence of multiple defects on a higher scale. In the case of formulation of microstructure for properties on the macro-scale, the microstructure's behaviour is taken as a situation of a material point on the macro-scale. The resulting properties are known as effective material properties.

The following section will focus on theoretical approximations for the effective mechanical properties and various analytical approaches will be discussed for macroscopic behaviour considering the influence of the microstructures. Various researchers proposed solutions for the micro-field variables. The very early studies of the topic include publications from JC Maxwell (1831-1879), Lord Raleigh (1842-1919) and A. Einstein (1879-1955). However, those studies were not under the topic of solid mechanics. Regarding the solid mechanics field, early studies include the theoretical contribution of Voigt (1850-1919) and Reuss (1900-1968), in their study of the elastic properties of a single crystal, as well as the contribution of R. Hill.

In the following paragraph, the emphasis will be on defining the mechanical and thermal behaviour of an inhomogeneous composite material, implementing continuous mechanics approaches. Regarding continuous mechanics, an essential parameter is the degree of inhomogeneity. The degree of inhomogeneity can be defined as in Equation 2.49 and it describes the elastic properties phase contrast.

$$E_{Inh} = \frac{E^{(i)}}{E^{(m)}} \quad \text{Equation 2.49}$$

$E^{(i)}$ represents the Young modulus of inhomogeneities and $E^{(m)}$ denotes the Young modulus for the matrix. It has been reported throughout the literature by (Thomason, 1996) through experimental studies and comparison with analytical models that, the higher the degree of inhomogeneity is, the higher the deviation from analytical predictions.

As will be discussed in detail throughout the next chapter, a hidden assumption for most micromechanical models is that length scales for an inhomogeneous material are well separated. This results in variables introduced into the system being able to be divided into two categories.

- Fast variables are considered to be the contribution to the micro-field which influence the response of the material on a larger scale, and
- Slow variables such as gradient of the field, which have no important contribution to the micro-field because the reflection on the local field is considered to be constant and can be replaced by a uniform applied field.

As a consequence, the total field which corresponds to an inhomogeneous material can be defined as the contribution of fast variables and slow variables. Equation 2.50 and Equation 2.51 states the aforementioned sentence. Where $\langle \bar{\varepsilon} \rangle$ corresponds to a macroscopic-far field strain, slow variable and $\dot{\varepsilon}(x)$ corresponds to local fluctuation- fast variables. Respectively $\langle \sigma \rangle$ and $\dot{\sigma}(x)$ stand for macroscopic far field stress and stress fluctuation. $\sigma(x)$ and $\varepsilon(x)$ correspond to local values of stress and strain respectively.

$$\varepsilon(x) = \langle \varepsilon \rangle + \dot{\varepsilon}(x) \quad \text{Equation 2.50}$$

$$\sigma(x) = \langle \sigma \rangle + \dot{\sigma}(x) \quad \text{Equation 2.51}$$

The contribution of fast variables can be expressed in the macroscopic behaviour of the material through their volume average. Equation 2.52 and Equation 2.53 show what are known as average strain and average stress theorems.

$$\langle \varepsilon \rangle = \frac{1}{\Omega_e} \int_{\Omega} \varepsilon(x) d\Omega \quad \text{Equation 2.52}$$

$$\langle \sigma \rangle = \frac{1}{\Omega_e} \int_{\Omega} \sigma(x) d\Omega \quad \text{Equation 2.53}$$

2.5.1 Strain and stress concentration tensors

Direct relation of the microscopic field variable and the macroscopic slow variables can be expressed through Equation 2.54. These equations are generally known as strain and stress concentration tensors, first introduced by Hill (1963) as influence tensors. Equation 2.54 and Equation 2.55 can be considered to express a localization relation.

$$\varepsilon(x) = \mathcal{A}(x)\langle\varepsilon\rangle \text{ or } \varepsilon_{ij}(x) = \mathcal{A}_{ijkl}(x)\langle\varepsilon_{kl}\rangle \text{ for } u_i = \varepsilon_{ij}x_j \quad \text{Equation 2.54}$$

$$\sigma(x) = \mathcal{B}(x)\langle\sigma\rangle \text{ or } \sigma_{ij}(x) = \mathcal{B}_{ijkl}(x)\langle\sigma_{kl}\rangle \text{ for } t_i = \sigma_{ij}n_j \quad \text{Equation 2.55}$$

$u_i = \varepsilon_{ij}x_j$ defines kinematic linear-Dirichlet boundary conditions, while $t_i = \sigma_{ij}n_j$ defines uniform traction-Neumann boundary conditions. A direct interpretation of Equation 2.54 and Equation 2.55 can lead to the conclusion that strain and stress concentration tensors are defined as the ratio between the local variable over the average value of stress and strain.

As reported by Hill, concentration tensors depend on the concentrations and phase modulus, while generally they exhibit a degree of asymmetry. The complete solution of the boundary value problem can be obtained through the fourth-order influence-concentration tensor, by considering information of the microstructure for the entire volume. In the case of Dirichlet, the boundary conditions of effective stiffness can be expressed as a function of the concentration tensor, in symbolic notation, as stated in Equation 2.56, while for Neumann boundary conditions, the expression can be observed in Equation 2.57.

$$C^{eff} = \langle C : \mathcal{A} \rangle \quad \text{Equation 2.56}$$

$$C^{eff} = \langle C^{-1} : \mathcal{B} \rangle^{-1} \quad \text{Equation 2.57}$$

Expression in an explicit representation of the influence tensor $\mathcal{A}_{ijkl}, \mathcal{B}_{ijkl}$ has always been a crucial and not trivial problem in the field of micromechanics. Due mainly to the random nature of the microstructure of short fibre composites and because of the high complexity of phase arrangement, exact explicit expressions cannot be given for strain or stress concentration tensors or the strain and stress micro-field.

Due to this reason, approximations of concentration tensors or micro-field variables can be approached through various assumptions. Those assumptions must not disturb the satisfaction of boundary conditions and in most cases are based on what is known as the “ergodic hypothesis”, which claims that for sufficiently large area-volumes, stochastically selected from a sample under study, exhibit a statistically equal phase arrangement and give raise to the averaged material properties.

It can be understood from Equation 2.56 and Equation 2.57 that calculation of effective stiffness properties can be seen as a weighted average approach on the microscopic elastic properties $C(x)$, in which the concentration tensor plays a role of weight average function. However, for real microstructures, the exact expression of microscopic elastic properties is not known and the corresponding influence tensor is neither known a priori. As a result, proper approximations have to be made with respect to information about the microstructure and the concentration tensor.

Through the following micromechanical models, presented in this chapter, various approaches to the determination of concentration tensors will be discussed. Considering a microstructure with discrete phases and exhibiting elastic properties, Equation 2.56 and Equation 2.57 may be expressed as summations shown in Equation 2.58 and Equation 2.59. Through the following formulation of effective stiffness, the subscript indicated the boundary conditions applied. D denotes Dirichlet boundary conditions while N denotes Neumann boundary conditions. f_k represents the volume of phase k . \mathcal{A}_k and \mathcal{B}_k are constant influence tensors which may be interpreted as the expression of the dependence of the average stress/strain field on the prescribed macroscopic analogues.

$$C_D^{eff} = \sum_{k=1}^n f_k C_k : \mathcal{A}_k \quad \text{Equation 2.58}$$

$$C_N^{eff} = \left(\sum_{k=1}^n f_k C_k^{-1} : \mathcal{B}_k \right)^{-1} \quad \text{Equation 2.59}$$

The above summation for the case of a two phase material can be expressed as in Equation 2.60 and Equation 2.61. Subscript I and M indicate properties for inhomogeneity and matrix respectively for the two distinct phases in the material.

$$C_D^{eff} = C_M + V_I (C_I - C_M) : \mathcal{A}_I \quad \text{Equation 2.60}$$

$$C_N^{eff} = (C_M^{-1} + V_I (C_I^{-1} - C_M^{-1}) : \mathcal{B}_I)^{-1} \quad \text{Equation 2.61}$$

2.5.2 Voigt approximation

The Voigt approximation (1889) is a very basic approximation and in general defines the upper limit of the reinforcing phenomenon for a given combination of materials. The Voigt model represents an expression of the minimum potential energy of a uniform strain field. The basic assumption for the Voigt model is expressed through Equation 2.62 and it states that both phases in the media experience the same strain. According to Equation 2.62, the uniform strain assumption leads to a unit concentration tensor, Equation 2.63. Effective stiffness according to the Voigt model is predicted as shown in Equation 2.64.

$$\varepsilon(x) = \langle \varepsilon \rangle = \text{constant} \quad \text{Equation 2.62}$$

$$\mathcal{A}_{ijkl} = \mathbf{I} \quad \text{Equation 2.63}$$

$$C_{Voigt}^{eff} = \sum_i^1 V_i C_i = V_f C_f + V_m C_m = C_m + V_f (C_f - C_m): \mathcal{A}_f \text{ for } \mathcal{A}_f = \mathbf{I} \quad \text{Equation 2.64}$$

Predictions of the Voigt model may deviate from experimental results for a short fibre composite, mainly because of the non-uniform strain field developed in the material due to the existence of inhomogeneity and also from the simplicity of the model which does not consider short fibres or any fibre's orientation.

2.5.3 Reuss approximation

Similarly to the Voigt approximation, for the Reuss approximation a uniform stress field is assumed, Equation 2.65.

$$\sigma(x) = \langle \sigma \rangle = \text{constant} \quad \text{Equation 2.65}$$

The uniform stress assumption leads to the conclusion that the stress concentration tensor must be unit, Equation 2.66. The Reuss model indicates the lower possible elastic properties between two constituents. Effective stiffness according to the Reuss model is shown in Equation 2.67.

$$\mathcal{B}_{ijkl} = \mathbf{I} \quad \text{Equation 2.66}$$

$$\frac{1}{C_{Reuss}^{eff}} = \sum_i^1 (V_i C_i^{-1})^{-1} = (C_m^{-1} + V_f (C_f^{-1} - C_m^{-1}): \mathcal{B}_f)^{-1} \text{ for } \mathcal{B}_f = \mathbf{I} \quad \text{Equation 2.67}$$

As in the previous case of the Voigt model, in reality, for heterogeneous material the stress field is not uniform and this is the main reason for the underestimated elastic properties of the model. For

both approximations, the Voigt and Reuss predictions regard homogeneous effective stiffness. For unidirectional arrangements of short, long and continuous fibres, the Reuss model can be used to estimate transverse effective stiffness. In that case, predictions will be closer to reality compared with the longitudinal estimations due to the fact that the more compliant phase will carry the load. A schematic representation of the Voigt and Reuss model can be seen in Figure 2.16. As indicated in the Figure 2.16, both models consider a material with two distinct phases and no information about the microstructure or inhomogeneity apart from the volume fraction.

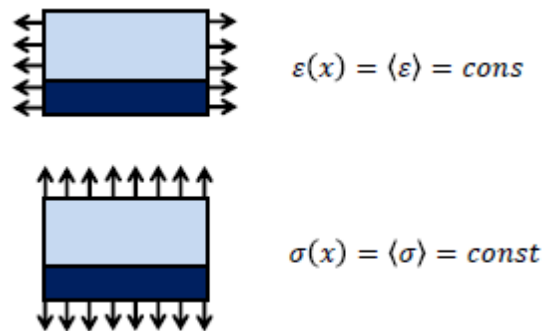


Figure 2.16 Schematic representation of the Voigt and Reuss models

A combination of both models indicates the broad bounds of a material. As shown in Equation 2.68, the Voigt approximation is the upper bound while the Reuss approximation is the lower bound.

$$\sum_i (V_i C_i^{-1})^{-1} \leq C^{eff} \leq \sum_i V_i C_i \quad \text{Equation 2.68}$$

Even if Voigt and Reuss bounds are very simple to use and offer a clear range for design, they have the major disadvantage that they don't include any information about the microstructure of the composite material, except for the volume content of each phase.

2.5.4 Shear lag model

The Shear lag model was a pioneering approach on micromechanics elasticity developed by Cox in 1951 and released in an article on the elasticity and strength of paper and other fibrous materials. The main assumption of the model is that the normal stress field developed in the fibre occurs due to shear stresses, transferred to fibres through the interphase region from matrix and fibre. A schematic illustration of the shear lag model can be seen in Figure 2.17.

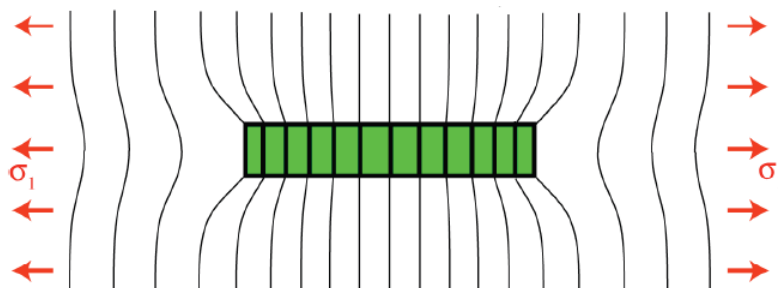


Figure 2.17 Schematic representation of the Shear-Lag model. Adapted from D. Hull

The main assumption of the shear lag model implies that shear stresses at any distance r in the matrix must be equal to the shear stress at the fibre surface in a distance r_f and that the shear stresses at the fibre surface τ_f must be equal to the normal stresses σ_f in the fibre. Equality of shear stresses between the matrix and fibre surface can be expressed through Equation 2.69 and Equation 2.70 while equality between normal stresses in the fibre and shear stresses on the fibre's surface can be shown in Equation 2.71.

$$2\pi r \tau_m = 2\pi r_f \tau_f \quad \text{Equation 2.69}$$

$$\frac{\tau_m}{\tau_f} = \frac{r_f}{r} \quad \text{Equation 2.70}$$

$$\frac{d\sigma_x}{dx} = \frac{-2\tau_f}{r_f} \quad \text{Equation 2.71}$$

For any two given phases, material shear strain can be expressed as shown in Equation 2.72.

$$\gamma = \frac{\tau_m}{G_m} = \frac{du_r}{dr} \quad \text{Equation 2.72}$$

While rearranging the terms we can conclude at Equation 2.73. Combining both expressions for shear stresses and integrating with general limits in the region between r and R Equation 2.74, an expression of the interphase shear stress can be derived, Equation 2.75 .

$$\gamma = \frac{\tau_m}{G_m} = \frac{\tau_f r_f}{G_m r} = \frac{du_r}{dr} \Rightarrow \frac{\tau_f r_f dr}{G_m r} = du_r \quad \text{Equation 2.73}$$

$$\int_{u_{r_f}}^{u_R} du_r = \frac{\tau_f r_f}{G_m} \int_{r_f}^R \frac{dr}{r} \Rightarrow [u_R - u_{r_f}] = \frac{\tau_f r_f}{G_m} \ln\left(\frac{R}{r_f}\right) \quad \text{Equation 2.74}$$

$$\tau_f = \frac{(u_R - u_{r_f}) G_m}{r_f \ln\left(\frac{R}{r_f}\right)} \quad \text{Equation 2.75}$$

On the above equation R represents the mean distance from centre to centre of fibres and depends on the fibres' package arrangement. As a consequence, distance R can be defined as a function of volume fraction for a given spatial arrangement in a composite. The combination of equations leads to Equation 2.76, from which the ratio between r_f and R can be replaced with a volume fraction expression. The value of $1/V_f$ corresponds to a hexagonal arrangement of fibres.

$$\frac{d\sigma_f}{dx} = \frac{-2(u_R - u_{r_f}) G_m}{r_f^2 \frac{1}{2} \ln\left(\frac{1}{V_f}\right)} \quad \text{Equation 2.76}$$

From the above equation, values for the displacement u_R and u_{r_f} are not known, but expressions of their derivatives can be defined. The differential expression of u_{r_f} , as shown in Equation 2.77, is equal to the normal strain in the fibre domain, while the differentiation of u_R expressed in Equation 2.78, defines the far field normal strain.

$$\frac{du_{r_f}}{dx} = \varepsilon_f = \frac{\sigma_f}{C_f} \quad \text{Equation 2.77}$$

$$\frac{du_R}{dx} = \varepsilon_c \quad \text{Equation 2.78}$$

With respect to the continuity of displacement at the interphase between fibre and matrix, and the assumption that displacement at the interphase and mean displacement in the fibre are equal, a differentiation of Equation 2.76 may be expressed as in Equation 2.79.

$$\frac{d^2\sigma_f(x)}{dx^2} = -\frac{2G_m}{r_f^2 \ln\left(\frac{R}{r_f}\right)} \left[\varepsilon_c - \frac{\sigma_f(x)}{C_f} \right] \quad \text{Equation 2.79}$$

The above equation consists of a second order linear differential equation. Solution of the differential equation can be obtained by implying the proper boundary conditions. An expression of the normal and shear stress distribution along the fibre is shown in Equation 2.80. B and D are constants which can be evaluated from the boundary conditions.

$$\sigma_f(x) = C_f \varepsilon_c + B \sinh(\eta x) + D \cosh(\eta x) \quad \text{Equation 2.80}$$

Parameter η is a characteristic parameter of the shear lag model and can be defined through Equation 2.81. According to the solution, the distribution of normal stresses in a fibre is equal to zero at both ends and has a maximum at the centre of the fibre. The opposite trend is predicted for the distribution of shear stresses. Shear stresses have maximum values at the ends of the fibre while they are equal to zero for the centre of the fibre. Effective stiffness properties can be described according to the shear lag model for a unidirectional short fibre composite as a modification of the Voigt model. Equation 2.82 shows predictions for the shear lag model.

$$\eta = \sqrt{\frac{2G_m}{r_f^2 C_f \ln(R/r_f)}} \quad \text{Equation 2.81}$$

$$C_{SL}^{eff} = \lambda V_f C_f + V_m C_m \quad \text{Equation 2.82}$$

Parameter λ is the parameter which considers all the necessary information derived from the aforementioned micromechanical analysis. As observed through Equation 2.83 λ is a function of the parameter η and the fibre length, while according to Equation 2.81, the η parameter includes information about the microstructure arrangement and elastic properties of the constituents.

$$\lambda = 1 - \frac{\tanh(\eta l/2)}{\eta l/2} \quad \text{Equation 2.83}$$

The Shear lag model is able to give relatively accurate predictions for the effective elastic properties of a heterogeneous media, but further than that, it can be used to evaluate the contribution of fibre length or spatial arrangement on the elastic properties or strength of composite materials. A further modification of the shear lag model was developed from Krenchel (1964), by adding an extra factor in order to account for the fibre's orientation.

2.5.5 Eshelby inclusion approximation

Sir Douglas Eshelby (1916-1981) was a British engineer with vital work and publications in the field of micromechanics. Eshelby's work is extensively used in various formulations of micro-mechanical problems. He published the main core of his work in 1957 on the proceeding of a conference from the Royal Aeronautical Society under the generic title: the determination of elastic field of an ellipsoidal inclusion and related problems. With this publication Sir Eshelby approaches the transformed inclusion problem, in order to derive a solution for the stress, strain and displacement fields for the inclusion and the matrix.

Originally, Eshelby's approach had nothing to do with composite materials. It was broadly used for phase-transformed metal alloys. The problem that Eshelby attempted to solve can be stated as the calculation of the stress, strain and displacement field of an inclusion with volume V_I and surface S_I , embedded in a linear elastic body with volume V_B and surface S_B when V_I undergoes a permanent deformation Figure 2.18.

Eshelby shows in a very elegant manner that this problem can be solved in four discrete virtual steps, by the superposition principle of linear elasticity and using the Green function. Eshelby's solution is valid for an unbounded domain which contains an inclusion with an elliptical shape. A description of the virtual four step experiment follows with an explanation on the equilibrium conditions for each step. Let us assume an inclusion with volume V_I , as shown in Figure 2.18, which is surrounded by a matrix material.

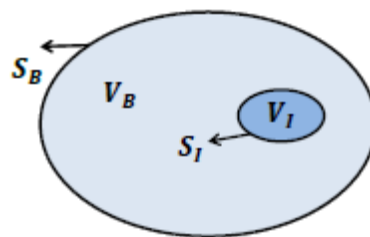


Figure 2.18 A single elliptical inclusion embedded in a matrix domain.

The whole body experiences no far field boundary conditions. The first step of the virtual experiment implies the removal of the inclusion from the surrounding domain, as shown in Figure 2.19. The stress and strain field in the inclusion and matrix are stated in Table 2-4.

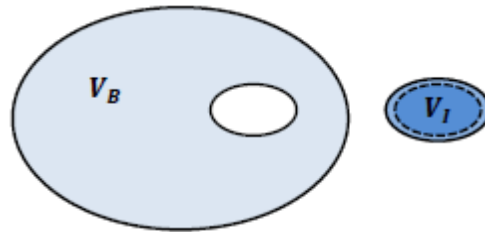


Figure 2.19 The first step involves the removal of the inclusion from the surrounding domain.

Once the inclusion is not surrounded by the matrix phase, it can expand due to the new degree of freedom which it experiences. The second step involves the application of a surface traction on the boundaries of the inclusion with the purpose of forcing the inclusion to return to its original shape as can be seen in Figure 2.20. The state of stress and strain fields for the inclusion and the matrix during the second step is stated through Table 2-4.

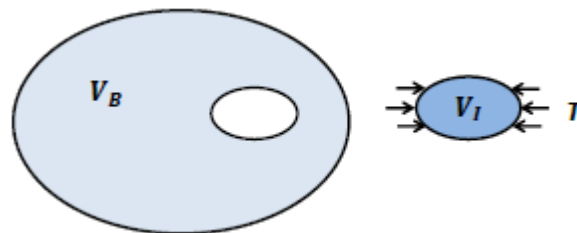


Figure 2.20 The second step involves the application of a surface traction on the boundaries of the inclusion

The third step of the virtual experiment regards the return of the inclusion into its original position within the matrix as can be seen in Figure 2.21. The inclusion can fit into the matrix again because during the second step the applied traction forces on the inclusion force it to return to its original shape. The strain and stress fields through the third step can be seen in Table 2-4.

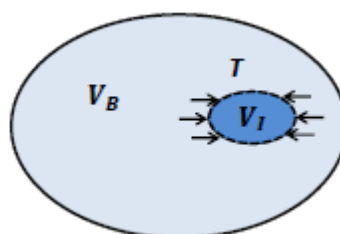


Figure 2.21 The third step of the virtual experiment regards the return of the inclusion into its original position within the matrix

The final step of the process, as shown in Figure 2.22, involves the removal of the applied traction and the application of an opposite and equivalent force acting on the surface of the inclusion. The stress and strain fields as a result of the last step can be seen in Table 2-4.

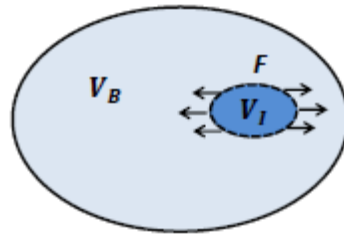


Figure 2.22 The final step of the process involves the removal of the applied traction and the application of an opposite and equivalent force acting on the surface of the inclusion.

Table 2-4. Stress, strain and displacement fields for the inclusion and the matrix according to Eshelby's approach.

	Matrix	Inclusion
Step 1		
Strain	$\varepsilon_{ij} = 0$	$\varepsilon_{ij} = \varepsilon_{ij}^*$
Stress	$\sigma_{ij} = 0$	$\sigma_{ij} = 0$
Displacement	$u_i = 0$	$u_i = \varepsilon_{ij}^* x_j$
Step 2		
Strain	$\varepsilon_{ij} = 0$	$\varepsilon_{ij} = \varepsilon_{ij}^e + \varepsilon_{ij}^* = 0$
Stress	$\sigma_{ij} = 0$	$\sigma_{ij} = C_{ijkl} \varepsilon_{ij}^e = -C_{ijkl} \varepsilon_{ij}^*$
Displacement	$u_i = 0$	$u_i = 0$
Step 3		
Strain	$\varepsilon_{ij} = 0$	$\varepsilon_{ij} = \varepsilon_{ij}^e + \varepsilon_{ij}^* = 0$

Stress	$\sigma_{ij} = 0$	$\sigma_{ij} = C_{ijkl} \varepsilon_{ij}^e = -C_{ijkl} \varepsilon_{ij}^*$
Displacement	$u_i = 0$	$u_i = 0$
Step 4		
Strain	$\varepsilon_{ij} = \varepsilon_{ij}^c$	$\varepsilon_{ij} = \varepsilon_{ij}^c$
Stress	$\sigma_{ij} = \sigma_{ij}^c$	$\sigma_{ij} = \sigma_{ij}^c = C_{ijkl} (\varepsilon_{kl}^c - \varepsilon_{kl}^*)$
Displacement	$u_i = u_i^c$	$u_i = u_i^c$

The above Table 2-4 properties denoted with the superscript "c" denote the constrained field caused by the presence of inhomogeneity and properties denoted with the superscript "e" denote the elastic strains of the inclusion which should cancel the eigen-strain. The displacement field on the existence of body force F on surface S_B can be expressed through the following integral, Equation 2.84

$$u_i^c(x) = \int_{S_0} F_j(\acute{x}) G_{ij}(x, \acute{x}) dS(\acute{x}) \quad \text{Equation 2.84}$$

where G_{ij} represents Green's function. By making use of the divergence theorem, the integral may be expressed as in Equation 2.85

$$u_i^c(x) = \int_{S_0} \sigma_{jk} n_k(\acute{x}) G_{ij}(x, \acute{x}) dS(\acute{x}) \quad \text{Equation 2.85}$$

The gradient of the displacement field can be expressed as the derivative of the above expression for displacement, shown in Equation 2.86.

$$u_{i,j}^c(x) = \int_{S_0} \sigma_{lk} n_k(\acute{x}) G_{il,j}(x, \acute{x}) dS(\acute{x}) \quad \text{Equation 2.86}$$

Respectively, expressions for strain and stress are presented in Equation 2.87 and Equation 2.88 and state:

$$\varepsilon_{ij}^c(x) = \frac{1}{2}(u_{i,j} + u_{j,i}) = \frac{1}{2} \int_{S_0} \sigma_{lk} n_k(\hat{x}) [G_{il,j}(x, \hat{x}) + G_{jl,i}(x, \hat{x})] dS(\hat{x}) \quad \text{Equation 2.87}$$

$$\sigma_{ij}^c(x) = C_{ijkl} \varepsilon_{kl}^c(x) \quad \text{Equation 2.88}$$

$$\varepsilon_{ij}^c = S_{ijkl} \varepsilon_{kl}^* \quad \text{Equation 2.89}$$

Constrained strain within the inclusion can be expressed as a function of eigen-strains through a fourth order tensor as stated in Equation 2.89. This fourth order tensor is known as the Eshelby tensor, Equation 2.89. The Eshelby tensor exhibits what is known as minor symmetry which can be expressed as shown in Equation 2.90, but no major symmetry. An explicit expression of the Eshelby tensor is not achievable for all the cases of inclusions or inhomogeneity. Only for the case of isotropic material, Eshelby's tensor has a close form representation and can be expressed as a function of elliptic integrals.

$$S_{ijkl} = S_{jikl} = S_{jilk} \quad \text{Equation 2.90}$$

$$S_{jikl} \neq S_{klij} \quad \text{Equation 2.91}$$

The conclusion of Eshelby's work is that for an inclusion with an elliptical shape which is surrounded by an infinite homogeneous matrix, Eshelby's tensor has constant elements, as a consequence of the stress and strain field within the inclusion domain, considered as being uniform or constant. This is the most valuable result from Eshelby's model.

An ellipsoidal domain is defined as the domain where α, β, γ satisfy Equation 2.92.

$$\left(\frac{x}{\alpha}\right)^2 + \left(\frac{y}{\beta}\right)^2 + \left(\frac{z}{\gamma}\right)^2 \leq 1 \quad \text{Equation 2.92}$$

where, α, β, γ are the three axes of the ellipses. For an isotropic medium closed analytical form of Eshelby's tensor for an elliptical inclusion can be calculated through elliptical integrals. For the

general case of spherical inclusion ($\alpha = \beta = \gamma$) Eshelby's tensor takes the following form Equation 2.93:

$$\mathbb{S}_{ijkl} = \frac{5\nu - 1}{15(1 - \nu)} \delta_{ij} \delta_{kl} + \frac{4 - 5\nu}{15(1 - \nu)} (\delta_{ik} \delta_{jl} + \delta_{il} \delta_{jk}) \quad \text{Equation 2.93}$$

where δ_{ij} is Kronecker delta which obeys the behaviour stated in Equation 2.94. ν represents the Poisson ratio of the matrix.

$$\delta_{ij} = \begin{cases} 0 & i \neq j \\ 1 & i = j \end{cases} \quad \text{Equation 2.94}$$

General expressions of Eshelby's tensor for elliptical inclusions are given in Appendix I. In the general case of elliptical inclusions where ($\alpha > \beta > \gamma$) Eshelby's tensor takes the following values, Equation 2.95. Solution for the I elliptical integrals can be found in Appendix .

$$\begin{aligned} \mathbb{S}_{1111} &= \frac{3}{8\pi(1 - \nu)} \alpha^2 I_{11} + \frac{1 - 2\nu}{8\pi(1 - \nu)} I_1 & \text{Equation 2.95} \\ \mathbb{S}_{1122} &= \frac{1}{8\pi(1 - \nu)} \beta^2 I_{12} + \frac{1 - 2\nu}{8\pi(1 - \nu)} I_1 \\ \mathbb{S}_{1133} &= \frac{1}{8\pi(1 - \nu)} \gamma^2 I_{13} + \frac{1 - 2\nu}{8\pi(1 - \nu)} I_1 \\ \mathbb{S}_{1212} &= \frac{\alpha^2 + \beta^2}{16\pi(1 - \nu)} I_{12} + \frac{1 - 2\nu}{16\pi(1 - \nu)} (I_1 + I_2) \\ \mathbb{S}_{1112} &= \mathbb{S}_{1223} = \mathbb{S}_{1232} = 0 \end{aligned}$$

2.5.6 Eshelby's approach to inhomogeneity

The previous calculation regards the situation of an inclusion embedded in an infinite matrix. Inclusion is defined as a domain in the matrix with the same elastic properties as the matrix. In the case of inhomogeneity the elastic properties are different from the matrix. Effective elastic properties for inhomogeneity can be approached through a technique called the Equivalent Inclusion Method. EIM implies that the inhomogeneity which has different elastic properties from the matrix and no eigenstrains will be replaced by a homogeneous inclusion which carries the appropriate equivalent eigenstrains in order to represent the inhomogeneity. The value of the equivalent eigenstrain must ensure that both inhomogeneous inclusion and the equivalent homogeneous inclusion experience the same stress field and constrained strain. As stated by

Eshelby (1957), the stress disturbance in an applied stress due to the presence of an inhomogeneity can be simulated by an eigenstress caused by an inclusion when the eigenstrain is chosen properly. Figure 2.23 shows a schematic representation of the equivalent inclusion method.

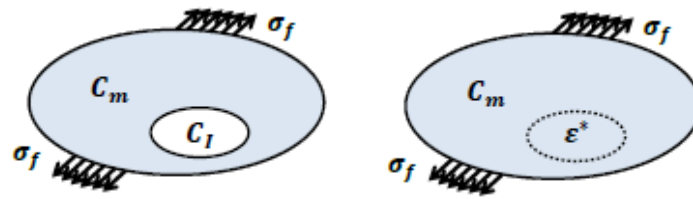


Figure 2.23 A schematic representation of the EIM

The stress field in the inhomogeneous inclusion can be expressed as in Equation 2.96

$$\sigma_I = C_I(\epsilon_c - \epsilon_t) \quad \text{Equation 2.96}$$

while the total amount of strain fields inside the inhomogeneity can be expressed as Equation 2.97:

$$\epsilon_I = \epsilon_c - \epsilon_t \quad \text{Equation 2.97}$$

The analogous stress field and total strain for the equivalent inclusion can be expressed as Equation 2.98 and Equation 2.99:

$$\sigma_m = C_m(\epsilon_c - \epsilon_\tau) \quad \text{Equation 2.98}$$

$$\epsilon_m = \epsilon_c - \epsilon_\tau \quad \text{Equation 2.99}$$

As mentioned, the stress field in both cases inside the inclusion must be the same. This can be expressed through Equation 2.100 in which the stress field is presented through stiffness and strain fields. By implementing Eshelby's tensor (Equation 2.89) Equation 2.100 takes the following form.

	$\sigma_I = C_I[\mathbb{S}\epsilon_\tau - \epsilon_t] = C_m[\mathbb{S} - \mathbf{I}]\epsilon_\tau$	Equation 2.100
$C_I(\epsilon_c - \epsilon_t) = C_m(\epsilon_c - \epsilon_\tau)$		

Under an applied far field strain ϵ_a strain in the inhomogeneity can be expressed as in Equation 2.101

	$\epsilon_i = \epsilon_a + \epsilon_c = [\mathbf{I} + \mathbb{S}C_m^{-1}(C_I - C_m)]^{-1}\epsilon_a$	Equation 2.101
--	--	-----------------------

From the previous expression it can be observed that the strain concentration tensor for the dilute case as a function of Eshelby's tensor can be given as in Equation 2.102. Similarly, the stress concentration tensor for the dilute case is defined as in Equation 2.103.

$$\mathcal{A}_{dil} = [I + \mathbb{S}C_m^{-1}(C_I - C_m)]^{-1} \quad \text{Equation 2.102}$$

$$\mathcal{B}_{dil} = [I + C_m(I - \mathbb{S})(C_I - C_m)]^{-1} \quad \text{Equation 2.103}$$

Effective stiffness for the dilute concentration tensor can be calculated according to Equation 2.104

$$C_{dil}^{eff} = C_m + V_I(C_I - C_m) : \mathcal{A}_{dil} \quad \text{Equation 2.104}$$

2.5.7 Self-consistent scheme

The self-consistent method was developed by Hill (1965) and implies the concept of an inhomogeneity embedded in the effective medium. The problem can be summarised as the calculation of effective properties considering a single inhomogeneity embedded in an unbounded domain. The self-consistent model is an implicit problem which needs an iterative numerical procedure in order to be solved. Schematic representation of the model can be seen in Figure 2.24.

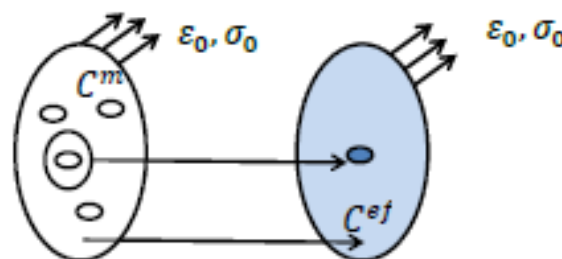


Figure 2.24 Schematic representation of the SCS

Effective property predictions of the self-consistent method are based on Equation 2.105 with a modification of the strain concentration tensor. According to the dilute model, strain concentration tensor can be expressed as in Equation 2.105.

$$\mathcal{A}_{dil} = [I + \mathbb{S}S_m(C_f - C_m)]^{-1} \quad \text{Equation 2.105}$$

$$\mathcal{A}_{SC} = [I + \mathbb{S}S_m(C_f - C_{SC})]^{-1}, \mathbb{S} = f(C_{SC}) \quad \text{Equation 2.106}$$

The modification for the self-consistent method regards all the parameters in the strain concentration tensor which represent the matrix. For the self-consistent scheme, those parameters represent the effective medium and are unknowns. Equation 2.106 shows the modification of the strain concentration tensor for the self-consistent approach. A flow chart of the iterative procedure needed to derive the effective material properties can be seen in Figure 2.25.

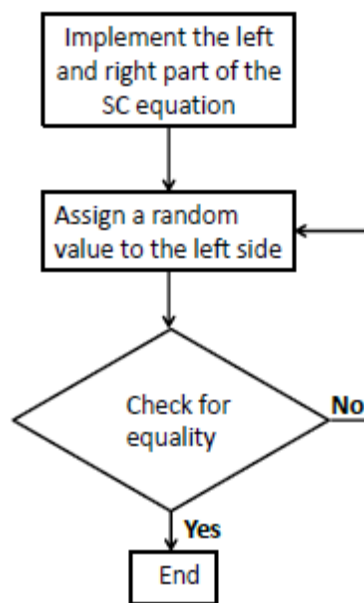


Figure 2.25 Flow chart of the SCS solver

2.5.8 Mori Tanaka scheme

Regarding the aforementioned models the assumption of a dilute model was used. The approximation of the dilute model implies that in the close vicinity of each inhomogeneity, the far field stresses or strains are dominant. As reported in the chapter for modelling strategies, the Mori-Tanaka scheme consists of an effective field approximation. The major contribution of the Mori-

Tanaka scheme is the ability of the model to account for interaction between inhomogeneities by superimposing an appropriate average matrix stress on the far field stress. Calculation of the average matrix stress is based on stresses acting on an inhomogeneity developed due to the presence of other inhomogeneities.

According to the M-T model, each inhomogeneity faces a loading condition which depends on the existence of other inhomogeneities introduced into the calculations via the average matrix stress. Calculations of the effective properties of a single inhomogeneity embedded in an infinite matrix, according to the M-T model, coincide with predictions from the dilute model. The strain concentration tensor for the M-T scheme is presented in Equation 2.107 and effective properties can be calculated with Equation 2.108.

$$\mathcal{A}_{MT} = [I + V_m \mathbb{S} S_m (C_f - C_{SC})]^{-1} \quad \text{Equation 2.107}$$

$$C_{MT}^{eff} = C_m + V_I (C_I - C_m) : \mathcal{A}_{MT} \quad \text{Equation 2.108}$$

2.5.9 Halpin-Tsai model

The Halpin-Tsai model consists of a semi-empirical approach derived from a reduced Hermans solution. The HT model is widely used mainly due to its simple algebraic calculations and the ability to provide reliable predictions. HT equations in their original form have the ability to predict effective properties of a unidirectional short fibre composite. Originally, the foundation of the model began from Herman and Hill based on a generalised self-consistent model. Equation 2.109 shows the basic form of the Halpin-Tsai model.

$$\frac{P}{P_m} = \frac{1 + \zeta \eta V_f}{1 - \eta V_f} \quad \text{Equation 2.109}$$

where η is a characteristic model's parameter which depends on the degree of inhomogeneity and the shape of the reinforcing agent. Parameter η is defined in Equation 2.110 while ζ is a parameter which considers the shape efficiency of the second phase and has a different value depending on the effective property under consideration.

$$\eta = \frac{\left(\frac{P_f}{P_m}\right) - 1}{\left(\frac{P_f}{P_m}\right) + \zeta} \quad \text{Equation 2.110}$$

Where P_f and P_m represent properties for the fibres and the matrix respectively as presented in Table 2-5.

Table 2-5. Parameters of the Halpin-Tsai model.

P	P_f	P_m	ζ	Property
E_{11}	E_f	E_m	$2(\mathcal{L}/d)$	Longitudinal modulus
E_{22}	E_f	E_m	2	Transverse modulus
G_{12}	G_f	G_m	1	Longitudinal shear modulus

Halpin and Kardor provided an in-depth analysis of HT equations, indicating that for extreme values of the ζ parameter, the HT model asymptotically approaches the Voight or Reuss models depending on if the value of ζ is very high or extremely low. Equation 2.111 and Equation 2.112 show the HT model for the case of $\zeta \rightarrow \infty$ and for the case of $\zeta \rightarrow 0$.

$$\zeta \rightarrow 0, \quad \frac{P}{P_m} = \frac{1}{1 - \eta V_f} = \frac{1}{P_m \left(\frac{V_f}{P_f} + \frac{1 - V_f}{P_m} \right)} \Rightarrow \frac{1}{P} = \frac{V_f}{P_f} + \frac{1 - V_f}{P_m} \quad \text{Equation 2.111}$$

$$\zeta \rightarrow \infty, \quad \frac{P}{P_m} = \frac{M_R + \zeta + \zeta(M_R - 1)V_f}{M_R + \zeta - (M_R - 1)V_f} = \frac{\infty}{\infty} = \frac{\lim_{\zeta \rightarrow \infty} \frac{d(M_R + \zeta + \zeta(M_R - 1)V_f)}{d\zeta}}{\lim_{\zeta \rightarrow \infty} \frac{d(M_R + \zeta - (M_R - 1)V_f)}{d\zeta}} \quad \text{Equation 2.112}$$

$$= P_f V_f + P_m (1 - V_f)$$

2.5.10 Analytical models comparison-Elastic properties

All the micromechanical models presented are able to predict effective mechanical properties and are often used for material characterisation. The accuracy of each model is strongly dependant on the initial assumption of each model. Semi-empirical models such as the Halpin-Tsai equations seem to be widely used in literature due to their simplicity and the clear physical meaning they exhibit. Mean field approaches such as the Eshelby-based model, are considered to be models able to reflect the presence of inhomogeneity in the media through average quantities. The following Figure 2.26 shows a comparison of predictions of longitudinal and transverse stiffness for aligned fibre orientation, while Figure 2.27 shows the prediction of effective stiffness in the case of randomly oriented fibres.

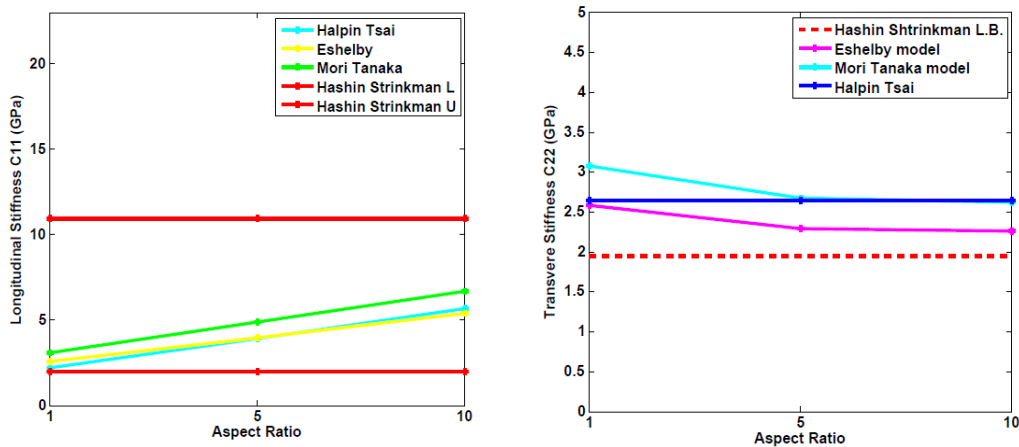


Figure 2.26 A comparison of predictions of longitudinal and transverse stiffness for aligned fibres orientation.

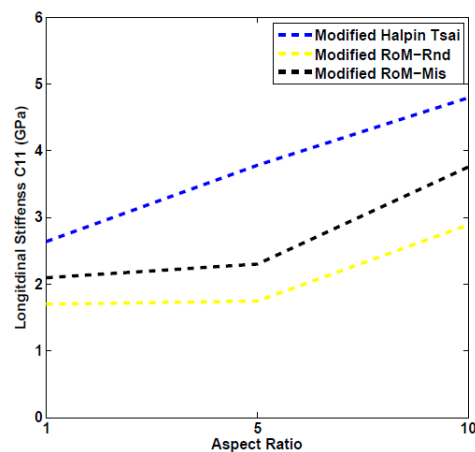


Figure 2.27 Prediction of effective stiffness in the case of randomly oriented fibres.

2.6 Thermal Conductivity

In an analogous approach, the mechanical properties calculation of thermal conductivity can be achieved through analytical micromechanical modelling. Thermal conductivity is a bulk property of a material analogous to elastic properties. It is one of the very weak properties of polymers and this is the main reason why polymers are widely used as thermal insulators. For that reason in the majority of polymer applications a reinforcing agent is used in order to increase or further decrease the thermal conductivity of the polymer.

As in the case of mechanical properties, thermal properties are also affected by various micromechanical parameters of a composite structure as fibre orientation distribution or fibre length distribution. In order to evaluate the contribution of each one of those parameters in the thermal macroscopic response of a short fibre composite, first the simpler case of aligned fibres must be study.

2.6.1 Halpin's Model

A widely used model for the prediction of longitudinal and transverse effective thermal conductivity is the Halpin's model. The model is used in a similar way to calculating the effective stiffness. Equation 2.113 and Equation 2.114 show the two main equations for calculating longitudinal and transverse thermal conductivity with Halpin's model.

$$K_1 = \frac{1 + 2(L/d)\mu_1 V_f}{1 - \mu_1 V_f} K_m \quad \text{Equation 2.113}$$

$$K_2 = \frac{1 + 2\mu_2 V_f}{1 - \mu_2 V_f} K_m \quad \text{Equation 2.114}$$

Micromechanical parameters such as the length and diameter of fibres or the degree of inhomogeneity are introduced into the main equations by parameters μ_1 and μ_2 . Solutions for μ_1 and μ_2 can be achieved through Equation 2.115 and Equation 2.116.

$$\mu_1 = \frac{K_{f1}/K_m - 1}{K_{f1}/K_m + 2L/d} \quad \text{Equation 2.115}$$

$$\mu_2 = \frac{K_{f2}/K_m - 1}{K_{f2}/K_m + 2} \quad \text{Equation 2.116}$$

2.6.2 Choy's model

(Choy, 1992) uses results from Halpin's equations, for longitudinal and transverse thermal conductivity in order to calculate the thermal conductivity of a composite material in a given angle. Equation 2.117 and Equation 2.118 shows the calculation of effective thermal conductivity for a given orientation.

$$K_1^i = K_1 \cos^2 \theta + K_2 \sin^2 \theta \quad \text{Equation 2.117}$$

$$K_2^i = K_1 \sin^2 \theta + K_2 \cos^2 \theta \quad \text{Equation 2.118}$$

Considering all the possible orientation angles in a composite the final thermal conductivity can be defined through

Equation 2.119 and Equation 2.120.

$$K_1^c = \frac{1}{2}(K_1 + K_2) + \frac{1}{2}V(K_1 - K_2) \quad \text{Equation 2.119}$$

$$K_2^c = \frac{1}{2}(K_1 + K_2) + \frac{1}{2}V(K_1 - K_2) \quad \text{Equation 2.120}$$

where V is the parameter which includes information about the orientation distribution and is given through Equation 2.121.

$$V = \frac{\lambda^2(1 + e^{-\lambda\pi/2})}{(\lambda^2 + 4)(1 - e^{-\lambda\pi/2})} \quad \text{Equation 2.121}$$

2.6.3 Nielsen's model

Nielsen's model is a similar approach to Halpin's equations, however Nielsen's model includes a parameter which accounts for the packing arrangement through the maximum achievable volume fraction. Longitudinal and transverse thermal conductivity of aligned composite can be predicted according to Nielsen's model through Equation 2.122 and Equation 2.123 respectively.

$$K_1 = \frac{1 + 2(L/d)\xi_1 V_f}{1 - \xi_1 \psi V_f} K_m \quad \text{Equation 2.122}$$

$$K_2 = \frac{1 + 0.5\xi_2 V_f}{1 - \xi_2 \psi V_f} K_m \quad \text{Equation 2.123}$$

For the above equations parameters ξ_1, ξ_2 and ψ take values resulting from Equation 2.124, Equation 2.125 and Equation 2.126.

$$\xi_1 = \frac{K_{f1}/K_m - 1}{K_{f1}/K_m + 2L/d} \quad \text{Equation 2.124}$$

$$\xi_2 = \frac{K_{f2}/K_m - 1}{K_{f2}/K_m + 0.5} \quad \text{Equation 2.125}$$

$$\psi = 1 + \left(\frac{1 - V_{f(max)}}{V_{f(max)}^2} \right) V_f \quad \text{Equation 2.126}$$

The value of the parameter ψ is strongly dependant on the maximum achievable volume fraction which is strongly affected by the dispersion state and the shape of the fillers. Nielsen's model and Halpin's equations give very similar results on the predictions of longitudinal thermal conductivity and a small difference on the transverse thermal conductivity.

Figure 2.28 shows a comparison of the predictions of longitudinal and transverse thermal conductivity for aligned fibres and a prediction on thermal conductivity for randomly oriented and misaligned fibres of the aforementioned analytical models.

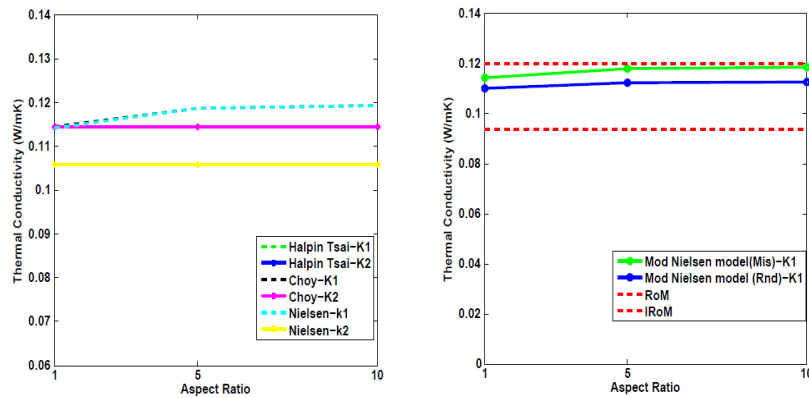


Figure 2.28 Comparison of analytical models predictions for Thermal conductivity

2.7 Linear Coefficient of Thermal Expansion

The coefficient of thermal expansion is defined as the linear change in the dimensions of the body per unit of temperature. This change of the original dimension of the body is a result of temperature change in the body. Throughout the following section various theoretical models for CTE predictions will be discussed.

2.7.1 Schapery's model

A model of calculating longitudinal and transverse CTE is Schapery's model. Schapery based his approach on an iso-strain behaviour of fibres and matrix. Equation 2.127 and Equation 2.128 show the calculation of longitudinal and transverse CTE according to Schapery's model.

Equation 2.127

$$\alpha_1 = \frac{E_f \alpha_f V_f + E_m \alpha_m \nu_m}{E_f V_f + E_m \nu_m}$$

Equation 2.128

$$\alpha_2 = (1 + \nu_f) \alpha_f V_f + (1 + \nu_m) \alpha_m \nu_m - \alpha_1 (\nu_f V_f + \nu_m \nu_m)$$

where in the above equation ν_f and ν_m represents the Poisson ratio for fibres and matrix respectively, while α_1 stands for the longitudinal CTE for the composite using Equation 2.127.

2.7.2 Shear Lag model

The second model for predictions of coefficient of thermal expansion has also a mechanics of materials approach and uses the efficiency coefficient as the shear Lag model in order to evaluate the effect of short fibre composites. According to Cox the calculation of efficiency factors is based on Equation 2.81 and Equation 2.83, while the longitudinal coefficient of thermal expansion can be calculated through Equation 2.129.

Equation 2.129

$$\alpha_1 = \frac{\lambda E_f \alpha_f V_f + E_m \alpha_m V_m}{\lambda E_f V_f + E_m V_m}$$

2.7.3 Halpin and Pagano's model

For the case of randomly oriented short fibre composite, Halpin and Pagano propose a model to calculate the overall coefficient of thermal expansion by considering the calculations of longitudinal and transverse thermal expansion from Schapery's model. In the case of two dimensional spaces Halpin and Pagano's model takes the form shown in Equation 2.130.

Equation 2.130

$$\alpha_c = \frac{\alpha_1 + \alpha_2}{2} + \frac{(E_{11} - E_{22})(\alpha_1 - \alpha_2)}{2[E_{11} + (1 + 2\nu_{12})E_{22}]}$$

where E_{11} and E_{22} represents the elastic modulus of the composite predicted for aligned fibres. Figure 2.29 shows a comparison of the predictions of longitudinal and transverse coefficient of thermal expansion for aligned fibres and a prediction of CTE for randomly oriented and misaligned fibres of the aforementioned analytical models.

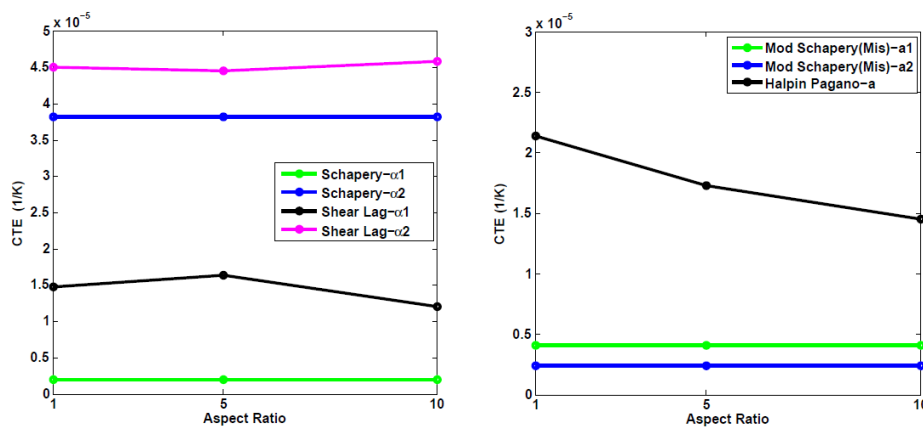


Figure 2.29 Comparison of analytical predictions for the Coefficient of Thermal Expansion.

2.8 Conclusions

Throughout chapter 2, various aspects of the field of linear continuum solid mechanics were presented with emphasis on the micromechanical analytical modelling and the major parameters affecting the performance of SFRC. The concept of inclusion and inhomogeneity was presented and the major differences were pointed out, while definitions for homogeneous and inhomogeneous media were given with the assumption that follows each definition. The symmetry of materials was discussed and various degrees of anisotropy were presented. The effect of material symmetry on the fourth order stiffness tensor was shown and the necessary independent elastic constant for each degree of anisotropy was reported. The concept of a high performance short fibre composite material was discussed through the analysis of the major factors affecting the mechanical behaviour of SFRC. Emphasis was given to the role of the physical properties of the constituents, the characteristics of the new system of materials, the contribution of FOD, FLD and volume fraction and the characteristics of the interface between fibre and matrix. Those parameters were presented in

detail, and various theoretical approaches for calculating their influence on the overall effective properties through performance factors were shown. A general report of various modelling strategies followed by pointing out the differences between different modelling approaches, and reporting their advantages and disadvantages. The presented approaches consist of the mean field approach and the periodic micro-field approach. The chapter concludes with a study of various micromechanical models for mechanical, thermal and thermo-mechanical property characterisation. The chapter considers the very generic bounds of Voigt and Reuss, which are used as a generic guide, the shear lag approximation, Eshelby's inclusion approach, the self-consistent scheme, the Mori-Tanaka scheme and the Halpin-Tsai equations. Each micromechanical model consists of a different approximation of the effective material properties. Assumption and calculation aspects were further discussed. Finally a comparison between the predictions of each model is presented. Analytical micromechanical models offer a direct answer to crucial initial design questions and material behaviour. Limitation of the analytical approach lies in the assumptions of each model. Whether this is expressed as limitations on the reinforced shapes, or loading transfer assumptions between matrix and fibre, or limitations in the volume fraction or the degree of inhomogeneity, there is a gap between the behaviour of the microstructure under various loading conditions and the mathematical model describing this condition. Numerical modelling aims to fill this gap and describe the behaviour of the microstructure under various loading conditions by its ability to locally simulate the microstructure of the material and consider any mechanism of loading transfer between matrix and fibres. This study aims to contribute to the field of material characterisation through numerical study by providing solutions to the material's physical properties based on computational models and compare them with analytical predictions.

3 Numerical modelling

Compared with the previously reported analytical micromechanical models, numerical models use a more direct approach regarding the calculation of effective material properties. General numerical approaches for material characterisation have been reported in Chapter 2 under the title of modelling strategies. This specific modelling approach requires high computational performance and the implementation of a numerical method in order to simulate the material's behaviour.

The most commonly used and continually developed numerical method for characterisation of materials properties is the finite element analysis (FEA). The method was developed in 1960 and since then, it has followed the exponential growth of computational performance. Nowadays the method is commercially coded and offered to users through various FEA packages. Engineering characterisation through numerical modelling can be obtained once the representative structure of the material is created and subjected to loading or boundary conditions. Effective material properties can be obtained through a homogenisation process on the resultant stress and strain fields after the numerical analysis.

The strong advantage offered by the numerical approach is that numerical modelling accounts for the contribution of each inhomogeneity on the macroscopic behaviour of the media, and calculations are based on a more realistic assumption regarding the microstructure. Furthermore, micromechanical parameters such as fibre length and fibre orientation are assumed to be a part of the microstructure and the interaction between those parameters is reflected in the calculated effective properties. One of the most crucial problems in simulating the behaviour of a short fibre composite is the actual representation of the microstructure of the composite. For periodic structures like unidirectional continued fibre composites, representation of the microstructure is a more trivial problem due to the periodicity of the microstructure. For random short fibre composites, the structure does not follow any periodic arrangement. In contrast, the arrangement of the microstructure has a random nature mainly due to the manufacturing processes. In that case, representation of the microstructure becomes more challenging and the actual size of the representative structure is one of the major parameters within the numerical investigation.

3.1 Packing problem

The problem that arises can be simply addressed as an arrangement of specific shape sub-domains in a bigger domain-container. The problem is known as the packing problem and it is a mathematical optimisation problem of packing objects in a container. The packing problem can be found in our daily lives especially within the merchant sector where everything needs to be packed into a closed volume. The question of an optimum packing arrangement or the maximum number of objects able to fill a closed volume is usually a part of each similar study.

The packing problem is directly related to the problem of short fibre composite modelling because fibres have to be packed in an optimum way on a volume element, otherwise it will be very difficult to reach the desired volume fraction. In order to overcome this problem engineers and

programmers developed algorithms to obtain an optimum solution for the packing problem of placing a second phase material in a matrix domain. The framework under which a solution can be obtained will be discussed in the next sub-section, while the challenges of a packing algorithm and the main assumptions will be presented in the next paragraphs.

Packing algorithms for short fibre composites were developed by various researchers. Approaches can be categorised as two dimensional and three dimensional representations. In general, three dimensional representations are more computationally expensive, however they represent the microstructure more accurately. For short fibre composites, fibres are represented as cylinders or ellipses for 3D and 2D respectively. The packing problem of SFRC is defined through placing cylinders or ellipses in a cubic or square domain by satisfying various criteria. Those criteria or restrictions ensure a closer representation of the macrostructure to the real structure of the material.

A basic criterion is the non-intersection between fibres, in addition to an optimum distance between fibres. In order to satisfy this criterion, the packing algorithm needs to calculate the distance between existing fibres and each new added fibre, and to reject fibres that do not satisfy the criterion. Each packing algorithm can be modified in order to fulfil the requirements of the developer. Various restrictions can be applied to control fibres orientation or fibre length or fibre behaviour in the bounds of the container. As a consequence, the more constrained parameters are introduced into the system, the higher the computational cost of the solution; however, this problem can be overcome by using high performance computers, or by implementing the appropriate assumptions in order to simplify the problem. Three dimensional ellipses and two dimensional elliptical shape representing fibres can be seen in Figure 3.1.

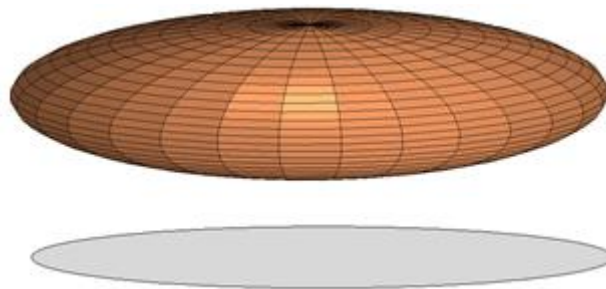


Figure 3.1 Three dimensional ellipses and two dimensional elliptical shape representing fibres.

Developed packing algorithms for short fibre composites include parameters which are seeded from random generators. Such parameters can be the space position for the centre of a fibre or the in-plane orientation and the length of each fibre. Parameters like distance between fibres can be restricted but they still have a random nature because they are strongly dependant on the space coordinate distribution. Efficiency of the packing algorithm is affected by various factors. The most dominant is the actual structure of the algorithm provided by the designer, however in any case parameters like fibre content and fibre length strongly influence the efficiency of the packing

algorithm and denote limitations. The very basic structure of a packing algorithm can be seen in Figure 3.2.

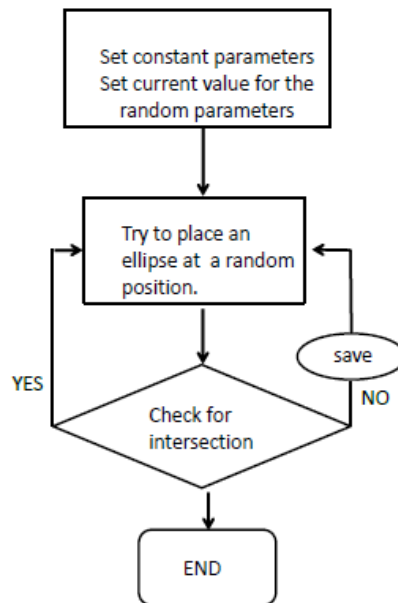


Figure 3.2 A very basic structure of a packing algorithm

As observed in the basic flow chart of Figure 3.2, a packing algorithm needs to be seeded with some constant parameters and some random parameters. The combination of those parameters reflects the actual position of the inclusion, which then passes through an intersection criterion. Accepted data will be stored while data which is not accepted will be rejected. The microstructure of a short fibre composite in reality has a random nature due to the manufacturing processes. This can be seen in Figure 3.3, showing an SEM picture of short fibre composite exhibiting the random nature of fibre orientation for short fibre composite.

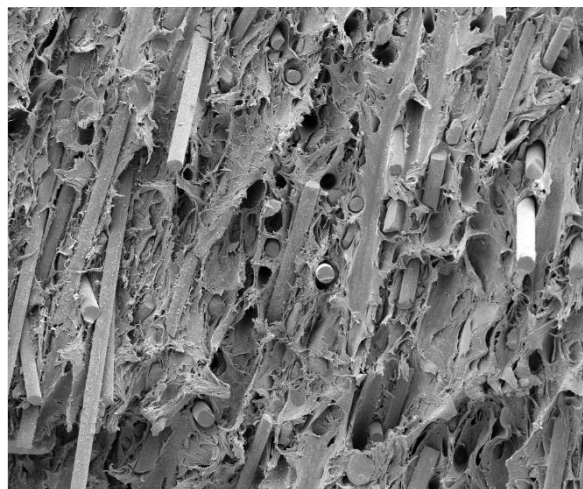


Figure 3.3 SEM picture of short fibre composite

Fibre length is reduced through the manufacturing process and fibre orientation (in-plane and out of plane) deviates from the flow direction due to the shear stresses developed in the material during the manufacturing process. For an accurate representation those characteristics of the microstructure must be introduced into the calculations through the packing arrangement obtained by the packing algorithm. This will slightly modify the flow chart in Figure 3.2 by adding a few branches to cover fibre length control, fibre orientation control and more random parameters. This will also increase the computational cost for obtaining a solution.

In the case of a 2D representation of the microstructure, the effect of fibre length can be fully covered, while with regards to the fibre orientation, the out of plane orientation of fibres is not covered. As a consequence, effective properties seem to be slightly overestimated for the two dimensional representation. Taking into consideration that measurements of the out of plane angle for short fibre composites show small deviation ($\pm 15^\circ$) from the flow direction, the assumption of a 2D plane stress or plane strain situation can be accepted as a less computationally expensive approach with accurate results.

One of the major challenges of building a representative structure for SFRC through a packing algorithm is the ability to obtain this microstructure, in a reasonable time for high volume fraction samples. Various solutions have been proposed in the literature to overcome this problem. A method to overcome the problem of high volume fractions is to place fibres into the square in a hierarchical manner. Fibres with high AR or higher length than the average value are always placed in the container first. It will be more difficult if we try to place them in the remaining space once short fibres have already been placed and the desirable volume fraction will probably not be achieved. A different approach is to obtain a solution without modifying the placing manner, however once a solution is achieved for volume fraction less than the desired, a further shrinkage of the container domain is possible and has as a result the increase of the volume fraction due to the decrease of the denominator as volume fraction is defined in Equation 2.41. In the case of three dimensional simulations, the maximum achievable volume fraction is less compared to the two dimensional simulations. The maximum achievable volume fraction for three dimensional simulations can go up to 35% by making use of the fibre local bending technique in order to take advantage of the intersected fibres and increase the volume fraction. Again, it must be mentioned that from the numerical point of view, the maximum achievable volume fraction is not an absolute number because it is strongly dependant on parameters such as fibre length, fibre orientation and whether it is in a 2D or 3D representation.

3.2 Representative Volume Element (RVE)

Computational micromechanics for material characterisation can be implemented under the framework of Representative Volume Element (RVE). An RVE is a way of connecting or bridging meso to macro scale. RVE is considered to be an element volume that is representative of the whole material structure. RVE can be seen as a small virtual specimen large enough to be representative of the macroscopic structure. The existence of RVE for the elastic response of various materials has

been proofed for various cases, however for cases of brittle or quasi-brittle material, the existence of RVE for the elastic, hardening or softening region of composite material is the field of current research.

3.2.1 Definition

Definitions of RVE vary depending on the approaching perspective of the author, however most of the definitions converge in a common base which states that RVE must be large enough to contain the necessary information of the microstructure and must also have the smallest possible size. According to (Hill, 1963) an RVE can be defined if it satisfied two criteria. First, it must be structurally entirely typical of the whole mixture on average and second, a sufficient number of inclusions are necessary in order to ensure independency of the effective properties with the surface values of traction and displacement. With respect to the (Drugan, 1996) definition, an RVE is considered as valid if it is chosen to be sufficiently large in comparison with the microstructural size. According to (Hashin, 1983), RVE can be representative if it is chosen to be large enough in order to include sufficient information about the microstructure; however it must be much smaller than the macroscopic body. Concluding the definition approaches for an RVE, the differences of an RVE with a unit cell (UC) must be addressed. A UC is defined as a realisation of the microstructure of a material. It may not be a representative of the material structure however it needs to include the information on the micro-structure of the material. On the other hand RVE is always a UC (in the sense that is a mimic of the micro-structure of the material) however an RVE is always a representative part of the material. The UC approach is more common for composite structures with periodic arrangements of fibres.

3.2.2 Length scales

In the present study we consider the lowest length scale to be the micro-scale, while the larger scale is considered a macro-scale and also commonly related to 'bulk' engineering materials. Between the micro and macro scales, the meso-scale can be defined. For the RVE definition (Ostoja-Starzewski, 1998) pointed out that statistical homogeneity and ergodicity of the material are necessary in order to determine an RVE and also that some scale λ of the material domain- sufficiently large in relation to the micro-scale d in order to ensure the independence of boundary conditions. Figure 3.4 is a schematic representation of the aforementioned.

Most micromechanical models are based on the assumption that length scales are well defined and separated. This can be understood as the contribution of the micro-structure which is reflected in the macro-scale through volume averages. More specifically, (Ostoja-Starzewski, 1998) reported that an RVE is clearly defined as a unit cell in a periodic microstructure, or in the case of random arrangements, as a volume with statistical homogeneity and *ergodic* properties which contains a very large number of inclusions.

The ergodic hypothesis implies that the heterogeneous material is assumed to be statistically homogeneous. Statistical homogeneity is the property of the material which ensures that results

have to be independent of the point of observation on the macro-scale. Figure 3.4 shows three different lengths involved in a multi-scale approach. λ represents the length on the structure scale while d represents the dimension of the defects and κ represents the characteristic length scale of the micro-structure. The meaning stated in the Ostaja-Starzewski definition can be partially expressed through Equation 3.1 that is also a condition that needs to be satisfied from the characteristic length scale in order for the material to be suitable for homogenisation.

$$\kappa \ll d \ll \lambda$$

Equation 3.1

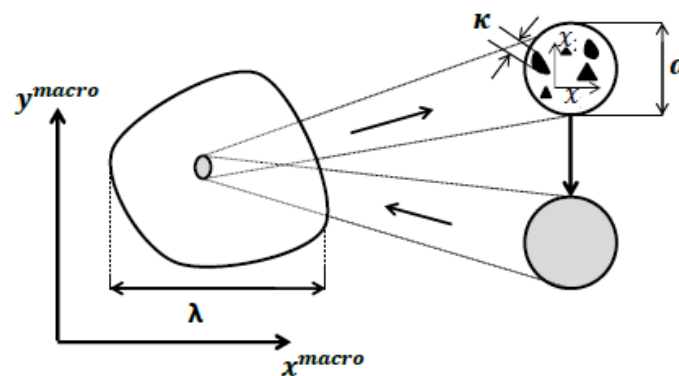


Figure 3.4 Three different lengths involved in a multi-scale approach. Adapted from Dietmar Gross

3.2.3 On the existence of RVE

By definition, once the RVE is validated for a specific combination of materials, this implies that the appropriate size of the volume can be found and that volume is able to represent a whole structure made out of the same material. Typical values for the size of RVE vary depending on the elastic properties of the constituents of the fibre content and on the aspect ratio of the reinforcing agent. Representative size of the developed UCs will be further discussed in the chapter 5.2.1. In the literature, various attempts were made in order to define an optimum size of the RVE. According to (Lemaitre, 1999), for three dimensional RVE, size must be roughly 0.1mm for metallic structures, around 1mm for polymers, 10mm for wood and 100mm for concrete. Considering the Lemaitre proposition it is clear that as long as more anisotropic materials are considered, the volume element needs higher sizes in order to be considered representative.

A different approach was proposed from (Van Mier, 2003). For concrete material they suggested that RVE size must be 3 to 5 or 7 to 8 times larger than the largest inclusion size. On the other hand, (Bazant, 2000) proposed a normalised equation for calculating the optimum size. They propose Equation 3.2 to represent the size of the RVE.

$$V = l^{n_d}$$

where n_d represents the number of spatial dimension, while l represents the characteristic length of the material which is defined as 2.7-3.0 times the maximum inclusion size. It is a common method to connect the length of the inclusion with the total size of the RVE.

The length of inclusions is a characteristic size of the micromechanical scale that can be connected with the characteristic size of the larger scale. However, as reported at the beginning of the paragraph, RVE size is not only dependant on the characteristic length of the microstructure, but also on the volume fraction and on the degree of inhomogeneity. A more accurate prediction of RVE size must include information about those parameters. A different approach for determining the existence of RVE is based on the numerical and statistical analysis of the resulting data. This process requires creating multiple realisations of the microstructure, at least five (this number is still under active research), and to subject them to far field loading conditions while recording the effective properties from the reaction of the loaded volume.

The next step involves the calculation of mean values and variance of the calculated effective property for the developed realisations. The last step in defining the appropriate RVE size requires setting a desired precision for the estimation of effective properties. That precision will work as a criterion for choosing the appropriate size of the RVE. Scatter from the average value of the five samples under investigation is a measurement of the representativeness of the volume element. Further details for the criterion will be given in the next section. Apart from the combination of numerical and statistical analysis, in order to determine the existence and the size of RVE, an analytical approach can be also used.

The analytical approach implies the solution of an explicit non-local constitutive equation. Calculations include the average strain field which varies with the position. The answer to the appropriate RVE size comes from the wave-length that has to be chosen in a way that the non-local term of the constitutive equation produces non-neglected corrections. It has to be mentioned that apart from numerical and analytical approaches in the validation and size determination of RVE, an experimental approach was also developed in order to answer the arising questions. Experimental approaches for validation and size determination is considered to be out of the scope of the current thesis and won't be further discussed.

3.3 Modelling SFRC

As reported, in order to numerically simulate a short fibre composite, an accurate representation of the microstructure must be created. Also, in a way, the RVE must ensure the continuity of the material and the continuity of local fluctuations, or in other words, ensure that the same response of the RVE can be found in any place of the material. This continuity condition is satisfied through the geometrical periodicity of the RVE. The term 'geometric periodicity' is used to describe how the

volume element is experiencing no wall effect. The wall effect is said to be the inability of inclusions to penetrate the boards of the square. A simple way of explaining the term geometric periodicity will be the ability of each inclusion once it exits the unit cell border to re-appear on exactly the opposite side. Realisations with geometric periodicity and realisations experiencing the wall effect can be seen in Figure 3.5.

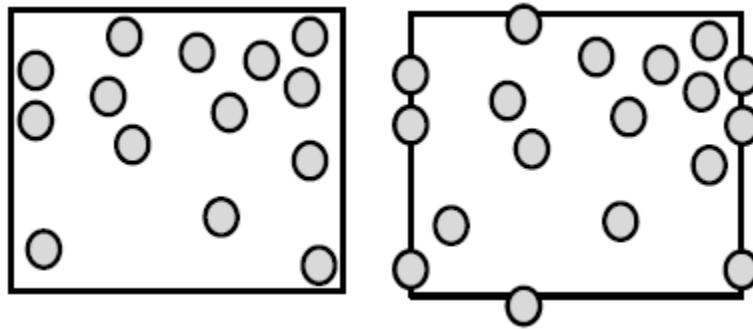


Figure 3.5 Unit cells structures of randomly distributed circular inclusions. The left unit cell has a defined wall effect while the unit cell on the right contains periodic boundaries.

Geometric periodicity ensures that repetition of the same volume element in both directions will cause a continued structure which consists of the same volume element. Creation of the microstructure can be obtained through a solution of the packing problem. For this purpose, a packing algorithm was developed in order to create two dimensional arrangements for ellipsoidal objects packed in a square domain experiencing geometric periodicity.

3.3.1 Implemented Algorithm

The first approach to developing the packing algorithm was based on the simple idea presented in Figure 3.6 through the flow chart.

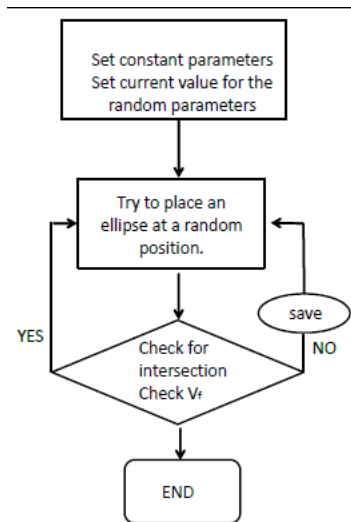


Figure 3.6 Simple structure of a packing algorithm.

The first developed algorithm for the purpose of this study was able to place circular objects on a square by controlling the distance from centre to centre. As observed in Figure 3.6, every new circular inclusion which entered the square was checked with all the existing inclusions in the square for intersection. The check was done with respect to the centre to centre distance. As in Figure 3.7, distance calculation was simplified as the application of Pythagoras's theorem between two points.

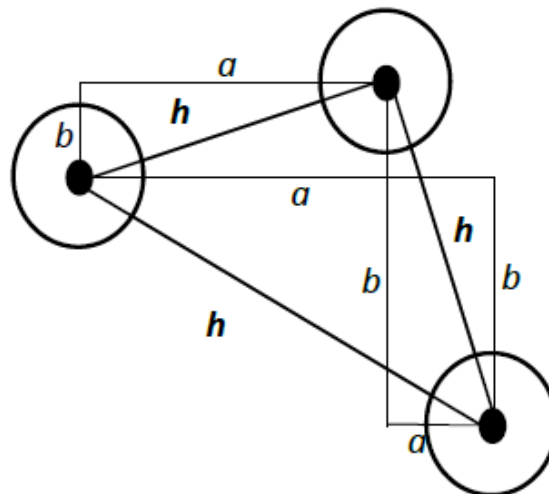


Figure 3.7 Calculation of distance between inclusions was based on centre to centre distance calculation.

Longitudinal and transverse distances between two points were calculated and the hypotenuse was used as a distance criterion. The flow chart of the specific algorithm can be seen in Figure 3.8.

Geometric periodicity was applied not to every circular inclusion in the square, but only to those inclusions exiting the boundaries of the container-square.

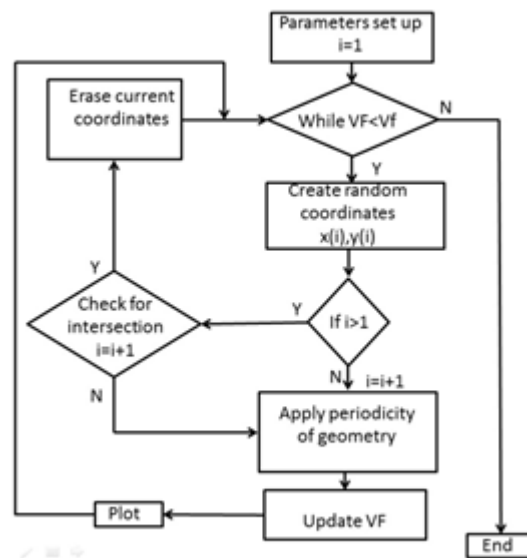


Figure 3.8 Flow chart of the initial algorithm able to produce a microstructure that consists of circular inclusions.

This requires an extra control loop in order to manipulate only inclusions at the walls of the square. The algorithm was used only as an initial starting point and has the major disadvantage of only being efficient for circular inclusions, or for inclusions with very low aspect ratio $AR \leq 2$. Another disadvantage of the algorithm is that it can reach high volume fractions only for circular inclusions, derived mainly from the criteria used for intersection.

It was shown that fibre simulation required an algorithm able to create and control the position of higher aspect ratio inclusions in a more efficient way. Further study on the packing problem led to the second developed algorithm for the microstructure of short fibre composite material. The flow chart of the second developed algorithm can be seen in Figure 3.9.

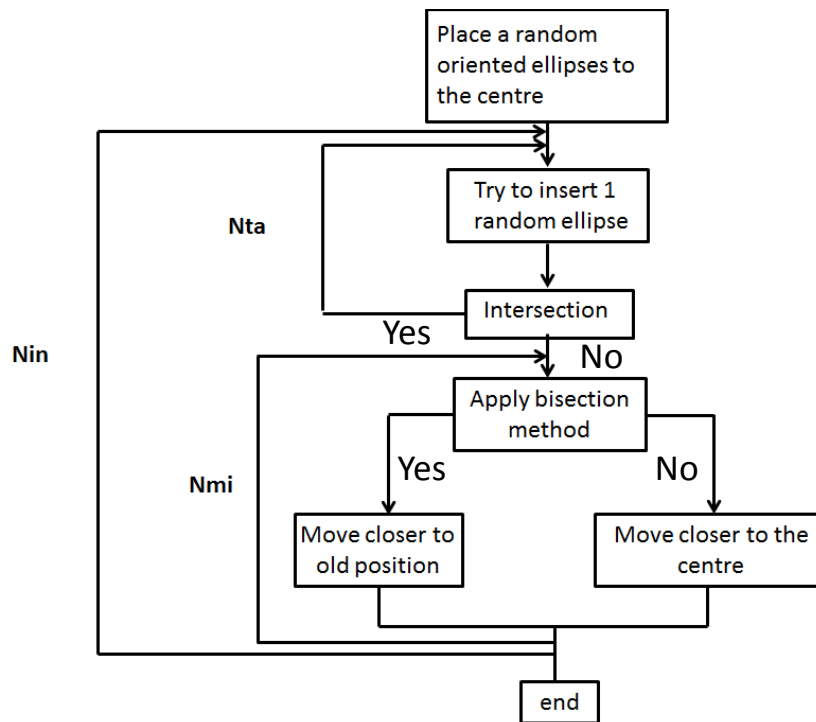


Figure 3.9 Flow chart of the algorithm used to develop various cases of SFRC microstructure.

The main differences between the latter and the former algorithm are the intersection criteria, the ability to solve problems with much higher AR, the different approach on the geometric periodicity and an extension loop for improving the potential for higher volume fractions. Also, the ability to create three different orientation cases (aligned, misaligned and randomly oriented fibres). The perimeter of each ellipsis is now approached by a polygon. The accuracy and the resolution of the polygon (number of vertices which comprise the polygon) is a choice of the user. Higher resolution polygons lead to a more geometrically accurate perimeter and a more realistic representation, but at the same time, the matrix which stores points of the perimeter becomes enormous as long as the user considers higher resolution polygons. In the case of the first algorithm, accuracy of the geometrical perimeter was approached by separating the angles to small intervals between $0 - 2\pi$. The resolution of the polygon also affected the accuracy of the intersection criterion and the time needed for the algorithm to respond. In general the number of vertices for a polygon was adjusted depending on the AR, where in most of the cases the resolution was set to 2^{10} .

The intersection criterion is no longer related to the centre of the inclusion, and it points at the perimeter of the inclusion. Points are compared using the equation of an ellipsis as it can be seen in Equation 3.3, and the intersection between fibres can be defined. Where dx represents the difference for the x coordinate between points on the perimeter of two ellipses. Similarly dy defines the difference for y coordinates on the perimeter between two ellipses. mfd represents the minimum fibre distance controlled by the algorithm user.

$$\left(\frac{dx}{\alpha}\right)^2 + \left(\frac{dy}{\beta}\right)^2 \geq 1 + mfd \quad \text{Equation 3.3}$$

As a consequence, ellipses with high aspect ratio have a larger perimeter and a rough surface so a higher polygon resolution is needed for that case. If a higher polygon resolution is not provided for a high AR microstructure, this may disturb the accuracy of the intersection criterion because it is based on the points of the perimeter. Another difference regarding the second algorithm in comparison with the first one, is the different way of implementing geometrical periodicity. Figure 3.10 shows how the second algorithm implements the concept of geometrical periodicity.

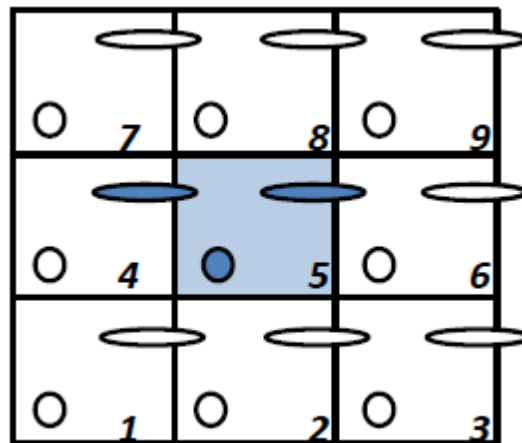


Figure 3.10 Implementation of geometrical periodicity.

The global coordinate system is placed on the left bottom edge of the square in the middle, square number 5. For every inclusion placed in the central square, eight inclusions were created immediately and occupied the analogous position on the eight squares surrounding the central one. In this way, it was ensured that every inclusion exiting the bounds of the square will appear on the opposite side, satisfying in this way the condition of geometrical periodicity. Square number five will be used as the periodic structure and the remaining eight squares will not participate any further in the analysis.

The additional section of the algorithm uses a bisection method in order to gather more fibres towards the centre and to increase the achievable volume fraction. The bisection method was developed as a root-finding method that repeatedly bisects an interval and selects a subinterval in which a root must lie. The bisection method is considered as being simple and robust but as a slow method for root-finding. Here the bisection method is implemented in order to optimise the maximum achievable volume fraction by rearranging the position of an accepted fibre towards the centre in order to make sure that space is used in the most efficient way.

A disadvantage of the second algorithm when compared with the first one is that the first one is able to control the total number of iterations by a volume fraction criterion. The algorithm keeps repeating its loops while the volume fraction is less than the desired one. The second algorithm does not use the volume fraction to define the iteration number of loops, but instead, a direct number of iterations is used as an input from the user. This implies a relation between the AR, the volume

fraction and the number of iterations in order to adjust those control parameters before running the algorithm to get the desired microstructure.

Studies comparing analyses of periodic microstructures in comparison with non-periodic microstructures show good agreement on tensile tests but a large deviation regarding shear tests. It was reported that non-periodic structures require higher sizes of RVE in order to predict accurate results. The concept of representative size is always strongly affected by the degree of accuracy that is needed. Additionally, there have been reports of the demand for high accuracy on non-periodic arrangements leading to extremely large RVE sizes.

3.3.2 Inclusion shape

Even if the appropriate projection of a three dimensional cylinder in two dimensions is a rectangle, the use of elliptical shape inclusions was preferred instead. The choice of elliptical domain ensures the minimisation of stress concentration points at the edge of the rectangle. The elliptical shape ensures a smooth slope from the middle of the ellipses to the edge, which confirms that no stress concentration will occur in the fibres' perimeter due to the shape of the inclusion. On the other hand, the sudden change of the geometry in a rectangle will cause serious problems for the UC to fulfil the ergodic hypothesis. The aspect ratio of a fibre is defined as the ratio between the length of the fibre over the diameter. In the case of elliptical shape inclusions the diameter is not constant and an average diameter or the maximum diameter may be used for AR calculations. Figure 3.11 shows the definition of aspect ratio for elliptical inclusions.

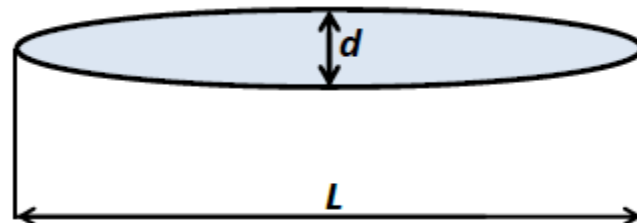


Figure 3.11 Aspect Ratio is defined as the ratio between fibre's length over the diameter.

Through literature it was observed that other variations of shapes are used in order to simulate cylindrical fibres in two dimensions. Regarding the very early simulations of microstructures rectangles were used. Implementation of rectangles in order to mimic 2D projection of cylindrical fibres introduces problems into the simulation as stress singularities. A solution for the stress singularities was proposed through the shape of sphere-cylinders. Sphere-cylinder consists of a rectangular body with two semi-circles at the edges.



Figure 3.12 Sphere-cylinder shape for 2D simulation of cylindrical fibres

3.3.3 In plane orientation distribution

The first step of the developed algorithm is the step which involves the declaration of constant parameters and random variables. Throughout this study, three random variables were considered. The first random variable is the coordinate of the centre of the ellipses. The second random variable is the fibre orientation and the third is the fibre length or aspect ratio. For all the models presented in this study, inclusions have random coordinates and the case of unidirectional fibres was first implemented. The second random variable implemented was the fibre's in-plane orientation. Three different variations of angle distribution will be presented through this study: unidirectional composite, randomly oriented composite and mis-oriented composite.

For randomly oriented composites the in-plane angle was able to take values in the closed interval between $0 - \pi$ (rad), and defined by a uniform distribution. The term 'closed interval' means that the interval includes its endpoints values. Figure 3.13 shows the in-plane angle distribution for a randomly oriented composite.

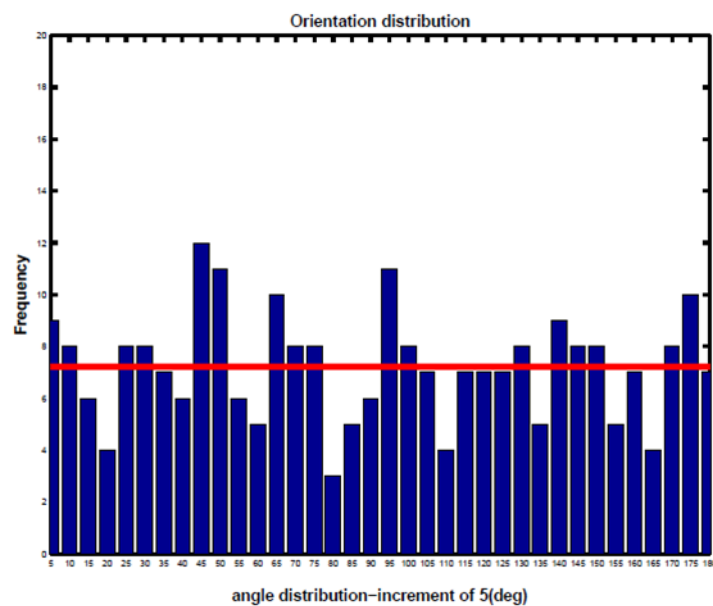


Figure 3.13 Orientation distribution for in-plane randomly oriented fibres.

It was observed that fibre orientation strongly influences the maximum achievable volume fraction and also the time that the algorithm needs in order to respond. Random values were seeded from a random number generator provided from Matlab by the command "*rand*" which creates uniformly distributed pseudorandom numbers on the open interval between $0 - 1$. The sequence of numbers produced by the aforementioned command is determined by the internal state of the uniform pseudorandom number generator that underlies the *rand* command.

In the case of mis-oriented fibres, the same command was used but restrictions on the angles were applied. In the plane angle for mis-oriented fibres it was restricted to take values on the close interval of $0 - 0.872$ (*rad*). By implementing this concept, the random nature of the in-plane angle was kept and simulation of mis-oriented microstructure was enabled. In-plane angle distribution for mis-oriented fibres can be seen in Figure 3.14.

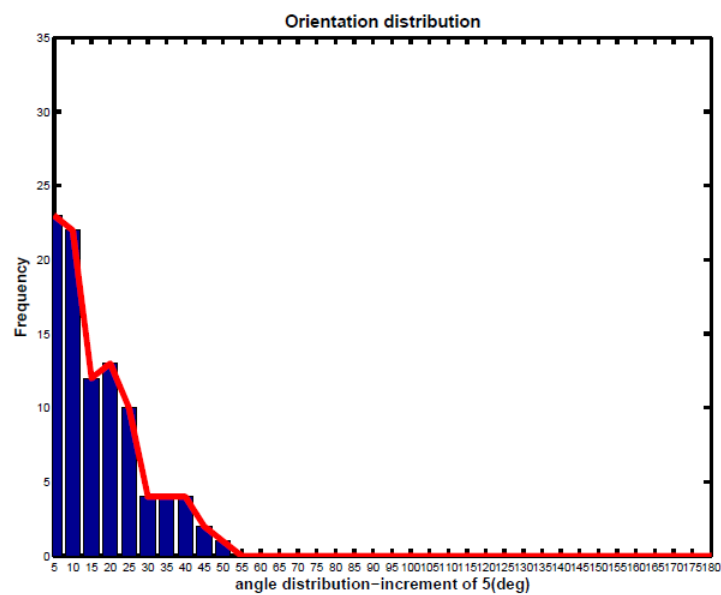


Figure 3.14 Distribution of fibres orientation for misaligned fibres.

3.3.4 Fibre length distribution

The third and last random variable is the fibre AR or fibre length. The variable was seeded from the same pseudorandom generator however restrictions were applied because fibre length could not be larger than the UC size. In order to overcome this difficulty, a function was implemented to modify results from the pseudorandom generator. The function considered the size of UC and the random parameter and can be expressed through Equation 3.4, where *a* and *b* denote the closed interval under investigation.

$$r = a + (b - a) * rand$$

Equation 3.4

Distribution of fibre length can be seen in Figure 3.15. The combination of random in-plane angle and random aspect ratio has a drastic influence on the achievable volume fraction and response time of the algorithm, hence in numerical simulations of short fibre composite, the random nature of fibres length must be considered.

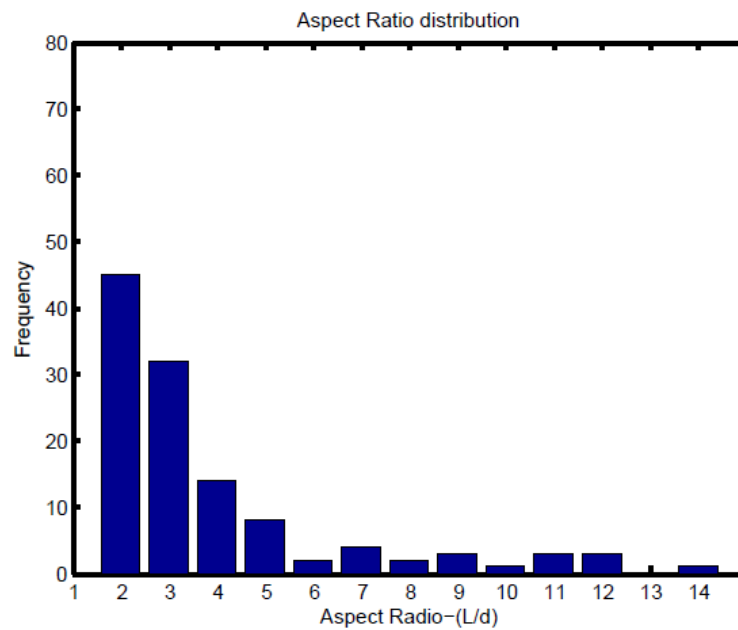


Figure 3.15 Distribution of fibre length-AR

Through the response of the aforementioned cases, the limitations and difficulties of the algorithm were raised. One of the major disadvantages is the response time in the case of high AR, or random in-plane orientation, or any combination of those two parameters; this topic will be further discussed in the next section. Also, the algorithm was not able to control the sequence of fibre length in a hierarchical way. Optimum solutions for the packing problem are an open research field which engineers and programmers are currently studying.

3.3.5 Algorithm time response

One of the main criteria for the efficiency of an algorithm is the time it needs to solve the problem. In the specific case of a packing problem, even for a given algorithm, there is no single answer because the response time depends on various parameters. The main parameters affecting the response time of the developed algorithm are:

- Aspect Ratio. The bigger the aspect ratio, the more difficult it is for the algorithm to place fillers in the container without any intersection. This mainly occurs because the higher the AR, the higher the possibility of intersection points, and the higher the possibility of rejection of a candidate fibre.
- Volume Fraction. Clearly there is a limitation on the maximum achievable volume fraction, which strongly depends on the fibre orientation and AR. However in general the higher the demand of V_f from the user, the more time the algorithm needs to solve the problem.
- Orientation. Orientation of fibres is also a parameter that strongly influences the time response of the algorithm. In general random orientations tend to need more time in order to be solved, mainly because the algorithm denotes numerous intersections and rejects numerous candidate fillers.
- UC size. As long as the size of a candidate RVE increases, the more fibres need to be included in the UC in order to reach the desirable V_f . As long as the number of fibres increases, the possibility of intersection between a new fibre and the existing fibres also increases. As a consequence the algorithm rejects higher number of fibres and needs more time to solve the problem for a desirable V_f .

In order to evaluate the efficiency of the developed algorithm, a built-in function was used at the beginning and at the end of the algorithm in order to count the time of response. In order to measure the actual time of results only, the time of creating the model of the microstructure was excluded from the measurement. Figure 3.16 shows the time response in minutes for cases of different orientation, different aspect ratio and different size. Bars are separated according to aspect ratio and orientation while each colour represents a different UC size.

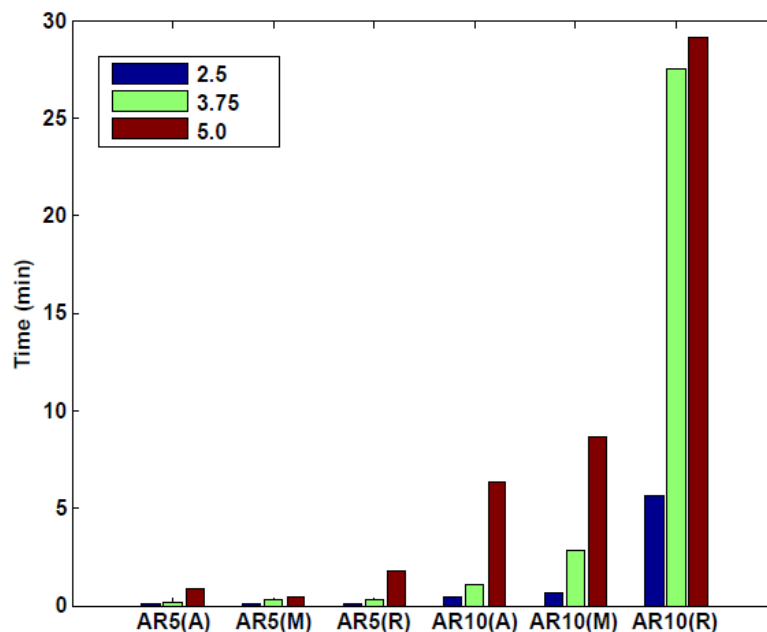


Figure 3.16 Time response of the developed algorithm for various values of AR and orientation.

3.4 Numerical models formation

The packing algorithm was developed in a Matlab programming environment and the developed microstructure was transferred to Abaqus FE commercial code through python scripting. Fibres were created through a process of partitioning a continuous media. The generated microstructure in Matlab was re-coded by python scripting language and introduced as a sketch which partitioned a two dimensional domain-container in order to create a two phase composite UC. Abaqus kernel can read-understand python scripts and turn them into geometrical configurations. A script is a text file containing scripting interface commands which can be interpreted directly by the kernel. Scripting in Abaqus has some major advantages. For example, by scripting, the whole process can be generated automatically, or a relatively minor change in the model can be done by changing a command instead of re-building the whole model.

Through the aforementioned advantages, a parametric study is also easier to execute. A characteristic python script of the microstructure is reported in Appendix II. The partitioning process separates a main domain into various subdomains in respect of the loaded part. By implementing the participation approach the discontinuity was introduced into the material as elliptical sub-domains with different elastic and thermal properties. By partitioning the two dimensional domain, the interface between fibres and matrix is assumed to be perfect. For the purposes of the current study, only linear properties will be investigated and further modelling of the interface is outside the scope of this study. The elastic and thermal properties of glass fibres and polypropylene can be seen in Table 3-1.

Table 3-1. Elastic and thermal properties of glass fibres and polypropylene.

Property	Glass fibres	Polypropylene
Young's Modulus (GPa)	73	1.2
Thermal Conductivity (W/mK)	0.05	0.15
Coefficient of Thermal Expansion (m/mK)	$4.3 * 10^{-6}$	$86.4 * 10^{-6}$

Models were meshed by using the environment of Abaqus 6.10 with two dimensional plane stress triangular elements. Those elements can be found in the Abaqus element library under the name *CPS3*. Figure 3.17 shows a typical example of a *CPS3* element.

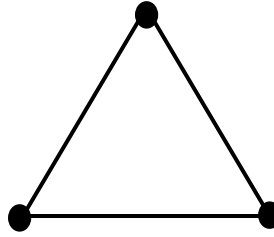


Figure 3.17 Plane stress element CPS3.

CPS3 are plane stress first order, linear triangular elements with three nodes and three faces. Each node has two kinematic degrees of freedom and a degree of rotation. Some characteristics of *CPS3* are their less than excellent convergence rate, their requirement of fine mesh to produce accurate results and a volumetric locking behaviour for incompressible materials.

It is known through finite element theory that quadrilateral elements produce more accurate results compared with triangular elements. In the specific study, the use of triangular elements was preferred due to the nature of the microstructure. The partitioning process of elliptical sub-domains of the two dimensional continued media, produces small areas which are extremely difficult to mesh with quadratic elements. The attempt to implement a quadratic element failed and an accurate meshing result was produced by only using triangular elements. *CPS3* offer a good meshing quality in a reasonable time and a low computational cost. The low computational cost is a result of the linear behaviour of the element and because it contains the minimum number of possible nodes. This was the main reason to develop a very fine mesh so that more accurate results can be obtained. In most cases for the developed models, the matrix domain was the one with areas that were very difficult to mesh. For this reason, and also to capture the developed stresses in the elliptical sub-domains, fibres and matrix were meshed with a different size. Element size for the fibres was chosen to be smaller compared with the element size of the matrix. A typical example of a meshed volume element can be seen in Figure 3.18.

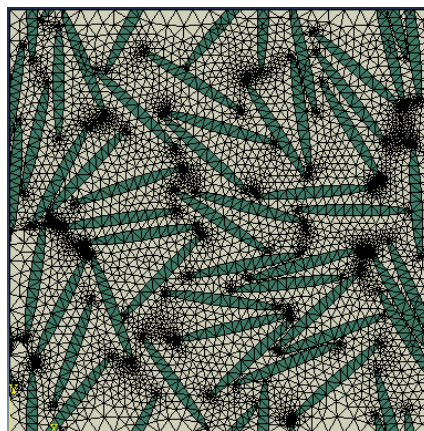


Figure 3.18 Typical mesh sample of randomly oriented UC.

Due to the difficulty of meshing the microstructure, in some cases high aspect ratio triangular elements were used to cover very demanding areas. For triangular finite elements, aspect ratio has the meaning of equal distance on the edge of the element with respect to a point on the centre of the element. This characteristic of the geometry of the elements can produce distorted elements during the analysis which shows locally stiffer behaviour due to this distortion. For every developed model, the actual number and the percentage of distorted elements was always calculated at the end of the analysis and models with distorted elements up to a certain limit were rejected for a lack of statistical homogeneity or for the local dominant behaviour. *CPS3* has an integration point placed in the middle of the triangle and standard linear shape functions are used to interpolate the edge displacement. Interpolation takes place according to the following Equation 3.5 and Equation 3.6 for "x" and "y" directions.

$$u = N_1x_1 + N_2x_2 + N_3x_3 \quad \text{Equation 3.5}$$

$$v = N_1y_1 + N_2y_2 + N_3y_3 \quad \text{Equation 3.6}$$

3.4.1 Boundary conditions

A key parameter of the effective properties derived from a multi-scale approach, such as the representative volume element framework, is the applied boundary conditions. Considering that the effective properties are calculated based on the developed stress and strain field in the RVE, which is a result of the applied boundary conditions, it can be understood that the selection of the appropriate boundary condition is a crucial step for numerical homogenisation methods.

There are mainly four different approaches on the concept of boundary conditions regarding simulating the RVE's response: Dirichlet boundary conditions, Neumann boundary conditions, the mixed boundary conditions and the periodic boundary conditions. Dirichlet boundary conditions are named after German mathematician Johann Peter Gustav Lejeune Dirichlet and are uniform kinematic boundary conditions, also known as the first type boundary conditions or the essential boundary conditions. As observed in Figure 3.19, uniform displacement is applied at the boundaries of a surface Γ_D .

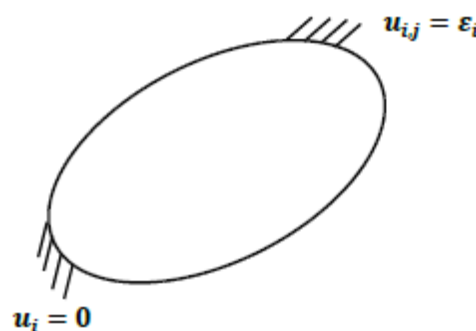


Figure 3.19 Dirichlet boundary conditions.

The second most commonly used boundary condition is the Neumann boundary condition. Neumann boundary conditions were named after German mathematician Carl Gottfried Neumann and are prescribed as uniform traction boundary conditions applied at the surface Γ_N , as can be seen in Figure 3.20. As reported by Hill, an RVE is considered to be well defined if results from those two different boundary conditions coincide.

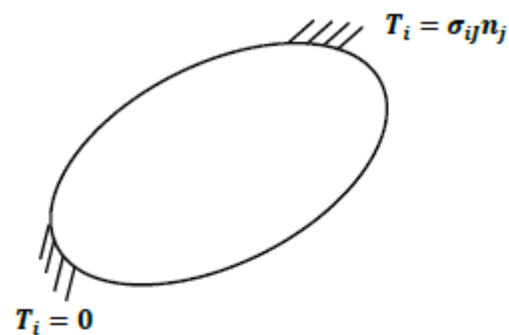


Figure 3.20 Neumann boundary conditions.

In the case of mixed boundary conditions, both cases of uniform displacement field and uniform traction field are applied simultaneously on a boundary surface Γ_M . For mixed boundary conditions, on a part of the boundary, uniform displacement is applied, while on a different part uniform traction boundary conditions are applied.

Periodic boundary conditions are widely used for multi-scale approaches. They are usually used in order to describe the conditions on the boundary of a small part located far away from the edge of a large system, which is the concept applied for representative volume simulations. Periodic boundary conditions are understood as the conditions which ensure compatibility by restricting nodes on the boundaries which are opposite each other to identically repeat their position before and after the deformation. Deformed bodies after implying periodic boundary conditions can be seen in Figure 3.21

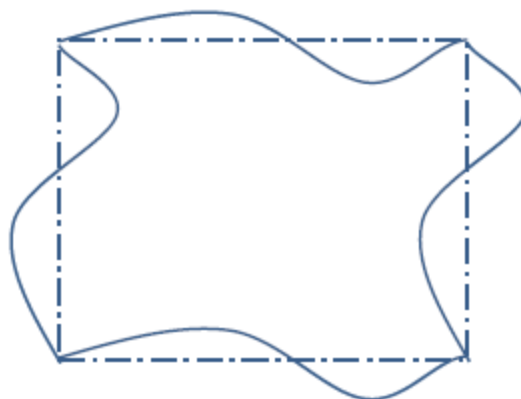


Figure 3.21 Periodic boundary conditions.

According to the periodicity assumption, the deformation of every boundary pair is equal and opposite in sign. For the thermal testing, boundary conditions were applied as temperature difference on the bounds of RVE. This temperature difference was able to create a heat flux field in the material which was then measured and values for the effective thermal conductivity were calculated. Figure 3.22 shows a typical example of RVE thermal loading for calculating longitudinal and transverse thermal conductivity.

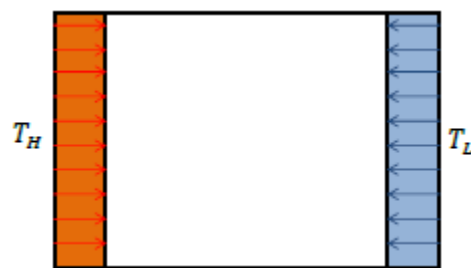


Figure 3.22 Boundary conditions for calculating longitudinal thermal conductivity.

For calculating the Linear Coefficient of Thermal Expansion (LCTE) the applied boundary conditions can be seen in Figure 3.23. As can be seen in Figure 3.23 the kinematic degrees of freedom on the surface-boards of the UC were fully constrained and a temperature difference was applied between left and right sides for longitudinal CTE and top and bottom for transverse CTE. As a result of the temperature difference thermal stresses were developed in the material while the macroscopic strains were equal to zero due to the kinematic constraints at the surface of the UC.

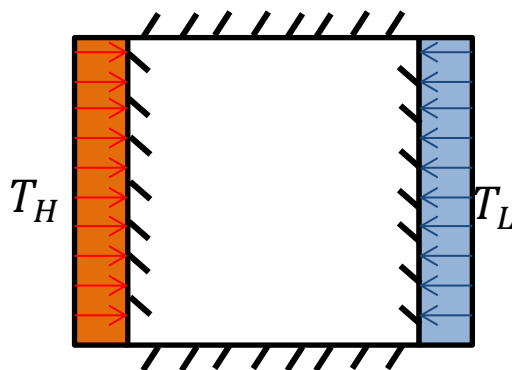


Figure 3.23 Boundary conditions for calculating Coefficient of Thermal Expansion.

Every developed RVE was examined for a mechanical, thermal and thermo-mechanical response in a concept of parametric study in which various parameters were changing for each case. A detailed report on the parametric study will take place in chapter 5. In order to derive the mechanical effective properties of a two phase short fibre composite, three mechanical virtual tests were performed for longitudinal tension, transverse tension and pure shear. Loading conditions for the cases of calculating the mechanical properties can be seen in Figure 3.24. Symbolic representation of the results from the applied loading conditions as seen in Figure 3.24, can be seen in Figure 3.25 for mechanical response and in Figure 3.26 for thermal response.

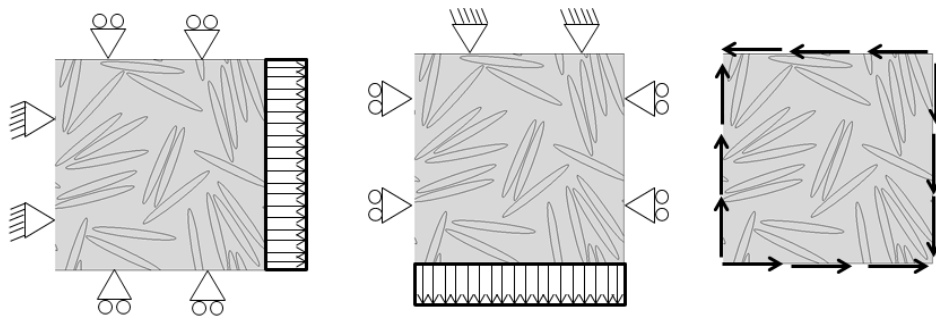


Figure 3.24 Loading conditions for effective longitudinal, transverse stiffness and effective shear stiffness.

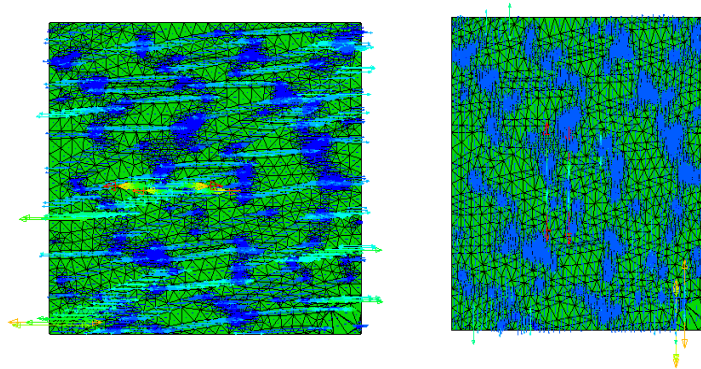


Figure 3.25 Symbolic representation of the developed stress field for longitudinal stiffness on the left and transverse stiffness on the right.

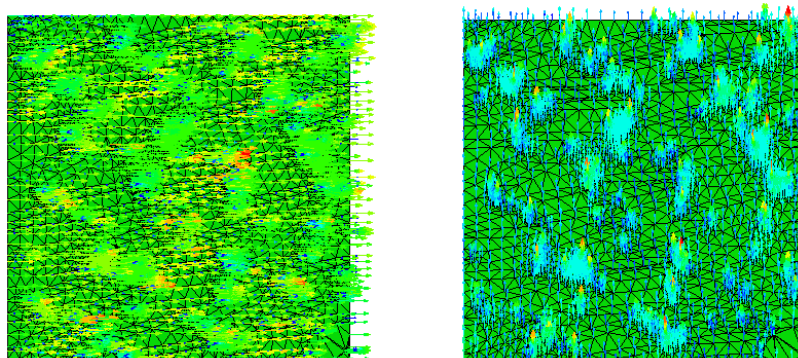


Figure 3.26 Symbolic representation of the developed stress field for longitudinal thermal conductivity on the left and transverse thermal conductivity on the right.

An output file from Abaqus was obtained after each analysis, which includes local values for stress, strain and volume of each element. Those files were then introduced into Matlab in which a developed script was able to further analyse data in order to obtain the average effective properties. A typical script for average effective properties can be seen in Appendix *III*.

3.5 Conclusions

In Chapter 3, various issues relating to the numerical modelling of short fibre composites were presented. The very basic problem of packing was first addressed and the major difficulties involved in finding a solution were presented, followed by further analysis of the proposed solution to the packing problem, through a developed packing algorithm. The main difficulties during the development of the algorithm were reported, followed by the limitations and the efficiency of the algorithm. The time response of the programme was discussed and the influence of various parameters on the time response of the algorithm were evaluated. The main assumptions of the modelling approach were presented and a discussion on the influence of those assumptions took place. Representation of fibres as elliptical domains was further discussed considering the advantages and disadvantages of this simplification. The concept of periodic and non-periodic microstructures was discussed and the way of implementing this periodicity was presented in detail. Definitions of the representative volume element were given and the common points on the different approaches from different researchers were reported. The differences between an RVE and a UC were also noted. The existence of RVE as a function of size was discussed and the implementation of length scales on the RVE concept was presented. A specific approach to the assumptions of modelling short fibre reinforced composite took place by analysing the simplification of the modelling microstructure with the properties of a real microstructure. The development of the packing algorithm using the Matlab programming package and the way of transferring the microstructure into the commercial FE software Abaqus through python scripting were presented. Finally, the various cases of boundary conditions used for RVE of microstructural units were addressed and advantages and disadvantages for each case were discussed.

4 Homogenisation approach

Homogenisation methods are widely used for material characterisation. The process of homogenisation involves the bridging of length scales. The purpose of the homogenisation methods is to obtain overall effective properties considering the response of the micro-structure. In a very general description, homogenisation can be seen as the characterisation of a material at lower scale where inhomogeneity exists, and its upscale to a fictitious energetically equivalent material. The concept of relating the microstructure with the overall composite response through a homogenisation process is taken into account by a representative volume element.

The opposite process of homogenisation is known as localisation process and is used for the local response of the material. The localisation process involves a “zooming in” on a smaller scale in the material. Localisation methods are generally more demanding than homogenisation due to the dependency of the local field with the micro-geometry of the constituents. For both cases, homogenisation and localisation, the main base of calculations is the geometry of the microstructure.

In the early years of development of homogenisation methods no computational power was available and as a result, various analytical homogenisation approaches have been developed. A few of those analytical homogenisation approaches were presented in chapter 2. Analytical homogenisation approaches can be described in two steps. The first step involves approximations of a local problem for a single inclusion embedded in an infinite matrix, and the second step consists of averaging the response of the local field. Under these considerations, as reported by (Klusemann, 2010) a homogenisation process requires:

- a) A simple structure which can be solved explicitly, such that a physical interpretation for the behaviour of all the components involved is possible.
- b) A valid structure for multiphase composites with various inclusion geometries, isotropy and anisotropies.
- c) An accurate model for the influence of various inclusion distributions and interactions between inclusions and their immediate surrounding matrix.

Even if the aforementioned analytical homogenisation approaches are widely used, none of them is accurately able to fulfil the previous requirements. The main drawback of the analytical processes lies in the assumption of the inclusion’s distribution and the considered material properties of the surrounding matrix. Homogenisation methods allow the calculation of effective material properties if the microstructure topology of the composite is known. The concept of homogenisation can be seen in Figure 4.1.



Figure 4.1 An illustration of the concept of homogenisation and length scales.

The homogenisation method aims to define an equivalent homogeneous media, able to replace the composite media with a homogeneous one in order to solve the problem of material characterisation using a global approach. The strong advantages of the method are that it needs only the information of the microstructure and that any kind of microstructure can be implemented. Apart from material characterisation of elastic properties, homogenisation methods can be accurately used for different fields, such as flow in porous media, heat transfer problems, viscoelastic related problems or coupling fields problems such as piezoelectric material analysis.

Throughout the following chapter, the topic of computational homogenisation will be discussed and the implemented homogenisation approach for this study will be further analysed. Through the second sub-section, Hill's condition for equivalent homogeneous media will be presented. Through the computational homogenisation approach the concept of representative volume element will be analysed and also the statistical analysis on RVE results will be explained. The fourth chapter concludes with a discussion on the properties under investigation and how those properties are affecting the accuracy of the RVE. A further discussion takes place about the effect of micromechanical parameters (aspect ratio, orientation and fibre length) on the results of the statistical analysis and also the size dependency of the RVE will be discussed.

4.1 Computational homogenisation

Computational homogenisation methods are implemented and treated in a similar way to analytical homogenisation methods. The aim of the process is to derive homogeneous properties of a material exhibiting a heterogeneous structure on a smaller scale. The main advantage of the numerical approach as compared with the analytical one is the ability of numerical homogenisation methods to account for multiple heterogeneities in the material, while the majority of analytical models are built-in with the basic assumption of analysing a heterogeneity embedded in an infinite matrix. This advantage provides the ability for the development of a more complex stress-strain field in the representative volume due to the interaction between heterogeneities.

A multi-scale approach from the computational point of view can be divided in three steps:

- during the first step the material is considered on a larger scale (macro-level),

- a further zooming in into the material is considered during the second step, where information of the micro or meso levels are derived.
- The third and final step involves the process of transferring information from the smaller scale to the macro-scale where the effective properties are calculated.

The aforementioned steps can be summarised as the process during which macro-level strains are introduced as boundary conditions into the lower scale, at which scale the material is considered as heterogeneous. A homogenisation process then takes place and effective properties can be calculated. The process of a multi-scale approach can be seen in the schematic in Figure 4.2.

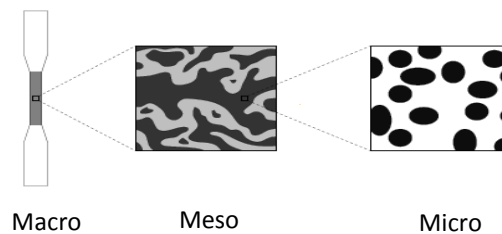


Figure 4.2 Schematic representation of the multi-scale approach. Adapted from Helmut J. Bohm.

The multi-scale approach from a macro scale to a smaller scale can be seen as that the macro-strains are translated through boundary conditions into the displacement field on a lower scale. Equation 4.1 shows a typical form of periodic boundary conditions where macro-strains and local displacement are connected.

$$u_i^t - u_i^b = \varepsilon^i (x_i^t - x_i^b)$$

Equation 4.1

On the other hand, connection of a meso or micro scale to a larger scale implies that information of the smaller scale must be used in order to upscale effective material properties. This process is called homogenisation and will be further analysed in the following chapter. The main computational homogenisation approaches that will be presented in this chapter are the Asymptotic Homogenisation Method, the Volume Average Homogenisation and the Reaction Force Approach. All of the aforementioned methods have been used widely in literature.

4.1.1 Asymptotic homogenisation approach.

A general definition of the asymptotic homogenisation approach is that of a method used to solve partial differential equations. The asymptotic homogenisation approach is a very good method for modelling physical procedures on a periodic structure taking place in a heterogeneous material. The physical procedure can be heat transfer, electric conductivity or mechanical loading. The main advantages of the AHM are the fact that it allows a significant reduction in the degrees of freedom involved in the problem and that it has the capability of calculating stress and strain fields on the micro-structure associated with the given macro-structural field. However, the method AHM has a restriction in that it can only be used with periodic arrangements.

The concept behind the asymptotic homogenisation scheme is that on a material volume \mathcal{H} as defined in Figure 4.3, consist of a heterogeneous microstructure define in a region \mathcal{F} , which exhibits geometrical periodicity. On the periodic representation of the microstructure \mathcal{F} , a coefficient ψ can be defined as the connection between micro- and macro scales, or can be seen as the connection between the characteristic dimension between the two length scales.

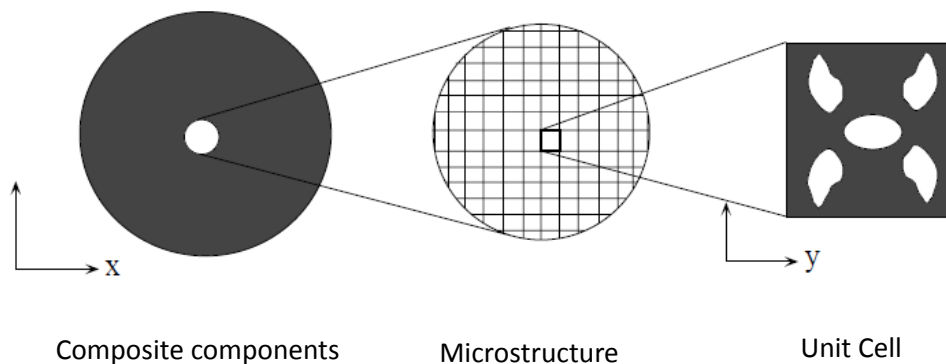


Figure 4.3 Asymptotic Homogenisation approach. Adapted from Helmut J. Bohm.

Once such a periodic structure is exposed to traction or kinematic boundary conditions, a periodic oscillation on the resulting stress and strain field will occur. The aforementioned oscillations are results of the periodicity of the microstructure and can be expressed as a function of the dimension coefficient ψ . Under the previous considerations, a clear separation of scales must occur. Let's clearly define the two different scales as x associated to the macro-scale and y associated to the microscale. As a result, it appears that variables associated to the referred fields depend on both x and y systems through Equation 4.2.

$$y = \psi/x \quad \text{Equation 4.2}$$

Function ψ exhibits a periodic behaviour in \mathcal{F} which is usually called \mathcal{F} -periodicity. As a consequence of the periodicity of function ψ in domain \mathcal{F} , the elasticity tensor in domain \mathcal{F} appears to exhibit the same periodicity. Therefore, material elastic properties are dependant on the response of the microstructure or of the domain \mathcal{F} . The last sentence can be expressed through Equation 4.3.

$$C_{ijkl} = C_{ijkl}(\mathcal{F}) \quad \text{Equation 4.3}$$

In the macro-scale system where the x dimension parameter is involved, heterogeneities of the microstructure appear in a periodic way of inversely proportionality of the parameter ψ . This can be expressed through Equation 4.4.

$$C_{ijkl} = C_{ijkl}(\psi) \quad \text{Equation 4.4}$$

With the assumption of infinitesimally small strains, the equilibrium condition on linear elasticity, the definition of stains and the constitutive equation for a linear elastic response can be seen through Equation 4.5, Equation 4.6 and Equation 4.7.

$$\frac{\partial \sigma_{ij}^{\psi}}{\partial x_{ij}^{\psi}} + f_i = 0 \quad \text{Equation 4.5}$$

$$\varepsilon_{ij}^{\psi} = \frac{1}{2} (u_{i,j}^{\psi} + u_{j,i}^{\psi}) \quad \text{Equation 4.6}$$

$$\sigma_{ij}^{\psi} = C_{ijkl}^{\psi} \varepsilon_{kl}^{\psi} \quad \text{Equation 4.7}$$

In the previous equations σ_{ij}^{ψ} and ε_{ij}^{ψ} represent Cauchy tensors for stresses and strains, the superscript ψ stands for the ψ, \mathcal{F} –periodicity of the given variable on the macro-coordinate system. Through the previous considerations the problem then can be summarised as the solution of the displacement field on the variation problem expressed through Equation 4.8.

$$\int_{\mathcal{H}} C_{ijkl}^{\psi} \frac{\partial u_k^{\psi}}{\partial x_l^{\psi}} \frac{\partial u_i^{\psi}}{\partial x_j^{\psi}} d\Omega \quad \text{Equation 4.8}$$

Considering the existence of two well separated scales which connect material properties of the micro-scale domain ψ and the macro-scale domain \mathcal{H} , the displacement field can be asymptotically approached as in Equation 4.9.

$$u_i^{\psi}(\mathbf{x}) = u_i^{(0)}(\mathbf{x}, \mathbf{y}) + \psi u_i^{(1)}(\mathbf{x}, \mathbf{y}) + \psi^2 u_i^{(2)}(\mathbf{x}, \mathbf{y}) + \dots \quad \text{Equation 4.9}$$

In the previous equation the terms $u_i^{(p)}(\mathbf{x}, \mathbf{y})$ are called correctors of order p or \mathcal{F} -periodic functions of the displacement field. Considering Equation 4.6 and the chain rule of function differentiation, the strain field can be asymptotically approximated as in Equation 4.10.

$$\varepsilon_{ij}^{\psi} = \psi^{-1} \varepsilon_{ij}^{(0)}(\mathbf{x}, \mathbf{y}) + \psi^0 \varepsilon_{ij}^{(1)} + \psi^1 \varepsilon_{ij}^{(2)} + \dots \quad \text{Equation 4.10}$$

Where in the previous equation ε_{ij}^p is defined as in Equation 4.11.

$$\varepsilon_{ij}^p = \frac{1}{2} \left(\frac{\partial u_i^{(p-1)}}{\partial x_j} + \frac{\partial u_j^{(p-1)}}{\partial x_i} + \frac{\partial u_i^{(p)}}{\partial y_j} + \frac{\partial u_j^{(p)}}{\partial y_i} \right) \quad \text{Equation 4.11}$$

Combining the previous equation with Equation 2.1 and making use of Equation 4.3, the stress field may be expressed in an asymptotic approach as can be seen in Equation 4.12.

$$\varepsilon_{ij}^{\psi} = \psi^{-1} \varepsilon_{ij}^{(0)}(\mathbf{x}, \mathbf{y}) + \psi^0 \varepsilon_{ij}^{(1)} + \psi^1 \varepsilon_{ij}^{(2)} + \dots \quad \text{Equation 4.12}$$

By implementing Equation 4.5 and considering the previous equation, a set of differential equations can be defined as a function of the parameter ψ . The solution of the set of differential equations, can be calculated recursively with respect to Dirichlet's and Neumann's boundary conditions. Each time a variable of $p - 1$ order is obtained, the calculation of the variable in p order is enabled. The method is widely used in the literature by numerous researchers for the purpose of material

characterisation. Despite the computational cost, the method has been reported as accurate enough for material characterisation.

4.1.2 Volume average method

A very direct way of obtaining the overall homogenised properties of a heterogeneous material is by calculating the volume average properties of the media. This can be implemented through the average stress and average strain theorems. The method is used on the resultant stress and strain field, on the representative volume. Local properties of the constituents and the geometric shape of the inclusions are strongly influence the developed microscopic stress and strain field. A volume average can be performed on the developed micro-stress and micro-strain field.

Through this process information of the local response of the structure are introduced into the calculations by the volume average. With respect to homogeneous stress boundary conditions (Neumann boundary conditions), traction is given as in Equation 4.13 and is supposed to be prescribed on the boundaries.

$$T = \Sigma \cdot n \quad \text{Equation 4.13}$$

here T denotes the surface traction while Σ denotes the known macroscopic stress tensor and n denotes the unit vector outward normal at the boundary. From the previous equation it can be proven that Σ is equal to the volume average stresses in the RVE. It can be shown that for every equilibrated stress field that obeys the scales separation assumption expressed through Equation 3.1, the macroscopic volume average stresses can be calculated through the average stress theorem. Equation 4.14 shows the process of calculating volume average stress.

$$\bar{\sigma}_{ij} = \int_V \sigma_{ij} dV \quad \text{Equation 4.14}$$

In a similar way, homogeneous strain boundary conditions (Dirichlet boundary conditions) are expressed through prescribed displacement at the boundary of the RVE which can be expressed through Equation 4.15

$$u = E \cdot x \quad \text{Equation 4.15}$$

Wherein the previous equation u expresses displacement on the boundaries of RVE, E represents the macroscopic strain tensor. The aforementioned approximation is valid as long as Equation 3.1 is satisfied. Equality of the macroscopic applied strain with the average strain in the RVE can be satisfied from every compatible strain field obeying Equation 4.15. The average strain can be expressed through Equation 4.16.

$$\bar{\varepsilon}_{ij} = \int_V \varepsilon_{ij} dV \quad \text{Equation 4.16}$$

For the implementation of the average stress and average strain theorems, in order to calculate the volume average stress and the volume average strain, integrals were approached as summations as expressed in Equation 4.17 and Equation 4.18.

$$\bar{\sigma}_{ij} = \sum_{k=1}^{NoE} \sigma_{ij}^k V^k \quad \text{Equation 4.17}$$

$$\bar{\varepsilon}_{ij} = \sum_{k=1}^{NoE} \varepsilon_{ij}^k V^k \quad \text{Equation 4.18}$$

where the superscript k refers to the k^{th} element and σ_{ij} and ε_{ij} are local quantities of stress and strain respectively measured from the integration point of every element. Figure 4.4 shows a triangular *CPS3* element and the position of the integration point.

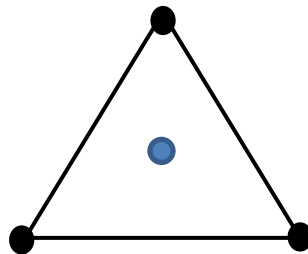


Figure 4.4 Plane stress triangular element with a single integration point

Where $\bar{\sigma}_{ij}$ and $\bar{\varepsilon}_{ij}$ represent the volume average quantities of stresses and strains respectively, while σ_{ij} and ε_{ij} represents the micro-stress and micro-strain field respectively, V represents the volume

of the RVE. The homogenisation process through volume average quantities is a process which needs information from the micro-scale. This information can be measured through the finite element analysis. Implementation of boundary conditions leads to a micro-stress and micro-strain field on the RVE. For every element, local quantities of stresses and strains are measured. Micro-stresses and micro-strains are then implemented into Equation 4.17 and Equation 4.18 and the volume average quantities are calculated. Further implementation of Equation 2.1 leads to the homogenised stiffness tensor. A detailed discussion will take place in chapter 4.3.

4.1.3 Reaction force homogenisation approach

A simpler and computationally less expensive approach when compared with the previous two homogenisation approaches is the reaction force homogenisation approach. The principal concept of the reaction force homogenisation approach comes from the classical definition of mechanical stress which is the division of the applied force with the cross section area as expressed through Equation 4.19.

$$\bar{\sigma}_{ij} = F_i^j A^{-1} \quad \text{Equation 4.19}$$

where for the above equation F_i^j represents the reaction force on the i direction for the j loading case on the boundary face of the area A . As reported from (Pan, 2008), even if the reaction force method is a very simple approach of calculating homogeneous stresses, comparing the time of response, the computational effort and the simplicity of use, results from the method show a comparable accuracy with the previous two homogenisation methods. For some cases of computational homogenisation, time response and computational cost are dominant parameters. For those cases the reaction force homogenisation approach is the ideal case.

4.2 Macro-homogeneity condition

Scale transition processes such as the homogenisation or localisation processes must satisfy the macro-homogeneity condition also known as the Hill-Mandel condition. Through the macro-homogeneity condition, the equivalence of the strain energy between the heterogeneous material and the equivalent homogeneous one is ensured. The Hill-Mandel condition can be expressed through Equation 4.20.

$$\frac{1}{2V} \int_V \sigma_{ij} \varepsilon_{ij} dV = \frac{1}{2} \bar{\sigma}_{ij} \bar{\varepsilon}_{ij} \quad \text{Equation 4.20}$$

For Equation 4.20 the consequence of the macro-homogeneity condition is that the fluctuation fields on the boundary of the RVE can be replaced by a homogeneous field.

4.3 Effective properties under investigation

For the purposes of this research, mechanical, thermal and thermo-mechanical properties were investigated. The appropriate boundary conditions were applied in order to cause the response of the effective stiffness in the longitudinal and transverse direction, as well as the response of the effective shear modulus. For the thermal properties, thermal conductivity of various cases of orientation for a two phase composite was calculated regarding the longitudinal and transverse directions. The thermo-mechanical property under investigation is the linear coefficient of thermal expansion. A solution for the linear coefficient of thermal expansion implies the application of thermal and kinematic boundary conditions, and from a numerical point of view, a coupling thermo-mechanical problem must be solved. Table 4-1 shows all the properties under investigation.

All the aforementioned properties were investigated with respect to fibre orientation, fibre aspect ratio, fibre length distribution and RVE size. Those were the main parameters of the study for the mechanical, thermal and thermo-mechanical behaviour of short fibre composite. For every case of loading conditions, the appropriate micro-quantity was measured on the integration point of every element. For the case of mechanical effective properties, longitudinal and transverse effective stiffness were calculated once measurement of micro-stresses, micro-strains and volume took place from every integration point in an element.

For calculating the longitudinal effective stiffness, stress σ_{11} and strain ε_{11} must be measured for every element with the value of the volume of the element. For the case of transverse effective stiffness, the analogous stress σ_{22} and strain ε_{22} must be measured along with the volume of the corresponding element. Stress and strain quantities represent the reaction of the heterogeneous material and are used through the average stress and average strain theorems as they were presented in the previous section.

Table 4-1 Properties under investigation

Symbol	Property	Orientation	Aspect Ratio	RVE size	Fibre length distribution
E_1	Longitudinal Stiffness				
E_2	Transverse Stiffness				

G_{12}	Shear modulus				
K_1	Longitudinal thermal conductivity	I. Aligned fibres II. Mis-aligned fibres III. Randomly oriented fibres	I. AR=1 II. AR=5 III. AR=10	I. RVE size=2.5 II. RVE size=3.75 III. RVE size=5.0	I. Constant fibre length II. Random fibre length
K_2	Transverse thermal conductivity				
a_1	Longitudinal coefficient of thermal expansion				
a_2	Transverse coefficient of thermal expansion				

4.3.1 Elastic properties

The effective mechanical properties are calculated as elements of the effective stiffness tensor for the case of two dimensional plane stress conditions. Boundary conditions were applied in such a way as for every virtual experiment-loading condition- samples were loaded macroscopically towards a single direction. As a consequence for every loading condition, just a single element of the strain tensor is active while all the remaining elements are zero. This can be seen in Equation 4.21 which shows the generalised expression for the one-dimension loading condition of Hooke's law for the two dimensional plane stress condition for calculating the longitudinal stiffness.

$$\begin{Bmatrix} \sigma_{11} \\ \sigma_{22} \\ \sigma_{12} \end{Bmatrix} = \begin{bmatrix} C_{11} & C_{12} & C_{16} \\ C_{21} & C_{22} & C_{26} \\ C_{16} & C_{26} & C_{66} \end{bmatrix} \begin{Bmatrix} \varepsilon_{11} \\ 0 \\ 0 \end{Bmatrix} \quad \text{Equation 4.21}$$

Expansion of the previous system of equations leads to a single equation with a single unknown as can be observed in Equation 4.22 , which has a trivial solution.

$$\sigma_{11} = C_{11}\varepsilon_{11} + C_{12}0 + C_{16}0 \quad \text{Equation 4.22}$$

For the case of calculating the transverse effective stiffness, the applied boundary conditions must ensure what is stated in Equation 4.23. For transverse effective stiffness the only element of macroscopic strain which is not zero must be the one which refers to the transverse direction's strains.

$$\begin{Bmatrix} \sigma_{11} \\ \sigma_{22} \\ \sigma_{12} \end{Bmatrix} = \begin{bmatrix} C_{11} & C_{12} & C_{16} \\ C_{21} & C_{22} & C_{26} \\ C_{16} & C_{26} & C_{66} \end{bmatrix} \begin{Bmatrix} 0 \\ \varepsilon_{22} \\ 0 \end{Bmatrix} \quad \text{Equation 4.23}$$

Expansion of the previous system of equations as in the case of longitudinal stiffness leads to the expression in Equation 4.24 with a single unknown as long as the remaining elements of the strain tensor are zero.

$$\sigma_{22} = C_{21}0 + C_{22}\varepsilon_{22} + C_{16}0 \quad \text{Equation 4.24}$$

In the case of effective shear modulus, only the last element of the strain tensor is active as can be seen in Equation 4.25

$$\begin{Bmatrix} \sigma_{11} \\ \sigma_{22} \\ \sigma_{12} \end{Bmatrix} = \begin{bmatrix} C_{11} & C_{12} & C_{16} \\ C_{21} & C_{22} & C_{26} \\ C_{16} & C_{26} & C_{66} \end{bmatrix} \begin{Bmatrix} 0 \\ 0 \\ \varepsilon_{12} \end{Bmatrix} \quad \text{Equation 4.25}$$

As a consequence, the system of equations is reduced, as in the previous two cases, to a single equation with a single unknown as stated in Equation 4.26.

$$\sigma_{12} = C_{61}0 + C_{62}0 + C_{66}\varepsilon_{12} \quad \text{Equation 4.26}$$

4.3.2 Thermal properties

For calculating the thermal effective properties, a similar procedure took place, with the main difference being the actual loading conditions applied on the bounds of RVE. In order to calculate the effective thermal conductivity, first the overall heat flux of the RVE must be calculated and results must be applied on Fourier's law for thermal conductivity. The time dependent form of Fourier's law can be seen in Equation 4.27.

$$\nabla \cdot (K\nabla T) = \rho C_p \frac{\partial T}{\partial t} \quad \text{Equation 4.27}$$

Where in the above equation ρ represents density of the material while C_p represents the specific heat. For the purpose of this research, thermal conductivity will be investigated for the steady-state condition. The steady-state condition describes the response of the material in terms of thermal conductivity, once every dynamic phenomenon that takes place through the heat transfer process is constant and does not cause any time-dependent changes on the spatial distribution of thermal conductivity.

A material, after a specific amount of time known as equilibration time, will reach a point in which there will be no time dependency. As a consequence of Equation 4.27 (Fourier's full version of heat transfer) all the partial derivatives of temperature with respect to time variables will vanish. The steady-state version of Fourier's thermal conductivity law can be seen in Equation 4.28.

$$q_i = K_i \frac{\partial T}{\partial i} \quad \text{Equation 4.28}$$

Effective homogenised thermal conductivity is calculated through a similar process, as described for effective mechanical properties. First, it must be noted that for thermal properties the UC was meshed with different element type. Elements with a code name *DC2D3* were used. *DC2D3* element is a diffusive 3-node linear heat transfer triangle and it has three integration points. Values for local heat flux were measured from every integration point of every element. Firstly an average quantity between the three integration points was considered and the total heat flux was calculated through a summation expressed in Equation 4.29.

$$Q_x = \sum_{i=1}^{NoE} q_i A_i \quad \text{Equation 4.29}$$

where for the above equation q_i represents the local heat flux measured from the i^{th} element, while A_i represents the area of the i^{th} element. The heat flux of every element was measured as the arithmetic average between the three integration points. In order to calculate the total average heat flux on the UC, the total area must be first calculated. The total area of the RVE is calculated through the summation expressed in Equation 4.30.

$$A_x = \sum_{i=1}^{NoE} A_i \quad \text{Equation 4.30}$$

In the above equation A_i represents the area of the i^{th} element. Once the total heat flux is calculated and the total area is known, the average heat flux of the RVE can be calculated through Equation 4.31.

$$q_i = Q_i/A \quad \text{Equation 4.31}$$

where for the above equation q_i represents the average heat flux on the i^{th} direction. The system of equations which needs to be solved in order to calculate the average heat flux can be seen in Equation 4.32.

$$\begin{pmatrix} q_x \\ q_y \\ q_z \end{pmatrix} = \begin{bmatrix} K_{xx} & K_{xy} & K_{xz} \\ K_{yx} & K_{yy} & K_{yz} \\ K_{zx} & K_{zy} & K_{zz} \end{bmatrix} \begin{pmatrix} \partial T / \partial x \\ \partial T / \partial y \\ \partial T / \partial z \end{pmatrix} \quad \text{Equation 4.32}$$

Again, as in the mechanical boundary conditions for each loading condition, only one of the temperatures gradients is not zero, the rest of them have no value! In this way the calculation of a single element of the effective thermal conductivity matrix was possible for every single loading condition.

4.3.3 Thermo-mechanical properties

For the case of thermo-mechanical loading conditions, in order to calculate the effective linear coefficient of thermal expansion, a combination of kinematic and thermal boundary conditions must

be applied on the borders of RVE. Figure 4.5 shows the applied boundary conditions for calculating the effective linear coefficient of thermal expansion.

As can be seen in Figure 4.5, the RVE is kinematically restricted all around the boundaries and a temperature difference is applied between the left and the right sides for longitudinal thermal expansion and from bottom to the top for transverse thermal expansion.

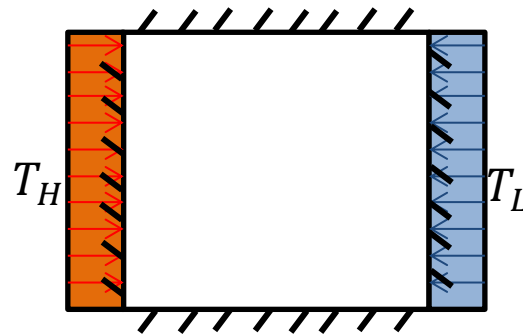


Figure 4.5 Applied boundary conditions for calculation of the CTE

The thermal difference on the bounds of the UC will cause a heat flux through the media and strains due to the different constituent's thermal expansion of the constituents will be developed. At the same time, the kinematic restrictions on the boundaries of the UC in combination with the developed strains will cause the rise of thermal stresses. In order to simulate this process, *CPE3T* elements from Abaqus library were used. *CPE3T* is a couples displacement-temperature linear triangular element.

Both developed stresses and strains in the UC are measured and the volume average quantities are calculated through the average stress and average strain theorems as they were presented in Equation 4.14 and Equation 4.16. Calculation of the effective linear coefficient of thermal expansion can be completed once the system of equations provided by Equation 4.33 is solved.

$$\begin{Bmatrix} \sigma_{11} \\ \sigma_{22} \\ \sigma_{12} \end{Bmatrix} = \begin{bmatrix} C_{11} & C_{12} & C_{16} \\ C_{21} & C_{22} & C_{26} \\ C_{16} & C_{26} & C_{66} \end{bmatrix} \begin{Bmatrix} \varepsilon_{11} + a_{11}\Delta T \\ \varepsilon_{22} + a_{22}\Delta T \\ \gamma_{12} + a_{33}\Delta T \end{Bmatrix} \quad \text{Equation 4.33}$$

From the above equations the macro-strains denoted as $\varepsilon_{11}, \varepsilon_{22}$ and ε_{33} are equal to zero as a consequence of the overall kinematic restrictions on the boundaries of the RVE. Stresses are calculated through the average stress theorem. The effective stiffness tensor is evaluated from the

pure mechanical homogenisation process and the same values were used for solving the thermo-mechanical problem.

4.4 RVE approach

All the aforementioned calculations were executed under the framework of a representative volume element. The real question that we are going to examine in this section is what is considered as representative and what process must take place in order to justify the representativeness of the unit cell. Also, the influence of various micromechanical parameters on the representativeness of the UC will be under discussion. The answer to this question comes from further statistical analysis of the results of the homogenisation process. For that purpose five realisations were developed for every combination possible.

In the following sub-section the concept of statistical analysis of the response of the composite material will be presented. A further explanation on the statistical test which was used will take place. An investigation of the influence of different parameters on the results of the statistical analysis will be carried out. That means that if we consider

- three different cases of orientation,
- three different cases of RVE's size,
- three different cases of aspect ratio and also
- investigation of seven different mechanical, thermal and thermo-mechanical properties
- for five developed "samples"

the number of differently solved models rises to more than 945.

4.4.1 Chi-square test

Having results for the five different realisations from every possible combination of the parameters under investigation, the next step is to normalise all the results with respect to the higher value of the five realisations. The normalisation process takes place in order to restrict all the values or different properties between the open interval of 0 – 1. As a consequence all the properties under investigation will have values on the same order of magnitude and a direct comparison can take place.

The statistical test which was used is the chi-square test. The chi-square test properties were investigated by a British mathematician named Karl Pearson at the beginning of the 20th century. The Chi-square test can be seen in Equation 4.34.

$$x^2 = \sum_{i=1}^{NoR} \frac{(O_i - E_i)^2}{E_i}$$

Equation 4.34

where for the above equation O_i represents the observed value for the i^{th} realisation, while E_i represents the expected value. The test actually calculates the deviation of the observed frequency with the expected frequency for a set of values and in combination with the statistical degrees of freedom of the problem, the test provides table values from which a decision about accepting or rejecting the results can be made. The test also provides a comparison between the observed values of a set which has properties of chi-square distribution and the expected value of the set. Table values for the chi-square test, for any degree of freedom and any level of accuracy, can be found in Appendix IV. Implementation of the Equation 4.34 and comparison of the equation results with the table values for a specific degrees of freedom and specific accuracy, will be the process by which we will examine whether the volume element is representative or not.

Throughout this study we observed that the results of the chi-square test are influenced by all the parameters that are introduced into the system as modifications of the microstructure. The main parameter that dramatically changes the results of the chi-square test is the UC size. This was expected from the beginning because as has been reported in literature the larger the size of UC, the more information it includes about the micro-structure, and as a consequence, the more representative it is. On the contrary, a very large UC is a computationally expensive problem to solve.

The real question about size has turned out to be “Which is the smallest representative size?” and also what parameters and to what degree they influence the representativeness of a UC. The smallest size is needed in order to save computational time and power. It was also observed that the results of the chi square test were also influenced from the property under investigation, the orientation of the inclusions, the aspect ratio and also the distribution of the fibre length. Throughout the following section, the influence of all the aforementioned parameters will be discussed and results from the chi square test will be provided.

4.4.2 Chi-square test and inclusion's orientation

It has been reported in the literature that periodic arrangements of micro-structure need a smaller RVE size in order to be representative and this is due to the repeated periodic micro-structure of the material. As a consequence, every parameter that enters the system and has a stochastic nature will influence the size of RVE, however it is under investigation if that influence is positive (leading to a smaller UC size) or negative (leading to a larger UC size). The first case under investigation is fibre spatial arrangements. The stochastic parameter in this case is the random position of the fibres. As observed in Figure 4.6, all the inclusions have the same aspect ratio, same orientation distribution and uniform length but they differ regarding the actual position of each inclusion in space, or the orientation of each individual inclusion. By examining the difference in the response of those five realisations, one will be in a position to understand if any movement of the inclusion in any other position in space will influence the effective properties of the UC. For representative sizes, the RVE is considered to be large enough so that derived effective properties are not influenced by the different fibre's position or any other parameter. Once the five realisations seen in Figure 4.6 have results that deviate from each other, that is a clear indication that the size of the UC is not big

enough to include all the necessary information for the response of the material and because each sample responds differently, under the same loading conditions, depending on its microstructure.

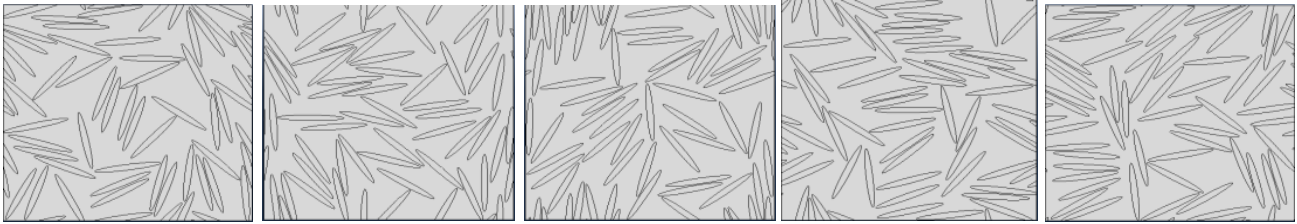


Figure 4.6 Five realisations of a UC consisting of the same V_f , the same AR, the same orientation distribution and the same UC size.

Through the following paragraphs, the influence of inclusion orientation on the value of the Chi-square test will be examined. Figure 4.7 shows the distribution of Chi-squares values with respect to the UC size for the three different cases of orientation distribution.

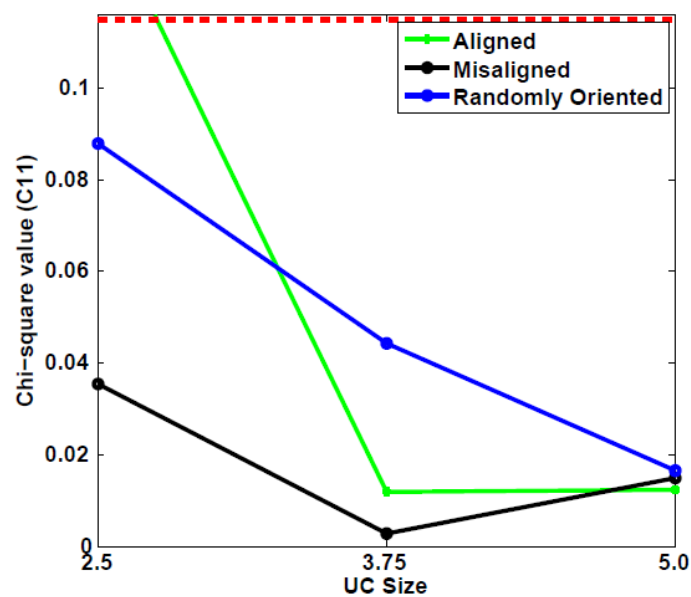


Figure 4.7 Chi-square values for longitudinal stiffness for realisations with AR=10 and three cases of orientations.

For the above figure, values of the chi-square test for the longitudinal effective stiffness with $AR = 10$ are presented. As can be observed in Figure 4.7, the chi-square test does not follow any linear pattern with respect to the inclusion's orientation. There is no linear relation between the number of stochastic parameters entering the system and the actual value of the chi-square test. This can be observed because aligned fibres have a higher chi-square value than randomly oriented fibres and the lowest chi-square value is for mis-aligned fibres, while for a linear relation one must expect the series to be aligned fibres, mis-aligned fibres and then randomly oriented fibres. This is a clear sign that the effective property, and as a consequence the chi-square value, are affected by multiple

parameters simultaneously and that the final result is a combination of those parameters and is dictated by the most dominant of those parameters.

In terms of stochastic parameters in the system, the case of randomly oriented fibres is the one with the most random parameters (position and orientation) that change for the five realisations. However, it seems that the number of stochastic parameters in the system is not the dominant variable that controls the chi-square behaviour of the material. A different trend can be seen in the case of the transverse effective stiffness for the same realisations. Chi square distribution for transverse stiffness as a function of fibre orientation can be observed in Figure 4.8. As was expected, the case of randomly oriented fibres shows the higher chi square value. This was expected once the random orientation reinforced the transverse direction due to the percentage of fibres oriented towards that direction, and also from the fact that random realisations have more stochastic parameters when compared with aligned fibres and mis-aligned fibres, and as a consequence the number of fibres reinforcing towards the transverse direction varies and this is reflected in the chi-square value.

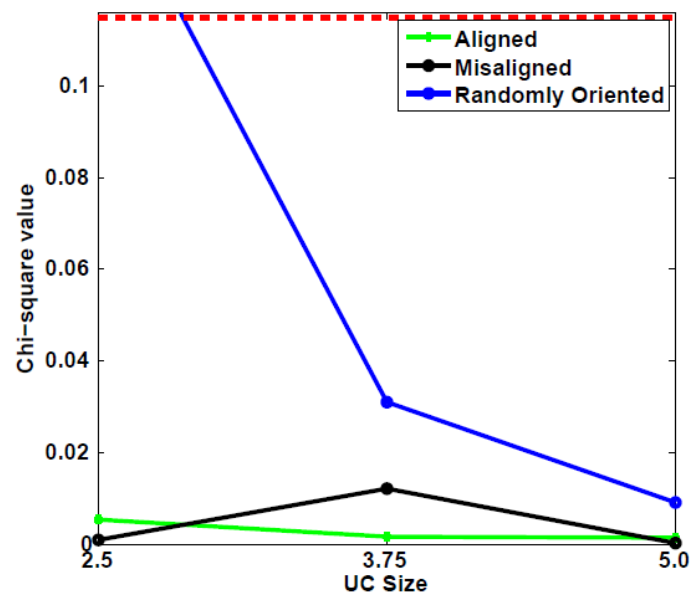


Figure 4.8 Chi-square values for transverse stiffness for realisations with $AR=10$ and three cases of orientations.

4.4.3 Chi square and aspect ratio

The second parameter under investigation for the values of the chi square test is the aspect ratio of the inclusions. For the purposes of this research, three different aspect ratio cases were examined in the case of uniform distribution length composite. Values of the chi-square will be compared for $AR = 1, 5, 10$. Results of the chi-square test for the same orientation and the same property but different aspect ratio can be seen in Figure 4.9.

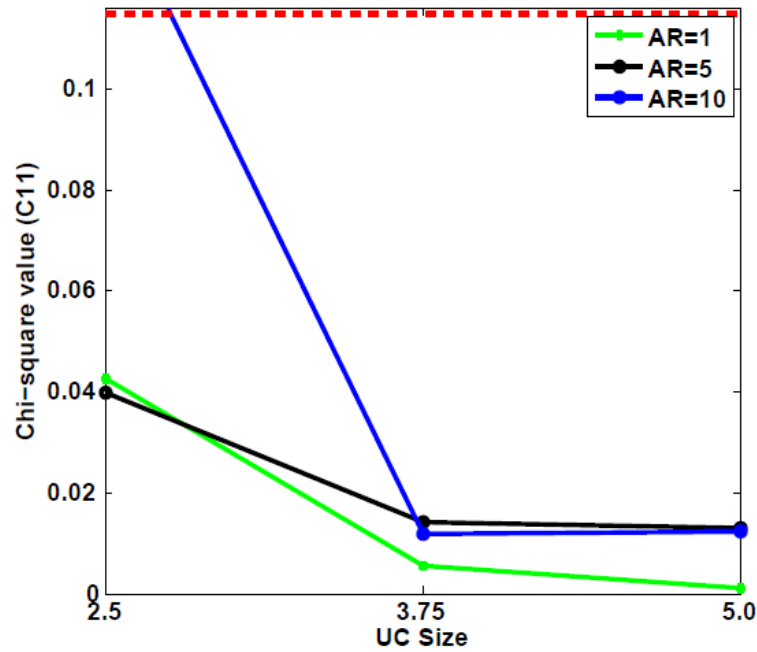


Figure 4.9 Chi-square value for longitudinal effective stiffness of aligned fibres as a function of AR.

For the above plot, the horizontal axis shows the three different UC sizes while the vertical axis shows the chi-square value. Figure 4.9 shows the influence of aspect ratio on Chi-square values for the longitudinal effective stiffness of aligned fibres composite. As can be observed, the aspect ratio has strongly influenced the chi-square value. Again, as in the previous case, the trend is not clear as aspect ratio is not the only parameter that influences the chi-square value. However, it is clear for longitudinal stiffness that the larger the aspect ratio is, the higher the chi-square value will be. This is related to the fact that by increasing the AR for aligned fibres, the property which is most affected is the longitudinal stiffness. In addition, aspect ratio is a parameter that is indirectly related to the size of RVE, which is the main reason why the chi-square values of the same aspect ratio decrease as the size of the RVE becomes larger.

The exact opposite trend on chi-square distribution was observed for the transverse effective stiffness of the same realisations as in the previous case. Figure 4.10 shows chi-square values for the transverse effective stiffness of aligned fibres composite.

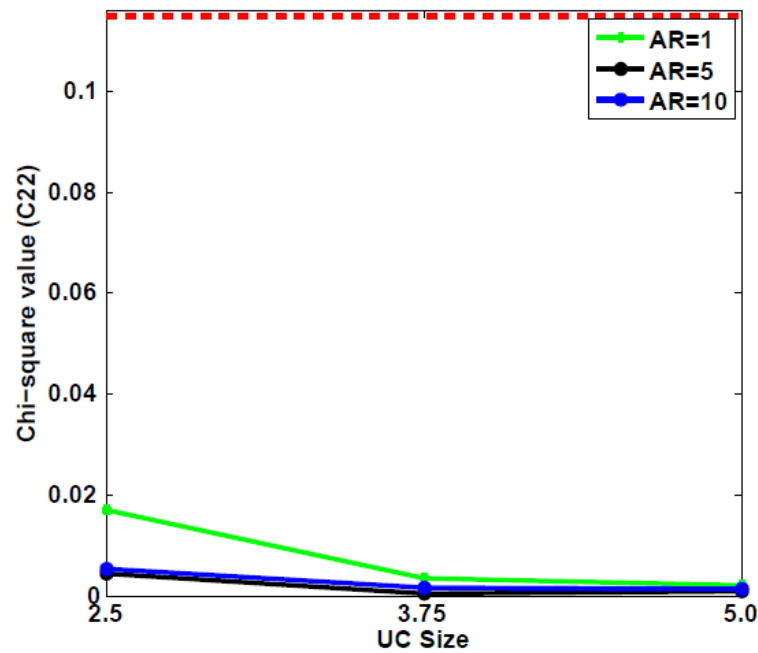


Figure 4.10 Chi-square value for transverse effective stiffness of aligned fibres as a function of AR.

As can be observed in Figure 4.10, for the case of the transverse effective stiffness, circular inclusions exhibit the highest deviation from the arithmetic average value. This is related to the most reinforced parameter but is a topic which will be discussed in the next paragraph because the phenomenon becomes clearer once the comparison of chi-square value is based on the effective properties.

4.4.4 Chi square and effective properties

In the following paragraph the influence of the chi-square test value with respect to effective properties will be examined. As shown in the previous sub-section, the same realisations show totally different trends for longitudinal effective stiffness and for transverse effective stiffness. This can be observed clearly in Figure 4.11 where the distribution of chi-square was plotted with respect to the UC size for three different effective mechanical properties.

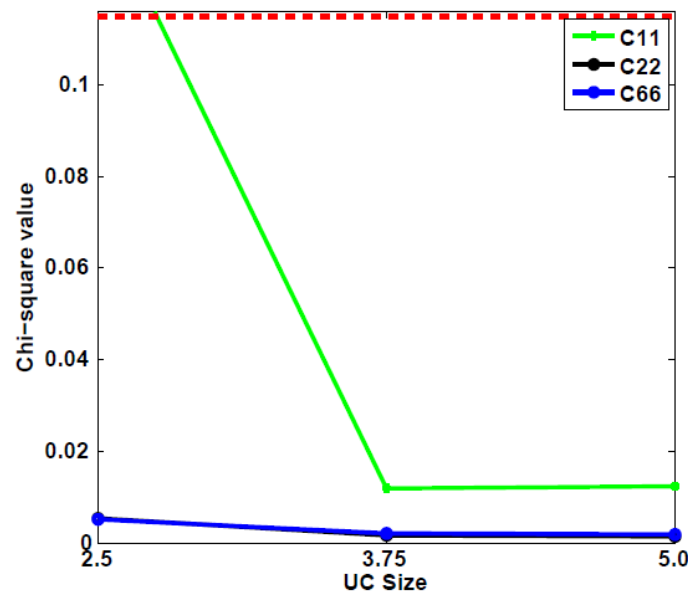


Figure 4.11 Chi square values for different mechanical properties for aligned fibres with AR=10.

Figure 4.11 shows the distribution of chi-square values for aligned fibres orientation with AR=10. As observed, the higher chi-square value belongs to the longitudinal effective stiffness. Up to this point, in order to appropriately interpret this behaviour one has to consider that fibres are oriented towards the longitudinal direction which is a parameter enhancing the longitudinal stiffness, and also that fibres have large aspect ratio (AR=10) which is also a second parameter enhancing the effective longitudinal stiffness. It then becomes clear that the parameter of the most reinforced property is a dominant parameter on the chi-square test. It was generally observed through the chi-square tests that if the orientation of fibres or the aspect ratio specifically reinforces any of the effective mechanical properties, then this property becomes the dominant parameter for the chi-square distribution. For the specific case shown in Figure 4.11, of the effective properties under investigation, longitudinal stiffness is the one which is more reinforced due to the fibre orientation and the fibre aspect ratio.

4.5 Conclusions

Throughout the previous chapter, the concept of computational homogenisation was discussed. The definition of the homogenisation process was given and the significance of the method on material characterisation was addressed. Various computational homogenisation approaches were presented and a discussion of the accuracy and the difficulty of implementation of each approach took place. The major homogenisation approaches, the asymptotic homogenisation method, the volume average and the reaction force methods, were further analysed. The macro-homogeneity condition

was presented and the concept of equivalent homogeneous media was discussed. A report on the effective properties under investigation follows. Longitudinal effective stiffness, transverse effective stiffness and effective shear modulus for the mechanical properties, while for the thermal properties the effective thermal conductivity was the property under investigation and for the thermo-mechanical simulations the effective linear coefficient of thermal expansion was the property under investigation. A detailed discussion on the implementation of boundary conditions and calculation of effective properties was presented. Finally, the chapter ends with a report on the statistical test. The question of the representative size has been answered through a statistical test. The chapter does not provide results from the chi-square test but a quality discussion on the importance of the test and the major factors affecting the test. Further investigation for the influence of various parameters on the chi-square value took place and the influence of the fibre orientation, aspect ratio, effective property and RVE size were discussed.

5 Results and discussion

Through the following chapter results from the developed numerical models are presented. The chapter is separated in two sections. Section 5.1 refer to mono-dispersed and section 5.2 for the non mono-dispersed fibre length. For both sections results are presented as a function of the parameters under investigation. Results from the chi-square test are presented first in order to clarify the representative sizes of a sample under consideration, and as a consequence the accurate results. The chapter concludes with a direct comparison of the representative results with various theoretical models as a function of the aspect ratio.

5.1 Mono-dispersed fibre length

As was discussed in chapter 2, fibre length is a parameter of the material mainly affected by the manufacturing process. Viscosities of the matrix polymer, volume fraction, and complexity of the mould are a few parameters of the manufacturing process which affect fibre length. Short fibre composite with mono-dispersed fibre length is not a common case. In the majority of short fibre composite products fibre length follows a distribution. The following analysis of the mono-dispersed fibre length aims to study the ideal case of fibre length for comparison with the more realistic case of fibre length distribution.

5.1.1 Chi-square results

The following plots show the chi-square distribution of the samples under investigation. The chi-square value was calculated as shown in Equation 4.34, by considering the five different realisations of each case. The five different realisations consist of the same fibre orientation, same UC size, same fibre aspect ratio and same volume fraction. The difference between them relies on the actual position of inclusions. Realisations represent a square region of the material taken in a random position. Any differences between the five realisations are a direct indication of non-uniformity in the response of the same material, or that the material is observed in a very local scale in which singularities are dominating the response of the material. An example of five realisations can be seen in Figure 5.1.

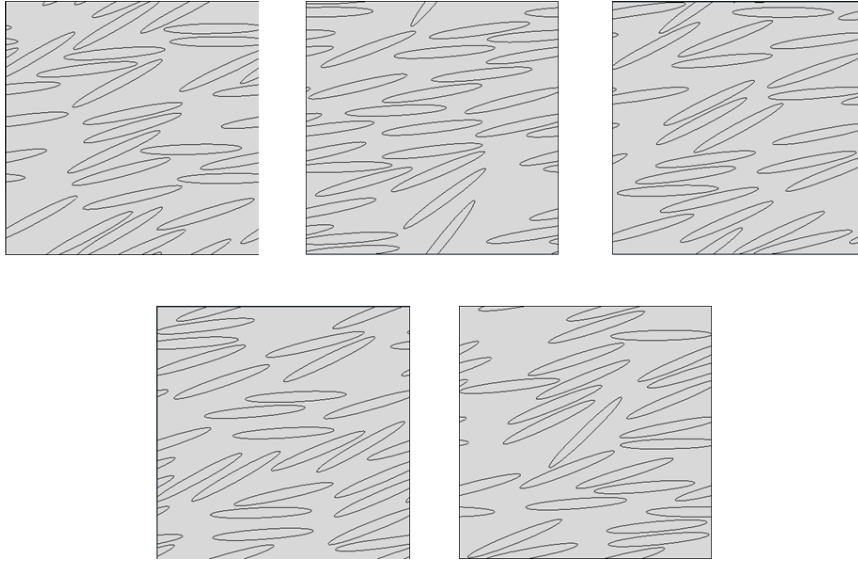


Figure 5.1 From every case of parameter combination, five realisations were developed in order to statistically study the results.

As has been reported in chapter 4, the Chi-square test can test the hypothesis of the representativeness of a UC's size. If the observed values of the effective property under investigation exhibit a major fluctuation with the expected value of the five realisations, it means that the size under study will show a relatively high chi-square value. As is been reported, chi-square test is a hypothesis test so the chi-square value resulting from a specific size analysis must be compared with a table value from the chi-square distribution. Combining the statistical degrees of freedom of the problem and the desired degree of accuracy, one is able to read a hypothesis test value from the chi-square distribution table (Appendix IV) and compare it with the resultant chi-square value. Any resultant chi-square value below the table distribution value can be considered as positively passing the hypothesis, any value above the chi-square table value is considered to fail the hypothesis test. Following the results of the hypothesis test results about the representativeness of the size can be made.

5.1.1.1 Chi-square Results-Mechanical properties

The first family of plots shown in

Figure 5.2 show the chi-square distribution regarding the mechanical properties of uniform length aligned short fibre composite for the cases of aspect ratio 1, 5 and 10. The horizontal axis of the plots shows the normalised UC size while the vertical axis indicates the resultant chi-square value for each size. Chi-square plots are categorized with respect to the orientation aspect ratio and property under investigation. By categorizing the plots in such a way gives the ability to investigate the contribution of each parameter on the chi square value.

Chi square plots for a uniform length distribution with respect to mechanical properties under investigation for perfectly oriented-aligned fibres, misaligned fibres and randomly oriented fibres are presented. The following

Figure 5.2 shows the chi-square value for mechanical properties of aligned fibres with respect to the normalised UC's value on the left side, and on the right side shows a picture of the realisation indicating the aspect ratio and the orientation.

5.1.1.1.1 Align fibres

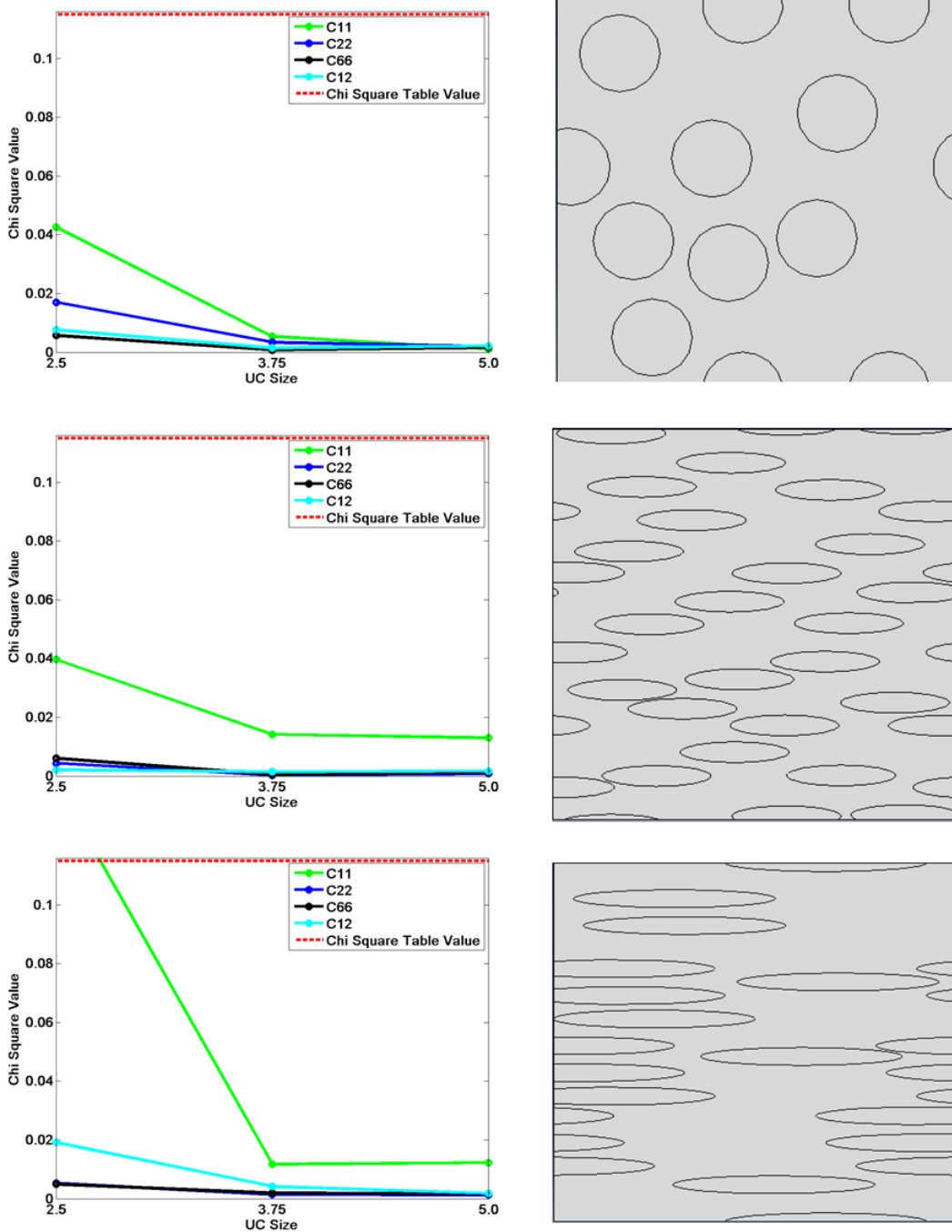


Figure 5.2 Chi-square results for uniform length aligned fibres.

Through

Figure 5.2 the chi-square value of aligned fibres is shown. It can be observed that:

1. for each individual plot the value of chi-square is decreasing as long as the UC size increases. This is a general trend which will be observed in all cases of chi-square test. This results from the fact that larger UC sizes include more fibres and as a consequence more information about the microstructure. This is something beneficial for the average properties of the UC. Larger UC sizes lead to fewer singularities due to the specific structure of each realisation. It must be emphasised that chi-square test is a criterion comparing the observed value of each realisation with the expected value calculated from the five different realisations.
2. Generally, as will be shown in this chapter, the AR in combination with fibre orientation, are parameters affecting the effective properties. In the specific case of aligned fibres an increase of AR leads to higher longitudinal effective stiffness. This can be seen by increasing the AR; the chi-square value of longitudinal stiffness increases and this is also why longitudinal stiffness has the highest chi-square value. This behaviour is not only reflected in the general trend of chi-square results but also in the actual values of the chi-square test.
3. Effective transverse stiffness and effective shear stiffness have lower chi-square values compared with longitudinal stiffness. This is also a phenomenon which can be explained by

the fact that transverse stiffness and shear stiffness do not experience strong enhancement from the increase of AR in the case of fully oriented-aligned fibres

5.1.1.1.2 Misaligned fibres

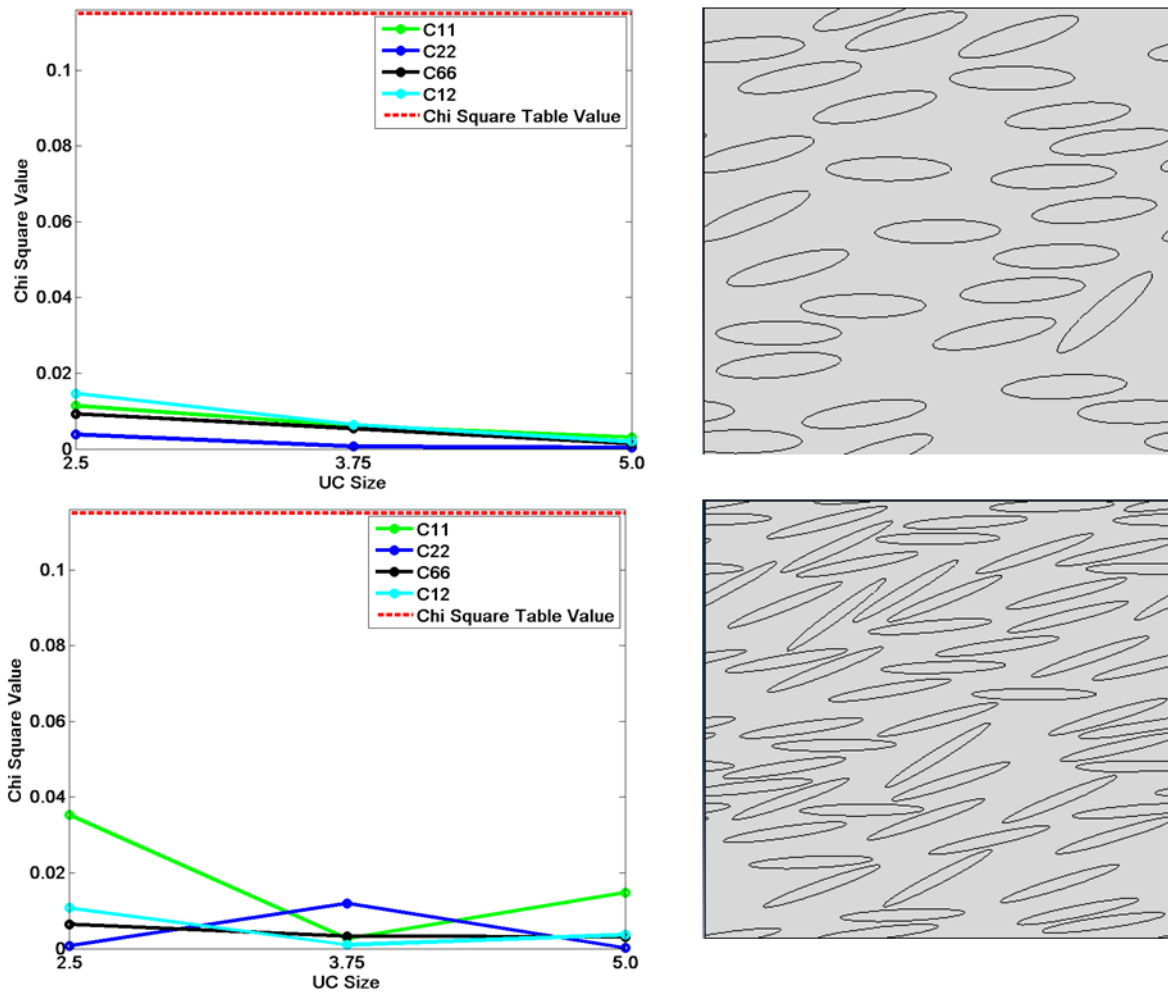


Figure 5.3 Chi-square results for uniform length misaligned fibres.

Figure 5.3 shows results of chi-square test for mechanical properties of misaligned fibres for $AR = 5$ and $AR = 10$. In the case of misaligned fibres an extra stochastic parameter is introduced into the system. However the stochastic behaviour of this parameter (fibre orientation) was restricted in order to get the misaligned orientation. The case of $AR = 1$ was omitted for all orientation cases except fully aligned fibres.

1. The first point under discussion is that the general trend of decrease of the chi-square value while AR increases is also observed for misaligned fibres.
2. For the case of $AR = 5$ it can be observed that chi-square values for effective longitudinal stiffness and effective shear stiffness are close to each other while the effective transverse stiffness has a lower value. This is a behaviour resulting from the contribution of orientation. As can be seen misaligned fibre UCs will exhibit lower longitudinal stiffness compared with aligned fibres and also higher effective transverse stiffness and effective shear stiffness. This

is the main reason why the absolute value of the chi-square test is lower for longitudinal effective stiffness.

3. For the case of $AR = 10$ the absolute value of the chi-square test is higher compared with the case of $AR = 5$, and this is again an indication of the contribution of AR in the case of the same orientation. The increase of AR seems to cause a deviation between the five values mainly relating to longitudinal effective stiffness.

For $AR = 10$ and for the cases of longitudinal and transverse stiffness it can be seen through Figure 5.3 that as the UC increases in some cases, the chi-square value increases. This behaviour arises from the fact that a combination of stochastic parameters in the system in some cases causes deviation between the observed and the expected value. However, this can be acceptable only for a few cases (not as a regular trend) and the way to overcome this barrier is to increase the number of realisations under study.

5.1.1.1.3 Randomly oriented fibres

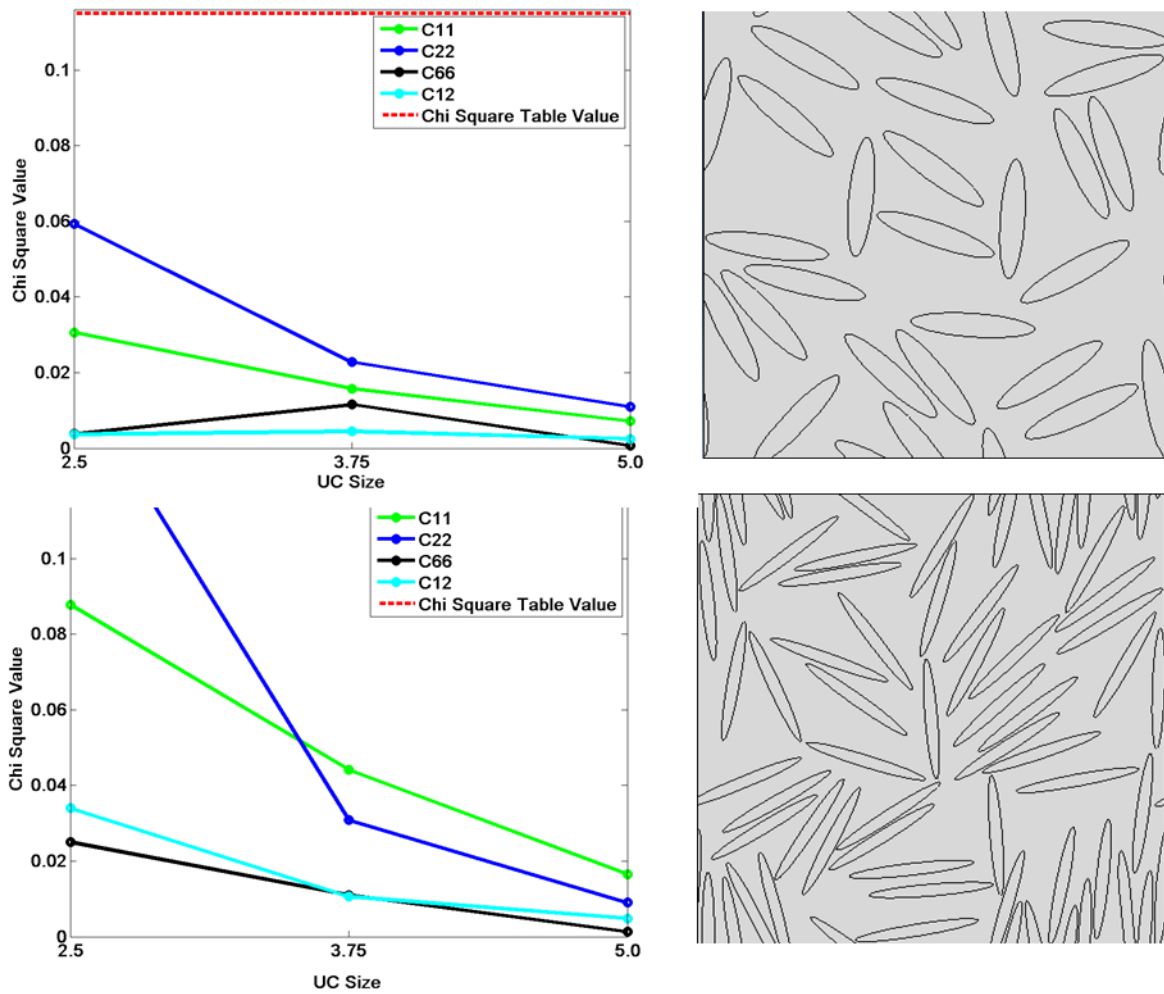


Figure 5.4 Chi-square results for uniform length randomly oriented fibres.

Figure 5.4 shows the chi-square test results for randomly oriented fibres. Again the case of $AR = 1$ has no meaning with random orientation. In the case of randomly oriented fibres the number of stochastic parameters in the system is the same as in the case of misaligned fibres, but in this case there is no restriction on the potential angle of each fibre. Fibre angles can take value on the closed interval between $0 - \pi$.

The following observation can be made:

1. The first comment about chi-square results of randomly oriented realisations is that the general trend of decrease of chi-square as UC size increases is also observed in this case.
2. The second comment regards the actual values of the test. Almost all effective properties have increased chi-square value and this is mainly caused by the stochastic parameters introduced into the system

3. It can be also observed that chi-square value for the effective transverse stiffness is the most dominant value of the chi-square test. This is mainly caused by the orientation and also by the AR. Analysing first the case of orientation, the case of randomly oriented fibres increases the actual number of fibres oriented towards the transverse direction. This causes a reinforcement of the effective transverse stiffness and at the same time, depending on the number of fibres oriented towards transverse direction, different realisations have different effective transverse stiffness. This points to a deviation of the observed values, and as a consequence a higher chi-square value.
4. It is also clear from the plots in Figure 5.4 that an increase in the AR increases the value of chi-square for all properties. This is something which was expected due to the reinforcing effect of randomly oriented fibres. In the case of randomly oriented fibres, the composite is enhanced in both directions and the effective shear stiffness is reinforced. As a consequence higher chi-square values were expected.

The following Table 5-1 includes all the results of the previous figures in a more integrated way. The table shows all the chi-square values for the mechanical properties of the samples under investigation. Results of the chi-square test regarding the table are categorized with respect to the orientation, the UC size and the aspect ratio.

Table 5-1 Chi-square results for mechanical properties.

Orientation	Normalised UC size	Property under investigation	Chi-square value		
			AR=1	AR=5	AR=10
Aligned	2.5	C_{11}	0.0426	0.0397	0.1415
	3.75	C_{11}	0.0054	0.0142	0.0117
	5.0	C_{11}	0.0011	0.0130	0.0123
	2.5	C_{22}	0.0169	0.0044	0.0052
	3.75	C_{22}	0.0034	0.0003	0.0014
	5.0	C_{22}	0.0020	0.0008	0.0013
	2.5	G_{12}	0.0057	0.0061	0.0050
	3.75	G_{12}	0.0008	0.0005	0.0019
	5.0	G_{12}	0.0016	0.0013	0.0017
Mis-aligned	2.5	C_{11}	0.0426	0.0114	0.0353

	3.75	C_{11}	0.0054	0.0061	0.0026
	5.0	C_{11}	0.0011	0.0031	0.0148
	2.5	C_{22}	0.0169	0.0039	0.0007
	3.75	C_{22}	0.0034	0.0006	0.012
	5.0	C_{22}	0.0020	0.0004	0.0002
	2.5	G_{12}	0.0057	0.0093	0.0064
	3.75	G_{12}	0.0008	0.0054	0.0032
	5.0	G_{12}	0.0016	0.0015	0.0031
Randomly oriented	2.5	C_{11}	0.0426	0.0306	0.0878
	3.75	C_{11}	0.0054	0.0157	0.0441
	5.0	C_{11}	0.0011	0.0072	0.0164
	2.5	C_{22}	0.0169	0.0593	0.15
	3.75	C_{22}	0.0034	0.0228	0.0308
	5.0	C_{22}	0.0020	0.0109	0.009
	2.5	G_{12}	0.0057	0.0038	0.025
	3.75	G_{12}	0.0008	0.0016	0.011
	5.0	G_{12}	0.0016	0.0006	0.0013

5.1.1.2 Chi-square Results-Thermal properties-Thermal Conductivity

The following family of plots relates to the chi-square results for thermal properties and more specifically to the longitudinal effective thermal conductivity and the transverse effective thermal

conductivity regarding all the cases of orientation and AR under investigation. The plots are separated for different aspect ratios.

5.1.1.2.1 Aligned fibres

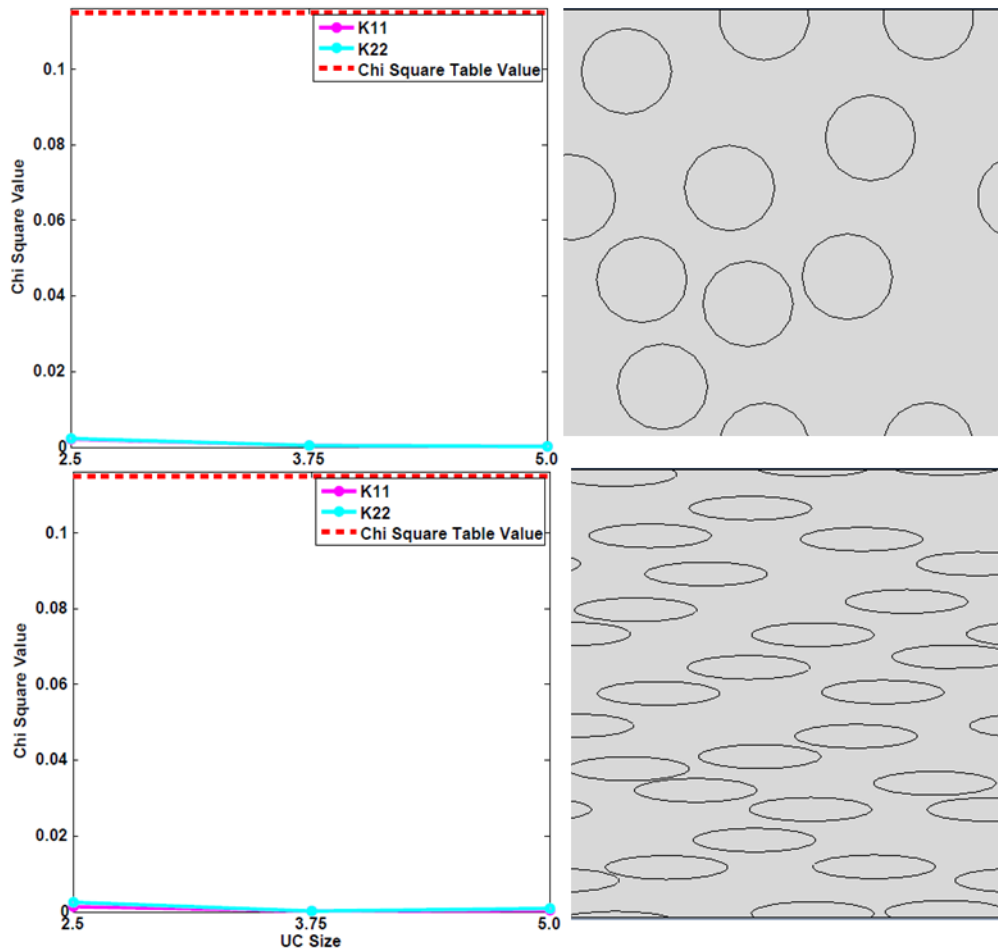


Figure 5.5 Chi-square results regarding the thermal conductivity for aligned uniform length fibres.

Figure 5.5 shows the longitudinal and transverse effective thermal conductivity for aligned fibres of $AR = 5$ and $AR = 10$. It can be observed that:

1. Comparing the chi-square value of thermal properties with chi-square value of mechanical properties, thermal properties seem to experience much less deviation between the observed and the expected value. It must be emphasised that expected and observed values entering the chi-square test are normalised and as a consequence for all the properties under investigation, all the values entering the test lie between the open interval of $0 - 1$. This enables a direct comparison between the chi-square behaviour of each property.
2. For the case of aligned fibres as shown in Figure 5.5, AR does not seem to affect the deviation between expected and observed value. Chi-square results are close to each other

in the case $AR = 5$ and $AR = 10$ and also values lay close to each other for the longitudinal effective conductivity and for the transverse effective conductivity.

3. The general trend of decrease of the chi-square value as the UC size increases was also observed for the longitudinal and transverse effective thermal conductivity of aligned fibres.

5.1.1.2.2 Misaligned fibres

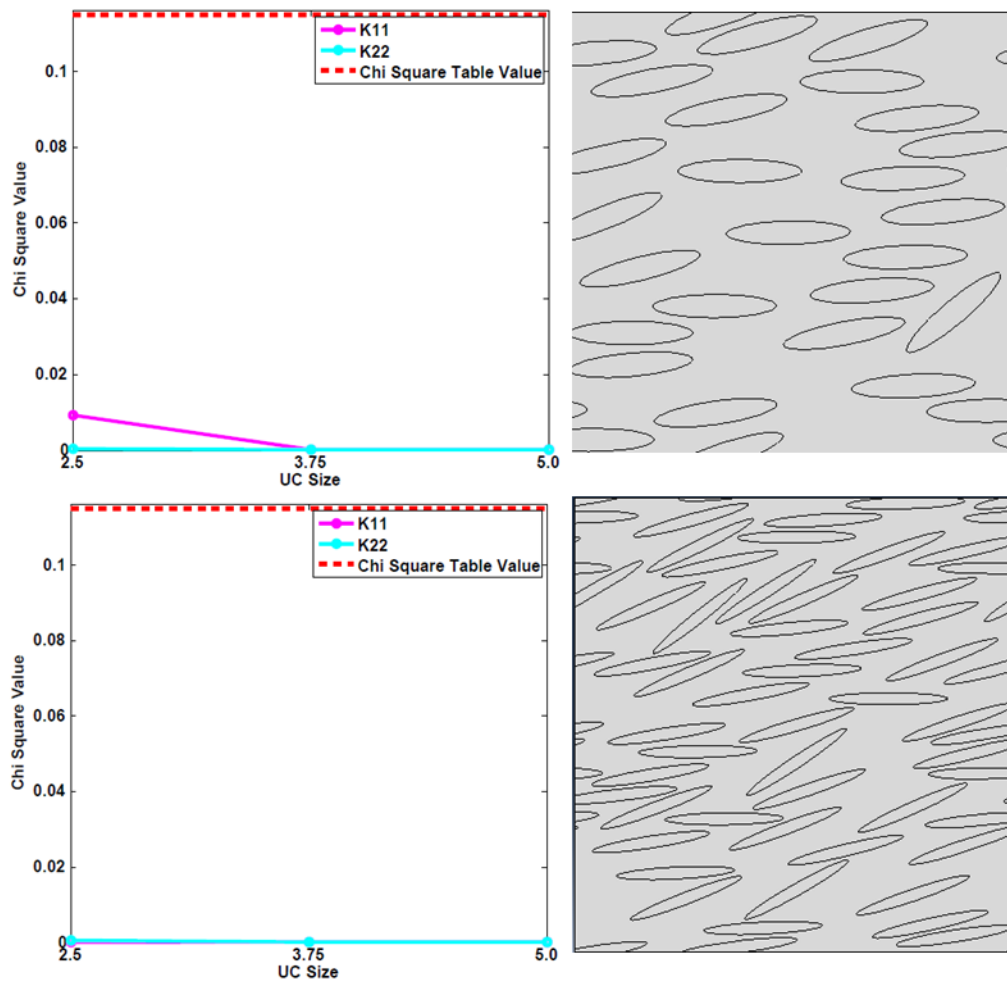


Figure 5.6 Chi-square results regarding the thermal conductivity for misaligned uniform length fibres.

Figure 5.6 shows results for the chi-square test for longitudinal and transverse effective thermal conductivity of misaligned fibres realisations. In a comparison of misaligned orientation with aligned fibres on Figure 5.5, it seems that:

1. The introduction of a new random parameter (fibre orientation) did not affect the chi-square value drastically. The general trend of chi-square value decrease with respect to UC size decrease is also observed.

2. In the case of $AR = 5$ longitudinal effective thermal conductivity seems to have an increased value of chi-square test when compared with $AR = 5$ and $AR = 10$ of aligned fibres.
3. On the contrary, the case of $AR = 10$ seems to have expected and observed values which are closer to each other. In the case of misaligned fibres $AR = 10$ seems to exhibit more uniform chi-square results. This is something which was observed for mechanical properties as well.

5.1.1.2.3 Randomly oriented fibres

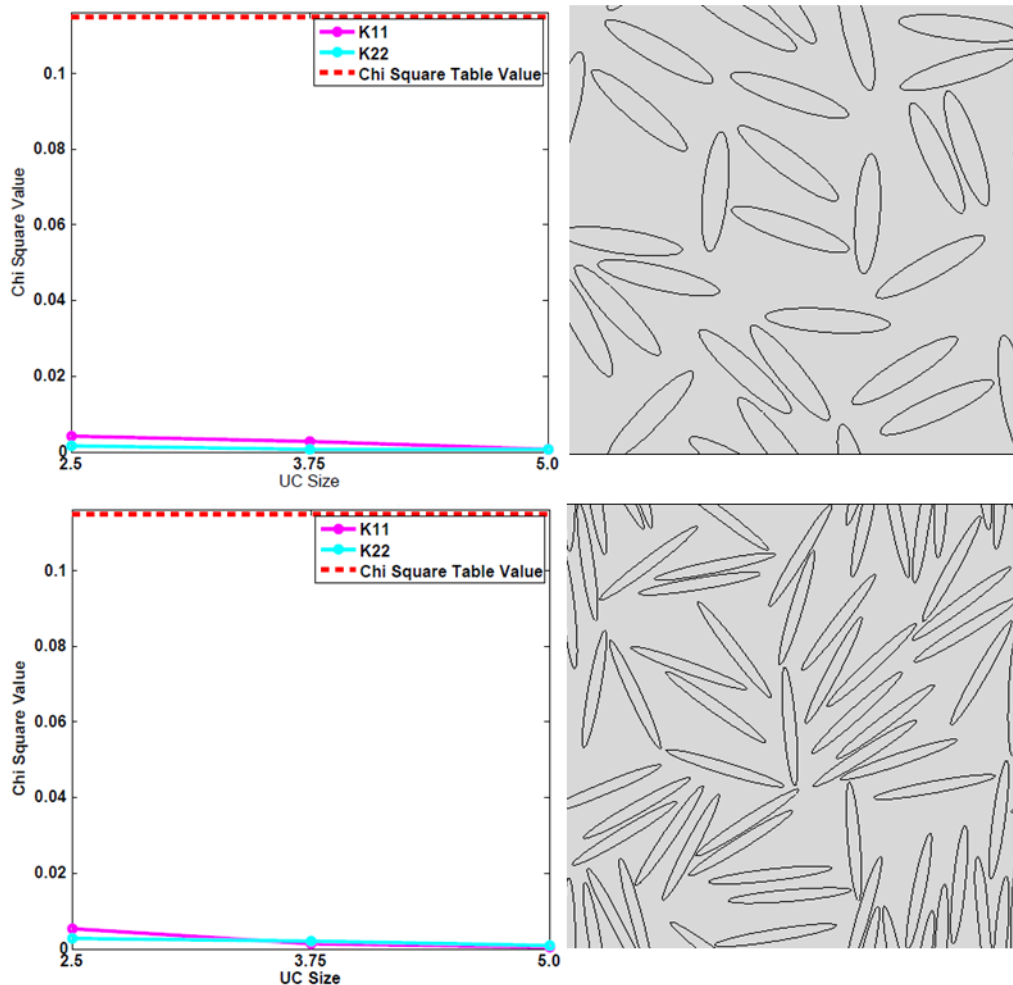


Figure 5.7 Chi-square results regarding the thermal conductivity for randomly oriented, uniform length fibres.

Figure 5.7 shows the chi-square results of longitudinal and transverse effective thermal conductivity for randomly oriented fibre realisations.

1. As in every case under investigation the general behaviour of decrease of the chi-square value was also observed in this case.

Comparing chi-square results in Figure 5.5, Figure 5.6 and Figure 5.7 it can be seen that:

2. in the case of randomly oriented fibres (Figure 5.7) the chi-square values are higher for both sets of parameters. Higher values were obtained as orientation changed from aligned to misaligned and randomly oriented, but also as the aspect ratio increased.
3. It must be noted that the case of randomly oriented fibres was the only case where the chi-square value of effective transverse thermal conductivity increased.

The following Table 5-2 includes all the information shown in the previous plots relating to the chi-square distribution with respect to the RVE size for the effective thermal conductivity, both longitudinal and transverse. Results for the chi-square distribution are shown with respect to the sample size, the orientation of fibres, the effective property and the aspect ratio.

Table 5-2 Chi-square results for thermal properties.

Orientation	Normalised UC size	Parameters under investigation	Chi-square values		
			AR=1	AR=5	AR=10
Aligned	2.5	K_{11}	0.002	0.0013	0.0015
	3.75	K_{11}	0.0004	0.0001	0.0005
	5.0	K_{11}	0.0001	0.0003	0.0004
	2.5	K_{22}	0.0021	0.0024	0.0038
	3.75	K_{22}	0.0003	0.0001	0.0010
	5.0	K_{22}	0.0001	0.0007	0.0006
Mis-aligned	2.5	K_{11}		0.0092	0.00007
	3.75	K_{11}		0.0002	0.000031
	5.0	K_{11}		0.0001	0.000035
	2.5	K_{22}		0.000244	0.000677
	3.75	K_{22}		0.0001781	0.000035
	5.0	K_{22}		0.0000917	0.0001186
Randomly oriented	2.5	K_{11}		0.0042	0.0053
	3.75	K_{11}		0.0026	0.0013

5.0	K_{11}		0.0005	0.0004
2.5	K_{22}		0.0016	0.002
3.75	K_{22}		0.0007	0.0021
5.0	K_{22}		0.0005	0.0008

5.1.1.3 Chi-square Results-Thermal properties-Coefficient of Thermal Expansion

The following family of plots show the chi-square distribution for the linear coefficient of thermal expansion, for aligned fibres, misaligned fibres and randomly oriented fibres for all the cases of orientation under investigation, and also for three different UC sizes and for longitudinal and transverse coefficient of thermal expansion.

5.1.1.3.1 Aligned fibres

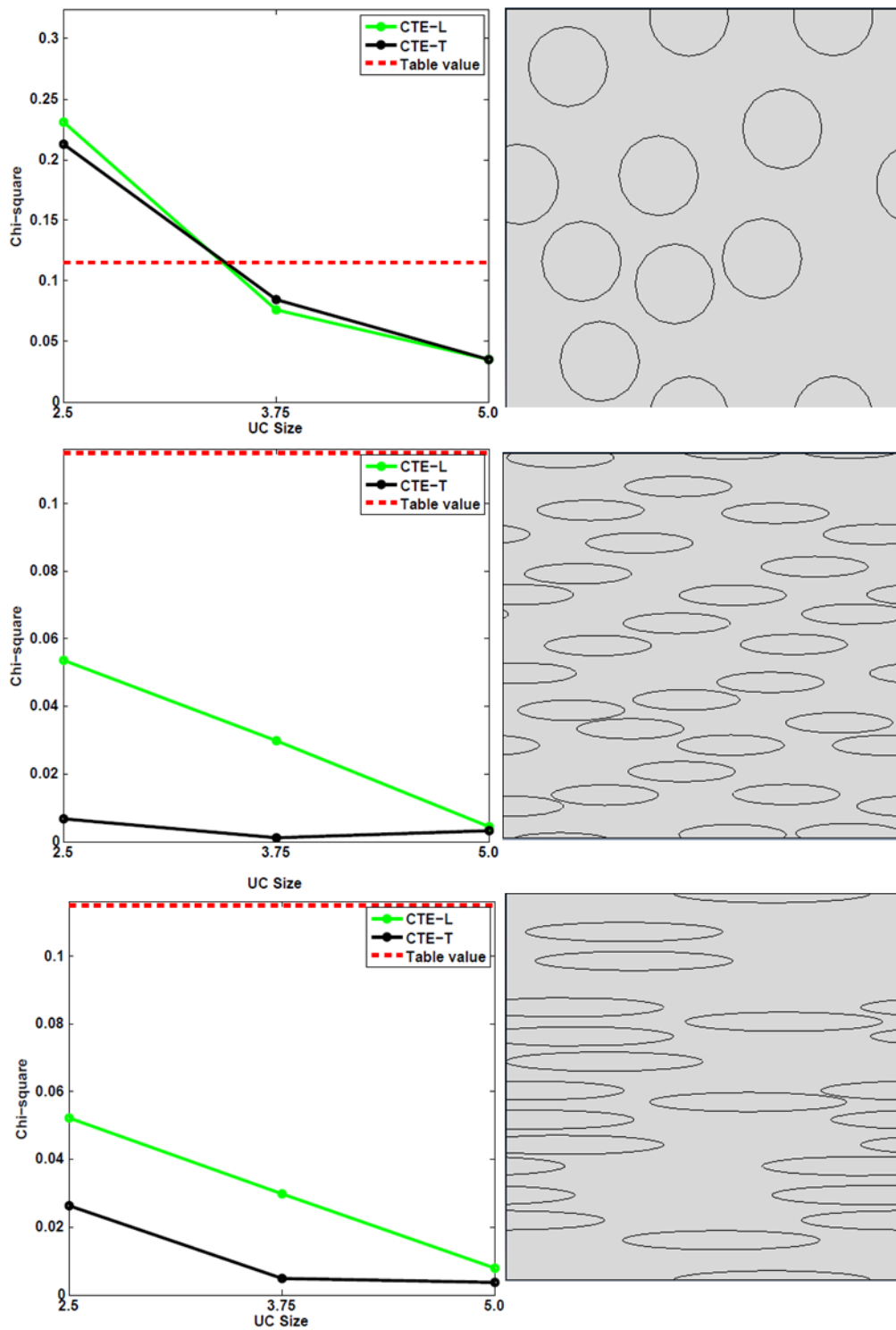


Figure 5.8 Chi-square results regarding the coefficient of thermal expansion for uniformly oriented-aligned fibres.

Figure 5.8 shows the results of the chi-square test on the effective longitudinal and transverse linear coefficient of thermal expansion for aligned fibres. As can be observed:

1. The general trend of chi-square value reduction with respect to UC size increase also takes place for CTE.
2. Regarding the increase of aspect ratio and the influence it has on effective longitudinal and transverse thermal conductivity, it can be seen that for $AR = 1$ values of the chi-square tests are almost the same, while as long as the AR increases the difference between longitudinal and transverse CTE increases.
3. It can also be observed that as long as the AR increases the actual value of the chi-square test decreases. In that case it can be said that the increase of AR has the opposite results comparing with chi-square results for mechanical and thermal properties.

5.1.1.3.2 Misaligned fibres

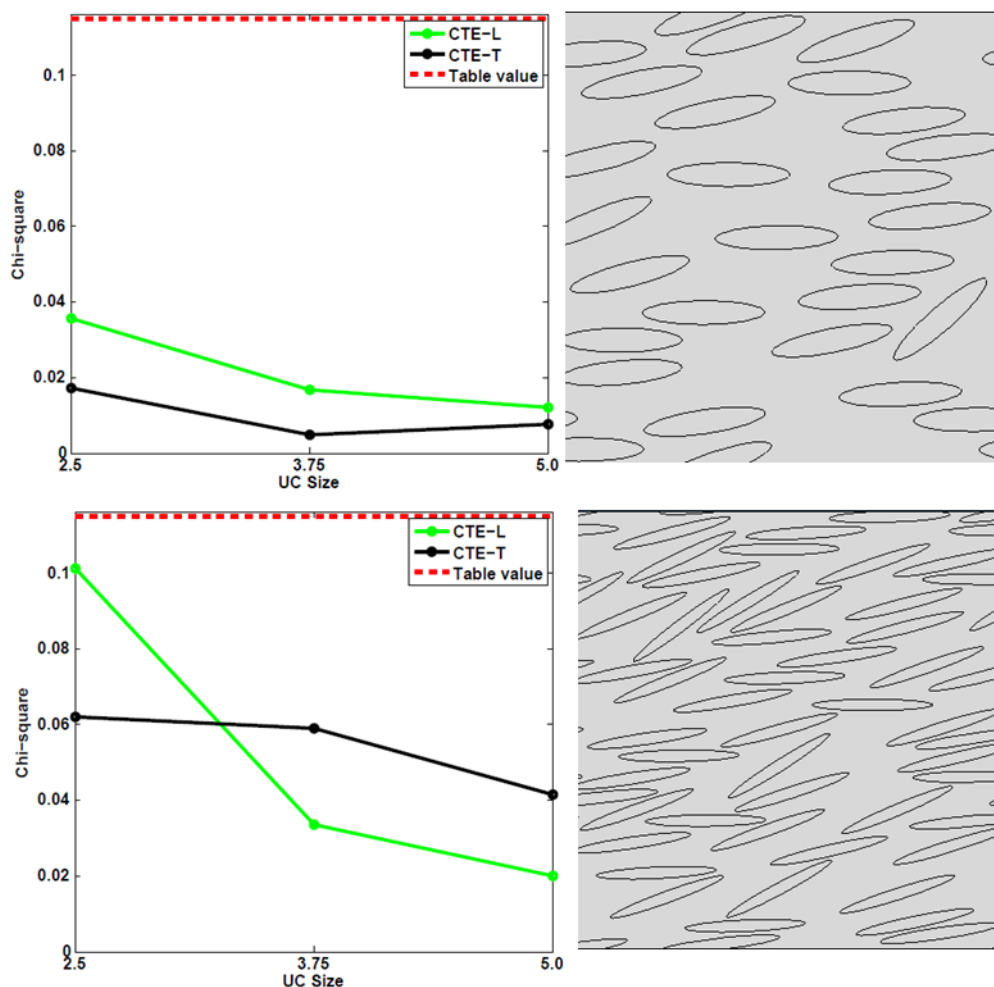


Figure 5.9 Chi-square results regarding the coefficient of thermal expansion for misaligned fibres.

Figure 5.9 shows the results of the chi-square test for the effective longitudinal and transverse linear coefficient of thermal expansion for misaligned fibres. As can be observed:

1. The general trend of chi-square value reduction with respect to UC's size increase also take place for CTE.

2. A direct comparison with aligned fibres in Figure 5.8 is that chi-square results for misaligned fibres are closer to each other than for longitudinal and transverse effective CTE. This behaviour arises from the different orientation.
3. It can be seen that effective transverse CTE has elevated chi-square values comparing when compared with aligned fibres. This can be observed in the effective properties as well.
4. AR seems to have a direct influence on the chi-square value. Misaligned fibres with $AR = 10$ have generally higher chi-square values when compared with $AR = 10$. This indicates that there is a strong influence on the CTE from AR which causes a deviation between the expected and the observed values.

5.1.1.3.3 Randomly oriented fibres

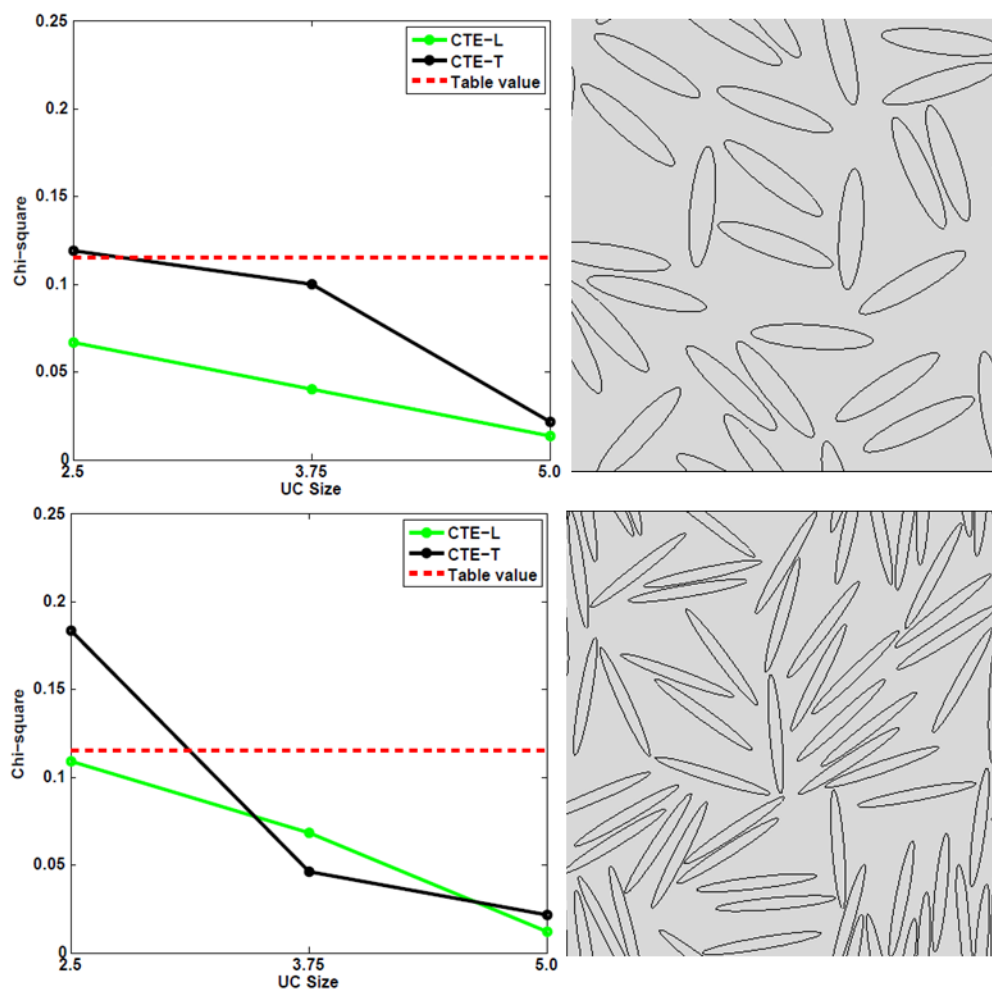


Figure 5.10 Chi-square results regarding the coefficient of thermal expansion for randomly oriented fibres.

Figure 5.10 shows results of the chi-square for longitudinal and transverse coefficient of thermal expansion of randomly oriented fibre realisations.

1. As in all the previous cases, as long as the UC size increases the chi-square value decreases.

2. In the case of randomly oriented fibres, chi square values are higher comparing compared with misaligned and aligned fibres. This is an indication that the accuracy of the results is strongly dependant on size when the property under investigation is CTE.
3. The influence of AR is also clear through Figure 5.4. Results from the observed and the expected values seem to deviate more as the AR increases. Again, this phenomenon is connected to the reinforcement of the property under investigation with respect to the AR and the orientation, however this is something which will be discussed in detail in the next section.

The following Table 5-3 includes all the information shown in the previous plots about the chi-square distribution with respect to the UC size for the longitudinal and transverse effective coefficient of thermal expansion. Results for the chi-square distribution are shown with respect to the sample size, the orientation of fibres, the effective property and the aspect ratio.

Table 5-3 Chi-square results for thermo-mechanical properties.

Orientation	RVE size	Chi-square	AR=1	AR=5	AR=10
Aligned	2.5	CTE_{11}	0.2315	0.0535	0.0521
	3.75	CTE_{11}	0.0759	0.0297	0.0297
	5.0	CTE_{11}	0.0347	0.0043	0.0078
	2.5	CTE_{22}	0.2129	0.0067	0.0262
	3.75	CTE_{22}	0.0842	0.001	0.0048
Mis-aligned	5.0	CTE_{22}	0.0348	0.0031	0.0037
	2.5	CTE_{11}		0.0355	0.1012
	3.75	CTE_{11}		0.0168	0.0335
	5.0	CTE_{11}		0.0119	0.02
	2.5	CTE_{22}		0.0172	0.062
Randomly	3.75	CTE_{22}		0.0048	0.059
	5.0	CTE_{22}		0.0076	0.0415
Randomly	2.5	CTE_{11}		0.0668	0.109

oriented					
	3.75	CTE_{11}		0.04	0.0683
	5.0	CTE_{11}		0.0131	0.0117
	2.5	CTE_{22}		0.119	0.1833
	3.75	CTE_{22}		0.1	0.0461
	5.0	CTE_{22}		0.0212	0.0215

5.1.2 Effective properties results

Effective mechanical, thermal and thermo-mechanical properties were studied with respect to various micromechanical parameters. The parameters which varied throughout this study were fibre aspect ratio, fibre orientation distribution, UC size and fibre length distribution. Aspect ratio was found to be a dominant parameter in the response of a short fibre composite, a fact which is also supported by theoretical-analytical models such as the shear lag model or Halpin-Tsai equations. Orientation was the second most influential parameter on the effective properties of the short fibre composite. The influence of the UC size can be clearly seen through the chi-square results, and it seems that higher UC sizes exhibit a more convergent behaviour compared with smaller UC sizes. The final parameter to be analysed is the fibre length distribution, which shows that if the appropriate condition between maximum fibre length and UC size is not satisfied, it can be a source of inaccuracy for the model.

5.1.2.1 Effective mechanical properties

The following family of plots show the distribution of the mechanical thermal and thermo-mechanical effective properties with respect to UC size as a function of fibre orientation with respect to AR. Each plot refers to a different UC size.

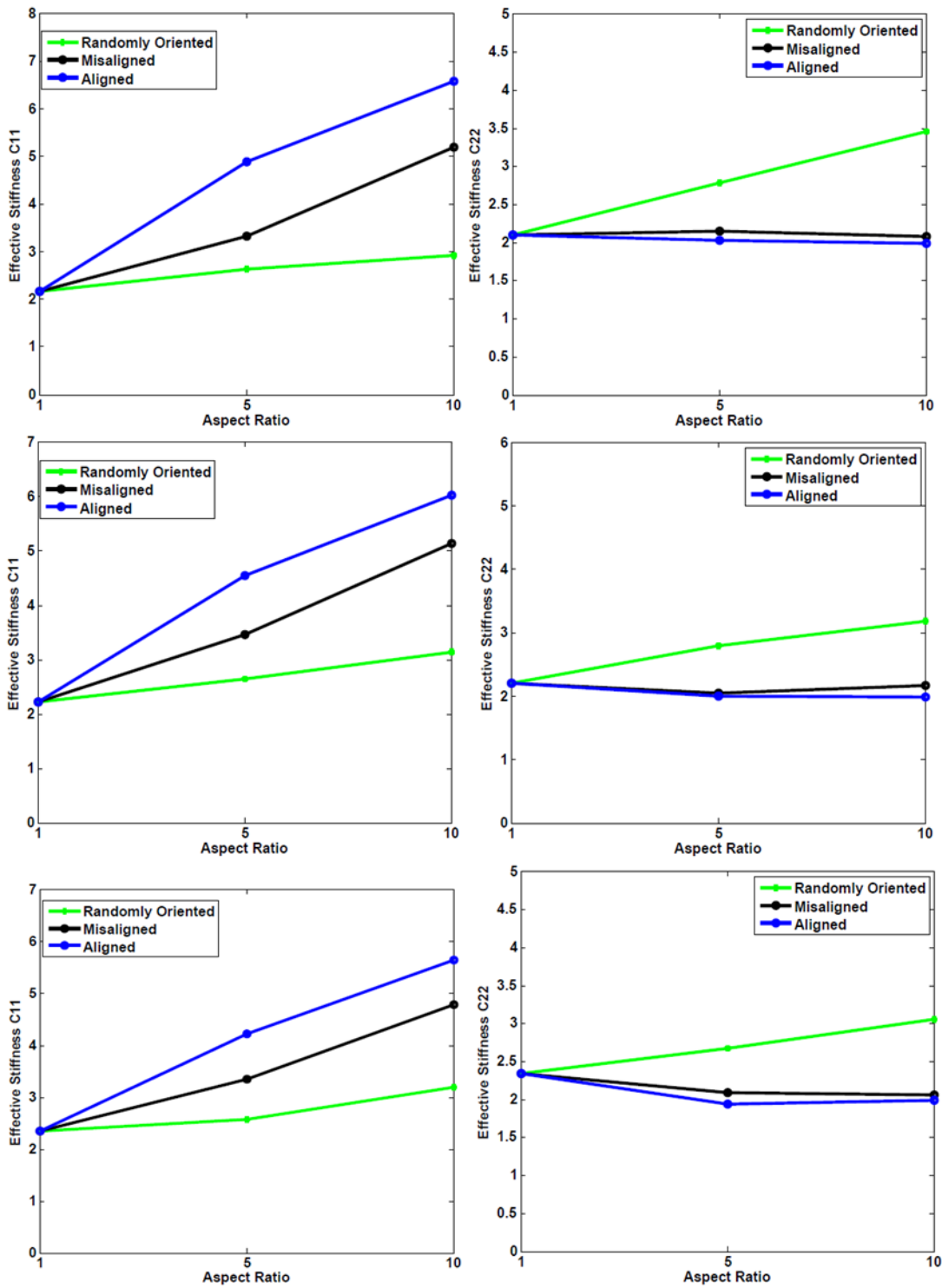


Figure 5.11 Effective mechanical properties results for uniform length fibres. Results are presented with respect to AR for all the cases of orientation under investigation.

Figure 5.11 shows the response of UC. On the left side of Figure 5.1 are results for the effective longitudinal stiffness and on the right side results for the effective transverse stiffness. Every row refers to a different UC size. The vertical axis on the plots refers to the effective property under investigation, while the horizontal axis refers to the value of aspect ratio.

As can be seen:

1. AR is a very crucial parameter for reinforcement. Analysing the left part of Figure 5.1, refers to effective longitudinal stiffness, as was expected for aligned fibres, UC seems to experience the most the reinforcement due to the increase in AR. Misaligned fibres follow with less reinforced property, while the least reinforced case of orientation, from the AR, are the randomly oriented realisations. The explanation for this behaviour is the combination of increased AR with orientation. For aligned fibres it was expected that an increase in AR will lead to a direct increase in the longitudinal stiffness. On the contrary for misaligned fibres and randomly oriented fibres, the percentage of fibres oriented towards the longitudinal direction is not enough to increase the longitudinal stiffness at the same rate as aligned fibres.
2. In the case of transverse effective stiffness, plotted on the right side of the Figure 5.11, the opposite trend can be observed. Higher transverse effective stiffness was observed for the case of randomly oriented fibres, while misaligned fibres exhibit lower effective transverse stiffness and finally aligned fibres shows the least effective transverse stiffness.
3. It is also interesting to report the behaviour of the effective transverse stiffness for each case of orientation with respect to AR. Randomly oriented UCs increase the effective transverse stiffness almost linearly with respect to AR increase. This is not the case for aligned and misaligned orientation. Aligned and misaligned realisations seems to be almost unaffected by the changes in AR. This mainly happens due to the lack of reinforcement on the specific direction of loading. As a result matrix is the main constituent that carries the load. This phenomenon can be predicted with analytical models.

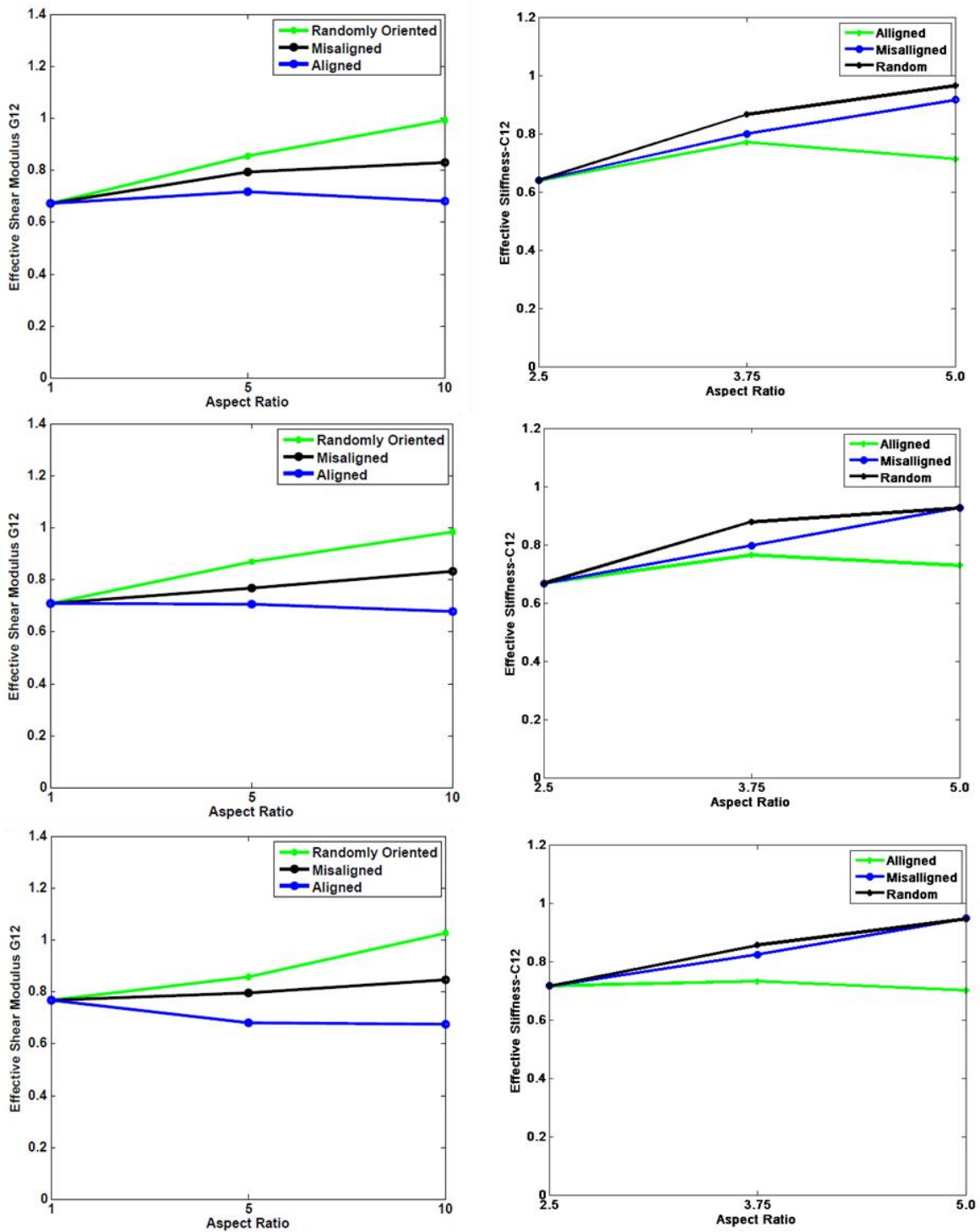


Figure 5.12 Effective shear properties results for uniform length fibres. Results are presented with respect to AR for all the cases of orientation under investigation.

Figure 5.12 show results for the effective shear stiffness. Each plot refers to a different UC size. Results follow the same trend as the effective transverse stiffness but in the case of shear stiffness this is a consequence of the orientation.

1. The orientation with the higher effective shear stiffness is the random orientation. This is due to the fact that randomly oriented fibres resist the shear deformation in a more efficient way compared with aligned and misaligned orientation.
2. Misaligned fibres seem to experience less shear stiffness compared with randomly oriented fibres, but higher stiffness compared with aligned fibres.
3. AR seems to have a strong effect on the random orientation, slightly increasing the effective shear stiffness for misaligned fibres and almost a negative contribution for aligned fibres.

The following Table 5-4 includes all the information shown in the previous plots about the effective mechanical properties under investigation with respect to the AR for the three cases of orientation and the three cases of UC size. Results for the effective mechanical properties are presented in the following table with respect to the sample size, the orientation of fibres, the effective property and the aspect ratio.

Table 5-4 Results for mechanical effective properties.

Orientation	Normalised UC size	Property under investigation	Effective property results		
			AR=1	AR=5	AR=10
Aligned	2.5	C_{11}	2.1597	4.8793	6.5723
	3.75	C_{11}	2.2163	4.5404	6.0217
	5.0	C_{11}	2.3518	4.2229	5.6344
	2.5	C_{22}	2.0943	2.0284	1.9849
	3.75	C_{22}	2.2045	1.9939	1.9849
	5.0	C_{22}	2.3408	1.9369	1.9897
	2.5	G_{12}	0.6721	0.7169	0.6799
	3.75	G_{12}	0.7071	0.7057	0.6784
	5.0	G_{12}	0.7668	0.6802	0.6751
Mis-aligned	2.5	C_{11}	2.1597	3.3310	5.1845

	3.75	C_{11}	2.2163	3.4584	5.1309
	5.0	C_{11}	2.3518	3.3387	4.7780
	2.5	C_{22}	2.0943	2.1436	2.0799
	3.75	C_{22}	2.2045	2.0479	2.1628
	5.0	C_{22}	2.3408	2.0845	2.0568
	2.5	G_{12}	0.6721	0.7935	0.8292
	3.75	G_{12}	0.7071	0.7676	0.8325
	5.0	G_{12}	0.7668	0.7953	0.8478
Randomly oriented	2.5	C_{11}	2.1597	2.6342	2.9177
	3.75	C_{11}	2.2163	2.6343	3.1292
	5.0	C_{11}	2.3518	2.5745	3.1904
	2.5	C_{22}	2.0943	2.7805	3.4560
	3.75	C_{22}	2.2045	2.7939	3.1832
	5.0	C_{22}	2.3408	2.6738	3.0561
	2.5	G_{12}	0.6721	0.8536	0.9925
	3.75	G_{12}	0.7071	0.8697	0.9857
	5.0	G_{12}	0.7668	0.8585	1.0263

5.1.2.2 Effective thermo-mechanical properties

Through the following paragraphs the effective properties of longitudinal and transverse thermal conductivity will be presented with respect to various parameters such as orientation, aspect ratio and UC size. In the second part of the sub-chapter the thermo-mechanical effective results are presented again with respect to various parameters such as orientation, aspect ratio and UC size.

5.1.2.2.1 Effective thermal conductivity

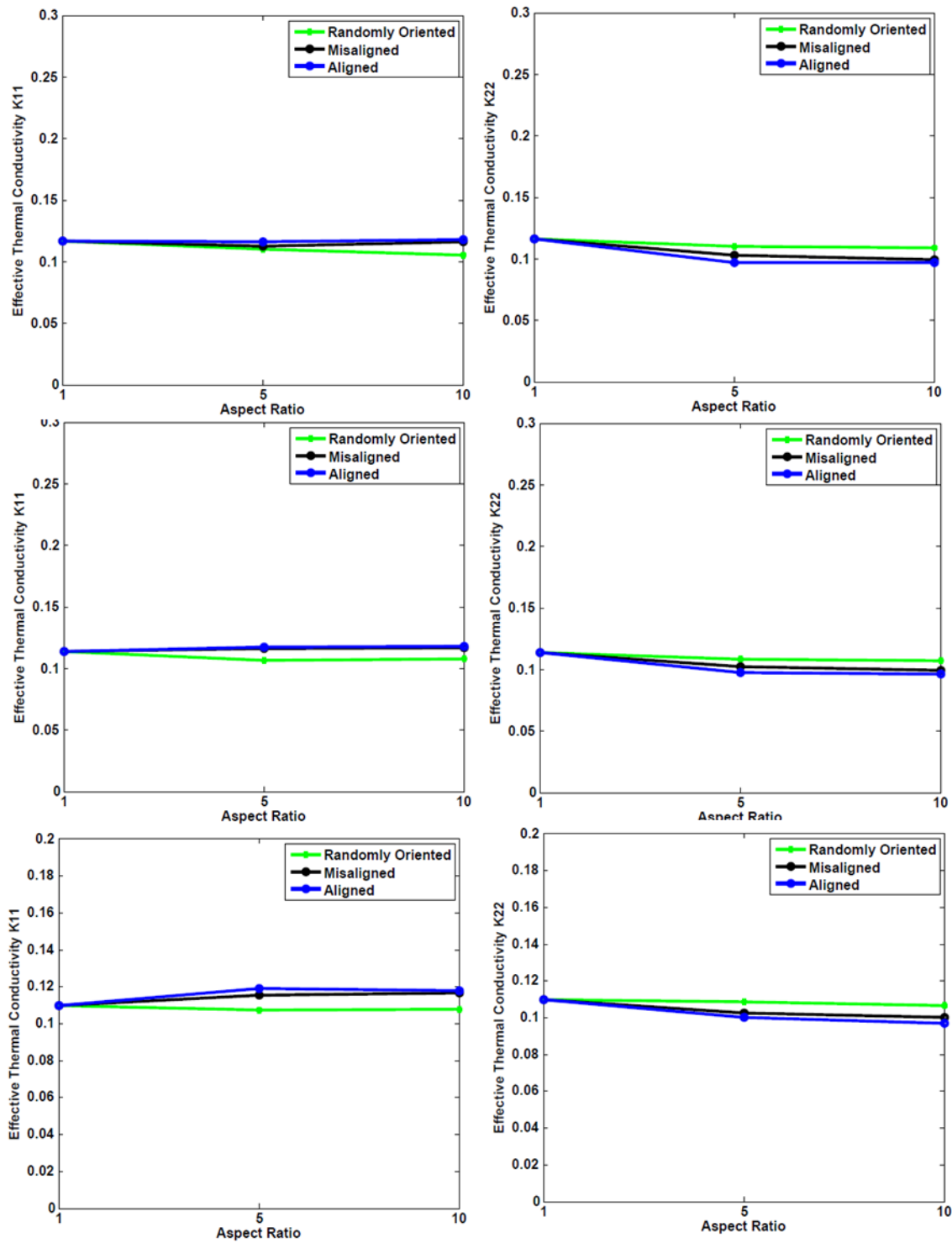


Figure 5.13 Effective thermal conductivity results for uniform length fibres. Results are presented with respect to AR for all the cases of orientation under investigation.

Figure 5.13 shows results for the effective thermal conductivity. Plots on the left side refer to longitudinal effective thermal conductivity while the plots on the right side of Figure 5.13 refer to the effective transverse thermal conductivity. Each row refers to a different UC size.

Analysing firstly the results on the left side of Figure 5.13, longitudinal effective thermal conductivity, it must be noticed that orientation is affecting the effective property.

1. Aligned fibres seem to be more conductive when compared with misaligned and randomly oriented. The lowest value of longitudinal thermal conductivity is in the case of randomly oriented fibres.
2. AR seems to make a small contribution to the property under investigation and only when it is combined with the appropriate orientation. For example, the same increase in the AR has a significant effect on randomly oriented fibres and almost no effect on aligned fibres.
3. In the case of transverse effective thermal conductivity, the exact opposite trend can be observed for both parameters (orientation and AR).
4. On the contrary to longitudinal effective stiffness, randomly oriented fibres seems to be more thermally conductive for the transverse direction, misaligned fibres less conductive and the orientation with the lowest transverse conductivity is the aligned fibres.
5. Regarding the AR, transverse effective thermal conductivity remains almost unaffected for the randomly oriented fibres as long as the AR increases, while misaligned and aligned fibres seems to slightly decrease as the AR increases.

The following Table 5-5 includes all the information shown in the previous plots regarding the effective thermal properties under investigation with respect to the AR for the three cases of orientation and the three cases of UC size. Results for the effective thermal conductivity for the longitudinal and transverse direction are presented in the following table with respect to the sample size, the orientation of fibres, the effective property and the aspect ratio.

Table 5-5 Results for effective thermal properties.

Orientation	Normalised UC size	Property under investigation	Effective property results		
			AR=1	AR=5	AR=10
Aligned	2.5	K_{11}	0.1168	0.1163	0.1180
	3.75	K_{11}	0.1136	0.1173	0.1181
	5.0	K_{11}	0.1097	0.1191	0.1176
	2.5	K_{22}	0.1160	0.0966	0.0970
	3.75	K_{22}	0.1136	0.0977	0.0964

	5.0	K_{22}	0.1096	0.0999	0.0969
Mis-aligned	2.5	K_{11}	0.1168	0.1124	0.1159
	3.75	K_{11}	0.1136	0.1161	0.1169
	5.0	K_{11}	0.1097	0.1152	0.1163
	2.5	K_{22}	0.1160	0.1032	0.0995
	3.75	K_{22}	0.1136	0.1022	0.0993
	5.0	K_{22}	0.1096	0.1026	0.0999
Randomly oriented	2.5	K_{11}	0.1168	0.0956	0.1053
	3.75	K_{11}	0.1136	0.1066	0.1076
	5.0	K_{11}	0.1097	0.1074	0.1077
	2.5	K_{22}	0.1160	0.0971	0.1090
	3.75	K_{22}	0.1136	0.1085	0.1071
	5.0	K_{22}	0.1096	0.1086	0.1065

5.1.2.2.2 Effective coefficient of thermal expansion

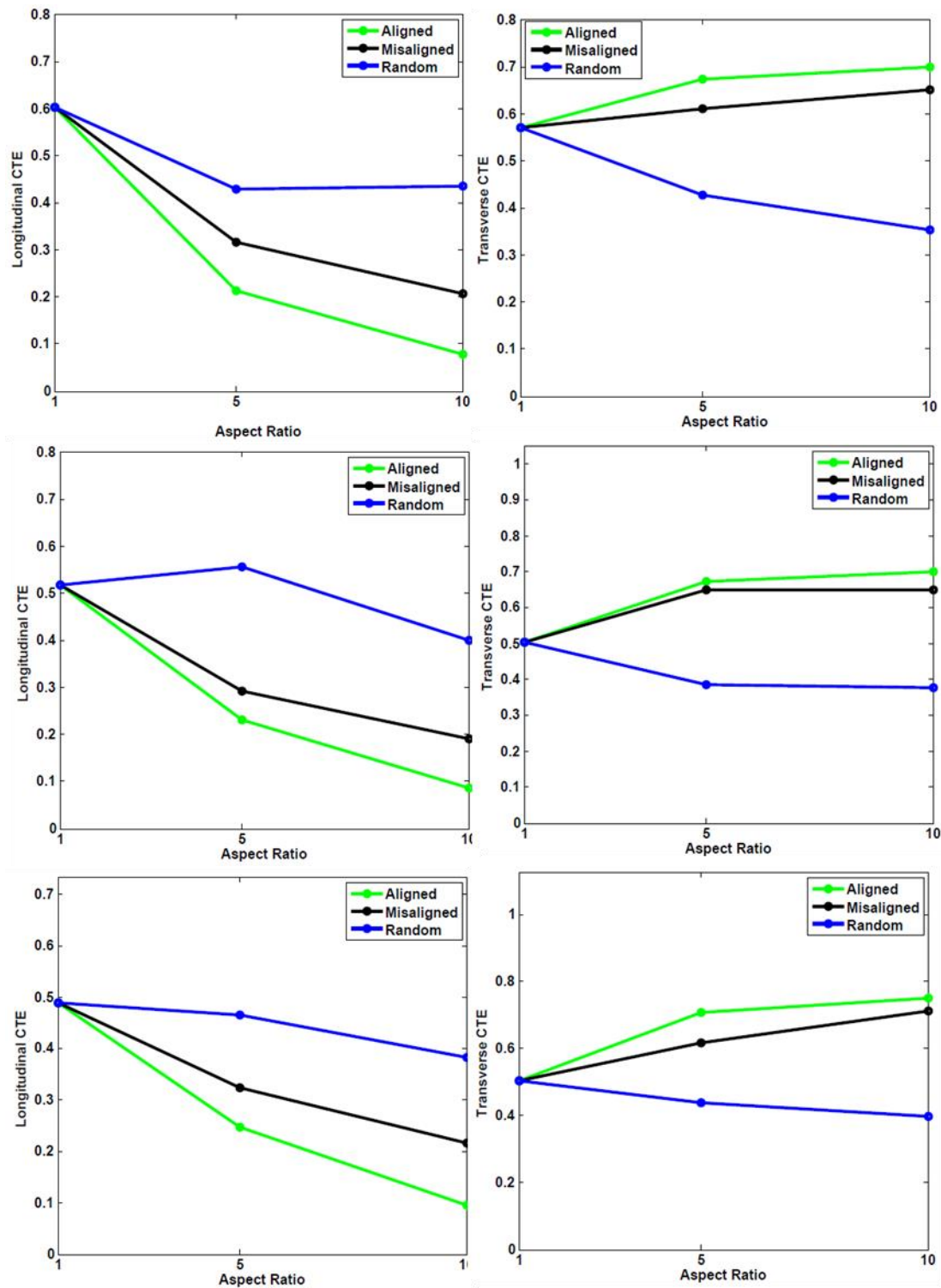


Figure 5.14 Effective CTE results for uniform length fibres. Results are presented with respect to AR for all the cases of orientation under investigation and units are $\frac{10^{-5}}{K}$.

Figure 5.14 shows the effective longitudinal and transverse coefficient of thermal expansion. The left side of Figure 5.14 refers to effective CTE for the longitudinal direction while the right side of Figure 5.14 refers to the effective CTE for the transverse direction.

As can be observed:

1. The longitudinal effective CTE randomly oriented fibres seems to have a higher CTE in comparison with misaligned fibres and randomly oriented fibres.
2. AR is also contributing in a negative way to longitudinal effective CTE. As can be observed, as the AR increases the effective longitudinal CTE decreases.
3. The opposite trend can be noticed for the effective transverse CTE with the exception of randomly oriented fibres. Firstly, in terms of orientation for effective transverse CTE, aligned fibres seems to have the higher CTE, while misaligned fibres have lower CTE and randomly oriented fibres have the lowest CTE.
4. Regarding the AR, CTE for realisations with aligned and misaligned fibres seems to increase as the AR increases (the opposite behaviour compared with longitudinal CTE) but in the case of randomly oriented realisations, CTE decreases as was observed for the longitudinal effective CTE.

The following Table 5-6 includes all the information shown in the previous plots about the effective thermo-mechanical properties under investigation with respect to the AR for the three cases of orientation and the three cases of UC size. Results for the effective coefficient of thermal expansion for the longitudinal and transverse direction are presented in the following table with respect to the sample size, the orientation of fibres, the effective property and the aspect ratio.

Table 5-6 Results for thermo-mechanical effective properties.

Orientation	RVE size	Property	AR=1	AR=5	AR=10
Aligned	2.5	CTE_{11}	$0.6035 * 10^{-5}$	$0.2130 * 10^{-5}$	$0.0774 * 10^{-5}$
	3.75	CTE_{11}	$0.5175 * 10^{-5}$	$0.2311 * 10^{-5}$	$0.0855 * 10^{-5}$
	5.0	CTE_{11}	$0.4887 * 10^{-5}$	$0.2472 * 10^{-5}$	$0.0953 * 10^{-5}$
	2.5	CTE_{22}	$0.5713 * 10^{-5}$	$0.6735 * 10^{-5}$	$0.6500 * 10^{-5}$
	3.75	CTE_{22}	$0.5040 * 10^{-5}$	$0.6735 * 10^{-5}$	$0.700 * 10^{-5}$
Mis-aligned	5.0	CTE_{22}	$0.5028 * 10^{-5}$	$0.7064 * 10^{-5}$	$0.7500 * 10^{-5}$
	2.5	CTE_{11}	$0.6035 * 10^{-5}$	$0.3156 * 10^{-5}$	$0.2063 * 10^{-5}$
	3.75	CTE_{11}	$0.5175 * 10^{-5}$	$0.2915 * 10^{-5}$	$0.2913 * 10^{-5}$

	5.0	CTE_{11}	$0.4887 * 10^{-5}$	$0.3241 * 10^{-5}$	$0.2166 * 10^{-5}$
	2.5	CTE_{22}	$0.5713 * 10^{-5}$	$0.6106 * 10^{-5}$	$0.6518 * 10^{-5}$
	3.75	CTE_{22}	$0.5040 * 10^{-5}$	$0.6488 * 10^{-5}$	$0.6489 * 10^{-5}$
	5.0	CTE_{22}	$0.5028 * 10^{-5}$	$0.6177 * 10^{-5}$	$0.7116 * 10^{-5}$
Randomly oriented	2.5	CTE_{11}	$0.6035 * 10^{-5}$	$0.4290 * 10^{-5}$	$0.4348 * 10^{-5}$
	3.75	CTE_{11}	$0.5175 * 10^{-5}$	$0.5562 * 10^{-5}$	$0.3995 * 10^{-5}$
	5.0	CTE_{11}	$0.4887 * 10^{-5}$	$0.4649 * 10^{-5}$	$0.3824 * 10^{-5}$
	2.5	CTE_{22}	$0.5713 * 10^{-5}$	$0.4281 * 10^{-5}$	$0.3533 * 10^{-5}$
	3.75	CTE_{22}	$0.5040 * 10^{-5}$	$0.3856 * 10^{-5}$	$0.3762 * 10^{-5}$
	5.0	CTE_{22}	$0.5028 * 10^{-5}$	$0.4389 * 10^{-5}$	$0.3980 * 10^{-5}$

5.2 Non mono-dispersed fibre length

Through the following sub-chapter chi-square results and effective properties results are presented for the elastic and the thermo-elastic responses of the material. The following paragraphs refer to the case of non-uniform fibre length. For the particular case being studied, fibre length distribution was seeded by a pseudorandom number generator as was presented in chapter 2.3.3.

5.2.1 Chi-square results

The following family of plots regards the chi square distribution and the effective mechanical, thermal and thermo-mechanical properties of realisations consisting of a randomly seeded fibre length. The distribution of fibre length can be characterised as uniform. Figure 5.15 shows the chi-square distribution for mechanical properties for aligned, misaligned and randomly oriented fibres. The horizontal axis indicates the size of the UC while the vertical axis defines the chi-square value of each property. Each plot refers to a different orientation. Chi square results for thermal properties

follow and the last chi square plots show the distribution of the test for thermo-mechanical properties.

5.2.1.1 Mechanical properties

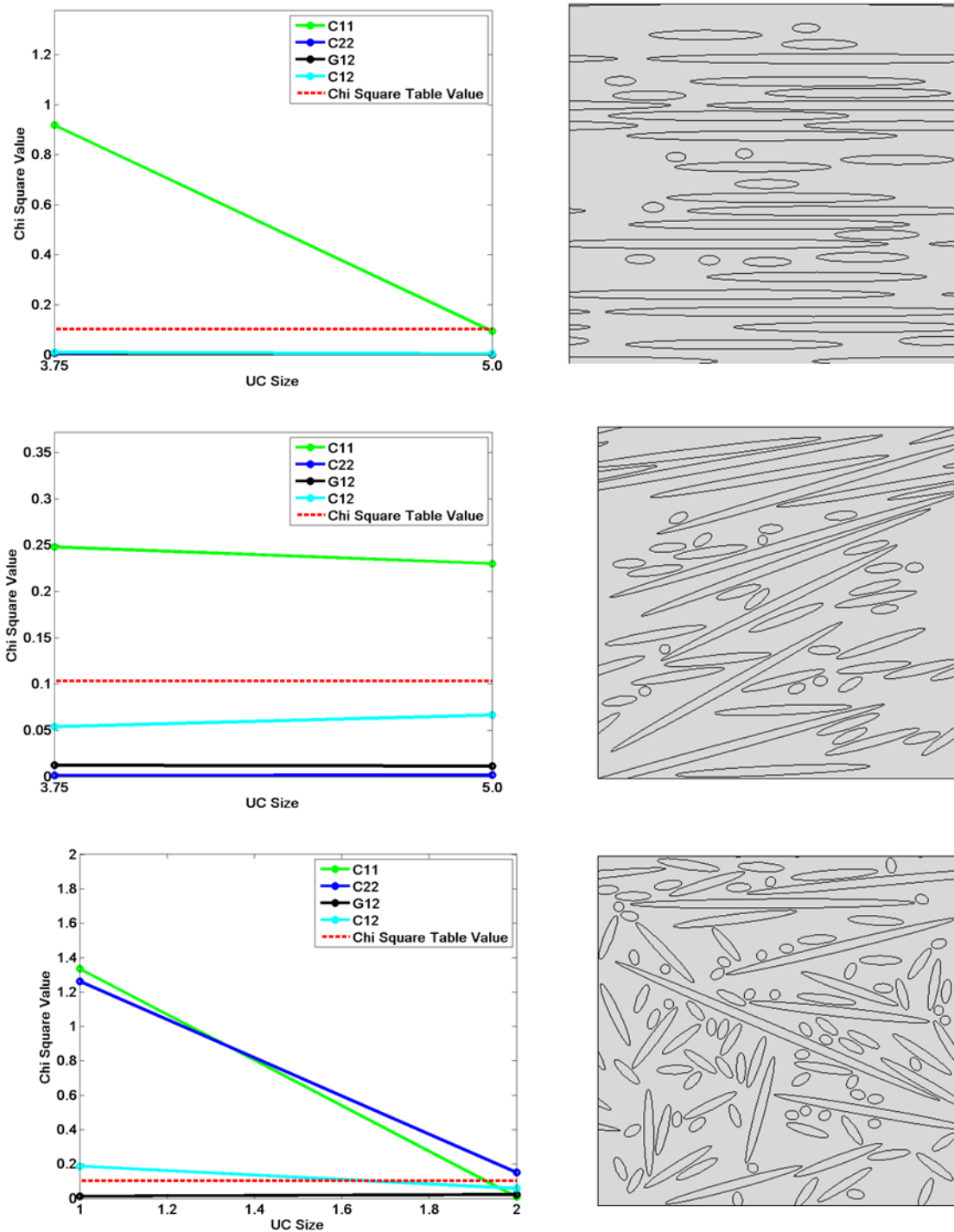


Figure 5.15 Chi-square results regarding the mechanical properties for non mono-disperse fibre length distribution, for three cases of orientation.

As can be seen in Figure 5.15 the general trend of the chi square values is to decrease as UC size increases. It can also be observed that:

1. Chi square values are higher in total compared with the chi-square values of mechanical properties of uniform fibres length realisations. This was expected since a new stochastic parameter has entered the system. As a consequence of increasing the uncertainty in the system, the deviation between the expected and the observed values of the five realisations' responses will increase.
2. As was observed for the mechanical properties of uniform length composite, for aligned fibres, the property with the higher chi-square value, so the greatest fluctuation in results is in the effective longitudinal stiffness. As was explained, this is due to the reinforcing contribution of oriented fibres. The main difference in that case is that the length of fibres is a random parameter for each realisation. As a result, the response of the material for five different realisations consisting of the same V_f and orientation varies depending on the stochastic fibre length. UC sizes that have chi-square values below the red discontinuous line on the plots do not experience any dependency of their response with the stochastic fibre length.
3. Comparing the chi-square values of the same mechanical property for a different case of orientation, it can be observed that randomly oriented fibre composite has the higher value for longitudinal, transverse stiffness and also for the effective shear stiffness. In the case of misaligned fibres results seems to have less deviation. This is reflected from the low high square values on the mechanical properties.
4. However compared with aligned fibres, transverse stiffness and shear stiffness have higher chi-square values.
5. Finally, for aligned fibres a large deviation was observed only for the case of longitudinal stiffness.

The following Table 5-7 includes all the information shown in the previous plots regarding the results of the chi-square test for the effective mechanical properties under investigation with respect to the three cases of orientation and the two cases of UC size. Results for the chi-square test for the longitudinal and transverse effective stiffness and for the effective shear stiffness are presented in the following Table 5-7 with respect to the sample size and the orientation of fibres.

Table 5-7 Chi-square results for mechanical properties of RLD.

Orientation	UC size	Property under investigation	Chi-square value
Aligned	2.5	C_{11}	Not-investigated
	3.75	C_{11}	0.9182
	5.0	C_{11}	0.0941
	2.5	C_{22}	Not-investigated
	3.75	C_{22}	0.0057
	5.0	C_{22}	0.0005
	2.5	G_{12}	Not-investigated
	3.75	G_{12}	0.0078
	5.0	G_{12}	0.0004
Mis-aligned	2.5	C_{11}	Not-investigated
	3.75	C_{11}	0.2480
	5.0	C_{11}	0.23
	2.5	C_{22}	Not-investigated
	3.75	C_{22}	0.0011
	5.0	C_{22}	0.0017
	2.5	G_{12}	Not-investigated
	3.75	G_{12}	0.0122
	5.0	G_{12}	0.0113
Randomly oriented	2.5	C_{11}	Not-investigated

	3.75	C_{11}	1.3356
	5.0	C_{11}	0.0085
	2.5	C_{22}	Not- investigated
	3.75	C_{22}	1.262
	5.0	C_{22}	0.1505
	2.5	G_{12}	Not- investigated
	3.75	G_{12}	0.0136
	5.0	G_{12}	0.0221

5.2.1.2 Thermal properties

The following family of plots regards the chi-square results for thermal properties and more specifically for the longitudinal effective thermal conductivity and the transverse effective thermal conductivity regarding all the cases of orientation and non mono-disperse fibre length. The plots are separated with respect to the fibres' orientation. The vertical axis indicates the chi-square value of each property while the horizontal axis indicates the UC size.

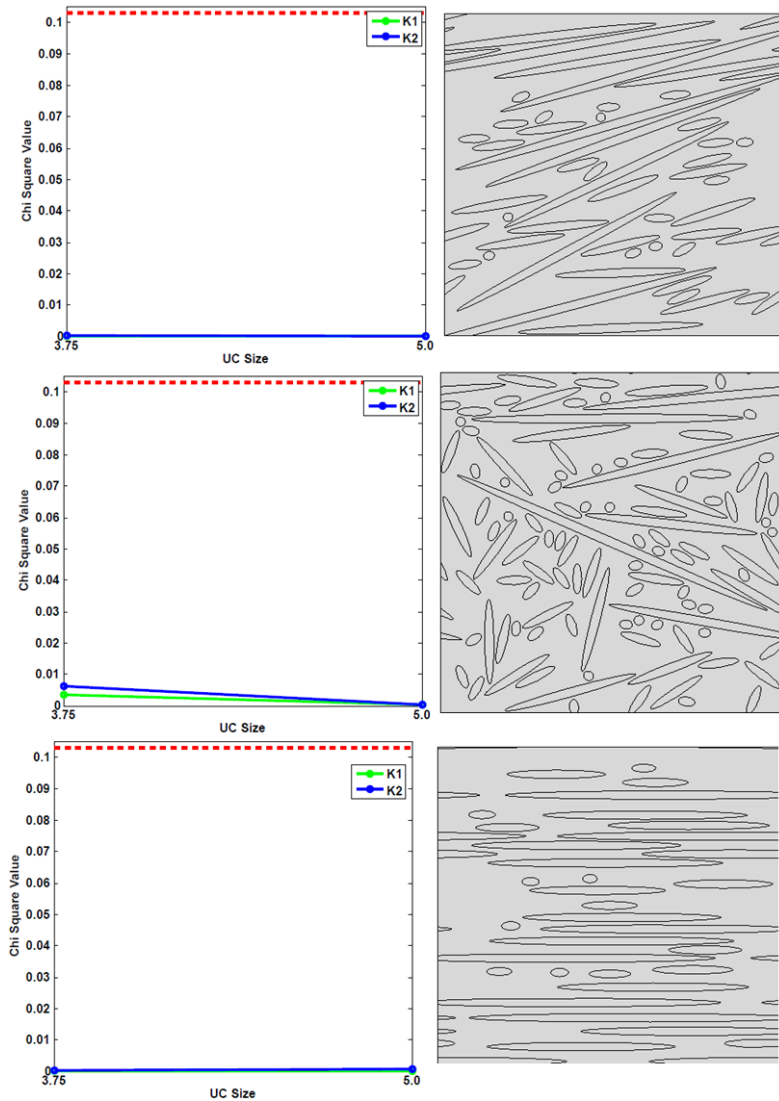


Figure 5.16 Chi-square results regarding the thermal conductivity for non mono-disperse fibre length distribution, for three cases of orientation.

As it can be seen in Figure 5.16 chi-square test results for the effective thermal conductivity have a very low value. A similar trend was observed for uniform fibre length. Results for the effective thermal conductivity seem to have very little deviation between the five realisations. It also seems not to be affected by the orientation. Only in the case of randomly oriented fibres a small increase in the chi-square value was observed, but this was still well below the criterion table value.

The following Table 5-8 includes all the information shown in the previous plots about the results of the chi-square test for the effective thermal properties under investigation with respect to the three cases of orientation and the two cases of UC size. Results for the chi-square test for the longitudinal and transverse effective thermal conductivity are presented in the following table with respect to the sample size and the orientation of fibres.

Table 5-8 Chi-square results for thermal properties of RLD.

Orientation	Normalised UC size	Property under investigation	Chi-square value	
Aligned	2.5	K_{11}	$0.1982 * 10^{-3}$	
	3.75	K_{11}	$0.1077 * 10^{-3}$	
	2.5	K_{22}	$0.3075 * 10^{-3}$	
	3.75	K_{22}	$0.6402 * 10^{-3}$	
	Mis-aligned	2.5	K_{11}	$0.1534 * 10^{-3}$
		3.75	K_{11}	$0.0947 * 10^{-3}$
2.5		K_{22}	$0.3826 * 10^{-3}$	
	3.75	K_{22}	$0.0654 * 10^{-3}$	
	Randomly oriented	2.5	K_{11}	0.0034
		3.75	K_{11}	0.0003
2.5		K_{22}	0.0063	
	3.75	K_{22}	0.0003	

5.2.1.3 Coefficient of thermal expansion

The following family of plots shows the chi-square distribution for the linear coefficient of thermal expansion, for non-uniform length, aligned fibres, misaligned fibres and randomly oriented fibres for all the cases of orientation under investigation and for two different UC sizes and for longitudinal and transverse coefficient of thermal expansion.

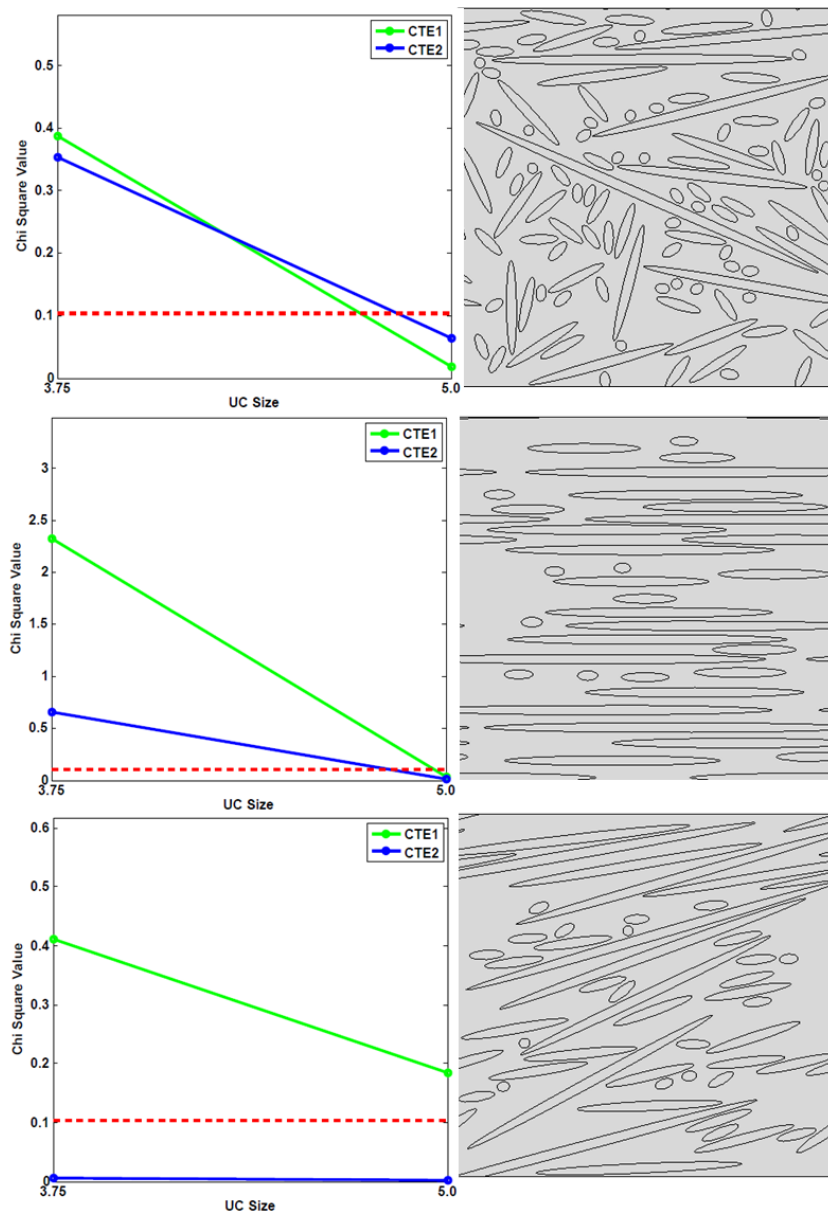


Figure 5.17 Chi-square results regarding the coefficient of thermal expansion for non mono-disperse fibre length distribution, for three cases of orientation.

As can be seen in Figure 5.17 chi-square values for the effective CTE for longitudinal and transverse direction are reduced as UC size increases. This trend was observed since the beginning of presenting the chi-square test and is also a general indication that the approach of a representative structure is pointing in the correct direction.

As can be observed the chi-square value differs depending on the property and on the orientation. As a general note it must be underlined that the first size under investigation is not representative in almost any case of random AR realisations. In some cases even the second-biggest size is not representative and larger UC realisations are needed. The higher chi-square value for longitudinal

CTE was in the case of aligned fibres, as was expected. For randomly oriented fibres both longitudinal and transverse CTE show very similar chi-square values, which means similar deviation between the observed and the expected value. This trend was observed in almost all cases of randomly oriented fibres and is a result of the isotropic response of randomly oriented short fibre composites. The case of misaligned fibres shows smaller value of chi-square test compared with the other two cases of orientation but the highest value on the second-larger UC size.

The following Table 5-9 includes all the information shown in the previous plots about the chi-square distribution with respect to the UC size for the longitudinal and transverse effective coefficient of thermal expansion. Results for the chi-square distribution are shown with respect to the UC size, the orientation of fibres and the effective property.

Table 5-9 Chi-square results for thermos-mechanical properties of RLD.

Orientation	Normalised UC size	Property under investigation	Random AR Chi-square value
Aligned	2.5	CTE_{11}	2.3212
	3.75	CTE_{11}	0.034
	2.5	CTE_{22}	0.6548
Mis-aligned	3.75	CTE_{22}	0.0111
	2.5	CTE_{11}	0.4111
	3.75	CTE_{11}	0.184
Randomly oriented	2.5	CTE_{22}	0.0053
	3.75	CTE_{22}	0.0016
	2.5	CTE_{11}	0.3867
Randomly oriented	3.75	CTE_{11}	0.0177
	2.5	CTE_{22}	0.353
	3.75	CTE_{22}	0.0637

5.2.2 **Effective mechanical properties**

The following plots are referring to effective properties. The first plots refer to mechanical properties, then thermal properties and thermo-mechanical properties. Figures are separated according to fibre orientation.

As in the case of uniform fibre length, effective mechanical, thermal and thermo-mechanical properties were studied with respect to various micromechanical parameters. The parameters that vary through the following results are fibre orientation distribution, UC size and fibre length distribution.

The following family of plots show the distribution of the mechanical thermal and thermo-mechanical effective properties with respect to UC size as a function of fibre orientation with respect to UC size. Each plot refers to a different fibre orientation.

5.2.2.1 Effective stiffness properties

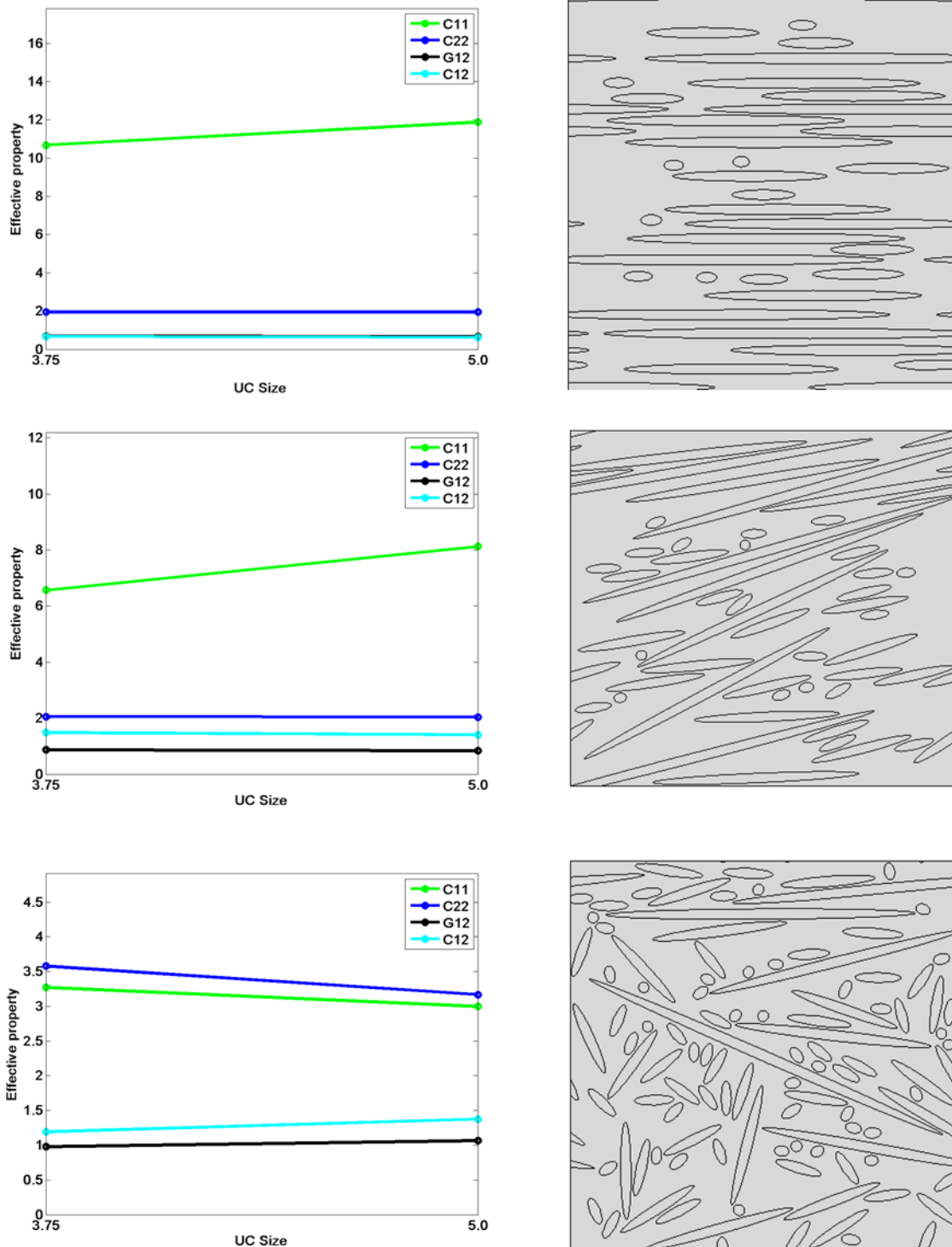


Figure 5.18 Mechanical effective properties for non mono-disperse fibre length for the three cases of orientation.

As it can be seen in Figure 5.18 each row represents different fibre orientation, and for each plot components of longitudinal, transverse and shear stiffness are presented.

1. As was observed for non-uniform length fibres the most reinforced parameter is the longitudinal stiffness.
2. Comparing results with the uniform fibre length it can be noted that non-uniform length shows higher effective mechanical properties.
3. However it is crucial to emphasise that results for the first UC size cannot be accepted as representative and also that uniform fibre lengths generally show much lower chi-square values, which is an indication of more accurate results.
4. Apart from the representativeness of results, the elevated stiffness is mainly caused by the percentage of fibres with an AR higher than 10. Fibres with $AR > 10$ offer the composite a higher degree of reinforcement.
5. As expected, higher longitudinal effective stiffness was observed for aligned fibres than misaligned fibres and the lower value of longitudinal effective stiffness is for randomly oriented fibres.
6. On the contrary, transverse effective stiffness has the higher value for randomly oriented fibres, while in the case of misaligned and aligned fibres very closed values were observed.
7. The same trend as transverse stiffness was observed for effective shear stiffness. The highest value was observed for randomly oriented fibres, while similar results were observed for misaligned and aligned fibres.

The following Table 5-10 includes all the information shown in the previous plots about the effective mechanical properties under investigation with respect to UC size for the three cases of orientation and the two cases of UC's size. Results for the effective mechanical properties are presented in the following table with respect to the sample size, the orientation of fibres and the effective property.

Table 5-10 Results of effective mechanical properties of RLD.

Orientation	Normalised UC size	Property under investigation	Random AR
Aligned	2.5	C_{11}	
	3.75	C_{11}	10.6836
	5.0	C_{11}	11.8822
	2.5	C_{22}	

	3.75	C_{22}	1.9512
	5.0	C_{22}	1.9509
	2.5	G_{12}	
	3.75	G_{12}	0.6837
	5.0	G_{12}	0.6587
Mis-aligned	2.5	C_{11}	
	3.75	C_{11}	6.567
	5.0	C_{11}	8.1329
	2.5	C_{22}	
	3.75	C_{22}	2.0599
	5.0	C_{22}	2.0380
	2.5	G_{12}	
	3.75	G_{12}	0.8716
	5.0	G_{12}	0.8341
Randomly oriented	2.5	C_{11}	
	3.75	C_{11}	3.2719
	5.0	C_{11}	2.9958
	2.5	C_{22}	
	3.75	C_{22}	3.579
	5.0	C_{22}	3.1664
	2.5	G_{12}	
	3.75	G_{12}	0.9786
	5.0	G_{12}	1.0645

5.2.3 Effective thermal conductivity

The following sub-chapter discusses effective property results for thermal conductivity. Results relate to the case of non mono-dispersed fibre length, the three cases of orientation (aligned, mis-oriented and random) and two UC sizes.

5.2.3.1 Effective thermal conductivity

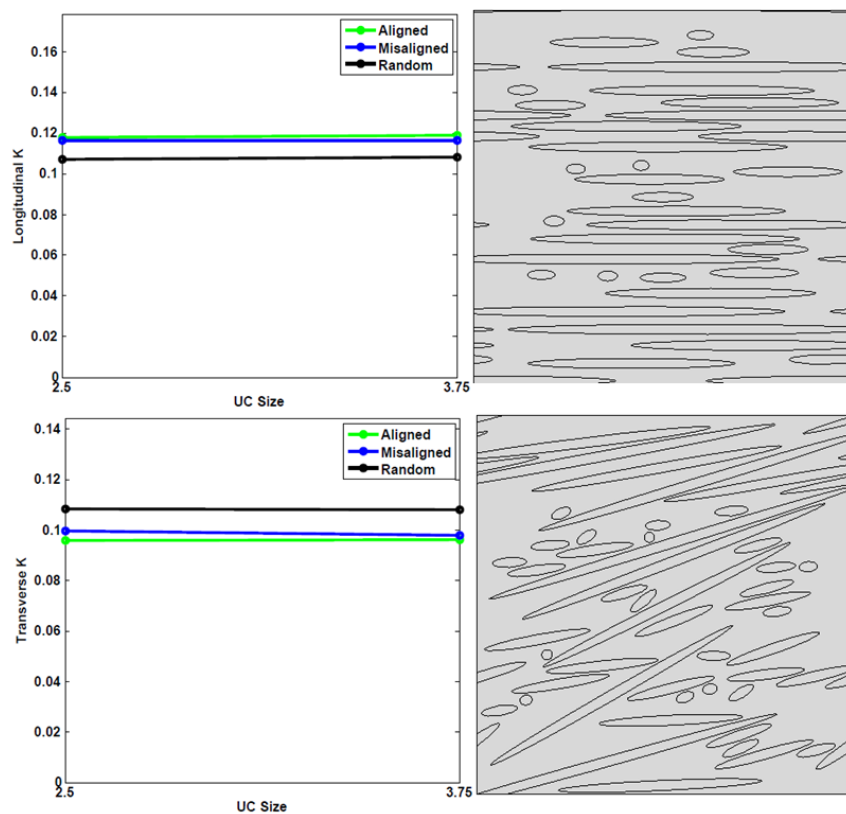


Figure 5.19 Thermal conductivity effective properties for non mono-disperse fibre length for the three cases of orientation.

Figure 5.19 shows results for the effective longitudinal and transverse thermal conductivity with respect to the UC size. The first row refers to longitudinal thermal conductivity while the second one refers to the thermal conductivity on the transverse direction. For each plot different colour refers to different orientations.

As can be seen in the plots of Figure 5.19

1. Results of the effective thermal conductivity differs with respect to the case of orientation but they slightly change with respect to the UC size. This is something which is also reflected in the chi-square plots by the very low value on the test.

2. Regarding the orientation, the response of realisation on thermal loading shows the opposite trend in terms of the direction of the property.
3. In the case of longitudinal effective stiffness, higher conductivity was observed for aligned fibres, misaligned fibres are less conductive and random fibres exhibit the less conductivity.
4. For thermal conductivity on the transverse direction the opposite trend was observed. Randomly oriented fibres show the higher conductivity, misaligned fibres show less conductivity while the lower conductivity value was observed for the case of aligned fibres.

The following Table 5-11 includes all the information shown in the previous plots about the effective thermal properties under investigation with respect to UC size for the three cases of orientation and the two cases of UC size. Results for the effective mechanical properties are presented in the following table with respect to the sample size, the orientation of fibres and the effective property.

Table 5-11 Results of effective thermal properties of FLD.

Orientation	Normalised UC size	Property under investigation	Effective property value
Aligned	2.5	K_{11}	0.1180
	3.75	K_{11}	0.1189
	2.5	K_{22}	0.0958
Mis-aligned	3.75	K_{22}	0.0962
	2.5	K_{11}	0.1166
	3.75	K_{11}	0.1166
Randomly oriented	2.5	K_{22}	0.0998
	3.75	K_{22}	0.0980
	2.5	K_{11}	0.1070
	3.75	K_{11}	0.102
	2.5	K_{22}	0.1084
	3.75	K_{22}	0.1083

5.2.3.2 Effective coefficient of thermal expansion

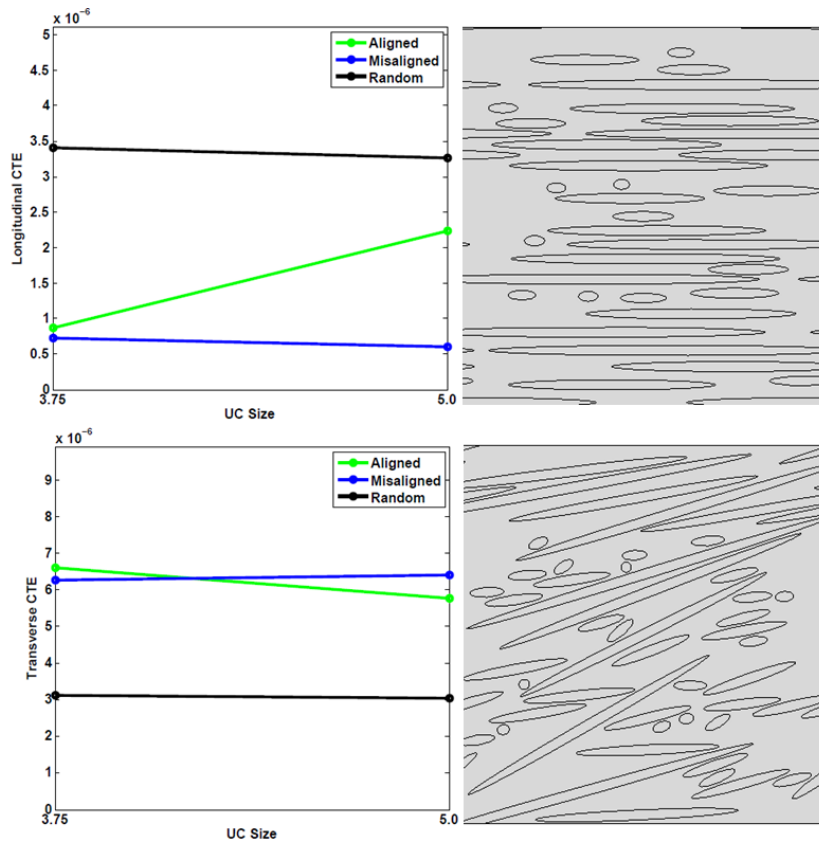


Figure 5.20 Coefficient of thermal expansion for non mono-disperse fibre length for the three cases of orientation.

Figure 5.20 shows the effective longitudinal and transverse CTE. The first row refers to the longitudinal CTE while the second one refers to the transverse CTE. For each plot a different colour indicates a different fibre orientation, while the vertical axis shows effective property results and the horizontal axis shows the UC size.

As can be seen:

1. The behaviour of the effective CTE with respect to UC size is constant except in the case of aligned fibres.
2. On the contrary a big difference can be observed for the case of different orientations. For longitudinal effective CTE randomly oriented fibres show the highest CTE, while aligned fibres follow and finally the lower value of CTE was observed for misaligned fibres.
3. Transverse effective CTE shows very closed values for aligned and misaligned orientations, while the smaller CTE value was observed for randomly oriented fibres.

Up to this point it must be emphasised that results have meaning only if the analogous chi-square results lay below the red discontinuous line so they can be considered as representative.

The following Table 5-12 includes all the information shown in the previous plots about the effective thermo-mechanical properties under investigation with respect to UC size for the three cases of orientation and the two cases of UC size. Results for the effective thermo-mechanical properties are presented in the following table with respect to the sample size, the orientation of fibres and the effective property.

Table 5-12 Results of the effective thermo-mechanical properties of FLD.

Orientation	Normalised UC size	Property under investigation	Effective property value
Aligned	2.5	CTE_{11}	$0.0863 * 10^{-5}$
	3.75	CTE_{11}	$0.2231 * 10^{-5}$
	2.5	CTE_{22}	$0.6598 * 10^{-5}$
	3.75	CTE_{22}	$0.577 * 10^{-5}$
Mis-aligned	2.5	CTE_{11}	$0.7212 * 10^{-6}$
	3.75	CTE_{11}	$0.605 * 10^{-6}$
	2.5	CTE_{22}	$0.6258 * 10^{-5}$
	3.75	CTE_{22}	$0.6398 * 10^{-5}$
Randomly oriented	2.5	CTE_{11}	$0.3405 * 10^{-5}$
	3.75	CTE_{11}	$0.3263 * 10^{-5}$
	2.5	CTE_{22}	$0.312 * 10^{-5}$
	3.75	CTE_{22}	$0.3045 * 10^{-5}$

5.3 Comparison with analytical models

Considering the mechanical, thermal and thermo-mechanical effective properties calculated from the numerical analysis a direct comparison with various analytical models will take place in the following section. The micromechanical analytical models which will be compared with numerical results were presented in chapter 2.

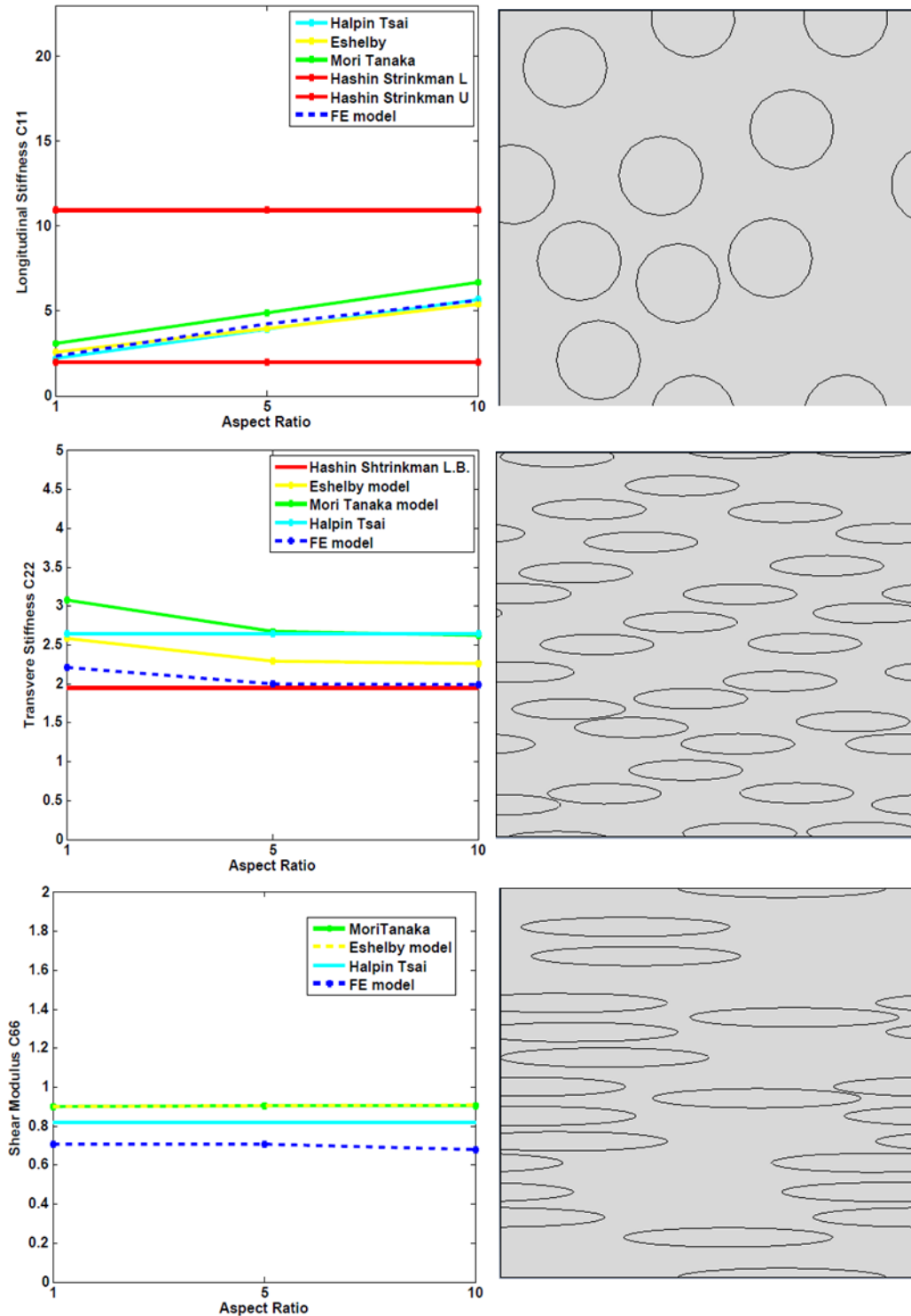


Figure 5.21 Comparison of FEA results with various analytical models for longitudinal transverse and shear stiffness

Comparison will take place as a function of AR and the majority of the following micromechanical models are able to consider any changes in the AR. The comparison is separated in terms of the property and the orientation.

Figure 5.21 shows effective properties calculated from numerical models in comparison with various analytical models. Results from numerical models were derived for normalised RVE size equal to 3.75. Each row on Figure 5.21 refers to a different property.

1. The first plot shows results for longitudinal stiffness of aligned fibres. As can be seen numerical results lay between Halpin-Tsai predictions, Mori-Tanaka and Eshelby predictions. With the red line the broad bounds of longitudinal and transverse direction are indicated. The numerical model is able to quite accurately simulate the reinforcement phenomenon of higher AR as the analytical models
2. The second plot refers to transverse stiffness of aligned fibres. As can be observed numerical models predictions lay below the Halpin-Tsai predictions, the Mori-Tanaka and Eshelby's predictions, and slightly above Hashin Strinkman's lower bound.
3. The third plot shows predictions for shear stiffness. Numerical predictions of shear stiffness seem to slightly underestimate the property compared with the predictions of analytical models. Finite element models lay below the predictions of Eshelby's model, Halpin-Tsai's model and Mori-Tanaka's model.

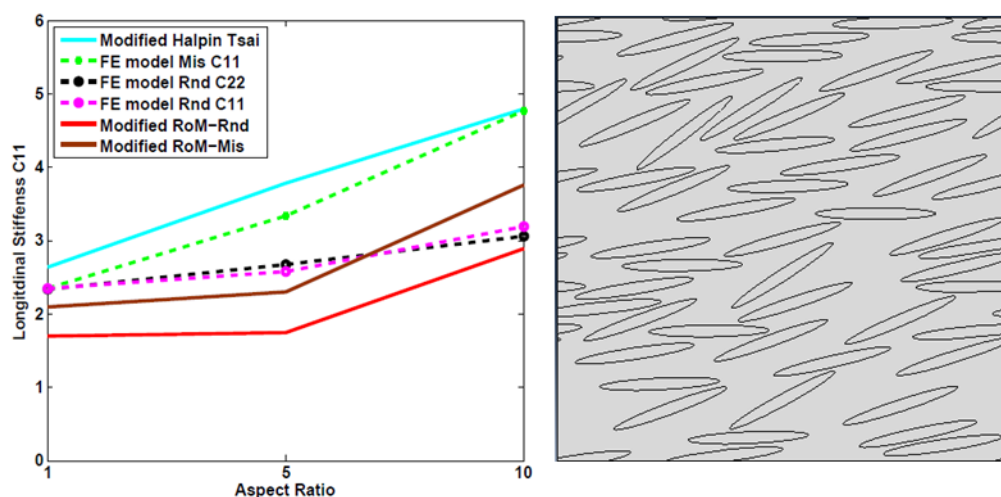


Figure 5.22 Comparison of FEA results with various analytical models for the case of randomly oriented and misaligned fibres

Figure 5.22 shows a prediction of the longitudinal and transverse stiffness of randomly oriented and misaligned fibres. For comparison with numerical models a modified version of the RoM was used based on the orientation distribution of the developed models. The factor modifying the RoM in order to account for misaligned and randomly oriented fibres was calculated based on the fibre orientation of the compared numerical model. Results show that numerical predictions for misaligned fibres and for randomly oriented fibres lay between the predictions of the analytical models.

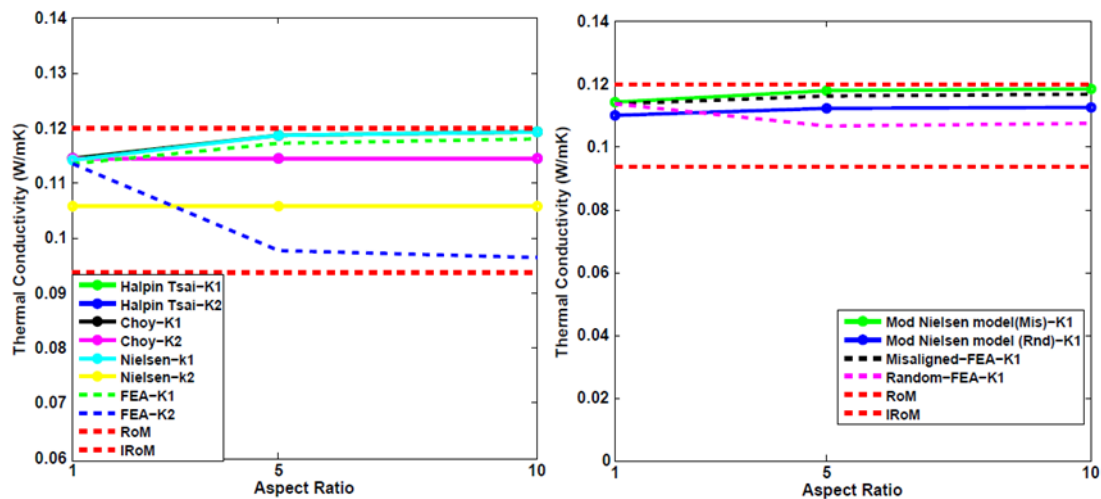


Figure 5.23 Comparison of FEA results with various analytical models for thermal conductivity for aligned and misaligned fibres.

Figure 5.23 shows a comparison between the predictions of various analytical models with the predictions of numerical models regarding the effective thermal conductivity. The plot on the left shows predictions of thermal conductivity on the longitudinal and transverse direction. As can be seen predictions of the numerical models lay between the general bounds of the RoM and the IRoM. Longitudinal effective conductivity follows the predictions of the Halpin-Tsai model while transverse thermal conductivity tends to asymptotically follow the lower bound.

The plot on the right side is a comparison between analytical and numerical models for misaligned and randomly oriented fibres. In the case of random orientation there is no longitudinal and transverse thermal conductivity because the general trend is an isotropic behaviour of the material due to the nature of reinforcement. As a result a single value of thermal conductivity was calculated, able to describe the thermal behaviour of the material in both directions. As can be seen predictions of the numerical models for misaligned and randomly oriented fibres are close to the predictions of

the modified Nielsen model and generally lay between the general bounds indicated with the red discontinuous line.

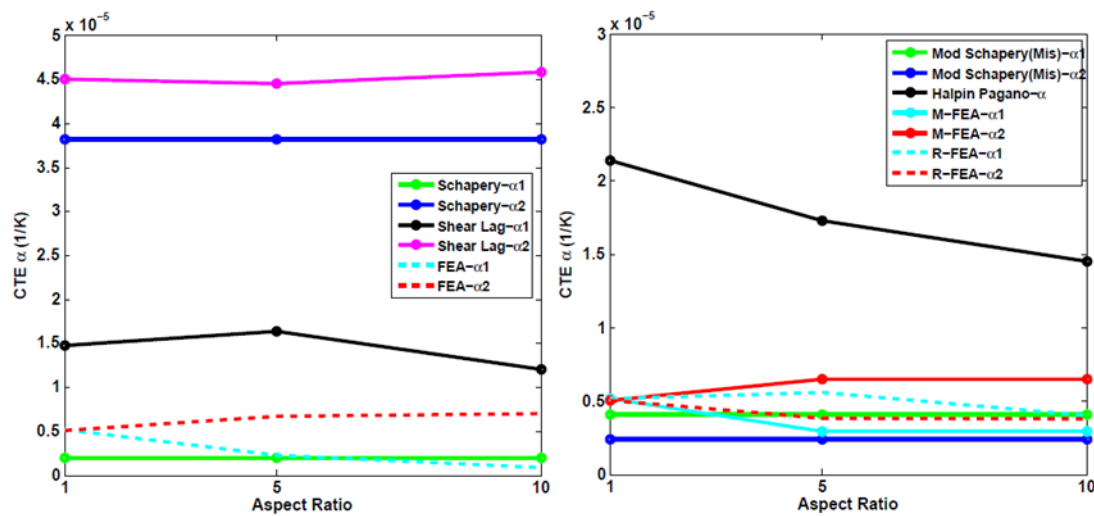


Figure 5.24 Comparison between FEA results and analytical models for coefficient of thermal expansion for aligned, misaligned and randomly oriented fibres.

Figure 5.24 shows a comparison between numerical models and analytical models for the predictions of effective coefficient of thermal expansion. The plot on the left side shows the prediction of longitudinal and transverse CTE for the case of fully aligned fibres. As can be seen finite element predictions for longitudinal CTE coincide with predictions from the Schapery model for longitudinal CTE while numerical calculations for the transverse CTE seems to deviate from the analytical predictions.

The plot on the right side of Figure 5.24 shows predictions of numerical and analytical models for the case of misaligned and randomly oriented fibres. Results seem to have a good agreement with predictions of the modified Schapery model, and to be well below the Halpin-Pangano model's predictions.

5.4 Conclusions

Throughout chapter 5 results from the numerical analysis were presented. The first section of the chapter deals with composite UCs consisting of uniform length fibres while the second section refers to non-uniform fibre length distribution. For each case of fibre length distribution (uniform or not) chi-square results are presented first and effective properties follow. Chi-square results are presented at the beginning of the chapter in order to emphasise their role. The effective properties results have no meaning if they are not interpreted in combination with the chi-square results.

The first section is divided in sub-sections with respect to the physical meaning of the properties under investigation. First the mechanical properties were presented, the thermal properties follow, while the thermo-mechanical properties are presented at the end.

Chi square results for mechanical properties show that in order to ensure that the UC is representative of the material, a size 3.75 times larger than the inclusion's larger dimension must be considered. The 3.75 normalised UC size satisfies the criterion for thermal and thermo-mechanical properties as well.

A strong dependency between the chi-square value and the fibre orientation, the AR and the property under investigation was observed. The last two parameters are not independent from each other. An increase in the AR leads to reinforcement of a specific property. Properties which are reinforced due to AR increase shows higher chi-square values. This is due to the fact that more reinforced properties tend to have a stronger dependency on the realisations. However this is not something independent of the fibre orientation. Increasing the AR will cause a direct increase in longitudinal stiffness for aligned fibres and an increase in the chi-square value of the specific orientation and property. However increasing the AR for randomly oriented fibres will not cause the same increase in the effective property and obviously not in the chi-square value. As a consequence the representativeness of the size is a property depending on the combination of AR and fibre orientation.

On the contrary, a common behaviour for all the properties under investigation and all the cases of AR and fibre orientation is the decrease of chi-square value with the increase in the UC size. This behaviour was observed for almost all the chi-square plots and as was mentioned previously, this is caused by the fact that larger UC sizes include more information about the structure and as a result the responses of the five realisations are closer to each other. Observed and expected values do not deviate.

As a consequence a conclusion regarding the first section of the chapter is that a UC is considered as representative of the material once it satisfies the chi-square criterion. Parameters such as AR and FO, and the combination of the two, strongly influence the representativeness of a UC's size. For the specific composite material under investigation (specific degree of inhomogeneity) and for the specific range of AR, the Representative Volume Element can be defined once the size of the UC is larger than 3.75 times the larger dimension of the inclusions.

The second sub-section of the chapter includes results for the effective properties under investigation. As in the first section of the chapter, results for mechanical properties are presented

first, while results for thermal and thermo-mechanical analysis follow. Through the analysis of the response of the material, the contribution of parameters such as AR or FO on the macroscopic effective properties was evaluated. AR seems to be a very dominant parameter for the mechanical properties of a composite material. It was clear from the results that higher AR leads to higher effective properties once it is combined with the proper orientation regarding the property of interest. Direct comparison of the effective properties with the same orientation but with different AR gives a clear picture of the enhancement of the mechanical properties with the increase of AR. However the enhancement does not take place for every property. In order to reinforce specific properties of the material, the increase in AR must be combined with the appropriate orientation for the specific property.

On the other hand a direct comparison with UC consisting of the same AR but different fibre orientation shows the importance of the appropriate orientation in order to get elevated mechanical properties. Nevertheless reinforcement of the same property due to different orientation is less in comparison with the degree of reinforcement on the same property when orientation is the same but AR changes.

A general orthotropic behaviour was observed in the case of aligned discontinuous fibres while the misaligned fibres showed a behaviour close to the special orthotropic. Randomly oriented fibres exhibit an almost isotropic behaviour. As a consequence of the symmetry of the material, aligned fibres lead to higher longitudinal effective stiffness while randomly oriented fibres lead to higher transverse effective stiffness and higher effective shear stiffness. It must be emphasised that reinforcement of each property is a combination of the AR and the orientation.

The influence on the mechanical properties from AR is strongly dependant on the property and on the orientation of fibres. For aligned fibres AR has a strong influence on the longitudinal stiffness while transverse stiffness and shear stiffness seem to be almost unaffected by the changes in AR. For misaligned fibres the case was slightly different. Longitudinal stiffness was again increased but at a lower rate compared with aligned fibres; also shear stiffness increased with respect to AR increase. For randomly oriented fibres longitudinal and transverse stiffness have almost the same value and the same influence once the AR increases. The case of shear stiffness for randomly oriented fibres is the only one in which the influence of AR on the shear stiffness is high. Shear stiffness seems to increase linearly with respect to AR. This is a phenomenon for effective shear stiffness which was observed only for the case of randomly oriented fibres.

Analysing the thermal and thermo-mechanical properties, chi square analysis indicates that chi-square value for thermal conductivity is very slightly influenced by the AR or fibre orientation. The Chi-square value for thermal conductivity is very low and well below the critical value. This is something which indicates that results from the five realisations concerning thermal conductivity converge to a specific value relatively easily. On the contrary, chi-square results for the effective CTE show a strong dependency on the chi-square results for AR and fibre orientation. More specifically, as can be seen in chi-square analysis, the first size under investigation turned out not to be representative. As a result representative volumes for that specific range of AR and the cases of orientation under study must be 3.75 times larger than the larger dimension of the inclusions.

Effective thermal conductivity shows similar trends as the chi-square values for thermal conductivity. A very small influence of the AR on the actual effective property was observed. Also the opposite

trend was observed regarding the direction of the property (longitudinal or transverse thermal conductivity) and the orientation of the fibres. In general the trend was for longitudinal thermal conductivity aligned fibres to show a more conductive response, while for the transverse effective thermal conductivity randomly oriented fibres show a more conductive response. The misaligned oriented fibres lay between aligned and randomly oriented fibres.

Regarding the effective coefficient of thermal expansion, a strong influence from both parameters (AR and orientation) was observed. More specifically for the longitudinal effective CTE as long as the AR increases the effective property decreases. This opposite trend was observed in the case of effective transverse CTE. The effective property increases as AR increases.

Effective thermal conductivity also shows a strong dependency on the fibre orientation. For transversely effective CTE aligned fibres have the higher effective property, while misaligned fibres exhibit lower CTE and randomly oriented fibres exhibit the lowest CTE. For transverse effective CTE the opposite trend was observed. Randomly oriented fibres exhibit the higher CTE with misaligned orientation following a similar trend. Aligned fibres exhibit much lower CTE compared with the other two cases of orientation.

Chi-square analysis of random length realisations for mechanical properties shows that there is a strong dependency of the results with the UC size. By far the 3.75 normalised UC size cannot be considered as representative. In some cases (misaligned fibres for longitudinal stiffness and random orientation for transverse stiffness) even the 5.0 normalised size is not representative.

Effective mechanical properties of stochastic length realisations exhibit higher stiffness for all the properties compared with uniform length realisations. However results from stochastic length realisations must be treated with care because chi square results show that at least the small size of the UC is not representative. The main reason for the elevated stiffness in comparison with uniform AR is the fact that stochastic length realisations include fibres with AR larger than 10 which enhanced the stiffness.

Chi-square plots for non-mono-dispersed realisations regarding effective thermal conductivity show similar results to the case of mono-dispersed fibres length. Deviation between the observed and the expected values of the material response seems to be very small and that is reflected as a very small chi-square value.

Effective thermal properties show no noticeable change with respect to the UC size. Between the longitudinal effective thermal conductivity and the transverse effective thermal conductivity the opposite trend was observed regarding the orientation of fibres. In the case of longitudinal thermal conductivity, aligned fibres exhibit the higher value with the misaligned fibres very close, having an almost similar response. Randomly oriented fibres exhibit the lower longitudinal thermal conductivity. In the case of transverse effective thermal conductivity randomly oriented fibres show the more conductive behaviour while misaligned and aligned oriented fibres exhibit lower thermal conductivity with very close results. Aligned fibres show the lowest transverse thermal conductivity.

Chi-square results for the coefficient of thermal expansion seem to have a very similar response to the chi-square results of the mechanical properties. Results for the normalised size of 3.75 cannot be

considered as representative for both longitudinal and transverse directions with an the exception of misaligned fibres and transverse CTE.

Regarding the effective thermo-mechanical properties, results show a strong dependency between the property and the size of the UC. This was clear from the chi-square analysis, however it is also obvious for the longitudinal effective CTE on the effective properties plots. Concerning the longitudinal effective CTE, randomly oriented fibres exhibit the higher CTE while misaligned fibres shows the lower CTE value. Both orientations shows gradual changes with respect to the size, while aligned fibres lay between the aforementioned orientation cases and change dramatically with the size. In general, for more accurate results regarding the case of stochastic fibre length, a larger UC size must be considered. As a consequence results can be under discussion, but is not the correct approach to derive conclusions about the response of the material.

The chapter concludes with a direct comparison of the numerical results with various analytical models and approaches. The analytical models under comparison have been discussed and presented in chapter 2. In general the comparison shows an acceptable agreement between the numerical method and the analytical models. Overall properties always lay between the general bounds of the constituents. More specifically, regarding the longitudinal stiffness of aligned fibres, numerical results show an excellent agreement with analytical predictions of theoretical and semi-empirical models. Transverse stiffness numerical results lay slightly below the theoretical models' predictions but above the general bounds. In the case of transverse stiffness it seems that the numerical model is able to capture a small reduction of the property as AR increases, a phenomenon that can't be captured with most analytical models. Effective shear stiffness is slightly underestimated compared with analytical predictions. Results for misaligned and randomly oriented numerical models were compared with modified analytical models. Analytical models were modified in order to be able to account for the fibre orientation. Results show good agreement for aligned fibres but also for randomly oriented fibres.

Thermal and thermo-mechanical results from numerical models were also compared with analytical models' predictions. Regarding the comparison of the effective thermal conductivity results for both cases of longitudinal and transverse thermal conductivity lay between the general bounds. Results for the longitudinal thermal conductivity seem to have an excellent agreement with predictions of analytical models, while results for the transverse thermal conductivity shows a dependency-reduction as AR increases, a behaviour which was not observed from the analytical models. Comparison of numerical results for thermal conductivity of randomly oriented fibres also shows a very good agreement with the modified versions of analytical models.

Regarding the comparison of numerical results of CTE with analytical predictions, the cases of aligned fibres, randomly oriented and misaligned fibres were examined. The comparison for aligned fibres shows a very good agreement regarding the longitudinal effective CTE, while the transverse CTE deviates from the analytical models' predictions. In the case of randomly oriented and misaligned fibres, results lay within the general bounds and show a good agreement with analytical predictions.

It must be emphasised that deviation of predictions from all the models is a parameter strongly dependant on the degree of inhomogeneity of the material. For this specific study the composite under investigation has a high degree of inhomogeneity.

6 Summary and conclusions

Composite material is without any doubt the material of the future. The lack of natural resources, the high demands of engineering materials, the elevated properties of composite structures and the new manufacturing processes for composite materials are a few of the driving forces towards the engineering material changes. Considering the aforementioned statement, a range of topics from the accurate simulation of the material's response to the after service life of the material, are arising. When designing and manufacturing composite material the impact of the material on the environment must always be considered. Thermoplastic composite material is a promising solution to the problem of after-service-life of composite materials. Through this thesis a computational approach to material characterisation was presented and the potential of using thermoplastic recycled material was examined. Through the following section the general conclusions for each chapter will be presented.

Chapter 1

Throughout chapter 1 several aspects regarding short fibre composites were covered. The main manufacturing processes were presented and the influence of each process on several parameters of the material was discussed.

The dominant factors affecting the macro-mechanical performance of SFRC were addressed and further discussion on the influence of those factors took place. The chapter covers through literature three aspects of material characterisation. Initially various theoretical approaches on the field of mechanical characterisation of material are presented. The second aspect is covered by the computational approach of material characterisation and the third aspect regards the experimental characterisation of materials. The fields of thermal and thermo-mechanical characterisation of materials, as reported in literature, are also covered while a general report on homogenisation approaches is also addressed.

Chapter 2

In chapter 2, various aspects of the field of linear continuous solid mechanics were presented with emphasis on the micromechanical analytical modelling of the major parameters affecting the performance of SFRC. The concept of inclusion and inhomogeneity was presented and the major differences were pointed out, while definitions for homogeneous and inhomogeneous media were given with the assumption that follows each definition. The symmetry of materials was discussed and various degrees of anisotropy were presented. The effect of material symmetry on the fourth order stiffness tensor was shown and the necessary independent elastic constants for each degree of anisotropy were reported. The concept of a high performance short fibre composite material was discussed through the analysis of the major factors affecting the mechanical behaviour of SFRC. Parameters such as fibre orientation, fibre length distribution, volume fraction and elastic properties of the constituent materials were covered. Those parameters were presented in detail with various theoretical approaches for calculating their influence on the overall effective properties through performance factors. A general report of various modelling strategies follows by pointing out the differences between different modelling approaches and reporting their advantages and disadvantages. The chapter concludes with a study of various micromechanical models for

mechanical, thermal and thermo-mechanical property characterisation. Each micromechanical model consists of a different approximation of the effective material properties. Assumption and calculation aspects were further discussed. Finally a comparison between the predictions of each analytical model is presented.

Chapter 3

Throughout chapter 3, various issues relating to the numerical modelling of short fibre composites were presented. The very basic problem of packing was first addressed and the major difficulties in finding a solution were presented. A further analysis of the proposed solution to the packing problem, through a developed packing algorithm follows. The main difficulties during the development of the algorithm were reported, followed by the limitations and the efficiency of the algorithm. The time response of the programme was discussed and the influence of various parameters on the time response of the algorithm were evaluated. The main assumptions of the modelling approach were presented and a discussion of the influence of those assumptions took place. Representation of fibres as elliptical domains was further discussed considering the advantages and disadvantages of this simplification. The concept of periodic and non-periodic microstructures was discussed and the way of implementing this periodicity was presented in detail. Definitions of the representative volume element were given and the common points in the different approaches of different researchers were reported. The differences between an RVE and a UC were also noticed. The existence of RVE as a function of size was discussed and the implementation of length scales on the RVE concept was presented. A specific approach to the assumptions of modelling short fibre reinforced composite took place by analysing the simplification of the modelling microstructure with the properties of a real microstructure. The chapter concludes by presenting the numerical model set-up. The development of the packing algorithm using the Matlab programming language and the way of transferring the microstructure to the commercial FE software Abaqus through python scripting were shown. Finally, the various cases of boundary conditions used for this type of problems were addressed and advantages and disadvantages for each case were discussed.

Chapter 4

In chapter 4, the concept of computational homogenisation was discussed. The definition of the homogenisation process was given and the significance of the method on material characterisation was addressed. Various computational homogenisation approaches were presented and a discussion around the accuracy and the difficulty of implementation of each approach took place. The major homogenisation approaches, the asymptotic homogenisation method, the volume average and the reaction force methods were further analysed. The macro-homogeneity condition was presented and the concept of equivalent homogeneous media was discussed. A report on the effective properties under investigation follows. Longitudinal effective stiffness, transverse effective stiffness and effective shear modulus for the mechanical properties, while for the thermal properties the effective thermal conductivity was the property under investigation and for the thermo-mechanical simulations the effective linear coefficient of thermal expansion was the property under

investigation. A detailed discussion on the implementation of boundary conditions and the calculation of effective properties was presented. Finally, the chapter ends with a report on the statistical test. The question of the representative size has been answered through a statistical test. The chapter does not provide results from the chi-square test but a quality discussion on the importance of the test and the major factors affecting the test. Further investigation for the influence of various parameters on the chi-square value took place and the influence of the fibre orientation, aspect ratio, effective property and RVE size were discussed.

Chapter 5

Throughout chapter 5 results from the numerical analysis were presented. The first section of the chapter deals with composite UCs consisting of uniform length fibres while the second section refers to non-uniform fibre length distribution. For each case of fibre length distribution (uniform or not) chi-square results are presented first and effective properties follow. Chi-square results are presented at the beginning of the chapter in order to emphasise their role. There is no meaning to the effective properties results if they are not interpreted in combination with the chi-square results. A detailed discussion of the results takes place for each family of plots throughout the chapter and useful information can be derived. Evaluation of the contribution of each micromechanical parameter under study took place for chi-square tests and for the actual effective properties. In general the analysis shows that the method of combined numerical and statistical methods can estimate accurately enough the effective properties of a composite material. Results show that reinforcement of the material through an increase of AR or fibre orientation towards the direction of the property under study causes an increase in the chi-square value, and as a consequence, an increase in the UC size, in order to be representative. Further than that through the specific research the assumption of a two dimensional approach was implemented in order to overcome computational power difficulties. Comparison with analytical models took place at the end of the chapter and was a verification that the two dimensional RVE were able to predict the mechanical, thermal and thermo-mechanical effective properties of a composite system. The major question regarding the representative size was answered through chi-square test. As was shown through the tests there is no clear contribution of a single parameter, but a combination of micromechanical parameters have to be considered in order to conclude about the influence on the representative size. For mono-dispersed fibre length chi-square results show that representative size exists for specific materials exhibiting a high degree of inhomogeneity, in all the cases of orientation and AR for square sizes 3.75 times larger than the larger dimension of the fibres. In the case of non mono-dispersed fibre length, the chi square test shows that larger sizes need to be considered in order to define the representative volume element.

Through this work a study of the numerical characterisation of short fibre reinforced thermoplastic took place. The study considers a solution to the packing problem of fibres, an analytical characterisation of short fibre materials, the development of numerical models, the parametric study of the mechanical, thermal and thermo-mechanical properties and statistical analysis on the effect of the representative size.

6.1 Recommendation for future work

The existing study can be an ideal base for further study on the field of computational characterisation. Any further future work must be oriented towards four main directions, namely packing algorithm further analysis on the 2D structures, implementation of 3D realisations and experimental study.

Packing algorithm

The packing algorithm implemented in a process as microstructure re-creations can always receive improvements. The current algorithm can be improved towards the following directions. Reach higher volume fraction using higher AR. Implement 3D realisations. Include a variety of shapes for inclusions and last but not least to create realisations of microstructures in a reasonable amount of time.

Extending the 2D analysis

Further work can potentially study realisations of SFRC with higher AR. The current study, investigate the effect of AR up to 10. A future work can implement higher AR in order to conclude on the AR of saturation effect regarding the specific short fibre composite. This will be useful because will provide the larger size of the RVE as size strongly depends on the AR. A further extension on the study of 2D structures can implement investigation of the interface between fibre and matrix. For the current study interface assumed to be perfect. Introduction of the interface region in simulations will provide a more realistic response of the material. Regarding the temperature properties, future work can be oriented in order to study conductivity and thermal expansion for temperature depending properties of the material and also study on the time depending thermal phenomenon.

3D simulations

Three dimensional simulations were not performed during this study. A three dimensional simulation will offer a more integrated view on the response of the material. Such an implementation will increase dramatically the computational cost but will provide a more realistic approach of the material. The three dimensional model can be integrated in order to include temperature and time depending properties. Up to this point a non-linear analysis can be performed by implementing experimental data from the non-linear region of the material or by performing a failure progress analysis. A study on the non-linear response of the material will provide information about the fracture mechanism of such a system of materials.

Experimental study

Experimental study will be useful in order to provide a direct comparison with computational models and also to provide information as the yield stress the ultimate stress or any viscoelastic response. All these information can be compared with computational results and also can be implemented on the computational models. In parallel with the mechanical or thermal testing is useful to perform some measurements on the samples as the mean fibre length, the mean fibre orientation, the fibre orientation distribution and the fibre length distribution. These measurements can potentially be the source of the random parameters introduced into the simulations.

7 Bibliography

Annapragada S Ravi and Dhavaleswarapu, Hemanth K Prediction of Effective Thermal Conductivity of Particulate Composites [Conference]. - West Lafayette : Composites Proceedings of Project, 2006.

Annapragada S Ravi and Sun, Dawei and Garimella, Suresh V Prediction of effective thermo-mechanical properties of particulate composites [Journal] // Computational materials science. - 2007. - Elsevier : Vol. 40. - pp. 255-266.

Astrom B. T Manufacturing of polymer composites [Book]. - [s.l.] : CRC Press, 1997.

Bazant Zdenek P and Novak, Drahomir Energetic-statistical size effect in quasibrittle failure at crack initiation ACI Materials Journal, ACI, 2000, 97 [Journal] // ACI Materials Journal. - 2000. - ACI : Vol. 97.

Benveniste Y A new approach to the application of Mori-Tanaka's theory in composite materials [Journal] // Mechanics of materials,. - 1987. - Elsevier, : Vols. 6,. - pp. 147-157.

Berger H and Kurukuri, S and Kari, S and Gabbert, U and Rodriguez-Ramos, R and Bravo-Castillero, J and Guinovart-Diaz, R Numerical and analytical approaches for calculating the effective thermo-mechanical properties of three-phase composites [Journal] // Journal of Thermal Stresses. - 2007. - Taylor & Francis : Vol. 30. - pp. 801-817.

Chen Chao-Hsun and Wang, Yuh-Chung Effective thermal conductivity of misoriented short-fiber reinforced thermoplastics [Journal] // Mechanics of materials. - 1996. - Elsevier : Vol. 23. - pp. 217-228.

Chin Wei-Kuo and Liu, Hsin-Tzu and Lee, Yu-Der Effects of fiber length and orientation distribution on the elastic modulus of short fiber reinforced thermoplastics [Journal] // Polymer Composite. - 1988. - Vol. 9. - pp. 27-35.

Choy CL and Leung, WP and Kowk, KW and Lau, Felix P Elastic moduli and thermal conductivity of injection-molded short-fiber--reinforced thermoplastics [Journal] // Polymer composites. - 1992. - Vol. 13. - pp. 69-80.

Cox HL The elasticity and strength of paper and other fibrous materials [Journal] // British journal of applied physics. - 1952. - IOP Publishing : Vol. 3. - p. 72.

Drugan WJ and Willis, JR A micromechanics-based nonlocal constitutive equation and estimates of representative volume element size for elastic composites [Journal] // Journal of the Mechanics and Physics of Solids. - 1996. - Elsevier : Vol. 44. - pp. 497-524.

Eshelby J. D The determination of the elastic field of an ellipsoidal inclusion, and related problems. [Journal] // Series A. Mathematical and Physical Sciences, Proceedings of the Royal Society of London. - 1957,. - The Royal Society, : Vols. 241,. - pp. 376-396.

Evans KE and Gibson, AG Prediction of the maximum packing fraction achievable in randomly oriented short-fibre composites [Journal] // Composites science and technology. - 1986,. - Elsevier, : Vols. 25,. - pp. 149-162.

Fu S.-Y. and Lauke B. & Mai, Y.-W. Science and engineering of short fibre reinforced polymer composites [Book]. - [s.l.] : Elsevier, 2009.

Fu Shao-Yun and Lauke, Bernd Effects of fiber length and fiber orientation distributions on the tensile strength of short-fiber-reinforced polymers [Journal] // Composites Science and Technology,. - 1996. - Elsevier : Vol. 56. - pp. 1179-1190.

Fu S-Y and Lauke, B and Mader, E and Yue, C-Y and Hu, X Tensile properties of short-glass-fiber-and short-carbon-fiber-reinforced polypropylene composites Composites Part A: [Journal] // Applied Science and Manufacturing. - 2000. - Elsevier : Vol. 31. - pp. 1117-1125.

Gitman IM and Askes, H and Sluys, LJ Representative volume: existence and size determination [Journal] // Engineering Fracture Mechanics. - 2007. - Elsevier : Vol. 74. - pp. 2518-2534.

Halpin J. & Kardos, J. The Halpin-Tsai equations: a review [Journal] // Polymer Engineering & Science. - 1976,. - Wiley Online Library, : Vol. 16. - pp. 344-352.

Hashin Z Analysis of composite materials—a survey [Journal] // Journal of Applied Mechanics. - 1983. - American Society of Mechanical Engineers : Vol. 50. - pp. 481-505.

Hatta H. & Taya, M. Effective thermal conductivity of a misoriented short fiber composite [Journal] // Journal of Applied Physics. - 1985. - AIP Publishing : Vol. 58. - pp. 2478-2486.

Hill R A self-consistent mechanics of composite materials [Journal] // Journal of the Mechanics and Physics of Solids. - 1965. - Elsevier : Vol. 13. - pp. 213-222.

Hill R. Elastic properties of reinforced solids: some theoretical principles [Journal] // Journal of the Mechanics and Physics of Solids. - 1963. - Elsevier : Vol. 11. - pp. 357-372.

Hine Peter J and Lusti, Hans Rudolf and Gusev, Andrei A Numerical simulation of the effects of volume fraction, aspect ratio and fibre length distribution on the elastic and thermoelastic properties of short fibre composites [Journal] // Composites science and technology. - 2002. - Elsevier : Vol. 62. - pp. 1445-1453.

Hua Yi and Gu, Linxia Prediction of the thermomechanical behavior of particle-reinforced metal matrix composites Composites Part B: [Journal] // Engineering. - 2013. - Elsevier : Vol. 45. - pp. 1464-1470.

Ionita A and Weitsman, YJ On the mechanical response of randomly reinforced chopped-fibers composites: Data and model [Journal] // Composites science and technology. - 2006. - Elsevier : Vol. 66. - pp. 2566-2579.

Iorga Lucian and Pan, Yi and Pelegri, Assimina Numerical characterization of material elastic properties for random fiber composites [Journal] // J. Mech. Mater. Struct. - 2008. - Vol. 3. - pp. 1279-1298.

Jules E Jao and Tsujikami, T and Lomov, SV and Verpoest, I Effect of Fibres Length and Fibres Orientation on the Predicted Elastic Properties of Long Fibre [Journal] // Composites Macromol. Symp. - 2004. - Vol. 17.

- Kacir L and Narkis, M and Ishai, O** Oriented short glass-fiber composites. I. Preparation and statistical analysis of aligned fiber mats [Journal] // Polymer Engineering & Science. - 1975. - Vol. 15. - pp. 525-531.
- Kamal Musa R and Song, Li and Singh, Peter** Measurement of fiber and matrix orientations in fiber reinforced composites [Journal] // Polymer composites. - 1986. - Wiley Online Library : Vol. 7. - pp. 323-329.
- Kari S and Berger, H and Gabbert, U** Numerical evaluation of effective material properties of randomly distributed short cylindrical fibre composites [Journal] // Computational materials science. - 2007. - Elsevier : Vol. 39. - pp. 198-204.
- Klusemann B and Svendsen, B** Homogenization methods for multi-phase elastic composites: comparisons and benchmarks [Journal] // Technische Mechanik. - 2010. - Vol. 30. - pp. 374-386.
- Lemaitre J and Sermage, JP and Desmorat, R** A two scale damage concept applied to fatigue [Journal] // International Journal of Fracture,. - 1999,. - Springer, : Vols. 97,. - pp. 67-81.
- Lusti Hans Rudolf and Hine, Peter J and Gusev, Andrei A** Direct numerical predictions for the elastic and thermoelastic properties of short fibre composites [Journal] // Composites science and technology. - 2002. - Elsevier : Vol. 62. - pp. 1927-1934.
- Milewski John V** A study of the packing of milled fiberglass and glass beads [Journal]. - 1974. - Taylor & Francis.
- Mori T and Tanaka, K** Average stress in matrix and average elastic energy of materials with misfitting inclusions [Journal] // Acta metallurgica. - 1973. - Elsevier : Vol. 21. - pp. 571-574.
- Mura Toshio** Micromechanics of defects in solids [Book]. - [s.l.] : Springer Science & Business Media, 1987. - 3.
- Nye JF** Plastic Deformation of Silver Chloride. I. Internal Stresses and the Glide Mechanism [Journal] // Proc R Soc A. - 1949. - Vol. 198. - pp. 190-204.
- Ostoja-Starzewski M** Random field models of heterogeneous materials International [Journal] // Journal of Solids and Structures. - 1998. - Elsevier : Vol. 35. - pp. 2429-2455.
- Pan Yi and Iorga, Lucian and Pelegri, Assimina A** Analysis of 3D random chopped fiber reinforced composites using FEM and random sequential adsorption [Journal] // Computational Materials Science. - 2008. - Elsevier : Vol. 43. - pp. 450-461.
- Ramani Karthik and Bank, Dave and Kraemer, Nick** Effect of screw design on fiber damage in extrusion compounding and composite properties [Journal] // Polymer composites. - 1995. - Wiley Online Library : Vol. 16. - pp. 258-266.
- Rosato Dominick V and Rosato, Donald V and Rosato, Marlene G** Injection molding handbook [Book]. - [s.l.] : Springer Science & Business Media, 2000.

Schapery Richard Allan Thermal expansion coefficients of composite materials based on energy principles [Journal] // Journal of Composite Materials. - 1968. - SAGE Publications : Vol. 2. - pp. 380-404.

Tandon GP and Weng, GJ The effect of aspect ratio of inclusions on the elastic properties of unidirectionally aligned composites [Journal] // Polymer composites. - 1984. - Wiley Online Library : Vol. 5. - pp. 327-333.

Thomason JL and Groenewoud, WM The influence of fibre length and concentration on the properties of glass fibre reinforced polypropylene: 2. Thermal properties [Journal] // Composites Part A: Applied Science and Manufacturing. - 1996. - Elsevier : Vol. 27. - pp. 555-565.

Thomason JL and Vlug, MA and Schipper, G and Krikor, HGLT Influence of fibre length and concentration on the properties of glass fibre-reinforced polypropylene: Part 3. Strength and strain at failure [Journal] // Composites Part A: Applied Science and Manufacturing. - 1996. - Elsevier : Vol. 27. - pp. 1075-1084.

Thomason JL and Vlug, MA Influence of fibre length and concentration on the properties of glass fibre-reinforced polypropylene: 1. Tensile and flexural modulus [Journal] // Composites Part A: Applied science and manufacturing. - 1996. - Elsevier : Vol. 27. - pp. 477-484.

Thomason JL Micromechanical parameters from macromechanical measurements on glass reinforced polypropylene [Journal] // Composites science and technology. - 2002. - Vol. 62. - pp. 1455-1468.

Thomason JL The influence of fibre length and concentration on the properties of glass fibre reinforced polypropylene: 5. Injection moulded long and short fibre PP [Journal] // Composites Part A: Applied Science and Manufacturing. - 2002. - Elsevier : Vol. 33. - pp. 1641-1652.

Van Mier JGM and Van Vliet, MRA Influence of microstructure of concrete on size/scale effects in tensile fracture [Journal] // Engineering fracture mechanics. - 2003. - Elsevier : Vol. 70. - pp. 2281-2306.

Vu-Khanh Toan and Denault, J and Habib, P and Low, A The effects of injection molding on the mechanical behavior of long-fiber reinforced PBT/PET blends [Journal] // Composites science and technology. - 1991. - Elsevier : Vol. 4. - pp. 423-435.

Wang Zhenqing and Wang, Xiaoqiang and Zhang, Jifeng and Liang, Wenyan and Zhou, Limin Automatic generation of random distribution of fibers in long-fiber-reinforced composites and mesomechanical simulation [Journal] // Materials & Design,. - 2011. - Elsevier : Vol. 32. - pp. 885-891.

Appendix I

Solution for the I elliptical integrals regarding the Eshelby's model:

$$I_1 = \frac{4\pi abc}{(a^2 - b^2)(a^2 - c^2)^{0.5}} [F(\theta, K) - E(\theta, K)]$$

$$I_3 = \frac{4\pi abc}{(b^2 - c^2)(a^2 - c^2)^{0.5}} \left[\frac{b(a^2 - c^2)^{0.5}}{ac} - E(\theta, K) \right]$$

Where

$$\theta = \arcsin \sqrt{\frac{a^2 - c^2}{a^2}}$$

$$k = \sqrt{\frac{a^2 - b^2}{a^2 - c^2}}$$

And

$$I_1 + I_2 + I_3 = 4\pi$$

$$3I_{11} + I_{12} + I_{13} = \frac{4\pi}{a^2}$$

$$3a^2 I_{11} + b^2 I_{12} + c^2 I_{13} = 3I_1$$

$$I_{12} = \frac{I_2 - I_1}{a^2 - b^2}$$

Standard Elliptical integrals are defined as:

$$F(\theta, k) = \int_0^{\theta} \frac{dw}{(1 - k^2 \sin^2 w)^{0.5}}$$

$$E(\theta, k) = \int_0^{\theta} (1 - k^2 \sin^2 w)^{0.5} dw$$

For an ellipsis where the third axis approaches infinity ($c \rightarrow \infty$) Eshelby's tensor takes the following expression:

$$S_{1111} = \frac{1}{2(1-\nu)} \left[\frac{b^2 + 2ab}{(a+b)^2} + (1-2\nu) \frac{b}{a+b} \right]$$

$$S_{2222} = \frac{1}{2(1-\nu)} \left[\frac{a^2 + 2ab}{(a+b)^2} + (1-2\nu) \frac{a}{a+b} \right]$$

$$S_{3333} = 0$$

$$S_{1122} = \frac{1}{2(1-\nu)} \left[\frac{b^2}{(a+b)^2} - (1-2\nu) \frac{b}{a+b} \right]$$

$$S_{2233} = \frac{1}{2(1-\nu)} \frac{2\nu a}{a+b}$$

$$S_{2211} = \frac{1}{2(1-\nu)} \left[\frac{a^2}{(a+b)^2} - (1-2\nu) \frac{a}{a+b} \right]$$

$$S_{3311} = S_{3322} = 0$$

$$S_{1212} = \frac{1}{2(1-\nu)} \left[\frac{a^2 + b^2}{2(a+b)^2} + \frac{(1-2\nu)}{2} \right]$$

$$S_{1133} = \frac{1}{2(1-\nu)} \frac{2\nu b}{a+b}$$

$$S_{2323} = \frac{a}{2(a+b)}$$

$$S_{3131} = \frac{b}{2(a+b)}$$

Appendix II

Characteristic python script for microstructure development:

```
from part import *

from material import *

from section import *

from assembly import *

from step import *

from interaction import *

from load import *

from mesh import *

from job import *

from sketch import *

from visualization import *

from connectorBehavior import *

mdb.models['Model-1'].ConstrainedSketch(name='__profile__', sheetSize=200.0)

mdb.models['Model-1'].sketches['__profile__'].rectangle(point1=(0.0, 0.0),
    point2=(30.0, 30.0))

mdb.models['Model-1'].sketches['__profile__'].EllipseByCenterPerimeter(axisPoint1=(24.34,19.77),
axisPoint2=(14.82,15.36), center=(15,15))

mdb.models['Model-1'].sketches['__profile__'].EllipseByCenterPerimeter(axisPoint1=(54.34,49.77),
axisPoint2=(44.82,45.36), center=(45,45))

mdb.models['Model-1'].sketches['__profile__'].EllipseByCenterPerimeter(axisPoint1=(54.34,19.77),
axisPoint2=(44.82,15.36), center=(45,15))

mdb.models['Model-1'].sketches['__profile__'].EllipseByCenterPerimeter(axisPoint1=(24.34,49.77),
axisPoint2=(14.82,45.36), center=(15,45))
```

```
mdb.models['Model-1'].sketches['__profile__'].EllipseByCenterPerimeter(axisPoint1=(26.23,20.91),  
axisPoint2=(17.71,18.72), center=(17.83,18.34))
```

```
mdb.models['Model-1'].sketches['__profile__'].EllipseByCenterPerimeter(axisPoint1=(-3.77,-9.09),  
axisPoint2=(-12.29,-11.28), center=(-12.17,-11.66))
```

```
mdb.models['Model-1'].sketches['__profile__'].EllipseByCenterPerimeter(axisPoint1=(-3.77,20.91),  
axisPoint2=(-12.29,18.72), center=(-12.17,18.34))
```

```
mdb.models['Model-1'].sketches['__profile__'].EllipseByCenterPerimeter(axisPoint1=(26.23,-9.09),  
axisPoint2=(17.71,-11.28), center=(17.83,-11.66))
```

```
mdb.models['Model-1'].sketches['__profile__'].EllipseByCenterPerimeter(axisPoint1=(30.21,25.06),  
axisPoint2=(22.61,22.13), center=(22.77,21.77))
```

```
mdb.models['Model-1'].sketches['__profile__'].EllipseByCenterPerimeter(axisPoint1=(0.21,-4.94),  
axisPoint2=(-7.39,-7.87), center=(-7.23,-8.23))
```

```
mdb.models['Model-1'].sketches['__profile__'].EllipseByCenterPerimeter(axisPoint1=(0.21,25.06),  
axisPoint2=(-7.39,22.13), center=(-7.23,21.77))
```

```
mdb.models['Model-1'].sketches['__profile__'].EllipseByCenterPerimeter(axisPoint1=(30.21,-4.94),  
axisPoint2=(22.61,-7.87), center=(22.77,-8.23))
```

```
mdb.models['Model-1'].sketches['__profile__'].EllipseByCenterPerimeter(axisPoint1=(26.58,19.4),  
axisPoint2=(19.5,16.53), center=(19.67,16.17))
```

```
mdb.models['Model-1'].sketches['__profile__'].EllipseByCenterPerimeter(axisPoint1=(-3.42,-10.6),  
axisPoint2=(-10.5,-13.47), center=(-10.33,-13.83))
```

```
mdb.models['Model-1'].sketches['__profile__'].EllipseByCenterPerimeter(axisPoint1=(-3.42,19.4),  
axisPoint2=(-10.5,16.53), center=(-10.33,16.17))
```

```
mdb.models['Model-1'].sketches['__profile__'].EllipseByCenterPerimeter(axisPoint1=(26.58,-10.6),  
axisPoint2=(19.5,-13.47), center=(19.67,-13.83))
```

```
mdb.models['Model-1'].sketches['__profile__'].EllipseByCenterPerimeter(axisPoint1=(37.32,9.81),  
axisPoint2=(22.89,9.86), center=(22.9,9.46))
```

```
mdb.models['Model-1'].sketches['__profile__'].EllipseByCenterPerimeter(axisPoint1=(7.32,39.81),  
axisPoint2=(-7.11,39.86), center=(-7.1,39.46))
```

```
mdb.models['Model-1'].sketches['__profile__'].EllipseByCenterPerimeter(axisPoint1=(37.32,39.81),  
axisPoint2=(22.89,39.86), center=(22.9,39.46))
```

```
mdb.models['Model-1'].sketches['__profile__'].EllipseByCenterPerimeter(axisPoint1=(7.32,9.81),  
axisPoint2=(-7.11,9.86), center=(-7.1,9.46))
```

```
mdb.models['Model-1'].sketches['__profile__'].EllipseByCenterPerimeter(axisPoint1=(18.49,20.75),  
axisPoint2=(17.25,20.73), center=(17.38,20.35))
```

```
mdb.models['Model-1'].sketches['__profile__'].EllipseByCenterPerimeter(axisPoint1=(-11.51,-9.25),  
axisPoint2=(-12.75,-9.27), center=(-12.62,-9.65))
```

```
mdb.models['Model-1'].sketches['__profile__'].EllipseByCenterPerimeter(axisPoint1=(-11.51,20.75),  
axisPoint2=(-12.75,20.73), center=(-12.62,20.35))
```

```
mdb.models['Model-1'].sketches['__profile__'].EllipseByCenterPerimeter(axisPoint1=(18.49,-9.25),  
axisPoint2=(17.25,-9.27), center=(17.38,-9.65))
```

```
mdb.models['Model-1'].sketches['__profile__'].EllipseByCenterPerimeter(axisPoint1=(15.88,19.32),  
axisPoint2=(14.74,19.52), center=(14.81,19.12))
```

```
mdb.models['Model-1'].sketches['__profile__'].EllipseByCenterPerimeter(axisPoint1=(45.88,-10.68),  
axisPoint2=(44.74,-10.48), center=(44.81,-10.88))
```

```
mdb.models['Model-1'].sketches['__profile__'].EllipseByCenterPerimeter(axisPoint1=(45.88,19.32),  
axisPoint2=(44.74,19.52), center=(44.81,19.12))
```

```
mdb.models['Model-1'].sketches['__profile__'].EllipseByCenterPerimeter(axisPoint1=(15.88,-10.68),  
axisPoint2=(14.74,-10.48), center=(14.81,-10.88))
```

```
mdb.models['Model-1'].sketches['__profile__'].EllipseByCenterPerimeter(axisPoint1=(19.19,8.22),  
axisPoint2=(15.26,6.77), center=(15.43,6.41))
```

```
mdb.models['Model-1'].sketches['__profile__'].EllipseByCenterPerimeter(axisPoint1=(-10.81,38.22),  
axisPoint2=(-14.74,36.77), center=(-14.57,36.41))
```

```
mdb.models['Model-1'].sketches['__profile__'].EllipseByCenterPerimeter(axisPoint1=(19.19,38.22),  
axisPoint2=(15.26,36.77), center=(15.43,36.41))
```

```
mdb.models['Model-1'].sketches['__profile__'].EllipseByCenterPerimeter(axisPoint1=(-10.81,8.22),  
axisPoint2=(-14.74,6.77), center=(-14.57,6.41))
```

```
mdb.models['Model-1'].sketches['__profile__'].EllipseByCenterPerimeter(axisPoint1=(20.95,27.01),  
axisPoint2=(7.36,26.5), center=(7.39,26.1))
```

```
mdb.models['Model-1'].sketches['__profile__'].EllipseByCenterPerimeter(axisPoint1=(50.95,-2.99),  
axisPoint2=(37.36,-3.5), center=(37.39,-3.9))
```

```
mdb.models['Model-1'].sketches['__profile__'].EllipseByCenterPerimeter(axisPoint1=(50.95,27.01),  
axisPoint2=(37.36,26.5), center=(37.39,26.1))
```

```
mdb.models['Model-1'].sketches['__profile__'].EllipseByCenterPerimeter(axisPoint1=(20.95,-2.99),  
axisPoint2=(7.36,-3.5), center=(7.39,-3.9))
```

```
mdb.models['Model-1'].sketches['__profile__'].EllipseByCenterPerimeter(axisPoint1=(28.65,8.37),  
axisPoint2=(24.8,6.61), center=(25,6.26))
```

```
mdb.models['Model-1'].sketches['__profile__'].EllipseByCenterPerimeter(axisPoint1=(-1.35,38.37),  
axisPoint2=(-5.2,36.61), center=(-5,36.26))
```

```
mdb.models['Model-1'].sketches['__profile__'].EllipseByCenterPerimeter(axisPoint1=(28.65,38.37),  
axisPoint2=(24.8,36.61), center=(25,36.26))
```

```
mdb.models['Model-1'].sketches['__profile__'].EllipseByCenterPerimeter(axisPoint1=(-1.35,8.37),  
axisPoint2=(-5.2,6.61), center=(-5,6.26))
```

```
mdb.models['Model-1'].sketches['__profile__'].EllipseByCenterPerimeter(axisPoint1=(29.04,26.72),  
axisPoint2=(25.02,26.42), center=(25.09,26.03))
```

```
mdb.models['Model-1'].sketches['__profile__'].EllipseByCenterPerimeter(axisPoint1=(-0.96,-3.28),  
axisPoint2=(-4.98,-3.58), center=(-4.91,-3.97))
```

```
mdb.models['Model-1'].sketches['__profile__'].EllipseByCenterPerimeter(axisPoint1=(-0.96,26.72),  
axisPoint2=(-4.98,26.42), center=(-4.91,26.03))
```

```
mdb.models['Model-1'].sketches['__profile__'].EllipseByCenterPerimeter(axisPoint1=(29.04,-3.28),  
axisPoint2=(25.02,-3.58), center=(25.09,-3.97))
```

```
mdb.models['Model-1'].sketches['__profile__'].EllipseByCenterPerimeter(axisPoint1=(25.09,28.22),  
axisPoint2=(20.02,28.2), center=(20.05,27.8))
```

```
mdb.models['Model-1'].sketches['__profile__'].EllipseByCenterPerimeter(axisPoint1=(-4.91,-1.78),  
axisPoint2=(-9.98,-1.8), center=(-9.95,-2.2))
```

```
mdb.models['Model-1'].sketches['__profile__'].EllipseByCenterPerimeter(axisPoint1=(-4.91,28.22),  
axisPoint2=(-9.98,28.2), center=(-9.95,27.8))
```

```
mdb.models['Model-1'].sketches['__profile__'].EllipseByCenterPerimeter(axisPoint1=(25.09,-1.78),  
axisPoint2=(20.02,-1.8), center=(20.05,-2.2))
```

```
mdb.models['Model-1'].sketches['__profile__'].EllipseByCenterPerimeter(axisPoint1=(14.65,8.1),  
axisPoint2=(5.66,6.54), center=(5.74,6.15))
```

```
mdb.models['Model-1'].sketches['__profile__'].EllipseByCenterPerimeter(axisPoint1=(44.65,38.1),  
axisPoint2=(35.66,36.54), center=(35.74,36.15))
```

```
mdb.models['Model-1'].sketches['__profile__'].EllipseByCenterPerimeter(axisPoint1=(44.65,8.1),  
axisPoint2=(35.66,6.54), center=(35.74,6.15))
```

```
mdb.models['Model-1'].sketches['__profile__'].EllipseByCenterPerimeter(axisPoint1=(14.65,38.1),  
axisPoint2=(5.66,36.54), center=(5.74,36.15))
```

```
mdb.models['Model-1'].sketches['__profile__'].EllipseByCenterPerimeter(axisPoint1=(18.18,4.22),  
axisPoint2=(13.19,4.45), center=(13.2,4.05))
```

```
mdb.models['Model-1'].sketches['__profile__'].EllipseByCenterPerimeter(axisPoint1=(48.18,34.22),  
axisPoint2=(43.19,34.45), center=(43.2,34.05))
```

```
mdb.models['Model-1'].sketches['__profile__'].EllipseByCenterPerimeter(axisPoint1=(48.18,4.22),  
axisPoint2=(43.19,4.45), center=(43.2,4.05))
```

```
mdb.models['Model-1'].sketches['__profile__'].EllipseByCenterPerimeter(axisPoint1=(18.18,34.22),  
axisPoint2=(13.19,34.45), center=(13.2,34.05))
```

```
mdb.models['Model-1'].sketches['__profile__'].EllipseByCenterPerimeter(axisPoint1=(24,3.83),  
axisPoint2=(21.42,3.95), center=(21.46,3.55))
```

```
mdb.models['Model-1'].sketches['__profile__'].EllipseByCenterPerimeter(axisPoint1=(-6,33.83),  
axisPoint2=(-8.58,33.95), center=(-8.54,33.55))
```

```
mdb.models['Model-1'].sketches['__profile__'].EllipseByCenterPerimeter(axisPoint1=(24,33.83),  
axisPoint2=(21.42,33.95), center=(21.46,33.55))
```

```
mdb.models['Model-1'].sketches['__profile__'].EllipseByCenterPerimeter(axisPoint1=(-6,3.83),  
axisPoint2=(-8.58,3.95), center=(-8.54,3.55))
```

```
mdb.models['Model-1'].sketches['__profile__'].EllipseByCenterPerimeter(axisPoint1=(29,19.76),  
axisPoint2=(27.93,20.09), center=(27.96,19.69))
```

```
mdb.models['Model-1'].sketches['__profile__'].EllipseByCenterPerimeter(axisPoint1=(-1,-10.24),  
axisPoint2=(-2.07,-9.91), center=(-2.04,-10.31))
```

```
mdb.models['Model-1'].sketches['__profile__'].EllipseByCenterPerimeter(axisPoint1=(-1,19.76),  
axisPoint2=(-2.07,20.09), center=(-2.04,19.69))
```

```
mdb.models['Model-1'].sketches['__profile__'].EllipseByCenterPerimeter(axisPoint1=(29,-10.24),  
axisPoint2=(27.93,-9.91), center=(27.96,-10.31))
```

```
mdb.models['Model-1'].sketches['__profile__'].EllipseByCenterPerimeter(axisPoint1=(10.01,16.7),  
axisPoint2=(7.83,16.01), center=(8.01,15.65))
```

```
mdb.models['Model-1'].sketches['__profile__'].EllipseByCenterPerimeter(axisPoint1=(40.01,-13.3),  
axisPoint2=(37.83,-13.99), center=(38.01,-14.35))
```

```
mdb.models['Model-1'].sketches['__profile__'].EllipseByCenterPerimeter(axisPoint1=(40.01,16.7),  
axisPoint2=(37.83,16.01), center=(38.01,15.65))
```

```
mdb.models['Model-1'].sketches['__profile__'].EllipseByCenterPerimeter(axisPoint1=(10.01,-13.3),  
axisPoint2=(7.83,-13.99), center=(8.01,-14.35))
```

```
mdb.models['Model-1'].sketches['__profile__'].EllipseByCenterPerimeter(axisPoint1=(11.92,3.2),  
axisPoint2=(9.96,3.36), center=(10.01,2.97))
```

```
mdb.models['Model-1'].sketches['__profile__'].EllipseByCenterPerimeter(axisPoint1=(41.92,33.2),  
axisPoint2=(39.96,33.36), center=(40.01,32.97))
```

```
mdb.models['Model-1'].sketches['__profile__'].EllipseByCenterPerimeter(axisPoint1=(41.92,3.2),  
axisPoint2=(39.96,3.36), center=(40.01,2.97))
```

```
mdb.models['Model-1'].sketches['__profile__'].EllipseByCenterPerimeter(axisPoint1=(11.92,33.2),  
axisPoint2=(9.96,33.36), center=(10.01,32.97))
```

```
mdb.models['Model-1'].sketches['__profile__'].EllipseByCenterPerimeter(axisPoint1=(29.74,30.58),  
axisPoint2=(18.58,29.2), center=(18.64,28.8))
```

```
mdb.models['Model-1'].sketches['__profile__'].EllipseByCenterPerimeter(axisPoint1=(-0.26,0.58),  
axisPoint2=(-11.42,-0.8), center=(-11.36,-1.2))
```

```
mdb.models['Model-1'].sketches['__profile__'].EllipseByCenterPerimeter(axisPoint1=(-0.26,30.58),  
axisPoint2=(-11.42,29.2), center=(-11.36,28.8))
```

```
mdb.models['Model-1'].sketches['__profile__'].EllipseByCenterPerimeter(axisPoint1=(29.74,0.58),  
axisPoint2=(18.58,-0.8), center=(18.64,-1.2))
```

```
mdb.models['Model-1'].sketches['__profile__'].EllipseByCenterPerimeter(axisPoint1=(16.75,16.92),  
axisPoint2=(9.4,14.85), center=(9.53,14.48))
```

```
mdb.models['Model-1'].sketches['__profile__'].EllipseByCenterPerimeter(axisPoint1=(46.75,46.92),  
axisPoint2=(39.4,44.85), center=(39.53,44.48))
```

```
mdb.models['Model-1'].sketches['__profile__'].EllipseByCenterPerimeter(axisPoint1=(46.75,16.92),  
axisPoint2=(39.4,14.85), center=(39.53,14.48))
```

```
mdb.models['Model-1'].sketches['__profile__'].EllipseByCenterPerimeter(axisPoint1=(16.75,46.92),  
axisPoint2=(9.4,44.85), center=(9.53,44.48))
```

```
mdb.models['Model-1'].sketches['__profile__'].EllipseByCenterPerimeter(axisPoint1=(17.73,21.4),  
axisPoint2=(7.89,17.8), center=(8.05,17.43))
```

```
mdb.models['Model-1'].sketches['__profile__'].EllipseByCenterPerimeter(axisPoint1=(47.73,-8.6),  
axisPoint2=(37.89,-12.2), center=(38.05,-12.57))
```

```
mdb.models['Model-1'].sketches['__profile__'].EllipseByCenterPerimeter(axisPoint1=(47.73,21.4),  
axisPoint2=(37.89,17.8), center=(38.05,17.43))
```

```
mdb.models['Model-1'].sketches['__profile__'].EllipseByCenterPerimeter(axisPoint1=(17.73,-8.6),  
axisPoint2=(7.89,-12.2), center=(8.05,-12.57))
```

```
mdb.models['Model-1'].sketches['__profile__'].EllipseByCenterPerimeter(axisPoint1=(20.99,25.78),  
axisPoint2=(13.91,23.27), center=(14.06,22.9))
```

```
mdb.models['Model-1'].sketches['__profile__'].EllipseByCenterPerimeter(axisPoint1=(50.99,-4.22),  
axisPoint2=(43.91,-6.73), center=(44.06,-7.1))
```

```
mdb.models['Model-1'].sketches['__profile__'].EllipseByCenterPerimeter(axisPoint1=(50.99,25.78),  
axisPoint2=(43.91,23.27), center=(44.06,22.9))
```

```
mdb.models['Model-1'].sketches['__profile__'].EllipseByCenterPerimeter(axisPoint1=(20.99,-4.22),  
axisPoint2=(13.91,-6.73), center=(14.06,-7.1))
```

```
mdb.models['Model-1'].sketches['__profile__'].EllipseByCenterPerimeter(axisPoint1=(6.34,21.63),  
axisPoint2=(2.37,18.34), center=(2.65,18.05))
```

```
mdb.models['Model-1'].sketches['__profile__'].EllipseByCenterPerimeter(axisPoint1=(36.34,-8.37),  
axisPoint2=(32.37,-11.66), center=(32.65,-11.95))
```

```
mdb.models['Model-1'].sketches['__profile__'].EllipseByCenterPerimeter(axisPoint1=(36.34,21.63),  
axisPoint2=(32.37,18.34), center=(32.65,18.05))
```

```
mdb.models['Model-1'].sketches['__profile__'].EllipseByCenterPerimeter(axisPoint1=(6.34,-8.37),  
axisPoint2=(2.37,-11.66), center=(2.65,-11.95))
```

```
mdb.models['Model-1'].sketches['__profile__'].EllipseByCenterPerimeter(axisPoint1=(31.01,2.88),  
axisPoint2=(24.73,3.1), center=(24.74,2.7))
```

```
mdb.models['Model-1'].sketches['__profile__'].EllipseByCenterPerimeter(axisPoint1=(1.01,32.88),  
axisPoint2=(-5.27,33.1), center=(-5.26,32.7))
```

```
mdb.models['Model-1'].sketches['__profile__'].EllipseByCenterPerimeter(axisPoint1=(31.01,32.88),  
axisPoint2=(24.73,33.1), center=(24.74,32.7))
```

```
mdb.models['Model-1'].sketches['__profile__'].EllipseByCenterPerimeter(axisPoint1=(1.01,2.88),  
axisPoint2=(-5.27,3.1), center=(-5.26,2.7))
```

```
mdb.models['Model-1'].sketches['__profile__'].EllipseByCenterPerimeter(axisPoint1=(28,1.92),  
axisPoint2=(20.82,2), center=(20.83,1.61))
```

```
mdb.models['Model-1'].sketches['__profile__'].EllipseByCenterPerimeter(axisPoint1=(-2,31.92),  
axisPoint2=(-9.18,32), center=(-9.17,31.61))
```

```
mdb.models['Model-1'].sketches['__profile__'].EllipseByCenterPerimeter(axisPoint1=(28,31.92),  
axisPoint2=(20.82,32), center=(20.83,31.61))
```

```
mdb.models['Model-1'].sketches['__profile__'].EllipseByCenterPerimeter(axisPoint1=(-2,1.92),  
axisPoint2=(-9.18,2), center=(-9.17,1.61))
```

```
mdb.models['Model-1'].sketches['__profile__'].EllipseByCenterPerimeter(axisPoint1=(23.52,14.77),  
axisPoint2=(19.78,14.6), center=(19.84,14.2))
```

```
mdb.models['Model-1'].sketches['__profile__'].EllipseByCenterPerimeter(axisPoint1=(-6.48,44.77),  
axisPoint2=(-10.22,44.6), center=(-10.16,44.2))
```

```
mdb.models['Model-1'].sketches['__profile__'].EllipseByCenterPerimeter(axisPoint1=(23.52,44.77),  
axisPoint2=(19.78,44.6), center=(19.84,44.2))
```

```
mdb.models['Model-1'].sketches['__profile__'].EllipseByCenterPerimeter(axisPoint1=(-6.48,14.77),  
axisPoint2=(-10.22,14.6), center=(-10.16,14.2))
```

```
mdb.models['Model-1'].sketches['__profile__'].EllipseByCenterPerimeter(axisPoint1=(26.55,18),  
axisPoint2=(24.46,17.06), center=(24.69,16.73))
```

```
mdb.models['Model-1'].sketches['__profile__'].EllipseByCenterPerimeter(axisPoint1=(-3.45,-12),  
axisPoint2=(-5.54,-12.94), center=(-5.31,-13.27))
```

```
mdb.models['Model-1'].sketches['__profile__'].EllipseByCenterPerimeter(axisPoint1=(-3.45,18),  
axisPoint2=(-5.54,17.06), center=(-5.31,16.73))
```

```
mdb.models['Model-1'].sketches['__profile__'].EllipseByCenterPerimeter(axisPoint1=(26.55,-12),  
axisPoint2=(24.46,-12.94), center=(24.69,-13.27))
```

```
mdb.models['Model-1'].sketches['__profile__'].EllipseByCenterPerimeter(axisPoint1=(18.87,22.13),  
axisPoint2=(17.73,22.39), center=(17.78,21.99))
```

```
mdb.models['Model-1'].sketches['__profile__'].EllipseByCenterPerimeter(axisPoint1=(-11.13,-7.87),  
axisPoint2=(-12.27,-7.61), center=(-12.22,-8.01))
```

```
mdb.models['Model-1'].sketches['__profile__'].EllipseByCenterPerimeter(axisPoint1=(-11.13,22.13),  
axisPoint2=(-12.27,22.39), center=(-12.22,21.99))
```

```
mdb.models['Model-1'].sketches['__profile__'].EllipseByCenterPerimeter(axisPoint1=(18.87,-7.87),  
axisPoint2=(17.73,-7.61), center=(17.78,-8.01))
```

```
mdb.models['Model-1'].sketches['__profile__'].EllipseByCenterPerimeter(axisPoint1=(24.93,14.83),  
axisPoint2=(22.4,13.97), center=(22.58,13.61))
```

```
mdb.models['Model-1'].sketches['__profile__'].EllipseByCenterPerimeter(axisPoint1=(-5.07,44.83),  
axisPoint2=(-7.6,43.97), center=(-7.42,43.61))
```

```
mdb.models['Model-1'].sketches['__profile__'].EllipseByCenterPerimeter(axisPoint1=(24.93,44.83),  
axisPoint2=(22.4,43.97), center=(22.58,43.61))
```

```
mdb.models['Model-1'].sketches['__profile__'].EllipseByCenterPerimeter(axisPoint1=(-5.07,14.83),  
axisPoint2=(-7.6,13.97), center=(-7.42,13.61))
```

```
mdb.models['Model-1'].sketches['__profile__'].EllipseByCenterPerimeter(axisPoint1=(6.92,22.22),  
axisPoint2=(3.15,21.99), center=(3.21,21.59))
```

```
mdb.models['Model-1'].sketches['__profile__'].EllipseByCenterPerimeter(axisPoint1=(36.92,-7.78),  
axisPoint2=(33.15,-8.01), center=(33.21,-8.41))
```

```
mdb.models['Model-1'].sketches['__profile__'].EllipseByCenterPerimeter(axisPoint1=(36.92,22.22),  
axisPoint2=(33.15,21.99), center=(33.21,21.59))
```

```
mdb.models['Model-1'].sketches['__profile__'].EllipseByCenterPerimeter(axisPoint1=(6.92,-7.78),  
axisPoint2=(3.15,-8.01), center=(3.21,-8.41))
```

```
mdb.models['Model-1'].sketches['__profile__'].EllipseByCenterPerimeter(axisPoint1=(5.16,22.98),  
axisPoint2=(4.19,23.14), center=(4.29,22.75))
```

```
mdb.models['Model-1'].sketches['__profile__'].EllipseByCenterPerimeter(axisPoint1=(35.16,-7.02),  
axisPoint2=(34.19,-6.86), center=(34.29,-7.25))
```

```
mdb.models['Model-1'].sketches['__profile__'].EllipseByCenterPerimeter(axisPoint1=(35.16,22.98),  
axisPoint2=(34.19,23.14), center=(34.29,22.75))
```

```
mdb.models['Model-1'].sketches['__profile__'].EllipseByCenterPerimeter(axisPoint1=(5.16,-7.02),  
axisPoint2=(4.19,-6.86), center=(4.29,-7.25))
```

```
mdb.models['Model-1'].sketches['__profile__'].EllipseByCenterPerimeter(axisPoint1=(10.29,24.74),  
axisPoint2=(6.06,24.42), center=(6.13,24.02))
```

```
mdb.models['Model-1'].sketches['__profile__'].EllipseByCenterPerimeter(axisPoint1=(40.29,-5.26),  
axisPoint2=(36.06,-5.58), center=(36.13,-5.98))
```

```
mdb.models['Model-1'].sketches['__profile__'].EllipseByCenterPerimeter(axisPoint1=(40.29,24.74),  
axisPoint2=(36.06,24.42), center=(36.13,24.02))
```

```
mdb.models['Model-1'].sketches['__profile__'].EllipseByCenterPerimeter(axisPoint1=(10.29,-5.26),  
axisPoint2=(6.06,-5.58), center=(6.13,-5.98))
```

```
mdb.models['Model-1'].sketches['__profile__'].EllipseByCenterPerimeter(axisPoint1=(29.62,27.76),  
axisPoint2=(27.4,27.76), center=(27.47,27.37))
```

```
mdb.models['Model-1'].sketches['__profile__'].EllipseByCenterPerimeter(axisPoint1=(-0.38,-2.24),  
axisPoint2=(-2.6,-2.24), center=(-2.53,-2.63))
```

```
mdb.models['Model-1'].sketches['__profile__'].EllipseByCenterPerimeter(axisPoint1=(-0.38,27.76),  
axisPoint2=(-2.6,27.76), center=(-2.53,27.37))
```

```
mdb.models['Model-1'].sketches['__profile__'].EllipseByCenterPerimeter(axisPoint1=(29.62,-2.24),  
axisPoint2=(27.4,-2.24), center=(27.47,-2.63))
```

```
mdb.models['Model-1'].sketches['__profile__'].EllipseByCenterPerimeter(axisPoint1=(8.02,5.4),  
axisPoint2=(5.64,5.49), center=(5.69,5.09))
```

```
mdb.models['Model-1'].sketches['__profile__'].EllipseByCenterPerimeter(axisPoint1=(38.02,35.4),  
axisPoint2=(35.64,35.49), center=(35.69,35.09))
```

```
mdb.models['Model-1'].sketches['__profile__'].EllipseByCenterPerimeter(axisPoint1=(38.02,5.4),  
axisPoint2=(35.64,5.49), center=(35.69,5.09))
```

```
mdb.models['Model-1'].sketches['__profile__'].EllipseByCenterPerimeter(axisPoint1=(8.02,35.4),  
axisPoint2=(5.64,35.49), center=(5.69,35.09))
```

```
mdb.models['Model-1'].sketches['__profile__'].EllipseByCenterPerimeter(axisPoint1=(31.58,30.15),  
axisPoint2=(28.46,29.85), center=(28.55,29.46))
```

```
mdb.models['Model-1'].sketches['__profile__'].EllipseByCenterPerimeter(axisPoint1=(1.58,0.15),  
axisPoint2=(-1.54,-0.15), center=(-1.45,-0.54))
```

```
mdb.models['Model-1'].sketches['__profile__'].EllipseByCenterPerimeter(axisPoint1=(1.58,30.15),  
axisPoint2=(-1.54,29.85), center=(-1.45,29.46))
```

```
mdb.models['Model-1'].sketches['__profile__'].EllipseByCenterPerimeter(axisPoint1=(31.58,0.15),  
axisPoint2=(28.46,-0.15), center=(28.55,-0.54))
```

```
mdb.models['Model-1'].sketches['__profile__'].EllipseByCenterPerimeter(axisPoint1=(12.58,12.34),  
axisPoint2=(11.83,12.67), center=(11.87,12.27))
```

```
mdb.models['Model-1'].sketches['__profile__'].EllipseByCenterPerimeter(axisPoint1=(42.58,42.34),  
axisPoint2=(41.83,42.67), center=(41.87,42.27))
```

```
mdb.models['Model-1'].sketches['__profile__'].EllipseByCenterPerimeter(axisPoint1=(42.58,12.34),  
axisPoint2=(41.83,12.67), center=(41.87,12.27))
```

```
mdb.models['Model-1'].sketches['__profile__'].EllipseByCenterPerimeter(axisPoint1=(12.58,42.34),  
axisPoint2=(11.83,42.67), center=(11.87,42.27))
```

```
mdb.models['Model-1'].sketches['__profile__'].EllipseByCenterPerimeter(axisPoint1=(28.04,17.14),  
axisPoint2=(26.81,17.24), center=(26.91,16.86))
```

```
mdb.models['Model-1'].sketches['__profile__'].EllipseByCenterPerimeter(axisPoint1=(-1.96,-12.86),  
axisPoint2=(-3.19,-12.76), center=(-3.09,-13.14))
```

```
mdb.models['Model-1'].sketches['__profile__'].EllipseByCenterPerimeter(axisPoint1=(-1.96,17.14),  
axisPoint2=(-3.19,17.24), center=(-3.09,16.86))
```

```
mdb.models['Model-1'].sketches['__profile__'].EllipseByCenterPerimeter(axisPoint1=(28.04,-12.86),  
axisPoint2=(26.81,-12.76), center=(26.91,-13.14))
```

```
mdb.models['Model-1'].sketches['__profile__'].EllipseByCenterPerimeter(axisPoint1=(14.58,3.17),  
axisPoint2=(13.43,3.49), center=(13.46,3.09))
```

```
mdb.models['Model-1'].sketches['__profile__'].EllipseByCenterPerimeter(axisPoint1=(44.58,33.17),  
axisPoint2=(43.43,33.49), center=(43.46,33.09))
```

```
mdb.models['Model-1'].sketches['__profile__'].EllipseByCenterPerimeter(axisPoint1=(44.58,3.17),  
axisPoint2=(43.43,3.49), center=(43.46,3.09))
```

```
mdb.models['Model-1'].sketches['__profile__'].EllipseByCenterPerimeter(axisPoint1=(14.58,33.17),  
axisPoint2=(13.43,33.49), center=(13.46,33.09))
```

```
mdb.models['Model-1'].sketches['__profile__'].EllipseByCenterPerimeter(axisPoint1=(11.94,20.39),  
axisPoint2=(10.66,20.04), center=(10.88,19.71))
```

```
mdb.models['Model-1'].sketches['__profile__'].EllipseByCenterPerimeter(axisPoint1=(41.94,-9.61),  
axisPoint2=(40.66,-9.96), center=(40.88,-10.29))
```

```
mdb.models['Model-1'].sketches['__profile__'].EllipseByCenterPerimeter(axisPoint1=(41.94,20.39),  
axisPoint2=(40.66,20.04), center=(40.88,19.71))
```

```
mdb.models['Model-1'].sketches['__profile__'].EllipseByCenterPerimeter(axisPoint1=(11.94,-9.61),  
axisPoint2=(10.66,-9.96), center=(10.88,-10.29))
```

```
mdb.models['Model-1'].sketches['__profile__'].EllipseByCenterPerimeter(axisPoint1=(5.05,24.64),  
axisPoint2=(3.01,24.95), center=(3.03,24.55))
```

```
mdb.models['Model-1'].sketches['__profile__'].EllipseByCenterPerimeter(axisPoint1=(35.05,-5.36),  
axisPoint2=(33.01,-5.05), center=(33.03,-5.45))
```

```
mdb.models['Model-1'].sketches['__profile__'].EllipseByCenterPerimeter(axisPoint1=(35.05,24.64),  
axisPoint2=(33.01,24.95), center=(33.03,24.55))
```

```
mdb.models['Model-1'].sketches['__profile__'].EllipseByCenterPerimeter(axisPoint1=(5.05,-5.36),  
axisPoint2=(3.01,-5.05), center=(3.03,-5.45))
```

```
mdb.models['Model-1'].sketches['__profile__'].EllipseByCenterPerimeter(axisPoint1=(6.46,27.06),  
axisPoint2=(4.72,27.28), center=(4.76,26.89))
```

```
mdb.models['Model-1'].sketches['__profile__'].EllipseByCenterPerimeter(axisPoint1=(36.46,-2.94),  
axisPoint2=(34.72,-2.72), center=(34.76,-3.11))
```

```
mdb.models['Model-1'].sketches['__profile__'].EllipseByCenterPerimeter(axisPoint1=(36.46,27.06),  
axisPoint2=(34.72,27.28), center=(34.76,26.89))
```

```
mdb.models['Model-1'].sketches['__profile__'].EllipseByCenterPerimeter(axisPoint1=(6.46,-2.94),  
axisPoint2=(4.72,-2.72), center=(4.76,-3.11))
```

```
mdb.models['Model-1'].sketches['__profile__'].EllipseByCenterPerimeter(axisPoint1=(7.01,9.26),  
axisPoint2=(4.86,8.38), center=(5.07,8.04))
```

```
mdb.models['Model-1'].sketches['__profile__'].EllipseByCenterPerimeter(axisPoint1=(37.01,39.26),  
axisPoint2=(34.86,38.38), center=(35.07,38.04))
```

```
mdb.models['Model-1'].sketches['__profile__'].EllipseByCenterPerimeter(axisPoint1=(37.01,9.26),  
axisPoint2=(34.86,8.38), center=(35.07,8.04))
```

```
mdb.models['Model-1'].sketches['__profile__'].EllipseByCenterPerimeter(axisPoint1=(7.01,39.26),  
axisPoint2=(4.86,38.38), center=(5.07,38.04))
```

```
mdb.models['Model-1'].sketches['__profile__'].EllipseByCenterPerimeter(axisPoint1=(4.31,2.88),  
axisPoint2=(2.04,2.87), center=(2.11,2.48))
```

```
mdb.models['Model-1'].sketches['__profile__'].EllipseByCenterPerimeter(axisPoint1=(34.31,32.88),  
axisPoint2=(32.04,32.87), center=(32.11,32.48))
```

```
mdb.models['Model-1'].sketches['__profile__'].EllipseByCenterPerimeter(axisPoint1=(34.31,2.88),  
axisPoint2=(32.04,2.87), center=(32.11,2.48))
```

```
mdb.models['Model-1'].sketches['__profile__'].EllipseByCenterPerimeter(axisPoint1=(4.31,32.88),  
axisPoint2=(2.04,32.87), center=(2.11,32.48))
```

```
mdb.models['Model-1'].sketches['__profile__'].EllipseByCenterPerimeter(axisPoint1=(22.43,12.08),  
axisPoint2=(20.3,12.15), center=(20.36,11.76))
```

```
mdb.models['Model-1'].sketches['__profile__'].EllipseByCenterPerimeter(axisPoint1=(-7.57,42.08),  
axisPoint2=(-9.7,42.15), center=(-9.64,41.76))
```

```
mdb.models['Model-1'].sketches['__profile__'].EllipseByCenterPerimeter(axisPoint1=(22.43,42.08),  
axisPoint2=(20.3,42.15), center=(20.36,41.76))
```

```
mdb.models['Model-1'].sketches['__profile__'].EllipseByCenterPerimeter(axisPoint1=(-7.57,12.08),  
axisPoint2=(-9.7,12.15), center=(-9.64,11.76))
```

```
mdb.models['Model-1'].sketches['__profile__'].EllipseByCenterPerimeter(axisPoint1=(10.67,28.34),  
axisPoint2=(10.1,28.69), center=(10.14,28.29))
```

```
mdb.models['Model-1'].sketches['__profile__'].EllipseByCenterPerimeter(axisPoint1=(40.67,-1.66),  
axisPoint2=(40.1,-1.31), center=(40.14,-1.71))
```

```
mdb.models['Model-1'].sketches['__profile__'].EllipseByCenterPerimeter(axisPoint1=(40.67,28.34),  
axisPoint2=(40.1,28.69), center=(40.14,28.29))
```

```
mdb.models['Model-1'].sketches['__profile__'].EllipseByCenterPerimeter(axisPoint1=(10.67,-1.66),  
axisPoint2=(10.1,-1.31), center=(10.14,-1.71))
```

```
mdb.models['Model-1'].sketches['__profile__'].EllipseByCenterPerimeter(axisPoint1=(10.89,22.42),  
axisPoint2=(9.78,22.6), center=(9.86,22.2))
```

```
mdb.models['Model-1'].sketches['__profile__'].EllipseByCenterPerimeter(axisPoint1=(40.89,-7.58),  
axisPoint2=(39.78,-7.4), center=(39.86,-7.8))
```

```
mdb.models['Model-1'].sketches['__profile__'].EllipseByCenterPerimeter(axisPoint1=(40.89,22.42),  
axisPoint2=(39.78,22.6), center=(39.86,22.2))
```

```
mdb.models['Model-1'].sketches['__profile__'].EllipseByCenterPerimeter(axisPoint1=(10.89,-7.58),  
axisPoint2=(9.78,-7.4), center=(9.86,-7.8))
```

```
mdb.models['Model-1'].sketches['__profile__'].EllipseByCenterPerimeter(axisPoint1=(12.35,2.33),  
axisPoint2=(9.64,2.32), center=(9.7,1.93))
```

```
mdb.models['Model-1'].sketches['__profile__'].EllipseByCenterPerimeter(axisPoint1=(42.35,32.33),  
axisPoint2=(39.64,32.32), center=(39.7,31.93))
```

```
mdb.models['Model-1'].sketches['__profile__'].EllipseByCenterPerimeter(axisPoint1=(42.35,2.33),  
axisPoint2=(39.64,2.32), center=(39.7,1.93))
```

```
mdb.models['Model-1'].sketches['__profile__'].EllipseByCenterPerimeter(axisPoint1=(12.35,32.33),  
axisPoint2=(9.64,32.32), center=(9.7,31.93))
```

```
mdb.models['Model-1'].sketches['__profile__'].EllipseByCenterPerimeter(axisPoint1=(27.24,21.87),  
axisPoint2=(26.1,21.95), center=(26.21,21.57))
```

```
mdb.models['Model-1'].sketches['__profile__'].EllipseByCenterPerimeter(axisPoint1=(-2.76,-8.13),  
axisPoint2=(-3.9,-8.05), center=(-3.79,-8.43))
```

```
mdb.models['Model-1'].sketches['__profile__'].EllipseByCenterPerimeter(axisPoint1=(-2.76,21.87),  
axisPoint2=(-3.9,21.95), center=(-3.79,21.57))
```

```
mdb.models['Model-1'].sketches['__profile__'].EllipseByCenterPerimeter(axisPoint1=(27.24,-8.13),  
axisPoint2=(26.1,-8.05), center=(26.21,-8.43))
```

```
mdb.models['Model-1'].sketches['__profile__'].EllipseByCenterPerimeter(axisPoint1=(30.15,12.75),  
axisPoint2=(26.91,12.85), center=(26.95,12.45))
```

```
mdb.models['Model-1'].sketches['__profile__'].EllipseByCenterPerimeter(axisPoint1=(0.15,42.75),  
axisPoint2=(-3.09,42.85), center=(-3.05,42.45))
```

```
mdb.models['Model-1'].sketches['__profile__'].EllipseByCenterPerimeter(axisPoint1=(30.15,42.75),  
axisPoint2=(26.91,42.85), center=(26.95,42.45))
```

```
mdb.models['Model-1'].sketches['__profile__'].EllipseByCenterPerimeter(axisPoint1=(0.15,12.75),  
axisPoint2=(-3.09,12.85), center=(-3.05,12.45))
```

```
mdb.models['Model-1'].sketches.changeKey(fromName='__profile__', toName=  
'skitso_1')
```

Appendix III

A typical script for calculating the average effective properties:

```

clc
clear all

load Rnd_AR5_40_1_T1.txt
load Rnd_AR5_40_2_T1.txt
load Rnd_AR5_40_3_T1.txt
load Rnd_AR5_40_4_T1.txt
load Rnd_AR5_40_5_T1.txt
load Rnd_AR5_40_1_T2.txt
load Rnd_AR5_40_2_T2.txt
load Rnd_AR5_40_3_T2.txt
load Rnd_AR5_40_4_T2.txt
load Rnd_AR5_40_5_T2.txt

% len =length of the RVE
len=60;

HFL56=Rnd_AR5_40_1_T1(:,3);
IVOL56=Rnd_AR5_40_1_T1(:,4);
s56=length(HFL56);

for i=1:3:s56

    av_HFL56(i)=(HFL56(i)+HFL56(i+1)+HFL56(i+2))/3;
    av_IVOL56(i)=(IVOL56(i)+IVOL56(i+1)+IVOL56(i+2))/3;
end

tav_HFL56=av_HFL56';
tav_IVOL56=av_IVOL56';

aHFL56=find(tav_HFL56);
aIVOL56=find(tav_IVOL56);
ss56=length(aHFL56);

for j=1:ss56
    Qx56(j)=tav_HFL56(aHFL56(j))*tav_IVOL56(aIVOL56(j));
end
tQx56=Qx56;

```

```
totQx56=sum(tQx56);
tAR56=sum(tav_IVOL56);
```

```
qx56=(totQx56/tAR56);
```

```
Kef56=(qx56*40)/90
```

```
%%%%%%%%%%%%%%%%%%%%%%%%%%%%%%%%%%%%%%%%%%%%%%%%%%%%%%%%%%%%%%%%%%%%%%%%
```

```
HFL57=Rnd_AR5_40_2_T1(:,3);
IVOL57=Rnd_AR5_40_2_T1(:,4);
s57=length(HFL57);
```

```
for i=1:3:s57
```

```
    av_HFL57(i)=(HFL57(i)+HFL57(i+1)+HFL57(i+2))/3;
    av_IVOL57(i)=(IVOL57(i)+IVOL57(i+1)+IVOL57(i+2))/3;
```

```
end
```

```
tav_HFL57=av_HFL57';
tav_IVOL57=av_IVOL57';
```

```
aHFL57=find(tav_HFL57);
aIVOL57=find(tav_IVOL57);
ss57=length(aHFL57);
```

```
for j=1:ss57
```

```
    Qx57(j)=tav_HFL57(aHFL57(j))*tav_IVOL57(aIVOL57(j));
```

```
end
```

```
tQx57=Qx57;
totQx57=sum(tQx57);
tAR57=sum(tav_IVOL57);
```

```
qx57=(totQx57/tAR57);
```

```
Kef57=(qx57*40)/90
```

```
%%%%%%%%%%%%%%%%%%%%%%%%%%%%%%%%%%%%%%%%%%%%%%%%%%%%%%%%%%%%%%%%%%%%%%%%
```

```
HFL58=Rnd_AR5_40_3_T1(:,3);
IVOL58=Rnd_AR5_40_3_T1(:,4);
s58=length(HFL58);
```

```
for i=1:3:s58
```

```
    av_HFL58(i)=(HFL58(i)+HFL58(i+1)+HFL58(i+2))/3;
    av_IVOL58(i)=(IVOL58(i)+IVOL58(i+1)+IVOL58(i+2))/3;
```

```
end
```

```
tav_HFL58=av_HFL58';
tav_IVOL58=av_IVOL58';
```

```

aHFL58=find(tav_HFL58);
aIVOL58=find(tav_IVOL58);
ss58=length(aHFL58);

for j=1:ss58
    Qx58(j)=tav_HFL58(aHFL58(j))*tav_IVOL58(aIVOL58(j));
end
tQx58=Qx58;
totQx58=sum(tQx58);
tAR58=sum(tav_IVOL58);

qx58=(totQx58/tAR58);

Kef58=(qx58*40)/90

%%%%%%%%%%%%%%%%%%%%%%%%%%%%%%%%%%%%%%%%%%%%%%%%%%%%%%%%%%%%%%%%%%%%%%%%

HFL59=Rnd_AR5_40_4_T1(:,3);
IVOL59=Rnd_AR5_40_4_T1(:,4);
s59=length(HFL59);

for i=1:3:s59

    av_HFL59(i)=(HFL59(i)+HFL59(i+1)+HFL59(i+2))/3;
    av_IVOL59(i)=(IVOL59(i)+IVOL59(i+1)+IVOL59(i+2))/3;
end

tav_HFL59=av_HFL59';
tav_IVOL59=av_IVOL59';

aHFL59=find(tav_HFL59);
aIVOL59=find(tav_IVOL59);
ss59=length(aHFL59);

for j=1:ss59
    Qx59(j)=tav_HFL59(aHFL59(j))*tav_IVOL59(aIVOL59(j));
end
tQx59=Qx59;
totQx59=sum(tQx59);
tAR59=sum(tav_IVOL59);

qx59=(totQx59/tAR59);

Kef59=(qx59*40)/90

%%%%%%%%%%%%%%%%%%%%%%%%%%%%%%%%%%%%%%%%%%%%%%%%%%%%%%%%%%%%%%%%%%%%%%%%

HFL60=Rnd_AR5_40_5_T1(:,3);
IVOL60=Rnd_AR5_40_5_T1(:,4);
s60=length(HFL60);

for i=1:3:s60

```

```

    av_HFL60(i)=(HFL60(i)+HFL60(i+1)+HFL60(i+2))/3;
    av_IVOL60(i)=(IVOL60(i)+IVOL60(i+1)+IVOL60(i+2))/3;
end

tav_HFL60=av_HFL60';
tav_IVOL60=av_IVOL60';

aHFL60=find(tav_HFL60);
aIVOL60=find(tav_IVOL60);
ss60=length(aHFL60);

for j=1:ss60
    Qx60(j)=tav_HFL60(aHFL60(j))*tav_IVOL60(aIVOL60(j));
end
tQx60=Qx60;
totQx60=sum(tQx60);
tAR60=sum(tav_IVOL60);

qx60=(totQx60/tAR60);

Kef60=(qx60*40)/90

%%%%%%%%%%%%%%

HFL56_2=Rnd_AR5_40_1_T2(:,3);
IVOL56_2=Rnd_AR5_40_1_T2(:,4);
s56_2=length(HFL56_2);

for i=1:3:s56_2

    av_HFL56_2(i)=(HFL56_2(i)+HFL56_2(i+1)+HFL56_2(i+2))/3;
    av_IVOL56_2(i)=(IVOL56_2(i)+IVOL56_2(i+1)+IVOL56_2(i+2))/3;
end

tav_HFL56_2=av_HFL56_2';
tav_IVOL56_2=av_IVOL56_2';

aHFL56_2=find(tav_HFL56_2);
aIVOL56_2=find(tav_IVOL56_2);
ss56_2=length(aHFL56_2);

for j=1:ss56_2
    Qx56_2(j)=tav_HFL56_2(aHFL56_2(j))*tav_IVOL56_2(aIVOL56_2(j));
end
tQx56_2=Qx56_2;
totQx56_2=sum(tQx56_2);
tAR56_2=sum(tav_IVOL56_2);

qx56_2=(totQx56_2/tAR56_2);

Kef56_2=(qx56_2*40)/90

```

```
%%%%%%%%%%%%%%%%%%%%%%%%%%%%%%%%%%%%%%%%%%%%%%%%%%%%%%%%%%%%%%%%%%%%%%%%
```

```
HFL57_2=Rnd_AR5_40_2_T2(:,3);
IVOL57_2=Rnd_AR5_40_2_T2(:,4);
s57_2=length(HFL57_2);
```

```
for i=1:3:s57_2
```

```
    av_HFL57_2(i)=(HFL57_2(i)+HFL57_2(i+1)+HFL57_2(i+2))/3;
    av_IVOL57_2(i)=(IVOL57_2(i)+IVOL57_2(i+1)+IVOL57_2(i+2))/3;
```

```
end
```

```
tav_HFL57_2=av_HFL57_2';
tav_IVOL57_2=av_IVOL57_2';
```

```
aHFL57_2=find(tav_HFL57_2);
aIVOL57_2=find(tav_IVOL57_2);
ss57_2=length(aHFL57_2);
```

```
for j=1:ss57_2
```

```
    Qx57_2(j)=tav_HFL57_2(aHFL57_2(j))*tav_IVOL57_2(aIVOL57_2(j));
```

```
end
```

```
tQx57_2=Qx57_2;
totQx57_2=sum(tQx57_2);
tAR57_2=sum(tav_IVOL57_2);
```

```
qx57_2=(totQx57_2/tAR57_2);
```

```
Kef57_2=(qx57_2*40)/90
```

```
%%%%%%%%%%%%%%%%%%%%%%%%%%%%%%%%%%%%%%%%%%%%%%%%%%%%%%%%%%%%%%%%%%%%%%%%
```

```
HFL58_2=Rnd_AR5_40_3_T2(:,3);
IVOL58_2=Rnd_AR5_40_3_T2(:,4);
s58_2=length(HFL58_2);
```

```
for i=1:3:s58_2
```

```
    av_HFL58_2(i)=(HFL58_2(i)+HFL58_2(i+1)+HFL58_2(i+2))/3;
    av_IVOL58_2(i)=(IVOL58_2(i)+IVOL58_2(i+1)+IVOL58_2(i+2))/3;
```

```
end
```

```
tav_HFL58_2=av_HFL58_2';
tav_IVOL58_2=av_IVOL58_2';
```

```
aHFL58_2=find(tav_HFL58_2);
aIVOL58_2=find(tav_IVOL58_2);
ss58_2=length(aHFL58_2);
```

```
for j=1:ss58_2
```

```

    Qx58_2(j)=tav_HFL58_2(aHFL58_2(j))*tav_IVOL58_2(aIVOL58_2(j));
end
tQx58_2=Qx58_2;
totQx58_2=sum(tQx58_2);
tAR58_2=sum(tav_IVOL58_2);

qx58_2=(totQx58_2/tAR58_2);

Kef58_2=(qx58_2*40)/90

```

```

%%%%%%%%%%%%%%%%%%%%%%%%%%%%%%%%%%%%%%%%%%%%%%%%%%%%%%%%%%%%%%%%%%%%%%%%

```

```

HFL59_2=Rnd_AR5_40_4_T2(:,3);
IVOL59_2=Rnd_AR5_40_4_T2(:,4);
s59_2=length(HFL59_2);

```

```

for i=1:3:s59_2

```

```

    av_HFL59_2(i)=(HFL59_2(i)+HFL59_2(i+1)+HFL59_2(i+2))/3;
    av_IVOL59_2(i)=(IVOL59_2(i)+IVOL59_2(i+1)+IVOL59_2(i+2))/3;

```

```

end

```

```

tav_HFL59_2=av_HFL59_2';
tav_IVOL59_2=av_IVOL59_2';

```

```

aHFL59_2=find(tav_HFL59_2);
aIVOL59_2=find(tav_IVOL59_2);
ss59_2=length(aHFL59_2);

```

```

for j=1:ss59_2

```

```

    Qx59_2(j)=tav_HFL59_2(aHFL59_2(j))*tav_IVOL59_2(aIVOL59_2(j));

```

```

end

```

```

tQx59_2=Qx59_2;
totQx59_2=sum(tQx59_2);
tAR59_2=sum(tav_IVOL59_2);

```

```

qx59_2=(totQx59_2/tAR59_2);

```

```

Kef59_2=(qx59_2*40)/90

```

```

%%%%%%%%%%%%%%%%%%%%%%%%%%%%%%%%%%%%%%%%%%%%%%%%%%%%%%%%%%%%%%%%%%%%%%%%

```

```

HFL60_2=Rnd_AR5_40_5_T2(:,3);
IVOL60_2=Rnd_AR5_40_5_T2(:,4);
s60_2=length(HFL60_2);

```

```

for i=1:3:s60_2

```

```

    av_HFL60_2(i)=(HFL60_2(i)+HFL60_2(i+1)+HFL60_2(i+2))/3;
    av_IVOL60_2(i)=(IVOL60_2(i)+IVOL60_2(i+1)+IVOL60_2(i+2))/3;

```

```

end

```

```
tav_HFL60_2=av_HFL60_2';
tav_IVOL60_2=av_IVOL60_2';
```

```
aHFL60_2=find(tav_HFL60_2);
aIVOL60_2=find(tav_IVOL60_2);
ss60_2=length(aHFL60_2);
```

```
for j=1:ss60_2
    Qx60_2(j)=tav_HFL60_2(aHFL60_2(j))*tav_IVOL60_2(aIVOL60_2(j));
end
tQx60_2=Qx60_2;
totQx60_2=sum(tQx60_2);
tAR60_2=sum(tav_IVOL60_2);

qx60_2=(totQx60_2/tAR60_2);

Kef60_2=(qx60_2*40)/90
```

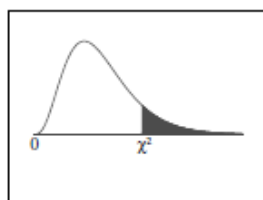
```
K_Eff_1=[Kef56 Kef57 Kef58 Kef59 Kef60]
mean_1=sum(K_Eff_1)/5
```

```
K_Eff_2=[Kef56_2 Kef57_2 Kef58_2 Kef59_2 Kef60_2]
mean_2=sum(K_Eff_2)/5
```

Appendix IV

Percentiles of the chi-square distribution

Chi-Square Distribution Table



The shaded area is equal to α for $\chi^2 = \chi^2_{\alpha}$.

<i>df</i>	$\chi^2_{.995}$	$\chi^2_{.990}$	$\chi^2_{.975}$	$\chi^2_{.950}$	$\chi^2_{.900}$	$\chi^2_{.100}$	$\chi^2_{.050}$	$\chi^2_{.025}$	$\chi^2_{.010}$	$\chi^2_{.005}$
1	0.000	0.000	0.001	0.004	0.016	2.706	3.841	5.024	6.635	7.879
2	0.010	0.020	0.051	0.103	0.211	4.605	5.991	7.378	9.210	10.597
3	0.072	0.115	0.216	0.352	0.584	6.251	7.815	9.348	11.345	12.838
4	0.207	0.297	0.484	0.711	1.064	7.779	9.488	11.143	13.277	14.860
5	0.412	0.554	0.831	1.145	1.610	9.236	11.070	12.833	15.086	16.750
6	0.676	0.872	1.237	1.635	2.204	10.645	12.592	14.449	16.812	18.548
7	0.989	1.239	1.690	2.167	2.833	12.017	14.067	16.013	18.475	20.278
8	1.344	1.646	2.180	2.733	3.490	13.362	15.507	17.535	20.090	21.955
9	1.735	2.088	2.700	3.325	4.168	14.684	16.919	19.023	21.666	23.589
10	2.156	2.558	3.247	3.940	4.865	15.987	18.307	20.483	23.209	25.188
11	2.603	3.053	3.816	4.575	5.578	17.275	19.675	21.920	24.725	26.757
12	3.074	3.571	4.404	5.226	6.304	18.549	21.026	23.337	26.217	28.300
13	3.565	4.107	5.009	5.892	7.042	19.812	22.362	24.736	27.688	29.819
14	4.075	4.660	5.629	6.571	7.790	21.064	23.685	26.119	29.141	31.319
15	4.601	5.229	6.262	7.261	8.547	22.307	24.996	27.488	30.578	32.801
16	5.142	5.812	6.908	7.962	9.312	23.542	26.296	28.845	32.000	34.267
17	5.697	6.408	7.564	8.672	10.085	24.769	27.587	30.191	33.409	35.718
18	6.265	7.015	8.231	9.390	10.865	25.989	28.869	31.526	34.805	37.156
19	6.844	7.633	8.907	10.117	11.651	27.204	30.144	32.852	36.191	38.582
20	7.434	8.260	9.591	10.851	12.443	28.412	31.410	34.170	37.566	39.997
21	8.034	8.897	10.283	11.591	13.240	29.615	32.671	35.479	38.932	41.401
22	8.643	9.542	10.982	12.338	14.041	30.813	33.924	36.781	40.289	42.796
23	9.260	10.196	11.689	13.091	14.848	32.007	35.172	38.076	41.638	44.181
24	9.886	10.856	12.401	13.848	15.659	33.196	36.415	39.364	42.980	45.559
25	10.520	11.524	13.120	14.611	16.473	34.382	37.652	40.646	44.314	46.928
26	11.160	12.198	13.844	15.379	17.292	35.563	38.885	41.923	45.642	48.290
27	11.808	12.879	14.573	16.151	18.114	36.741	40.113	43.195	46.963	49.645
28	12.461	13.565	15.308	16.928	18.939	37.916	41.337	44.461	48.278	50.993
29	13.121	14.256	16.047	17.708	19.768	39.087	42.557	45.722	49.588	52.336
30	13.787	14.953	16.791	18.493	20.599	40.256	43.773	46.979	50.892	53.672
40	20.707	22.164	24.433	26.509	29.051	51.805	55.758	59.342	63.691	66.766
50	27.991	29.707	32.357	34.764	37.689	63.167	67.505	71.420	76.154	79.490
60	35.534	37.485	40.482	43.188	46.459	74.397	79.082	83.298	88.379	91.952
70	43.275	45.442	48.758	51.739	55.329	85.527	90.531	95.023	100.425	104.215
80	51.172	53.540	57.153	60.391	64.278	96.578	101.879	106.629	112.329	116.321
90	59.196	61.754	65.647	69.126	73.291	107.565	113.145	118.136	124.116	128.299
100	67.328	70.065	74.222	77.929	82.358	118.498	124.342	129.561	135.807	140.169

Publications

CONFERENCE PROCEEDINGS

1. Ioannis, Ioannou, Hodzic Alma, Gitman Inna, Soutis Costas, and M. A. Almaadeed. "Numerical Characterisation of Random Glass Fibre Composite Material" Proc. ECCM15, 24-28 June 2012, Venice, Italy.
2. Ioannis, Ioannou, Hodzic Alma, Gitman Inna, Soutis Costas, and M. A. Almaadeed. "Numerical Investigation of the Mechanical Properties and Thermal Conductivity of Short Fibre Thermoplastic Composites." Proc. DFC12/S16, 8-11 April 2013, Cambridge, England.
3. Ioannis, Ioannou, Hodzic Alma, Gitman Inna, Soutis Costas, and M. A. Almaadeed. "Investigation of Thermal and Mechanical Properties of Short Fibre Thermoplastic Composites." Proc. ICCS17, 17-21 June 2013, Porto, Portugal.
4. Ioannis, Ioannou, Hodzic Alma, Gitman Inna, Soutis Costas, and M. A. Almaadeed. "Numerical analysis of Micromechanical Aspects in Short Fibre Composite." Proc. 34th Riso International Symposium on Material Science. 2-5 September 2013, Roskilde, Denmark.
5. Ioannis, Ioannou, Hodzic Alma, Gitman Inna, Soutis Costas, and M. A. Almaadeed. "Investigation of Micromechanical Parameters on the Mechanical and Thermal Response of Short Fibre Composite" Proc. ECCM16, 22-26 June 2014, Seville, Spain.

JOURNAL PUBLICATIONS

1. Ioannis, Ioannou, Hodzic Alma, Gitman Inna, Soutis Costas, and M. A. Almaadeed. "Micro-Mechanical Parameters in Short Fibre Composite." Applied Composite Materials 21, no. 1 (2014): 197-211.

PAPERS IN PREPARATION

1. Ioannis, Ioannou, Hodzic Alma, Gitman Inna, Soutis Costas, and M. A. Almaadeed. "Numerical Investigation of Thermal and Thermo-Mechanical Effective Properties for Short Fibre Composites - I.-Thermal Properties"

2. Ioannis, Ioannou, Hodzic Alma, Gitman Inna, Soutis Costas, and M. A. Almaadeed.
“Numerical Investigation of Thermal and Thermo-Mechanical Effective Properties for Short Fibre Composites – *II*-Fibre Length Distribution”